UNIVERSITÉ LAVAL

Bottom-up Photochemical Synthesis of Structurally Defined Graphene Nanoribbons and Conjugated Polymers

Thèse

Dandan Miao

Doctorat en chimie
Philosophiæ doctor (Ph. D.)

Québec, Canada

Résumé

Le graphène peut être considéré comme l'un des matériaux les plus prometteurs pour les composants électroniques pratiques en raison de ses excellentes propriétés de transport de charge, de sa surface spécifique très élevée, de sa conductivité thermique excellente et de sa grande résistance mécanique. Cependant, ce graphène bidimensionnel est un semiconducteur à bande interdite nulle, ce qui limite son application pratique dans les dispositifs électroniques. L'une des méthodes les plus prometteuses pour ouvrir une bande interdite est le confinement structurel du graphène en bandes étroites, définies comme des nanorubans de graphène (GNR). La bande interdite des GNR peut être contrôlée avec précision par la largeur et la configuration des bords, ce qui donne aux GNR des propriétés optiques et électroniques réglables.

La synthèse ascendante en solution est l'une des stratégies les plus prometteuses pour préparer des GNR structurellement bien définis avec des propriétés optiques et électroniques ajustables. Contrairement aux méthodes descendantes, la stratégie ascendante permet un contrôle précis de la largeur et de la configuration des bords des GNR. Une stratégie couramment utilisée, la réaction de cyclodéshydrogénation catalysée par l'acide de Lewis, appelée réaction de Scholl, a été largement utilisée pour synthétiser une grande variété de GNR bien définis sur des précurseurs de polyphénylène. Cependant, la réaction de Scholl présente de sérieux inconvénients qui limitent la portée et la polyvalence de cette réaction. Le premier est sa faible régiosélectivité qui entraîne des défauts de structure et affecte les propriétés des GNR. Ensuite, les réarrangements indésirables et l'utilisation d'un catalyseur métallique peuvent conduire à la formation de sous-produits. De plus, l'introduction de groupes fonctionnels sensibles aux oxydants et d'hétérocycles riches en électrons est difficile à réaliser en raison des conditions de réaction difficiles, qui limitent la diversité des propriétés structurelles et électroniques des GNR.

Notre groupe a récemment développé une synthèse de nanographènes et de GNR à l'aide de la réaction de cyclodéhydrochloration photochimique (CDHC) sur des précurseurs de

polyphénylène polychlorés. La réaction CDHC possède une haute régiosélectivité et se déroule sans réarrangement ni formation de sous-produits. De plus, la réaction CDHC est conduite sans catalyseur métallique ni oxydant dans des conditions très douces, permettant ainsi l'introduction de différents groupes fonctionnels et hétérocycles sur le GNR afin de moduler leurs propriétés optoélectroniques. En comparant avec la réaction de Scholl, la réaction CDHC permet de mieux contrôler les configuration de bord des GNR. Cette thèse présente en détail l'utilisation de la réaction CDHC pour la préparation de GNR et étudie avec soin les propriétés structurelles et optoélectroniques des GNR produits. Tout d'abord, les GNR asymétriques et latéralement symétriques ont été préparés pour démontrer la régiosélectivité, le contrôle des configuration de bord et l'efficacité de la réaction photochimique CDHC. Ensuite, les GNR à bord thiophène ont été synthétisés pour montrer la polyvalence de la réaction CDHC et étudier l'influence de l'introduction de groupes fonctionnels riches en électrons sur les structures et les propriétés optoélectroniques des GNR. Ensuite, les polymères échelle conjugués (CLP) contenant des unités pyrrole riches en électrons ont été synthétisés pour montrer la compatibilité de la réaction du CDHC avec des groupes fonctionnels très riches en électrons et le rendement élevé de la réaction du CDHC. Enfin, divers dérivés d'ullazine fusionnés avec des hétérocycles riches en électrons ou pauvres en électrons ont été préparés et une série de polymères donneurs-accepteurs conjugués (D-A CP) ont été synthétisés et ces polymères ont été utilisés avec succès dans les cellules solaires à polymères et ont présenté des performances très prometteuse, indiquant l'efficacité, la polyvalence et le caractère pratique de la réaction photochimique CDHC.

Abstract

Graphene is considered as one of the most promising materials for practical electronic components because of its outstanding charge transport properties, very high specific surface area, excellent thermal conductivity, and high mechanical strength. However, this two dimensional graphene is a zero band gap semiconductor, which limits its practical application in electronic devices. One of the most promising methods to open a band gap is the structural confinement of graphene into narrow strips, which is defined as graphene nanoribbons (GNRs). The band gap of GNRs can be precisely controlled by the width and edge configuration, providing GNRs with tunable optical and electronic properties.

Bottom-up, solution-phase synthesis is one of the most promising strategies to prepare structurally well-defined GNRs with tunable optical and electronic properties. Unlike the top-down methods, the bottom-up strategy allows a precise control over the width and edge configuration of GNRs. One of the most commonly used strategy, the Lewis acid catalyzed cyclodehydrogenation reaction, known as the Scholl reaction, has been widely used to synthesize a large variety of well-defined GNRs on polyphenylene precursors. However, the Scholl reaction possesses some serious drawbacks that limit the scope and versatility of this reaction. First is its poor regioselectivity that results in structural defects to affect the properties of GNRs. Then the undesired rearrangements and the use of a metal catalyst can lead to the formation of by-products. Moreover, the introduction of oxidant-sensitive functional groups and electron-rich heterocycles is difficult to achieve due to the harsh reaction conditions, which limits the diversity of structural and electronic properties of GNRs.

Recently, our group reported the synthesis of nanographenes and GNRs using the photochemical cyclodehydrochlorination (CDHC) reaction on polychlorinated polyphenylene precursors. The CDHC reaction possesses high regioselectivity and it proceeds without rearrangements or the formation of side-products. Furthermore, the CDHC reaction is conducted without metal catalyst and oxidant under very mild conditions, thus enabling the

introduction of different functional groups and heterocycles onto the GNRS to modulate their optoelectronic properties. And comparing with the Scholl reaction, the CDHC reaction provides better control over the edge configuration of the GNRs. This paper investigates in detail the usefulness of the CDHC reaction for the preparation of GNRs and carefully studies the structural and optoelectronic properties of the GNRs produced. First the laterally symmetrical and unsymmetrical GNRs were prepared to demonstrate the regioselectivity, edge configuration control, and efficiency of the photochemical CDHC reaction. Then the thiophene-edged GNRs were synthesized to show the versatility of the CDHC reaction and study the influence of the introduction of electron-rich functional groups on the structures and optoelectronic properties of GNRs. Then, the conjugated ladder polymers (CLPs) containing electron-rich pyrrole units were synthesized to show the compatibility of the CDHC reaction with very electron-rich functional groups and the high efficiency of the CDHC reaction. Finally various π-extended ullazine derivatives fused with electron-rich or electron-poor heterocycles were prepared and a series of conjugated donor-acceptor polymers (D-A CPs) were synthesized and these polymers were successfully employed in the polymer solar cells and exhibited very promising performances, indicating the efficiency, versatility and practicality of the photochemical CDHC reaction.

Table of Content

List of Tables

List of Figures

List of Schemes

List of Abbreviations

AFM = Atomic Force Microscopy
APPI = Atmospheric Pressure Photo-Ionization
BHJ-PSCs = Bulk Heterojunction Polymer Solar Cells
Bu_4NPF_6 = Tetrabutylammonium hexafluorophosphate
C-C = Carbon-Carbon
CDHC = Cyclodehydrochlorination
CNTs = Carbon Nanotubes
CLPs = Conjugated Ladder Polymers
CV = Cyclic Voltammetry
CVD = Chemical Vapor Deposition
d = Doublet
D-A CPs = Donor-Acceptor Conjugated Polymers
dba = Dibenzylideneacetone
DCM = Dichloromethane
DFT = Density Functional Theory
DIO = Diiodooctane
DMF = Dimethylformamide
DP = Degree of Polymerization
DPP = Diketopyrrolopyrrole
dppf = 1,1'-Bis(diphenylphosphino)ferrocene
DSC = Differential Scanning Calorimetry
DSSCs = Dye-sensitized Solar Cells
dtbpf = 1,1′-Bis(di-*tert*-butylphosphino)ferrocene
E_g^{elec} = Electrochemical Bandgap
E_g^{opt} = Optical Bandgap
FETs = Field-Effect Transistors
FF = Fill Factor
FMN = Flavin Mononucleotide
FT-IR = Fourier-transform Infrared
GNRs = Graphene Nanoribbons
GO = Graphene Oxide
GONRs = Graphene Oxide Nanoribbons
GSs = Graphene Sheets

h = Hour

HOMO = Highest Occupied Molecular Orbital

HRMS = High Resolution Mass Spectra

I_{on}/I_{off} = On-Off ratio

ICT = Intramolecular Charge Transfer

IID = Isoindigo

ITO = Indium Tin Oxide

J_{sc} = Short-circuit Current Density

J-V = Current density-voltage

LC-MS = Liquid Chromatography-Mass Spectrometry

LUMO = Lowest Unoccupied Molecular Orbital

m = Multiplet

MWCNTs = Multi-Walled Carbon Nanotubes

NGs = Nanographenes

NIR = Near-Infrared

NMR/RMN = Nuclear Magnetic Resonance/ Résonance Magnétique Nucléaire

OFETs = Organic Field-Effect Transistors

OLEDs = Organic Light Emitting Diodes

OPVs = Organic Photovoltaics

PAHs = Polycyclic Aromatic Hydrocarbons

PCE = Power Conversion Efficiency

PDAs = Polydiacetylenes

PDIs = Perylene Diimides

PEI = Polyethylenimine

P3HT = Poly(3-hexylthiophene)

PMMA = Poly(methyl methacrylate)

PmPV = Poly(*m*-phenylene-co-2,5-dioctoxy-*p*-phenylenevinylene)

PPh_3 = Triphenylphosphine

PVP = Polyvinylpyrrolidone

RMS = Root-Mean-Square

s = Singlet

SCE = Saturated Calomel Electrode

SDS = Sodium Dodecyl Sulphate

SEC = Size-exclusion Chromatography

SPhos = 2-Dicyclohexylphosphino-2′,6′-dimethoxybiphenyl

SPS = Solvent Purifier System

STM = Scanning Tunnelling Microscopy

SWCNTs = Single-Walled Carbon Nanotubes

t = Triplet

TBPA = Tris(4-bromophenyl)ammoniumyl hexachloroantimonate

TCB = 1,2,4-Trichlorobenzene

TCE = Tetrachloroethane

TEM = Transmission Electron Microscopy

TFA = Trifluoroacetic acid

TfOH = Triflic acid

T_g = Glass Transition Temperature

TGA = Thermogravimetric Analysis

THF = Tetrahydrofuran

TLC = Thin Layer Chromatography

TOF = Time-of-Flight

TPD = Thienopyrroledione

UHV = Ultra-High Vacuum

UV = Ultraviolet

UV-vis = Ultraviolet-visible

V_{oc} = Open-circuit Voltage

XPhos = 2-Dicyclohexylphosphino-2′,4′,6′-triisopropylbiphenyl

XPS = X-ray Photoelectron Spectroscopy

$Đ$ = Dispersity Index

ϕ_F = Quantum Yield

Acknowledgements

First of all, I would like to thank Prof. Dr. Jean-Fran ̧ois Morin. Four years ago, when I was in China, I was very interested in his research group and I applied to come to his group to do my PhD. I really appreciate him for giving me this opportunity to work in his lab and work on the graphene nanoribbons project. He is the most patient and kind professor I have ever met. I sincerely appreciate his selfless support and understanding both on my research project and on my life. Whenever I encounter problems in my research, he always gives me helpful suggestions and guidance, most importantly, he trusts me and gives me great confidence in conducting my research work. I would say, without him, I can't finish my PhD so smoothly.

I would also like to thank Dr. Maxime Daigle. When I came to the lab on the first day, I met him, my colleague Maxime Daigle, he took me to the lab, introduced me in detail the equipment and instruments of the lab. At first, I worked with him on his project, he taught me a lot, from the most basic experimental operations to how to conduct research project independently, he gave me advice and guidance, making me quickly become familiar with my project, and I could work on my project myself. He is both the best research partner and the most important friend in my life.

I would also like to thank Dr. Cyril Aumaitre. He helped me a lot in my project. He is an expert in polymer solar cells and when I did this part of work in my project, he really gave me a lot of useful suggestions and helped me to accomplish all the work. I really appreciate him for his help and guidance to achieve the exciting collaboration results.

I would also like to thank all the colleagues in the Morin's research group. They are all kind persons and whenever I have a problem, whether in my project or in my life, they are always there to help. They often invite me to attend their party, so that I can enjoy the warmth in a foreign country, which allows me to conduct my research work more freely.

I would also like to thank Prof. Dr. Matteo Tommasini and Dr. Andrea Lucotti (Department of

Chemistry, Materials and Chemical Engineering “G. Natta”, Politecnico di Milano) for their kindly collaboration in the Raman analysis and DFT calculations.

Finally, I would like to thank my parents and my husband Mr. Tiezhu Liu for their continuous support and understanding, which gave me confidence and strength to overcome all kinds of difficulties and complete my PhD studies.

Foreword

The content of chapter 2 and 4 are identical to the published papers but have been reformatted to ensure the coherence of the thesis.

Chapter 2: Dandan Miao[a], Maxime Daigle[a], Andrea Lucotti[b], Joël Boismenu-Lavoie[a], Matteo Tommasini [b], and Jean-François Morin*[a]. Toward thiophene-annulated GNRs, *Angewandte Chemie International Edition*, **2018**, *57*, 3588-3592.

Contribution: I am the first author and I am the principal contributor. I have designed and synthesized the molecules. I also have done the characterization (NMR, UV-Vis and photoluminescence, FT-IR). I also have written the manuscript. Andrea Lucotti and Matteo Tommasini performed the Raman spectroscopy and DFT calculations. Joël Boismenu-Lavoie helped to design the model compounds. Prof. Claudine Allen helped for the measurements of quantum yields. Yannick Ledemi, Samuel Ouellet and Prof. Denis Boudreau helped for time-resolved photoluminescence spectroscopy measurements. Maxime Daigle and Jean-François Morin have contributed to the manuscript writing and edition.

Chapter 4: Dandan Miao[a], Cyril Aumaitre[a], and Jean-François Morin*[a]. Photochemical synthesis of π-extended ullazine derivatives as new electron donors for efficient conjugated D-A polymers, *Journal of Materials Chemistry C*, **2019**, *7*, 3015-3024.

Contribution: I am the first author and I am the principal contributor. I have designed and synthesized the molecules. I also have done the characterization (UV-Vis-NIR, CV). I also have written the manuscript. Cyril Aumaitre helped in the polymer solar cells application. Cyril Aumaitre and Jean-François Morin have contributed to the manuscript writing and edition.

Introduction

Graphene

Graphene (as is shown in Figure I.1), a single layer of carbon atoms arranged in a two-dimensional honeycomb lattice. Since first isolated in 2004 by Geim and Novoselov *et al.*,[1,2] graphene has quickly become a hot research topic in many research areas. Many extraordinary properties of graphene have been reported, such as extremely high charge carrier mobility (> 200 000 cm^2 V^{-1} s^{-1}, several orders of magnitude higher than silicon),[3] high specific surface area (2630 m^2 g^{-1}),[4] excellent thermal conductivity (~ 5000 W m^{-1} K^{-1}),[5] good mechanical properties with a high Young's modulus (1.0 TPa),[6] and unexpectedly high optical transparency (~ 97.7%).[7] All of these excellent properties make graphene a promising material for practical applications in future electronics[8,9] and optical electronics.[10-12]

With all of these excellent properties and promising applications, a variety of synthetic methods have been developed for the large scale synthesis of graphene, such as solution exfoliation of graphite,[13-15] chemical reduction of graphene oxide (GO),[16,17] epitaxial growth on a silicon carbide (SiC) substrate,[18-20] and chemical vapor deposition (CVD) on transition-metals surfaces.[21-23] Chemical vapor deposition (CVD) has proven to be the most efficient synthetic method for preparing large-area, well controlled graphene sheets.

However, for the application of graphene in electronic devices, in addition to the quality and scale of synthesis, the graphene sheets need to be transfered from the metal surfaces onto the dielectric substrate.[24-26] Besides, even though graphene possesses a lot of extraordinary properties, it is intrinsically semi-metallic due to its zero-bandgap nature.[27] The absence of bandgap means that the conductivity in graphene cannot be switched off, which definitely hinders its semiconducting applications in electronic devices, such as field-effect transistors (FETs) devices.[28] Many approaches have been employed to open a bandgap in graphene, one of the most promising methods is the quantum confinement of graphene into high aspect ratio

strips (with lateral width less than 50 nm), which are defined as graphene nanoribbons (GNRs). Both theoretical and experimental studies proved that large and tunable bandgap can be obtained in GNRs.[29,30] Thus, GNRs have become one of the most promising materials for the next generation semiconductor electronic devices.

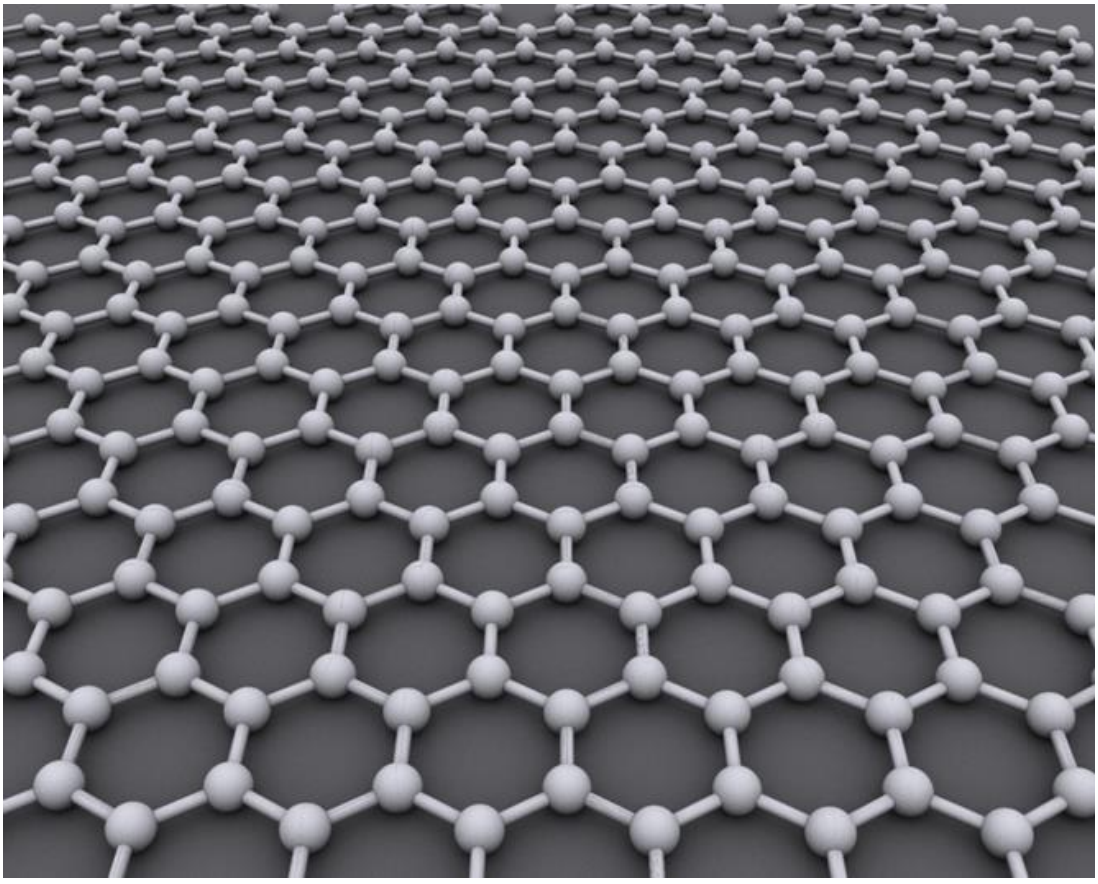

Figure I.1. Graphene is an atomic-scale hexagonal lattice made of carbon atoms.

Graphene Nanoribbons

The electronic properties of graphene nanoribbons (GNRs) are critically dependent on their width and edge structures.[31] According to the obtained edge structures, there are typically three types of GNRs, namely armchair GNR,[32] zigzag GNR[33], "cove"-type GNR[34] and chiral GNR[35]. (as is shown in Figure I.2).

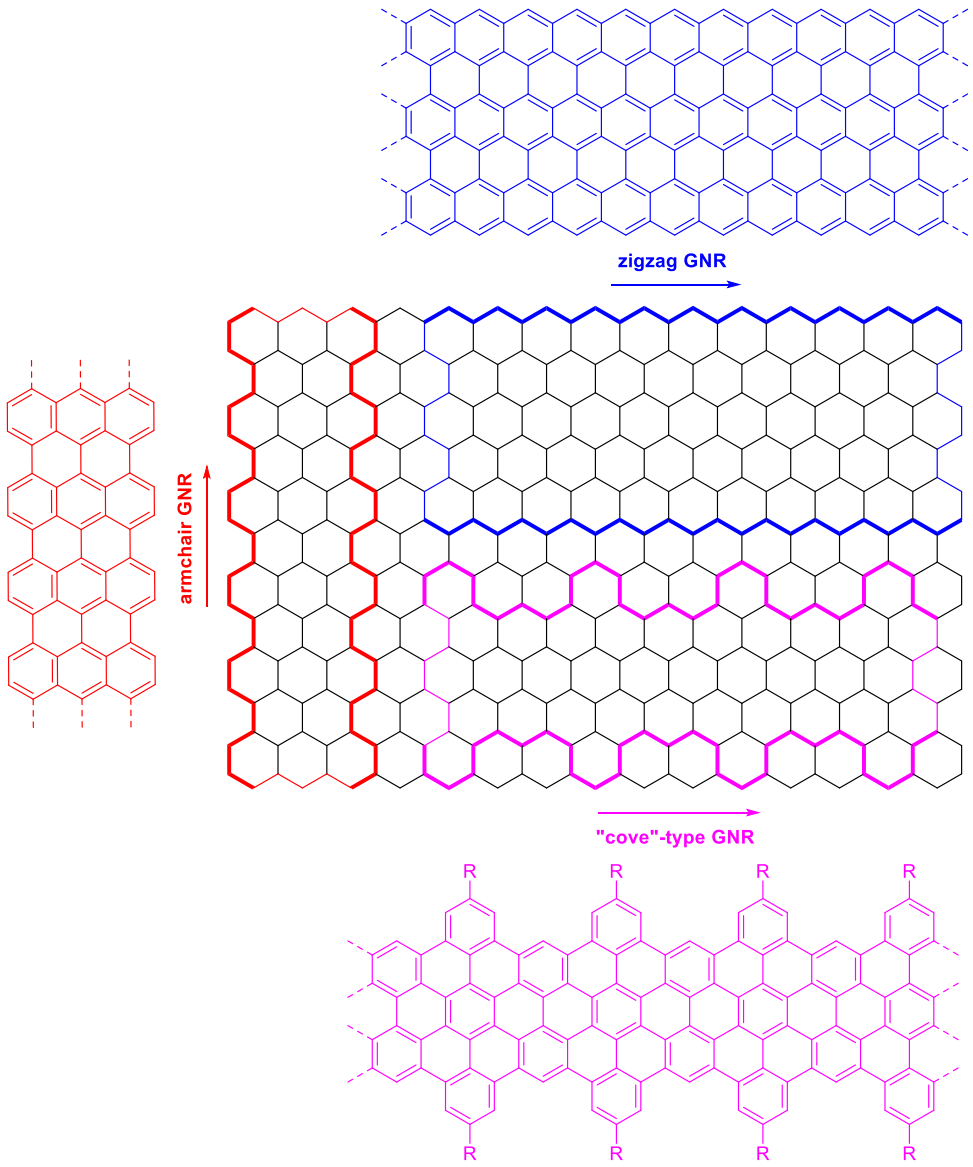

Figure I.2. Three edge structures for graphene nanoribbons: armchair GNR, zigzag GNR and "cove"-type GNR. Reproduced from Ref. [32-34].

It has already been reported that the bandgap of GNRs is inversely proportional to its lateral width,[30,36,37] which means the bandgap increases as the lateral width decreases (as is shown in Figure I.3). Thus, due to the close relationship between the physical structure and electronic properties of GNRs, it is imperative to find a synthetic method in which the structure of GNRs can be precisely controlled on the atomic scale.

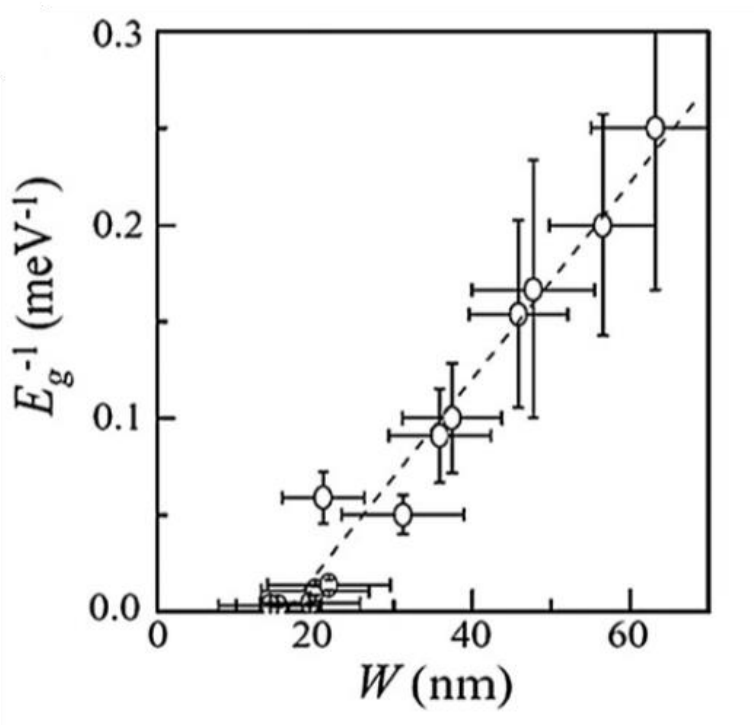

Figure I.3. The relationship between the reciprocal of energy gap E_g and the width of GNRs. Reproduced from Ref. [30].

"Top-down" synthesis of GNRs

Initially, GNRs with various lateral widths (5 nm-500 nm) have been successfully synthesized from larger carbon materials such as graphite, carbon nanotubes (CNTs) and graphene using the so-called "top-down" approach including the sonochemical extraction of expanded graphite, unzipping of CNTs and lithography of graphene. Although these "top-down" approaches proved to be useful in preparing GNRs and studying their electronic properties, obtaining the GNRs with lateral width down to 5 nm and controlling the uniform edge structures is still challenging.

Sonochemical extraction of graphite

The first "top-down" strategy is the sonochemical extraction of expanded graphite. Dai *et al*[38] first reported in 2008 the synthesis of GNRs with lateral width down to sub 10 nm by the

solution-phase sonication and functionalization of expanded graphite in the presence of poly(*m*-phenylene-co-2,5-dioctoxy-*p*-phenylenevinylene) (PmPV) (Figure I.4b). Cheng *et al*[39] reported in 2010 the sonochemical cutting of the graphene sheets (GSs) in a mixture of 0.1 wt% polyvinylpyrrolidone (PVP) and 0.1 wt% sodium dodecyl sulphate (SDS) into long and narrower than 20 nm GNRs (Figure I.4c-d). In 2015, Ju *et al*[40] reported the GNRs as small as 10 nm in width formed by the sonochemical graphene unzipping using flavin mononucleotide (FMN) as a surfactant (Figure I.4a).

The sub-10 nm wide GNRs were employed to fabricate field-effect transistors (FETs) by Dai *et al*[41] in 2008, and the FET devices showed on-off ratio (I_{on}/I_{off}) up to 10^6 at room temperature and on-state current density as high as ~ 2000 μA/μm. The sub-10 nm wide GNRs based FETs are comparable in performance with small diameter carbon nanotubes (CNTs) devices, but the GNRs have the advantages of all-semiconducting devices. These excellent performances indicated the high quality of the obtained GNRs. However, this method suffered from low reproducibility, low yields, and uncontrollable edge structure and lateral width.

Unzipping of CNTs

The second "top-down" strategy is the longitudinal unzipping of CNTs.[42-46] In 2009, Tour *et al*[42] first reported the unzipping of CNTs through a solution-based oxidative process (as is shown in Figure I.5). Similar to the exfoliation of graphite, multi-walled carbon nanotubes (MWCNTs) were treated with a mixture of concentrated sulfuric acid (H_2SO_4) and potassium permanganate ($KMnO_4$) and the MWCNTs were unzipped in a linear longitudinal direction to generate graphene oxide nanoribbons (GONRs) with length of ~ 4 μm and lateral width of >100 nm. The subsequent reduction of GONRs with hydrazine (N_2H_4) was unable to remove all the oxygen-containing functionalities and even optimized method[44] reported later can only produced GONRs (length of > 5 μm, width of 75-200 nm) with fewer structural defects. The structural defects affect the electronic properties of the obtained GNRs and the large lateral widths make it hard to open a bandgap.

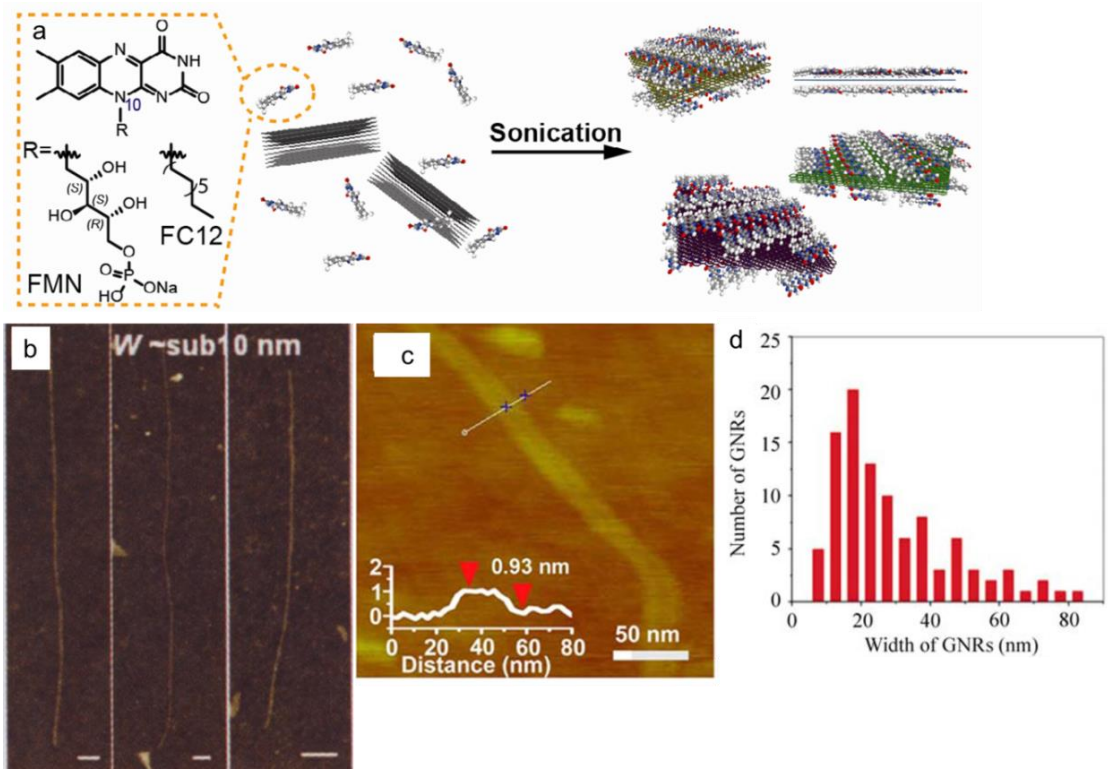

Figure I.4. a) Schematic illustration of FMN-assisted graphene dispersion using a sonochemical method. Reproduced from Ref. [40]. b) AFM image of GNRs with the lateral width sub 10 nm. Reproduced from Ref. [38]. c) AFM image of GNRs with width narrower than 20 nm and d) width distributions of GNRs produced by sonochemical method. Reproduced from Ref. [39].

Later, GNRs with narrower width (10-20 nm) and smooth edges were prepared through the Ar plasma etching of MWCNTs partly embedded in a poly(methyl methacrylate) (PMMA) film (Figure I.6).[43] This polymer-protected plasma etching method was applied on an aligned array of single-walled carbon nanotubes (SWCNTs) to obtain highly aligned, narrower (sub-10 nm) GNRs.[45] FETs devices were fabricated based on these GNRs and an on-off ratio (I_{on}/I_{off}) up to 10^3 at room temperature was obtained, indicating the high quality of GNRs obtained by this method.

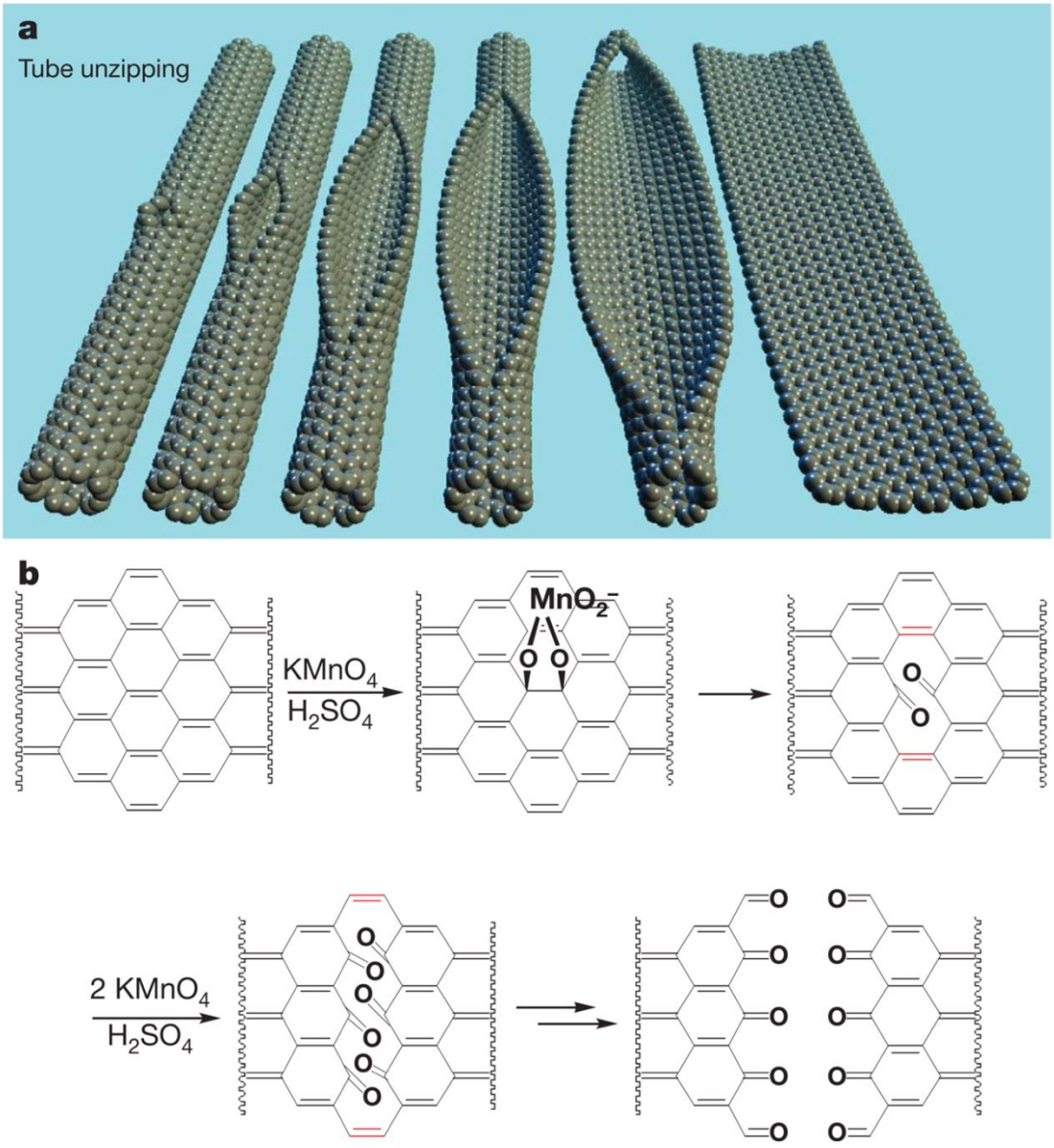

Figure I.5. a) Schematic illustration of the unzipping of CNTs to prepare GNRs. b) The proposed chemical mechanism of CNTs unzipping. Reproduced from Ref. [42].

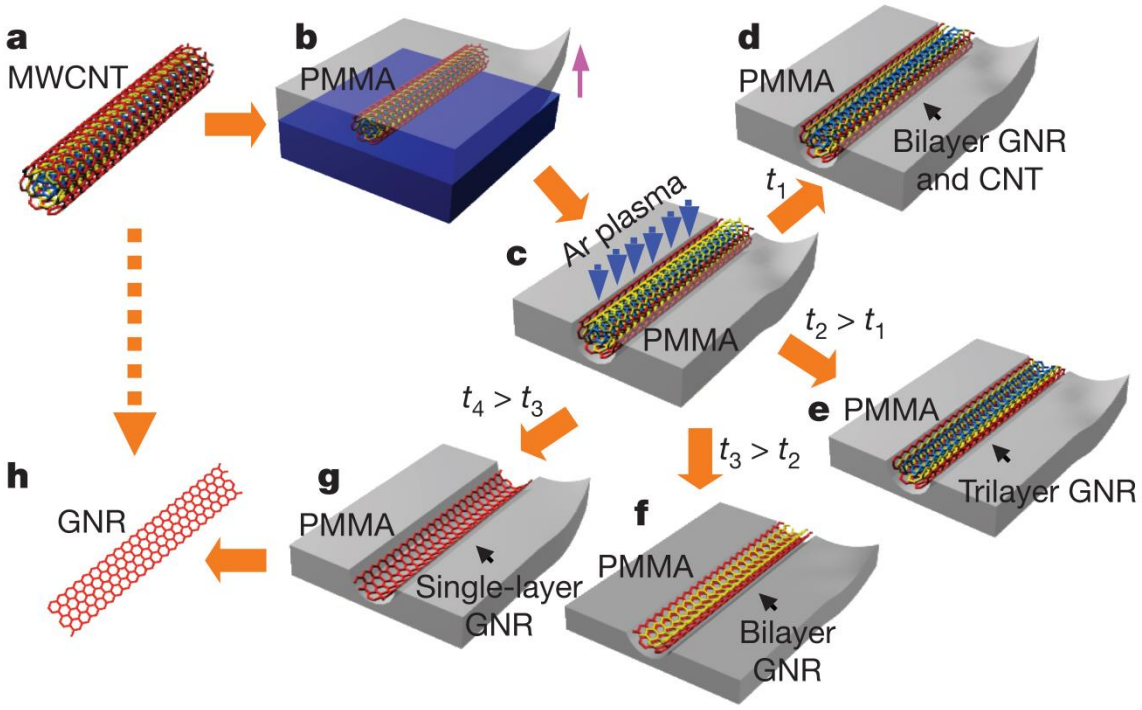

Figure I.6. Schematic illustration of the unzipping of CNTs through the polymer-protected Ar plasma etching method. Reproduced from Ref. [43].

Lithography of graphene

Another "top-down" strategy is the lithography of graphene. First reported in 2007 by Avouris *et al*,[47] graphene was patterned using electron-beam lithography first, then an oxygen plasma etching process was applied to make GNRs with widths range from 20 to 500 nm. The electronic properties of these GNRs were studied by Kim *et al*[30] and they observed that the bandgap scales inversely with the lateral width, demonstrating the ability of lithography to design the bandgap of GNRs. Later, in 2009, this method was optimized by using chemically synthesized nanowires as the protection mask, followed by the oxygen plasma etching to obtain GNRs with lateral width down to 6 nm (Figure I.7).[48] By tuning the diameter of the nanowire and the etching time, the lateral width of GNRs can be controlled. Reported by Liu *et al*[49] in 2011, highly aligned GNRs arrays with widths less than 10 nm were fabricated by self-masked plasma etching of wrinkle engineering CVD-graphene. FETs devices showed an on-off ratio

(I_{on}/I_{off}) of ~ 30, suggesting a bandgap of ~ 0.1 eV. Although the lithographic of graphene possesses the advantages of generating aligned GNRs, the low reproducibility and the edge defects (roughness and disorder) are still large problems.

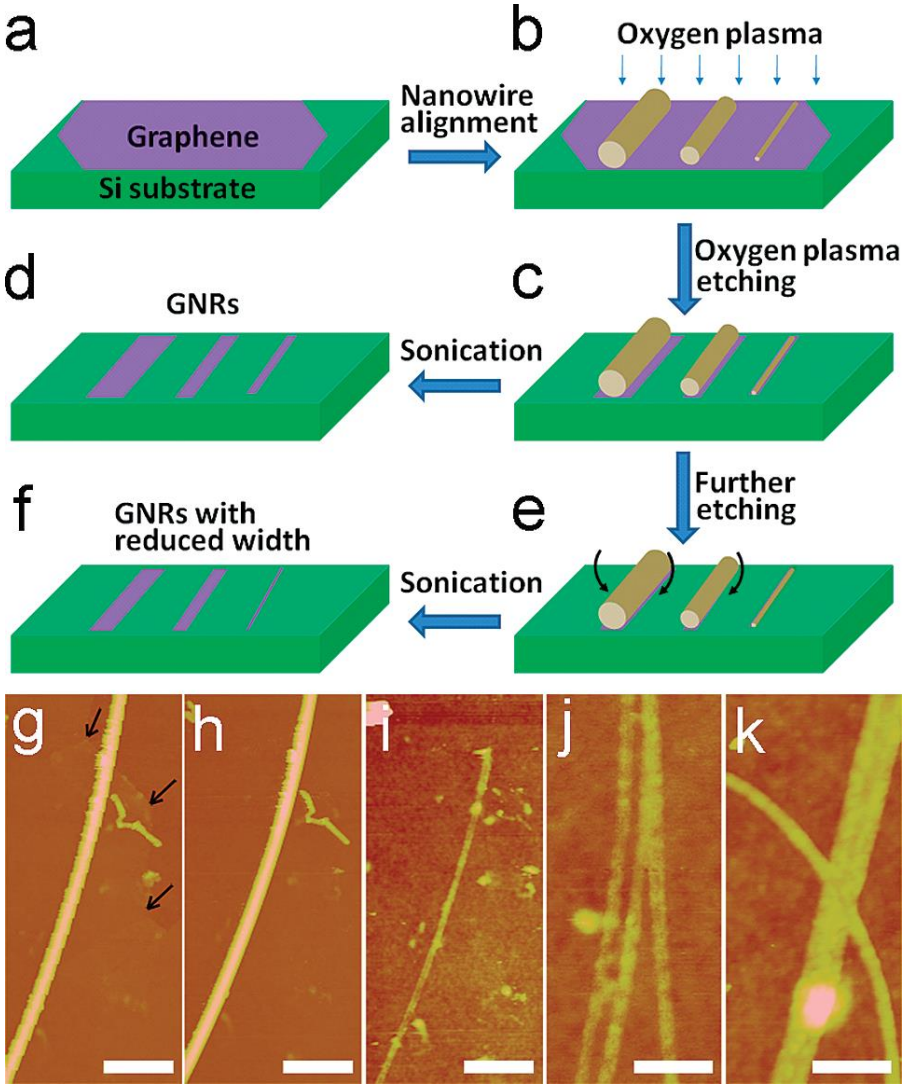

Figure I.7. a-f) Schematic illustration of the lithography process to obtain GNRs by an oxygen plasma etching with a nanowire as the protection mask. g, h) AFM images of a nanowire protection mask on top of the graphene before (g) and after (h) oxygen plasma etching. i) AFM image of the obtained GNRs after sonication removing the nanowire mask. j-k) AFM images of branched and crossed GNRs from merged and crossed nanowire masks. Reproduced from Ref. [48].

The "top-down" methods proved to be useful in preparing GNRs which exhibited excellent semiconducting properties with high on-off ratio (*e.g.* 10^6) and high mobility (*e.g.* 1500 $cm^2 V^{-1} s^{-1}$). However, these methods suffer from low yields, low reproductivity, different lateral widths and random edge structures, which strongly affect their electronic properties and ultimately hinders their practical applications in electronic devices. Besides, in order to open sufficient bandgaps for high on/off ratio FETs devices, the lateral width should be narrowed down to sub-5 nm,[50] which is hard to be achieved by the "top-down" methods. Therefore, it is very important to find a synthetic approach where the lateral width and edge structure can be precisely controlled on the atomic scale.

"Bottom-up" synthesis of GNRs

In contrast, "bottom-up" approach enables the synthesis of various GNRs with well-defined structures, narrow lateral width (sub-5 nm), as well as heteroatom doping. Starting from carefully designed small molecules, followed by a polymerization and cyclodehydrogenation, the lateral width, edge structure and heteroatoms doping of GNRs can be precisely controlled. The "bottom-up" approach can be accomplished both on metal surfaces under ultra-high vacuum (UHV) conditions and in solution, which are surface-assisted and solution-mediated approach.

Surface-assisted approach

The surface-assisted synthesis of GNRs was first reported by Müllen and Fasel *et al*[32] in 2010 (Figure I.8). The steps are described in Figure I.8a: the dibrominated monomer was deposited on the metal surface through vacuum sublimation, and annealed at 200 ℃ to generate the dehalogenated intermediates through surface-catalyzed carbon-halogen bond cleavage, which diffused along the surface and formed the carbon-carbon (C-C) bonds between each monomer to give the precursor polymer chains. Subsequently, the polyphenylene precursors were graphitized through the surface-assisted cyclodehydrogenation at higher annealing temperature

400 ℃ to result in the GNRs whose lateral width and edge structure are precisely controlled. By using two different monomers 10,10'-dibromo-9,9'-bianthryl and 6,11-dibromo-1,2,3,4-tetraphenyltriphenylene, *N* = 7 armchair GNR and chevron-type GNR were obtained (Figure I.8b). Insitu high-resolution scanning tunnelling microscopy (STM) visualization and X-ray photoelectron spectroscopy (XPS) analysis confirmed the successful synthesis of the GNRs.

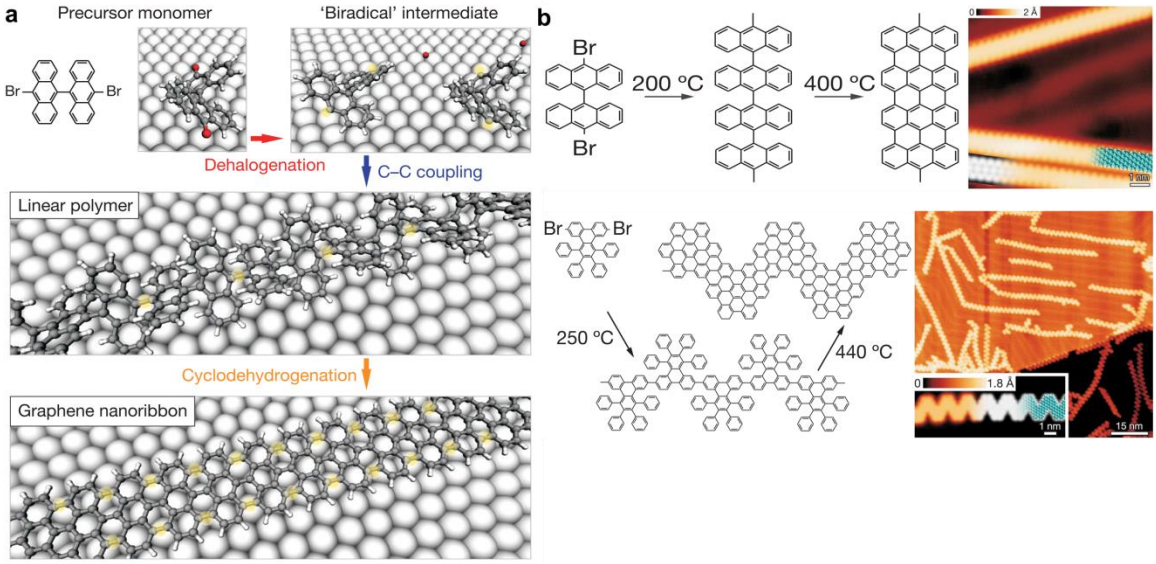

Figure I.8. a) Schematic illustration of the steps for surface-assisted synthesis of GNRs. b) Reaction schemes for *N* = 7 armchair GNR and chevron-type GNR, as well as their STM images. Reproduced from Ref. [32].

In 2013, a wider *N* = 13 armchair GNR was reported by Crommie's group.[51] As is shown in Figure I.9a, from an extended dibrominated monomer, laterally extended *N* = 13 armchair GNR could be synthesized by the surface-assisted approach. Notably, the extended *N* = 13 armchair GNR have a bandgap of 1.4 eV, which is about 1.0 eV lower than the bandgap for *N* = 7 armchair GNR (2.3 eV), indicating the engineering of electronic properties. Moreover, except for the modifications of width and edge structures, the tuning of the electronic structures of GNRs can be achieved by heteroatom doping, including N,[52-55] B,[56,57] and S.[58] For example, chevron-type N-doped GNRs with different degrees of N-doping were synthesized by using

two different N-doped monomers (Figure I.9b-c).[52,53,55] Both theoretical and experimental results showed that the N-doping lowered the electronic energy levels of the GNRs while the bandgap remains unaffected. The energy levels change precisely according to the degree of N-doping, indicating that by controlling the heteroatoms doping, the electronic structures of GNRs can be precisely tuned.

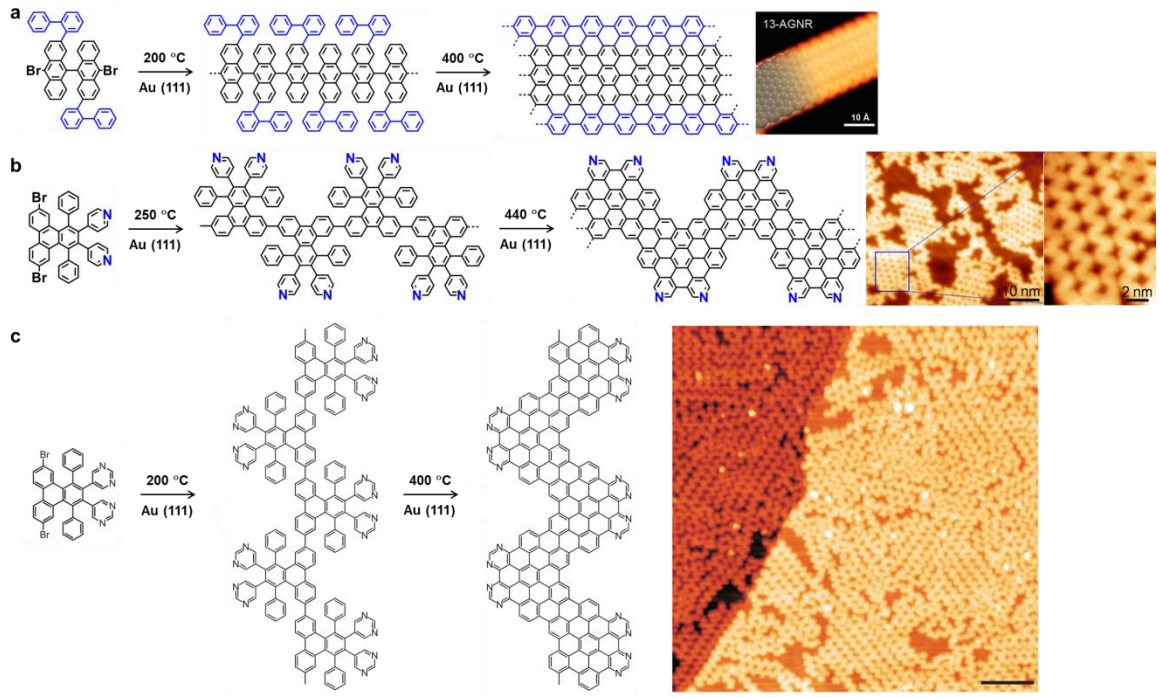

Figure I.9. a) Surface-assisted synthesis of laterally extended N = 13 armchair GNR and its STM image. Reproduced from Ref. [51]. b, c) Surface-assisted synthsis of N-doped GNRs and their STM images. Reproduced from Ref. [52, 53, 55].

The surface-assisted approach enables the synthesis of atomically precise GNRs with different widths, edge structures, and heteroatoms doping. The structures of the GNRs can be clearly characterized using the insitu high-resolution STM. However, the surface-assisted approach requires a very complicated fabrication process, the yield is low, and the obtained GNRs are all bound to the metal surfaces, making it hard to transfer them onto other dielectric substrates for further studies on their electronic properties and hindering their practical application in electronic devices.

Solution-mediated approach

The solution-mediated approach enables the large-scale synthesis of structurally well-defined GNRs, and it also enables the introduction of alkyl chains at the peripheral positions to prevent the π-π stacking aggregation between each ribbon and allow for their liquid-phase processability. Polyphenylene precursors are prepared from precisely designed monomers through a variety of polymerization reactions like Suzuki polymerization, Yamamoto polymerization, and Diels-Alder polymerization, followed by the graphitization or planarization by oxidative cyclodehydrogenation (the Scholl reaction) to obtain GNRs with precisely controlled structures, increased solubility and heteroatoms doping.

In 2008, Müllen and co-workers first reported the solution-mediated synthesis of linear, 2D *N* = 9 armchair GNRs via the Suzuki polymerization followed by the Scholl reaction (Figure I.10).[59] With dimethyl-octyl on the edges, the as-obtained GNRs possess improved solubility, and thus allowing for liquid-phase processing and STM analysis. The STM analysis indicated that the length of the GNRs was only up to 12 nm. The reason for obtaining such short GNRs is the low degree of polymerization due to the high steric hindrance between the two monomers, as well as the high rigid polyphenylene backbone structure.

In order to obtain the longitudinally extended GNRs, the more efficient AA-type Yamamoto polymerization was employed to synthesize high molecular weight polyphenylene precursors. In 2012, Müllen *et al*[60] reported the synthesis of laterally and longitudinally extended GNRs on the polyphenylene precursor synthesized by AA-type Yamamoto polymerization (Figure I.11). By the high efficient AA-type Yamamoto polymerization, a polyphenylene precursor with a number-average molecular weight ($\overline{Mn}$) of 44 000 g mol^{-1} was obtained, clearly higher molecular weight values obtained compared to the A_2B_2-type Suzuki polymerization. The obtained laterally extended GNRs possesses a lateral width of 1.54-1.98 nm with broad absorption extended to near-infrared (NIR) region and an optical bandgap as low as ~ 1.12 eV. The low bandgap GNRs have been successfully employed in optoelectronic devices, like

organic photovoltaics, as electron donor materials.[61] Later in 2014, an even wider N = 18 armchair GNRs with a lateral width of ~ 2.1 nm was reported by Müllen, Samori *et al* (Figure I.11).[62] They blended it with poly(3-hexylthiophene) (P3HT) and fabricated the thin-film organic field-effect transistors (OFETs). They fabricated devices with various GNRs loading ratios, and notably, the device with 24% GNRs exhibited a large field-effect mobility (7.3×10^3 cm^2 V^{-1} s^{-1}), which is four-fold higher than pure P3HT. What's more, the photoresponse of the transistors were measured to investigate the potential application of these OFETs in optoelectronics and they found the photoresponse of the GNRs-P3HT transistors was two-fold higher than that of the pure P3HT transistor. These results indicate that the performance of the device is enhanced in the presence of GNRs and this suggests the potential application of GNRs in the optoelectronic devices.

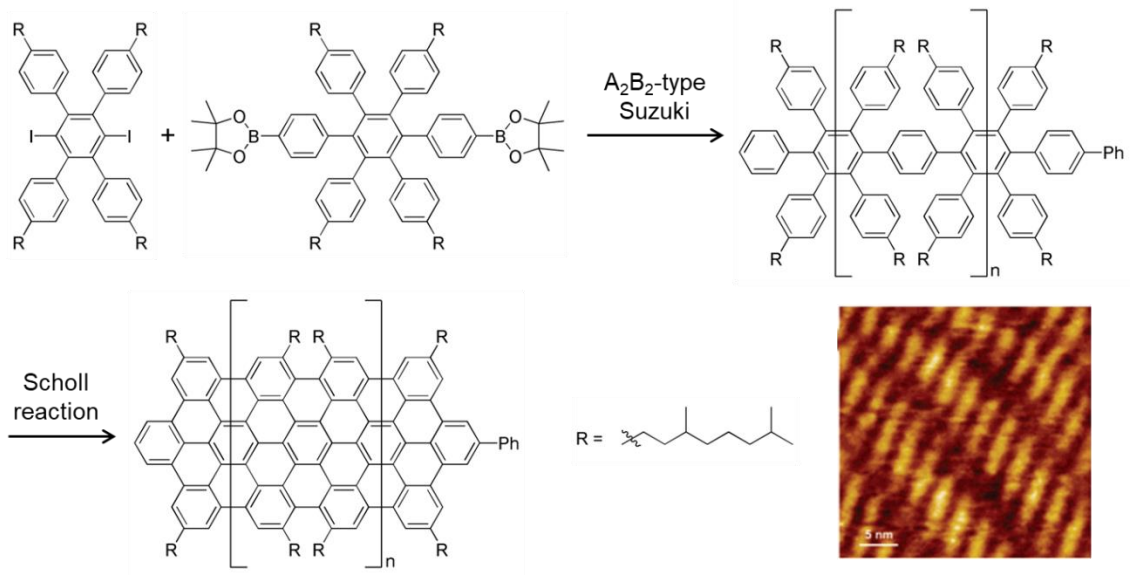

Figure I.10. Solution-mediated synthesis of N = 9 armchair GNRs through A_2B_2-type Suzuki polymerization and its STM image. Reproduced from Ref. [59].

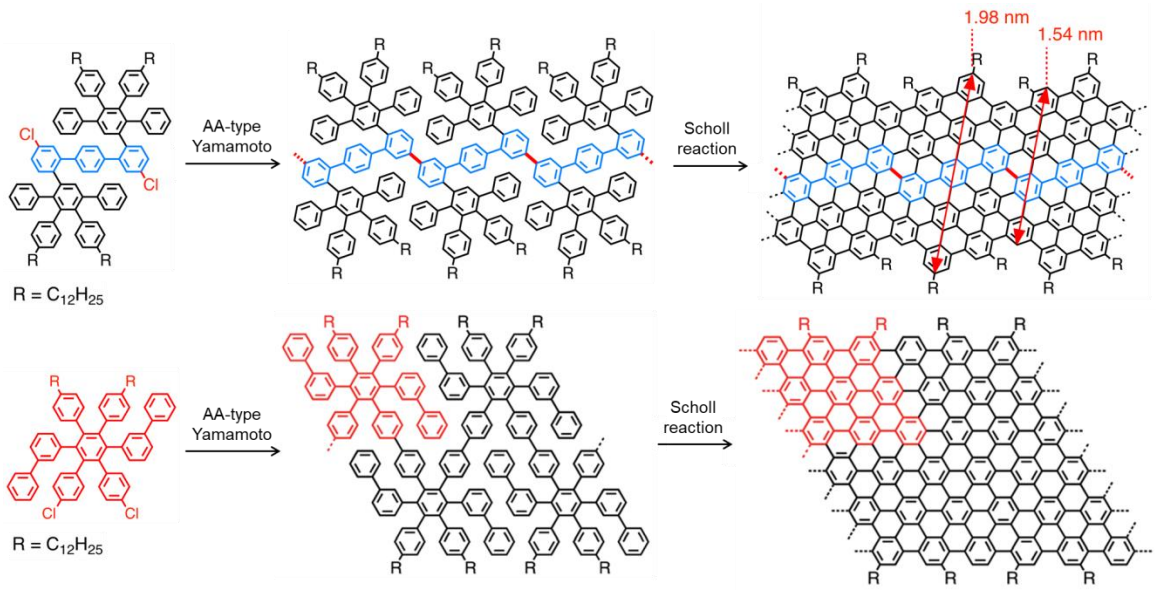

Figure I.11. Solution-mediated synthesis of laterally extended GNRs through AA-type Yamamoto polymerization. Reproduced from Ref. [60, 62].

As described above, laterally extended GNRs could be successfully synthesized through the AA-type Yamamoto polymerization. However, the obtained GNRs were shorter than 50 nm, which is not long enough for the fabrication of single-GNR-based FETs devices. Thus, developing a method for the synthesis of longitudinally extended GNRs with length > 100 nm is highly required. In 2014, Müllen and co-workers[63] first reported the synthesis of a "cove"-type GNRs through the AB-type Diels-Alder polymerization, with lateral width of 0.69-1.13 nm and length over 600 nm (Figure I.12). Mischa Bonn's group applied non-contact, ultrafast terahertz (THz) photoconductivity analysis and found the GNRs had an excellent intrinsic mobility.[64] Later, Chongwu Zhou's group[65] successfully deposited the GNRs on the SiO_2 surface and fabricated single-GNR-based transistors, which confirmed the semiconducting property of the GNRs and demonstrated the potential application value of chemically synthesized GNRs in the future electronic devices and sensors. The laterally extended GNRs were obtained later with broad absorption into the NIR region and a lowered optical bandgap of ~ 1.2 eV.[66] THz photoconductivity measurements showed it possessed excellent intrinsic

mobility, similar as the above narrower GNRs.[64]

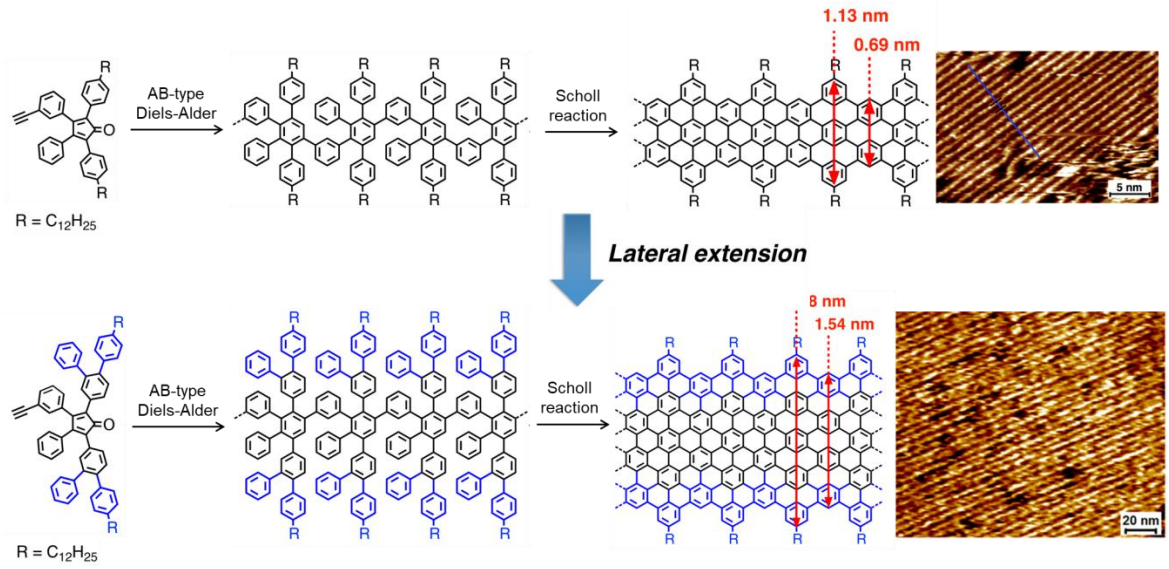

Figure I.12. Solution-mediated synthesis of laterally and longitudinally extended GNRs through AB-type Diels-Alder polymerization. Reproduced from Ref. [63, 66].

In addition to controlling the lateral width and edge structure, heteroatoms doping is also an efficient method to modulate the electronic properties of GNRs. Jo *et al*[67] synthesized the N-doped GNRs with different degrees of N-doping (Figure I.13). They found that with increasing the degree of N-doping, the hole mobility of the GNRs decreased while the electron mobility increased. The electron mobility of the GNRs with the highest degree of N-doping is 0.102 $cm^2 V^{-1} s^{-1}$, which is two orders of magnitude higher than that of non-doped GNRs. These results indicate that by N-doping the charge-transport behavior of the GNRs could be changed from ambipolar to n-type semiconductor.

Scholl reaction

The last and most important step in the "bottom-up" approach is the graphitization of polyphenylene precursors into GNRs. The most widely used method is the intramolecular oxidative cyclodehydrogenation reaction, which is known as Scholl reaction. Pioneered by Müllen and co-workers, various GNRs with different length, width, edge structures, as well as

heteroatoms doping have been synthesized by Scholl reaction.[68-70] The obtained GNRs were successfully employed in electronic devices, like photovoltaics and field-effect transistors. However, the Scholl reaction also possesses some drawbacks, like incomplete graphitization, low regioselectivity, undesired rearrangements and incompatibility with electron-rich functional groups.

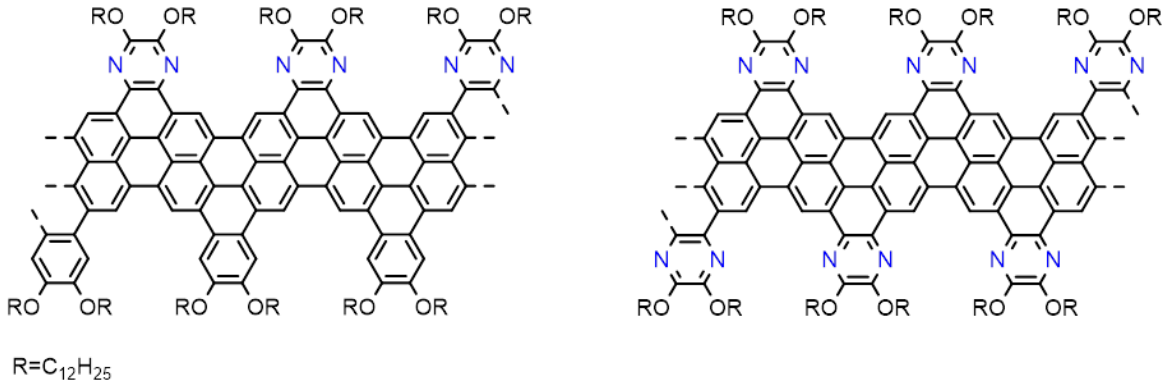

Figure I.13. Solution-mediated synthesis of N-doped GNRs through A_2B_2-type Suzuki polymerization. Reproduced from Ref. [67].

Müllen *et al*[71,72] reported that when applying the Scholl reaction, the starting material could be partially cyclized because of the incomplete reactions, and the use of metal chlorides ($FeCl_3$, $AlCl_3$) could create hydrochloric acids, thus generating chlorinated byproducts. Another drawback of the Scholl reaction is the poor regioselectivity of cyclization,[73-79] which will generate structurally undefined GNRs. For example, Durola and co-workers[78] reported the unexpected regioselectivity of intramolecular Scholl reactions on pentaphenylene compounds (Figure I.14). When applying the Scholl reaction on tetrasubstituted quinquephenyl, the highly congested helicenic isomer tetrabenzanthracene was formed predominantly in 80 % yield, while the flat counterpart dibenzo[5]helicene was obtained in only 8 % yield. In 2016, Israel Agranat's group[74] reported the intramolecular Scholl reaction of 1-benzoylpyrene and found the poor regioselectivity of Scholl reaction generates the formation of 42% five-member ring product and 21% six-member ring compound. The Scholl reaction also suffers from undesired

rearrangements,[80-84] which interfere with the construction of certain architectures. For example, in 2008 King *et al*[81] reported the Scholl reaction of 3,3',4,4'-tetramethoxybiphenyl. Because of the skeletal rearrangements involved by the phenyl shift, the oxidation occurred on the rearranged skeleton and an unexpected isomer was obtained, while the expected product was not formed (as is shown in Figure I.15). This indicates that the rearrangements in the Scholl reaction will affect the construction of a particular structure.

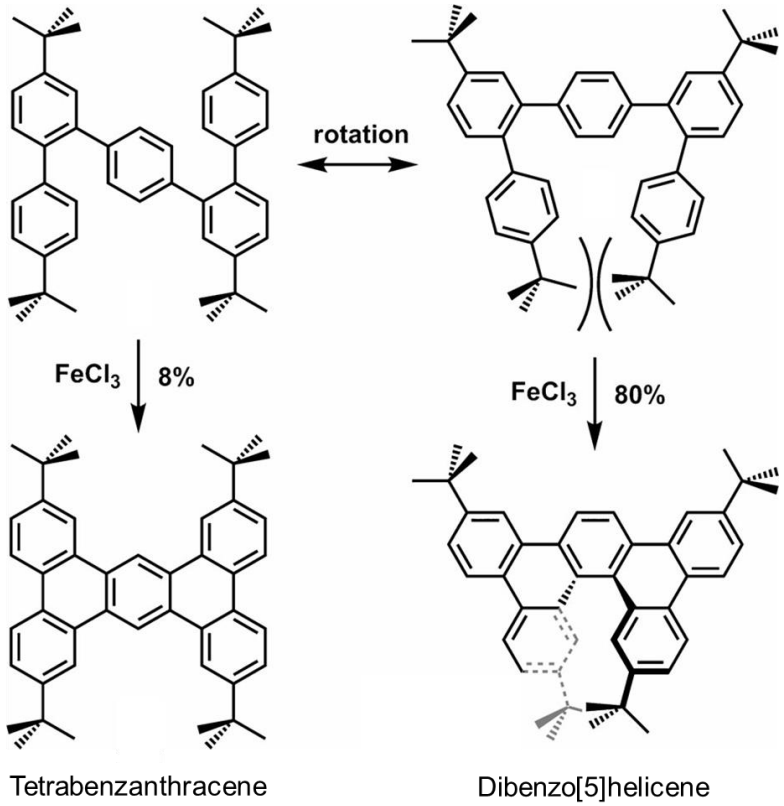

Figure I.14. Unexpected regioselectivity of an intramolecular Scholl reaction that leads to the formation of highly congested [5]helicenes. Reproduced from Ref. [78].

In addition, the harsh reaction conditions (Lewis acids, protic acids) make it hard for the introduction of oxidant-sensitive functional groups and electron-rich heterocycles, thus limiting the scope and versatility of the Scholl reaction. Therefore, only electron-poor and chemically robust pyridine, pyrimidine, naphthalene monoimide, and perylene monoimide moieties can be used as edge units to modulate the electronic properties of GNRs.[52,85,86] Thus, a milder method

to prepare GNRs that will allow the introduction of a large variety of functional groups and heterocycles, both electron-poor and electron-rich, is thus highly desirable.[87,88]

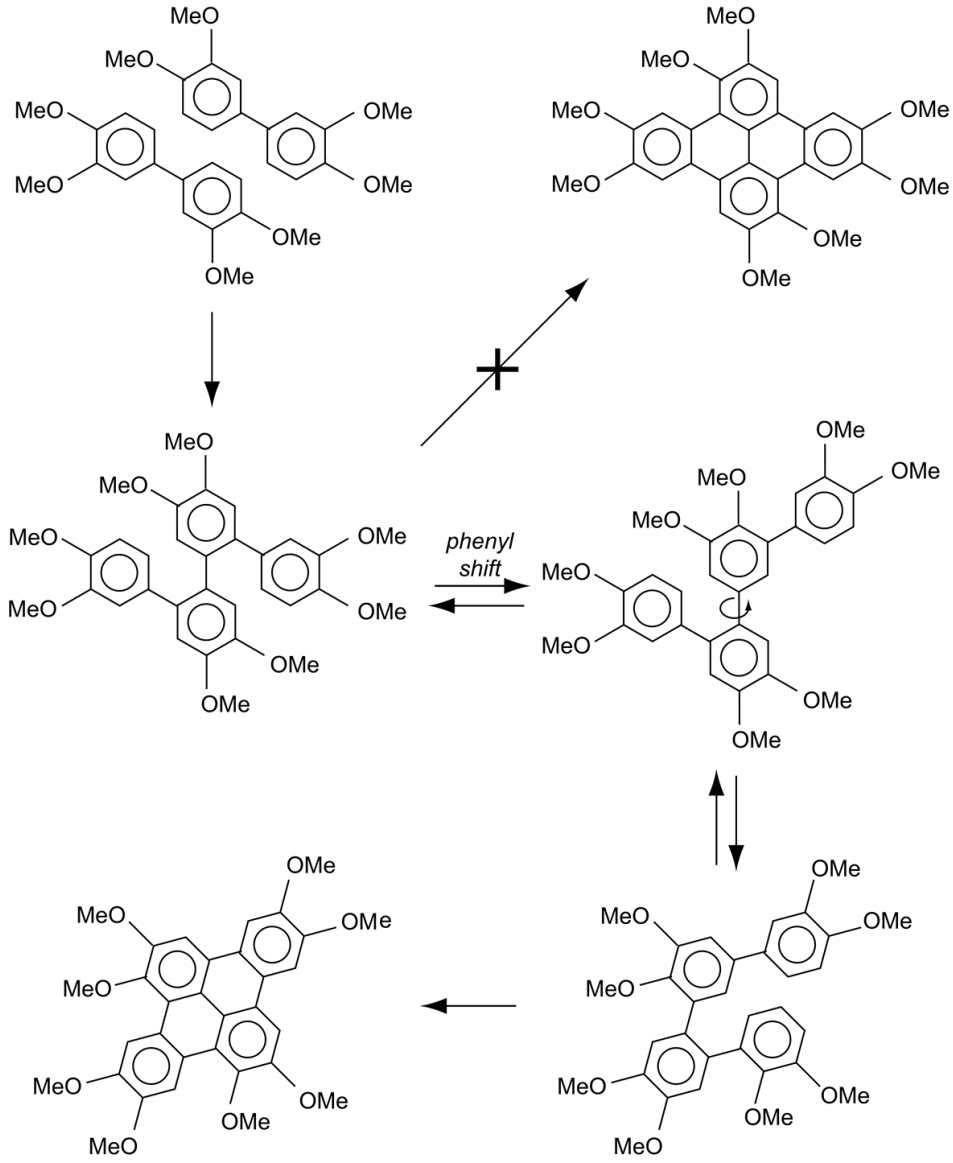

Figure I.15. Scholl reaction of 3,3',4,4'-tetramethoxybiphenyl. Reproduced from Ref. [81].

Synthesis of GNRs through alkyne benzannulation

In order to circumvent some of the drawbacks of the Scholl reaction, other methods with non-oxidative and relatively mild reaction conditions have been employed to synthesize GNRs,

like alkyne benzannulation.[89-94] Alkyne benzannulation reactions can proceed by using electrophilic reagents,[95-97] Brønsted acids,[98-101] π-Lewis acids,[102-106] and radical reagents.[107,108] A variety of nanographenes (NGs) and pyrenacenes (pyrene, peropyrene, teropyrene, etc., which can be viewed as GNR oligomers) have been successfully synthesized based on alkyne benzannulation. In 1994, Swager and co-workers[90] reported the synthesis of a very narrow GNRs with increased solubility by a Brønsted acid (trifluoroacetic acid, TFA) catalyzed alkyne benzannulation (Figure I.16). This strategy enables the introduction of alkyl substitution (R) to increase the solubility and the obtained GNRs possesses a high molecular weight of $\overline{Mn}$ = 45 000-55 000 g mol^{-1}. Later, Wu, Zhao *et al*[91] synthesized more conjugated and planar pyrene-based GNRs using a similar method (Figure I.16).

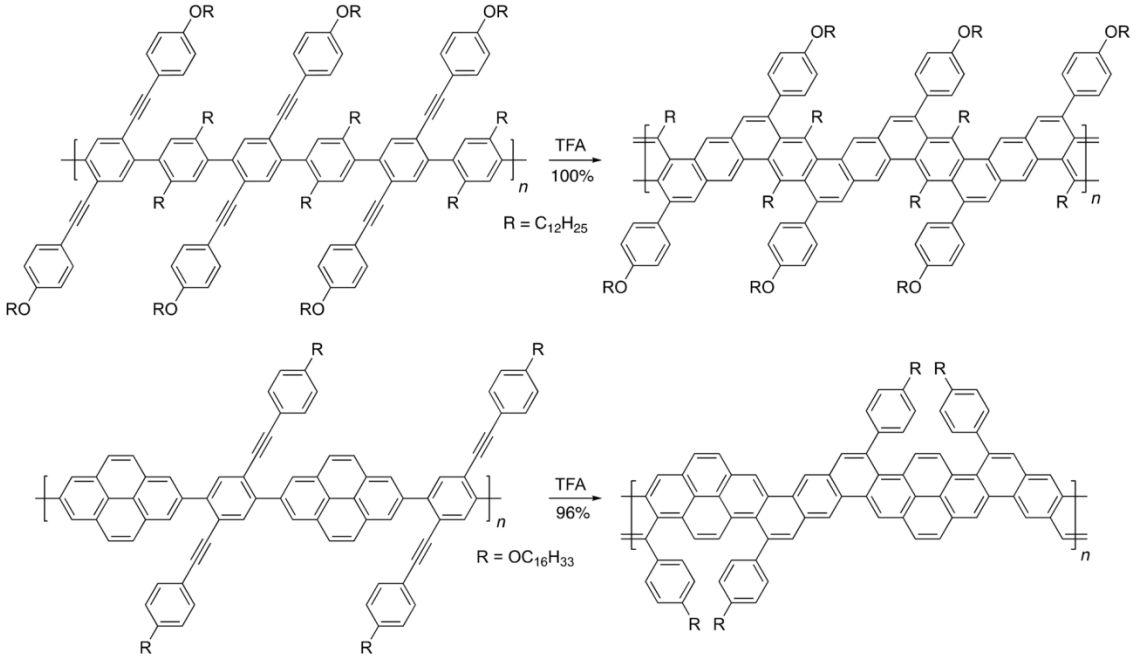

Figure I.16. Synthesis of GNRs by alkyne benzannulation. Reproduced from Ref. [90, 91].

Chalifoux's group reported the synthesis of a series of pyrene, peropyrene, and teropyrene derivatives through the alkyne benzannulation promoted by Brønsted acids.[109] Since the electron-rich ethynyl aryl groups are tolerant to the reaction conditions, they thought the ethynyl thiophene moieties would also be tolerant to Brønsted acid condition and undergo

facile benzannulation. Interestingly, thiophene-functionalized pyrene, peropyrene, and teropyrene derivatives were successfully synthesized through the alkyne benzannulation promoted by a stronger Brønsted acid triflic acid (TfOH) (Figure I.17). The introduction of electron-donating thiophene substituents is very interesting for the p-type semiconducting materials. The obtained pyrenes, peropyrenes, and teropyrenes showed good solubility in many commonly used organic solvents, which enabled the characterization of their physical properties. Their interesting photophysical properties make them very promising materials for optoelectronic devices.

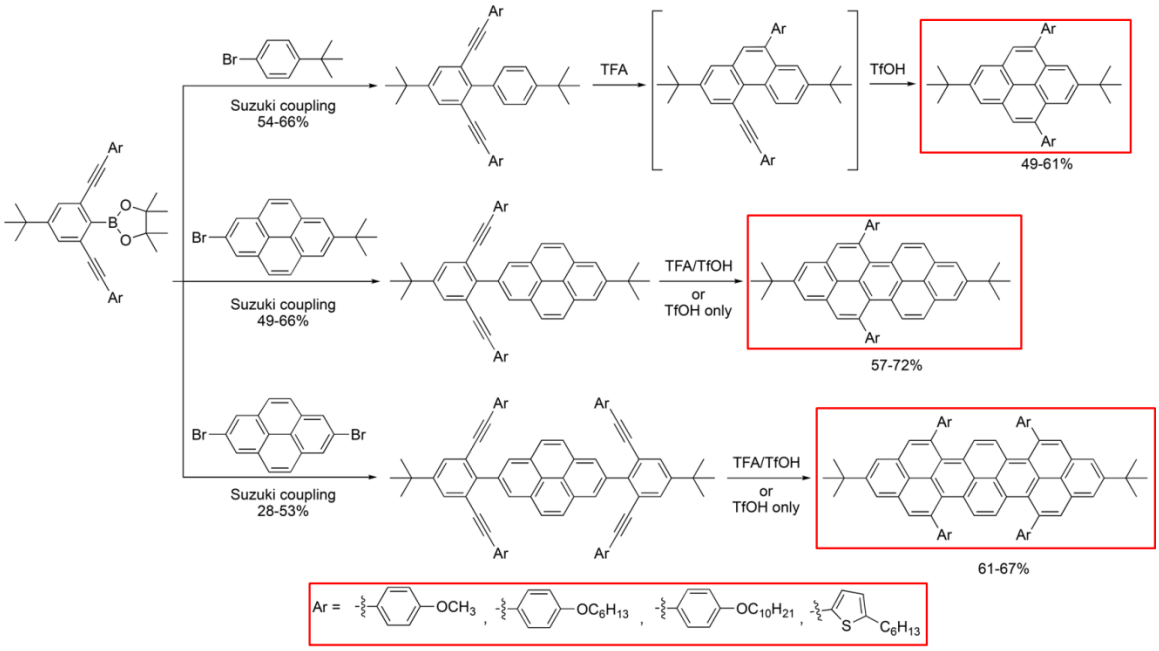

Figure I.17. Synthesis of pyrene, peropyrene, and teropyrene derivatives through two-fold and four-fold alkyne benzannulation promoted by Brønsted acids. Reproduced from Ref. [109].

The pyrene, peropyrene, and teropyrene derivatives can be viewed as armchair GNRs oligomers. Their successful synthesis through alkyne benzannulation exemplifies the application of this method for the preparation of GNRs. Chalifoux and co-workers[92] reported the synthesis of soluble and narrow GNRs through Brønsted acid-promoted alkyne benzannulation (Figure I.18).

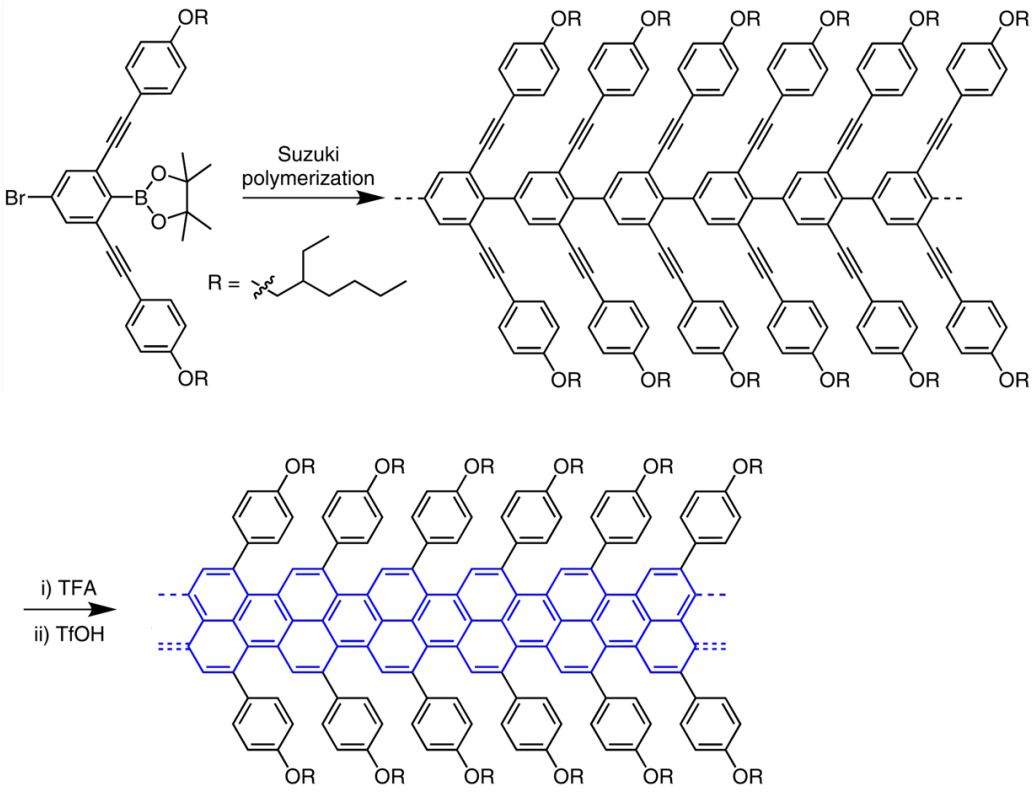

Figure I.18. Synthesis of GNRs through alkyne benzannulation promoted by Brønsted acids. Reproduced from Ref. [92].

The alkyne benzannulation employs non-oxidative and relatively milder reaction conditions than the Scholl reaction and has proven to be useful in synthesizing a variety of NGs, pyrenacenes, as well as GNRs. However, the electron-rich ethynyl aryl groups are necessary for the 6-*endo-dig* cyclization, which makes it hard to modulate the electronic and optical properties through the substituent effects.

Synthesis of GNRs through thermal polydiacetylene aromatization

Rubin *et al*[110,111] reported the bottom-up synthesis of GNRs through the thermal polydiacetylene aromatization. The approach contains two steps : first a butadiyne-containing monomer undergoes crystalline-state topchemical polymerization to form the polydiacetylenes (PDAs), then the PDAs undergoes a solid-state thermal aromatization under argon or vacuum

atmosphere without the need for additional reagents (as is shown in Figure I.19).

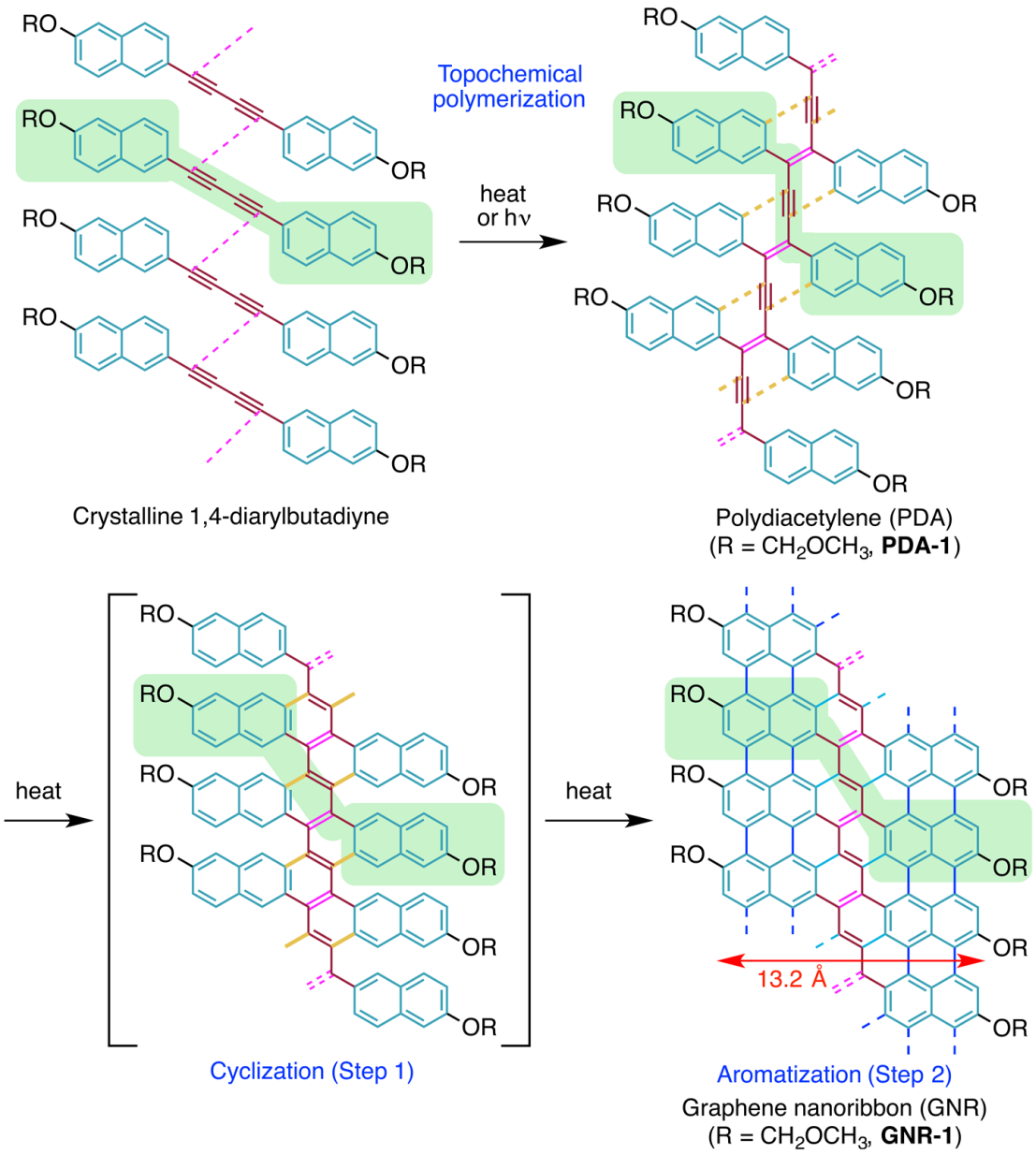

Figure I.19. Bottom-up synthesis of GNRs through thermal polydiacetylene aromatization. Reproduced from Ref. [111].

Both the alkyne benzannulation and the thermal polydiacetylene aromatization possess milder reaction conditions than the Scholl reaction and avoid some of the drawbacks of the Scholl reaction. A variety of GNRs with various widths and edge structures have been prepared by

these methods, however only all-phenyl GNRs have been prepared by these methods.

Mallory reaction

Besides the Scholl reaction, photocyclization can also be used to create a sp^2 carbon atoms network, such as the Mallory photocyclization reaction (as is shown in Figure I.20). Unlike the harsh conditions employed in the Scholl reaction, the photochemical reaction doesn't need metal-catalyst, or acids, and can be regarded as one of the greenest synthetic approaches. The Mallory photocyclization reaction (also called photochemical intramolecular oxidative dehydrogenation) has proven to be an efficient photochemical method for the synthesis of carbon nanomaterials, polycyclic aromatic hydrocarbons (PAHs), and heteroaromatics.[112-114]

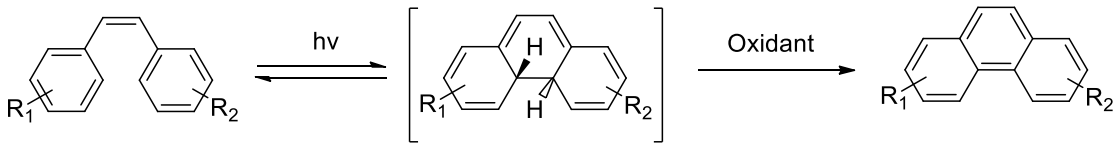

Figure I.20. Reaction process of Mallory photocyclization reaction. Reproduced from Ref. [112].

A variety of extended perylene diimides (PDIs),[115-117] N-heteroarenes,[118] as well as cove-edge GNRs[119] and helical GNRs[120] have been synthesized by the Mallory photocyclization reaction. As is shown in Figure I.21, Nuckolls, Zhu and Miyata *et al*[119] synthesized long (~ 5 nm), atomically precise and soluble GNRs, with the alternating electron deficient perylene diimides and electron rich alkoxy pyrene subunit, the donor-acceptor GNRs absorb at very long wavelength and can be used as electron-acceptor in highly efficient organic photovoltaics (OPVs).

However, one of the major shortcomings of the Mallory reaction is the use of an oxidant (I_2, O_2). The use of the oxidant often leads to side reactions, which will decrease the product yield and purity.[121,122]

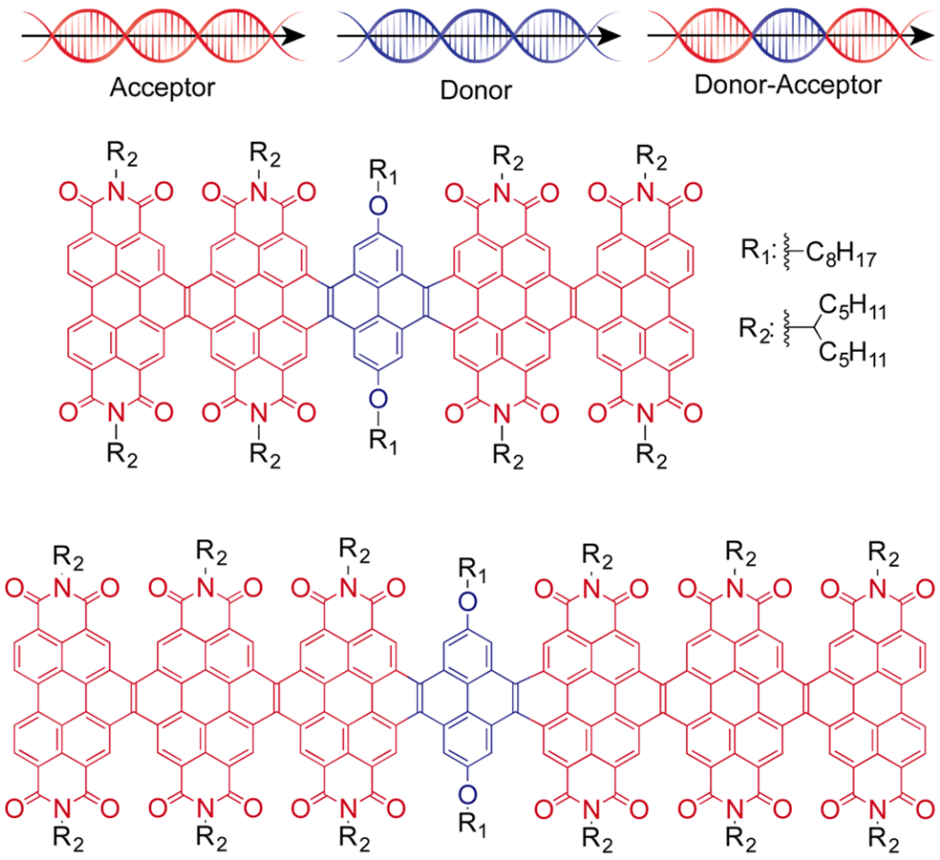

Figure I.21. Two donor-acceptor cove-edge GNRs. Reproduced from Ref. [119].

Photochemical cyclodehydrochlorination (CDHC) reaction

To avoid using the oxidant, a similar reaction, the intramolecular photochemical cyclodehydrochlorination (CDHC) reaction was developed in 1970s.[123,124] Unlike the photochemical intramolecular oxidative dehydrogenation, in which the loss of H_2 is facilitated by the oxidant, the CDHC reaction achieves the formation of polycyclic aromatic hydrocarbons (PAHs) by the loss of HCl molecules without the use of an oxidant. The reaction process of the photochemical CDHC reaction is shown in Figure I.22.

However, very few reports mention using the CDHC reaction for the synthesis of PAHs, probably due to the dominant position of the Scholl reaction in the synthesis of PAHs. Recently, Hartley *et al*[84,125] reported the synthesis of dibenzo[*fg*,*op*]naphthacenes with liquid crystalline

properties through the planarization of *o*-phenylene tetramers (Figure I.23) using the photochemical CDHC reaction. It is known that the *o*-phenylenes always undergo backbone rearrangements under the Scholl reaction for planarization, while skeletal rearrangements have been overcome by using the photochemical CDHC reaction on chlorinated *o*-phenylene tetramers precursor), as is shown in Figure I.23.

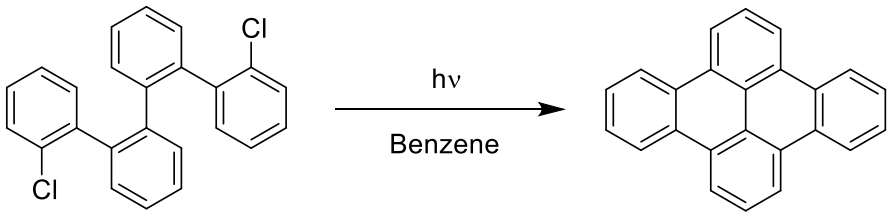

Figure I.22. Diagram of the photochemical CDHC reaction process. Reproduced from Ref. [123].

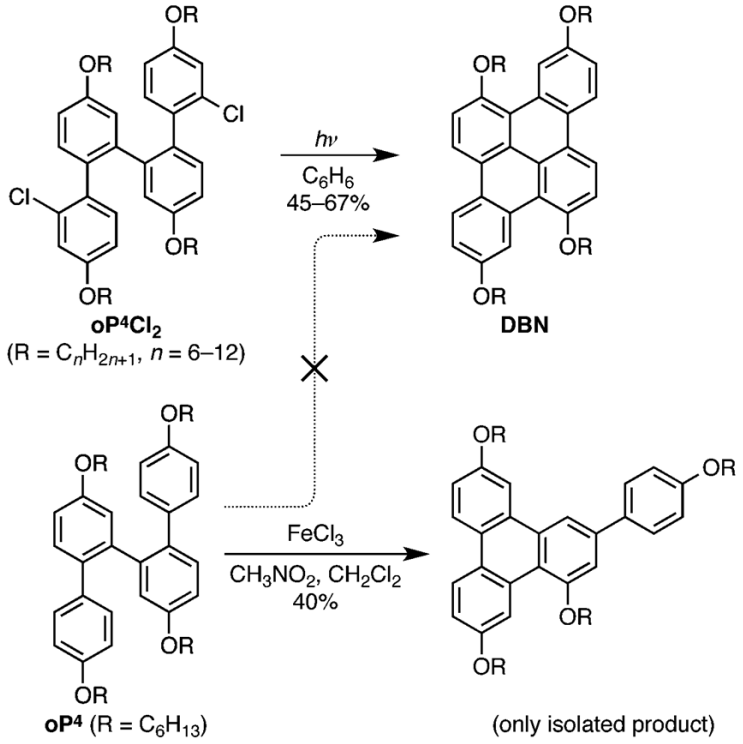

Figure I.23. Planarization of *o*-phenylene tetramers by photochemical CDHC reaction (top) and Scholl reaction (bottom). Reproduced from Ref. [84].

Zhang *et al*[126] reported the photocyclization of 2-chloro-*N*- (ω-arylalkyl)-3-acylindoles to afford π-expanded heterocycles using the photochemical CDHC reaction. A series of phenanthro[9,10-*d*]imidazoles containing electron-donating and electron-withdrawing substituents and various heterocyclic units were successfully converted into π-expanded heterocycles by the photochemical CDHC reaction.[127-129] Bath *et al*[130] employed the photochemical CDHC reaction to prepare phenanthro[9,10-*c*]thiophenes. These results indicate that the photochemical CDHC reaction can be performed on molecules containing heterocycles, and both electron-rich and electron-poor substituents are tolerated to the CDHC reaction. Figure I.24 shows the several heterocycles synthesized by the photochemical CDHC reaction.

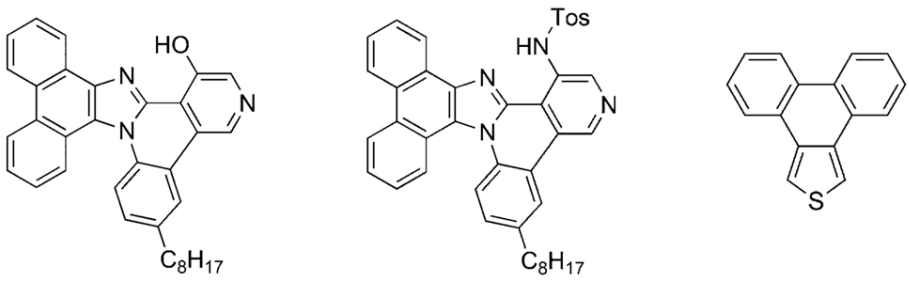

Figure I.24. Several heterocycles structures synthesized by photochemical CDHC reaction. Reproduced from Ref. [127, 130].

The photochemical CDHC reaction is really attractive for synthesizing carbon nanomaterials (NGs, GNRs) for several reasons. First, it is regioselective, meaning that it won't result in structural isomers like the Scholl reaction, which guarantees the purity of the obtained GNRs. Second, it proceeds without rearrangement, meaning that well-defined structures that are not accessible with the Scholl reaction can be obtained with the photochemical CDHC reaction. Moreover, the mild reaction conditions (absence of metal catalyst and oxidant) enable the introduction of various functional groups, both electron-rich and electron-poor heterocycles, onto the GNRs to further modulate their structural and electronic properties. In addition, it possesses a better control over the edge structures of NGs and GNRs than the Scholl reaction.

Inspired by the many advantages of the photochemical CDHC reaction and the successful

results in the synthesis of various PAHs by this reaction, our group has successfully synthesized larger and more complicated NGs using this reaction (Figure I.25).[131] As is shown in Figure I.25, a carefully designed chlorinated precursor with chlorine atoms at the specific positions was prepared firstly, and subsequently the chlorinated precursor was irradiated in a solution under ultraviolet (UV) light to achieve the full aromatization. For most of reactions, the yields are relatively high, and the reaction proceeds cleanly with the desired product precipitating from the solution in a pure form. Moreover, we demonstrated the regioselectivity, high efficiency (usefulness in multiple cyclization processes and successful synthesis of sterically hindered, contorted NGs), and better edge configuration control of the CDHC reaction. Most importantly, the versatility of the CDHC reaction was demonstrated by the successful synthesis of both electron-rich (thiophene) and electron-poor (pyridine) substituents fused NGs, meaning that the CDHC reaction is compatible with various heterocycles.

Inspired by these excellent results in synthesizing NGs, we focused on using the CDHC reaction to synthesize GNRs with good solubility, well-defined lateral width and edge structures. In 2017, we reported the first well-defined, helically coiled GNRs synthesized from a polychlorinated polyphenylenes precursor by the photochemical CDHC reaction (Figure I.26).[132] The structures of the obtained GNRs were confirmed by ^{1}H NMR, FT-IR, XPS, TEM, and Raman spectroscopy. The electronic and optical properties of the GNRs were carefully characterized by UV-vis absorption and photoluminescence analysis. The successful synthesis of the GNRs demonstrated the regioselectivity and high efficiency of the photochemical CDHC reaction and enabled us to study further the CDHC reaction in synthesizing a variety of GNRs with various width, edge structures, and heteroatoms doping.

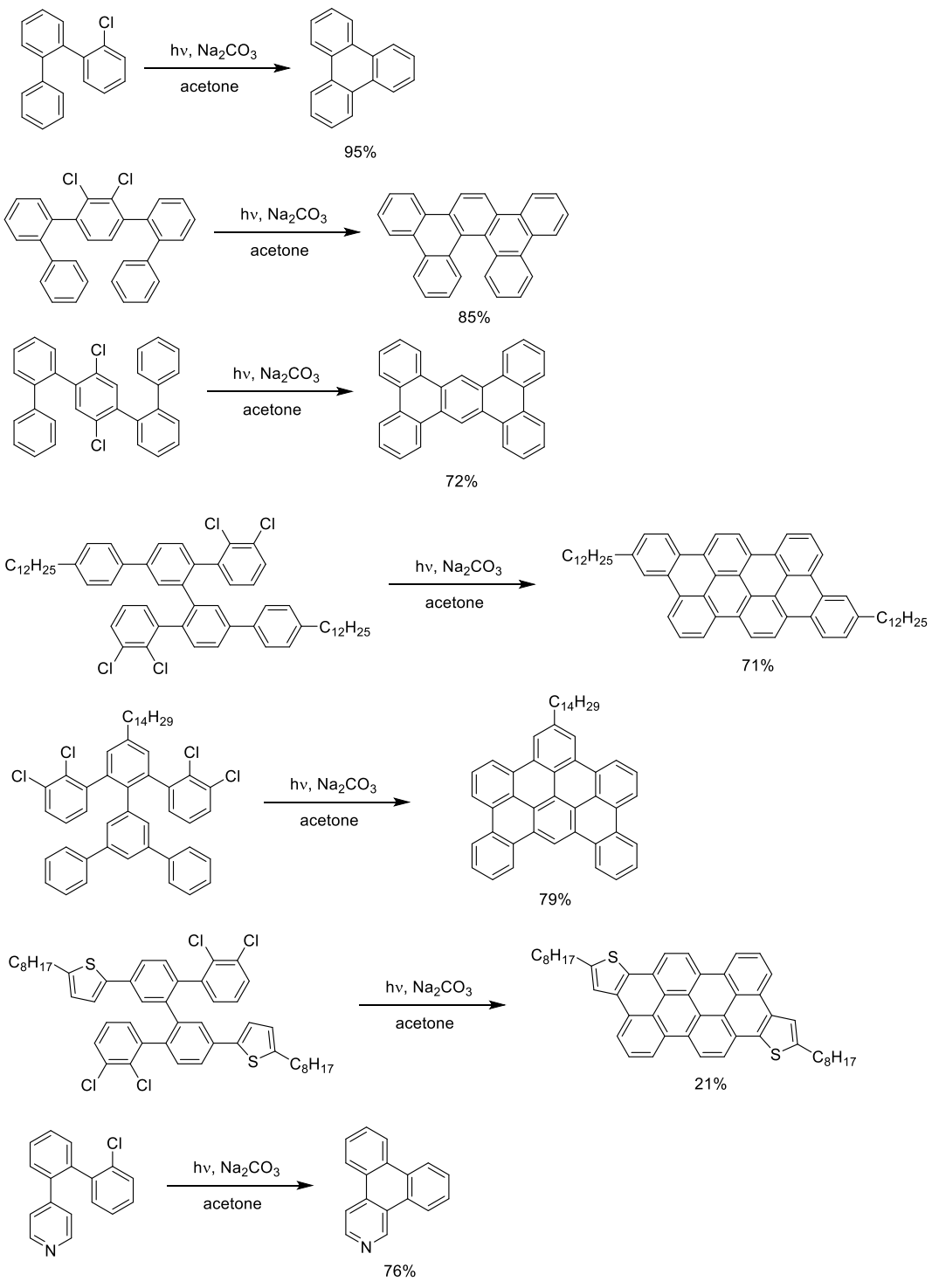

Figure I.25. Synthesis of NGs using the photochemical CDHC reaction. Reproduced from Ref. [131].

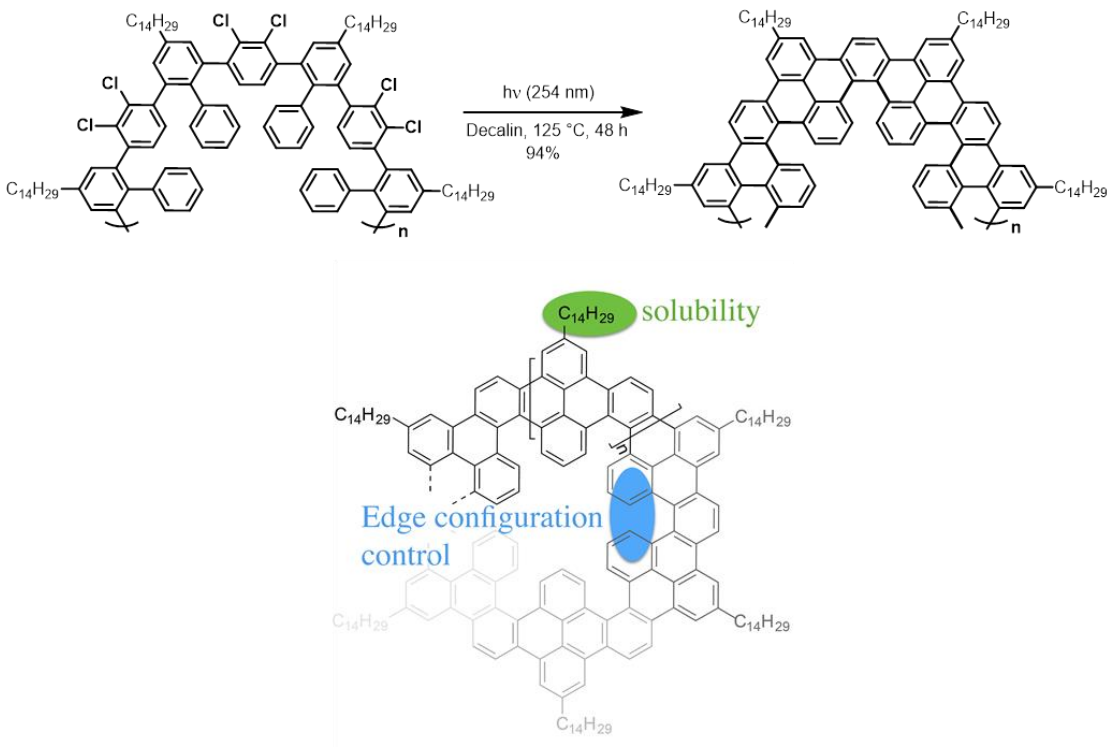

Figure I.26. Synthesis of helically coiled GNRs using the photochemical CDHC reaction. Reproduced from Ref. [132].

Motivation and objectives

As described above in section 1.2, “top-down” methods proved to be useful in preparing GNRs which exhibited excellent semiconducting properties with high on-off ratio and high mobility, while these methods lack control on the lateral width and edge structure, which strongly affect their electronic properties and hinders their practical applications in electronic devices. In contrast, GNRs with well-defined structures, narrow lateral width (sub-5 nm), as well as heteroatom doping can be fabricated by the “bottom-up” method based on surface-assisted and solution-mediated approach.

The surface-assisted approach enables the growth of atomically precise GNRs directly on the metal surfaces, and the structures of the GNRs can be clearly characterized using the in-situ high-resolution STM. However, it requires a very complicated fabrication process, the yield is low and the obtained GNRs are all bound to the metal surfaces. This makes it hard to transfer them onto other dielectric substrates for further studies on their electronic properties and hinders their practical application in electronic devices.

In contrast, the solution-mediated approach enables the large-scale synthesis of structurally well-defined GNRs, and it also enables the introduction of alkyl chains at the peripheral positions to increase the liquid-phase processability. It is one of the most promising strategies to prepare structurally well-defined GNRs with tunable optical and electronic properties. The most widely used method for the graphitization of polyphenylene precursors into GNRs is the intramolecular oxidative cyclodehydrogenation reaction, which is known as Scholl reaction. However, the Scholl reaction possesses some serious drawbacks that limit the scope and versatility of this reaction. First is its poor regioselectivity that results in structural defects to affect the properties of GNRs. Then, the undesired rearrangements and the use of a metal catalyst can lead to the formation of by-products. Moreover, the introduction of oxidant-sensitive functional groups and electron-rich heterocycles is difficult to achieve due to the harsh reaction conditions, which limit the diversity of structural and electronic properties of

GNRs.

In order to circumvent some of the drawbacks of the Scholl reaction, other methods with non-oxidative and relatively mild reaction conditions have been employed to synthesize GNRs, such as alkyne benzannulation and thermal polydiacetylene aromatization. However, only all-phenyl GNRs have been prepared by these methods, a milder method to prepare GNRs that will allow the introduction of a large variety of functional groups and heterocycles, both electron-poor and electron-rich, is thus highly desirable. Recently, our group reported the synthesis of nanographenes and GNRs using the photochemical cyclodehydrochlorination (CDHC) reaction on polychlorinated polyphenylene precursors. The CDHC reaction possesses high regioselectivity and it proceeds without rearrangements. Furthermore, the CDHC reaction is conducted without metal catalyst and oxidant under very mild conditions, thus enabling the introduction of different functional groups and heterocycles onto the GNRS to modulate their optoelectronic properties. And comparing with the Scholl reaction, the CDHC reaction provides better control over the edge configuration of the GNRs. This thesis investigates in detail the usefulness of the CDHC reaction for the preparation of a variety of GNRs with various width, edge structures, and heteroatoms doping, and carefully studies the structural and optoelectronic properties of the GNRs produced.

Regioselective synthesis of GNRs by photochemical CDHC reaction

First, in order to test the usefulness of the photochemical CDHC reaction in synthesizing GNRs, two polychlorinated polyphenylene precursors (as is shown in Figure I.27) have been designed. After applying the CDHC reaction on the two precursors, two narrow GNRs, both laterally symmetrical (GNR1) and unsymmetrical (GNR2) GNRs can be synthesized (Figure I.27). The structures of the obtained GNRs can be confirmed by ^{1}H NMR, FT-IR, and XPS analysis. The successful synthesis of these two structurally defined GNRs will demonstrate the regioselectivity, edge configuration control, and high efficiency of the photochemical CDHC reaction.

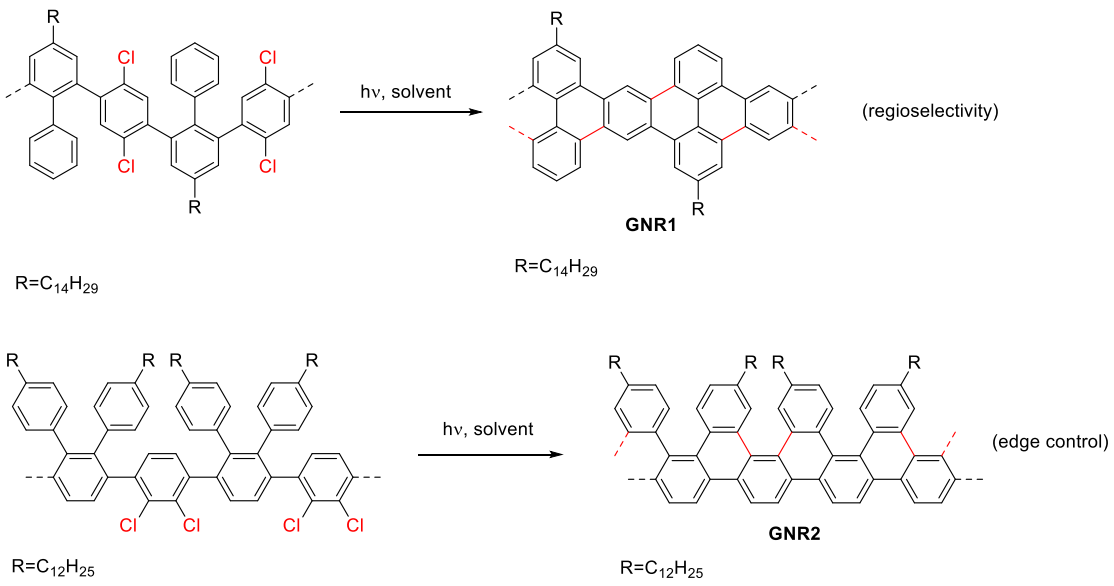

Figure I.27. Regioselective synthesis of GNR1 and GNR2 by the photochemical CDHC reaction.

Toward thiophene-annulated GNRs

Then, in order to test the versatility of the CDHC reaction, two narrow GNRs (*o*T-GNR and *p*T-GNR), both consisting in a "ladderized" poly(*p*-phenylene) polymer backbone (in blue, Figure I.28) annulated with [2,3]thiophene units have been designed. The successful introduction of electron-rich thiophene heterocycle into GNRs will demonstrate the versatility of the CDHC reaction, and the influence of the introduction of electron-rich functional groups on the structures and optoelectronic properties of GNRs can be carefully studied through a series of analytical methods.

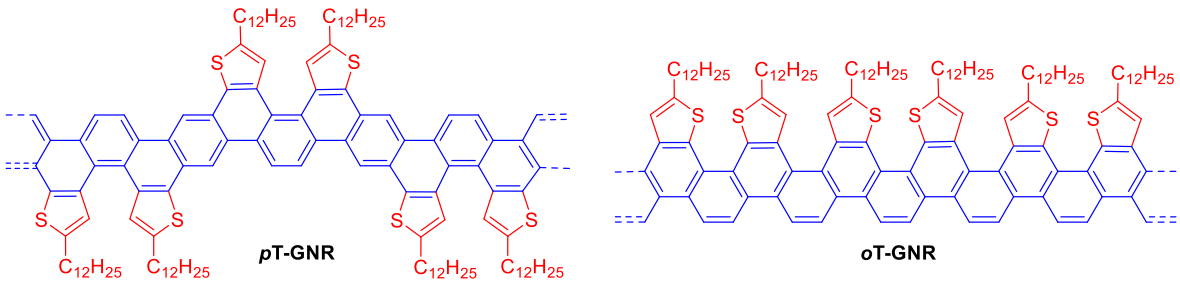

Figure I.28. Structures of *p*T-GNR and *o*T-GNR.

Photochemical synthesis of conjugated ladder polymers containing pyrrole units

As a second step, linear and helical conjugated ladder polymers (L-CLP and H-CLP) bearing electron-rich pyrrole units have been designed (Figure I.29). The successful synthesis will indicate the compatibility of the CDHC reaction with very electron-rich functional groups and the high efficiency of the CDHC reaction. The strong electron-donating properties of the pyrrole units in the polymer backbone make the polymer very electron-rich and lead to excellent optoelectronic properties. Promising applications can be explored on these polymers.

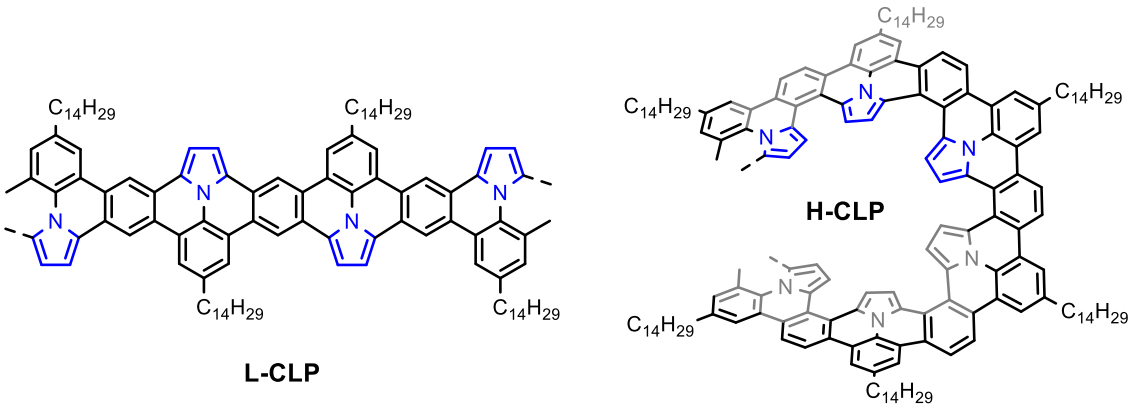

Figure I.29. Structures of the conjugated ladder polymers L-CLP and H-CLP.

Photochemical synthesis of π-extended ullazine derivatives as new electron donors for efficient conjugated D-A polymers

Finally, various π-extended ullazine derivatives annulated with either electron-poor pyridine or electron-rich thiophene units have been designed to further test the versatility and praticality of the photochemical CDHC reaction (Figure I.30). The strongest electron-donor derivative with one pyrrole and two thiophene rings will be copolymerized with three electron-deficient monomers to provide a series of conjugated donor-acceptor polymers (D-A CPs). Then, these polymers will be employed in the polymer solar cells to test their performances.

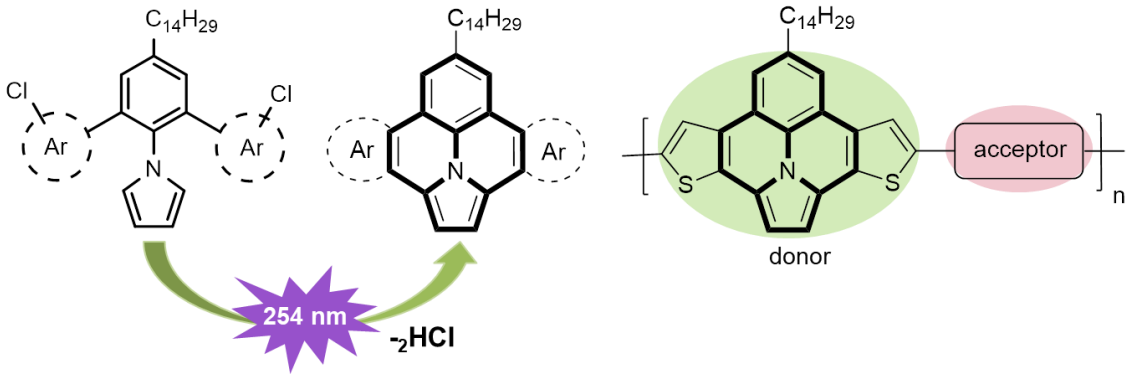

Figure I.30. Schematic illustration of the synthesis of ullazine derivatives through the CDHC reaction and the structure of the D-A CPs.

Chapter 1. **Regioselective Synthesis of Graphene Nanoribbons by Photochemical Cyclodehydrochlorination**

Dandan Miao[a] and Jean-François Morin*[a]

a) Département de Chimie et Centre de Recherche sur les Materiaux Avancés (CERMA), Université Laval, Pavillon A.-Vachon, 1045 Ave de la Médecine, Québec QC, Canada G1V 0A6

In preparation.

1.1. Résumé

De nouveaux nanorubans de graphène (GNR) ont été préparés à partir de précurseurs de polyphénylène polychlorés par la réaction de cyclodéhydrochloration photochimique (CDHC). La préparation réussie des GNR à symétrie latérale et asymétrique démontre la régiosélectivité, le contrôle des configuration de bord et l'efficacité de la réaction CDHC. La RMN ^{1}H, la FT-IR et le XPS ont confirmé les structures des GNR. Les propriétés optiques et électroniques des GNR ont été soigneusement étudiées par analyse UV-vis et par photoluminescence. Les GNR asymétriques latéralement et asymétriques ont une bande interdite de 3.10 eV et 2.70 eV, respectivement, les deux sont très émissifs dans la région visible.

1.2. Abstract

Novel graphene nanoribbons (GNRs) were prepared from polychlorinated polyphenylene precursors by the photochemical cyclodehydrochlorination (CDHC) reaction. The successful preparation of both laterally symmetrical and unsymmetrical GNRs demonstrates the regioselectivity, edge configuration control, and efficiency of the CDHC reaction. ^{1}H NMR, FT-IR, and XPS confirmed the structures of the GNRs. The optical and electronic properties of the GNRs were carefully studied by UV-vis and photoluminescence analysis. The laterally symmetrical and unsymmetrical GNRs has a bandgap of 3.10 eV and 2.70 eV, respectively, both are highly emissive in the visible region.

1.3. Introduction

Graphene can be considered as one of the most promising materials for electronic components due to its outstanding charge transport properties, high specific surface area, excellent thermal conductivity, and high mechanical strength.[2,133,134] However, the two dimensional graphene is a zero band gap semiconductor, which limits its practical application in electronic devices.[28,135,136] Many approaches have been developed to open the band gap,[137-140] one of the most promising

methods is the formation of graphene nanoribbons (GNRs) through quantum confinement at nanometer scale.[36,38] The band gap of GNRs can be precisely controlled by the width and edge configuration,[61,141,142] providing GNRs with tunable optical and electronic properties. Thus, it's crucial to find a synthetic method in which the structure of GNRs can be precisely controlled on the atomic scale.

Bottom-up, solution-phase synthesis is one of the most promising strategies to prepare structurally well-defined GNRs.[85,143,144] Unlike the top-down methods that include the cutting of graphene,[30] sonochemical extraction from expanded graphite,[38] and "unzipping" of carbon nanotubes,[42] the bottom-up strategy allows a precise control over the width and edge configuration of GNRs. Among the most commonly used strategy, the Lewis acid catalyzed cyclodehydrogenation reaction, known as Scholl reaction,[76] has been widely used to synthesize a large variety of structurally well-defined GNRs on polyphenylene precursors.[63,66,145-148] However, the Scholl reaction possesses some serious drawbacks that limit the scope and versatility of this reaction. One of the disadvantages is the poor regioselectivity, which results in structural defects that affect the properties of GNRs.[77] Then the undesired rearrangements and the use of a metal catalyst can lead to the formation of by-products.[149] In addition, the harsh reaction conditions make it difficult to introduce oxidant-sensitive functional groups and electron-rich heterocycles, which limits the diversity of structural and electronic properties of GNRs.[150]

Recently, our group reported the synthesis of nanographenes and GNRs by the photochemical cyclodehydrochlorination (CDHC) reaction on the polychlorinated polyphenylene precursors.[87,88,131,132] The photochemical CDHC reaction proceeds with high regioselectivity and without rearrangements or the formation of side-products. Moreover, the CDHC reaction is conducted without metal catalyst and oxidant, under milder reaction conditions than the Scholl reaction, and is compatible with different functional groups and heterocycles. And comparing with the Scholl reaction, the CDHC reaction provides better control over the edge configuration

of the GNRs.

Here, two narrow GNRs were prepared from polychlorinated polyphenylene precursors by the photochemical CDHC reaction (Scheme 1.1). The successful synthesis of both laterally symmetrical (GNR1) and unsymmetrical (GNR2) GNRs demonstrates the regioselectivity, edge configuration control, and efficiency of the CDHC reaction. The structures and properties were carefully characterized by ^{1}H NMR, FT-IR, XPS, UV-vis and photoluminescence analysis.

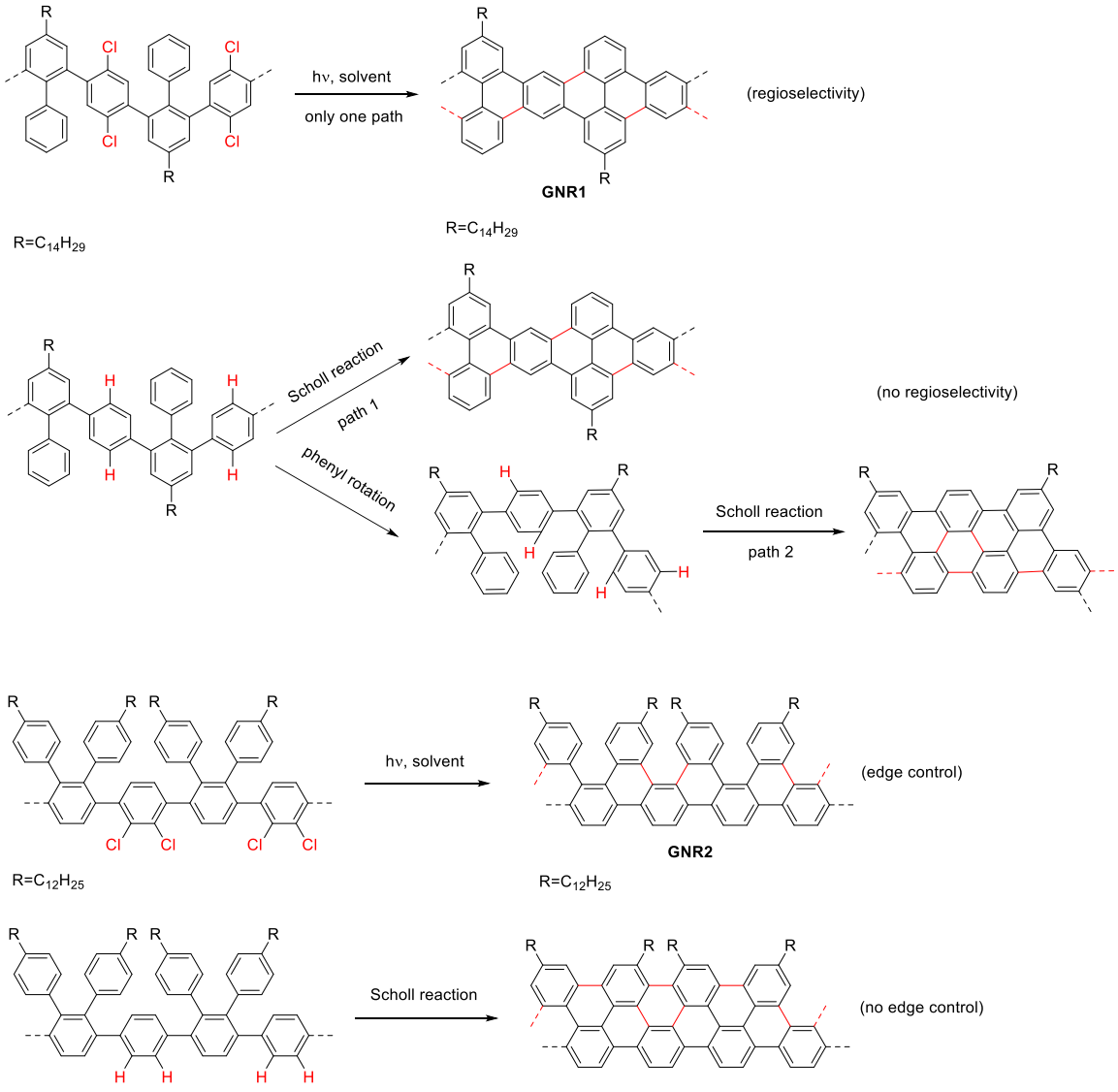

Scheme 1.1. Different reaction pathways for the CDHC and Scholl reactions on the same structural precursors. The newly formed bonds are shown in red.

1.4. Results and Discussion

1.4.1. Synthesis

The synthesis of GNR1 and GNR2 is shown in Scheme 1.2. Prior to the synthesis of the GNRs, model compound **4** was synthesized to optimize the CDHC reaction conditions. Previously, we performed the CDHC reaction in acetone and benzene under room temperature, unfortunately the yields are not high enough.[131] In our latest study, we found decahydronaphthalene (decalin) to be a very good solvent for the CDHC reaction since it is very stable upon UV irradiation and allows the reaction to reach a very high temperature, sufficent to overcome the solubility issues, especially in the case of polymers.[87,88,132] Fortunately, compound **4** was obtained in 95% yield after the irradiation of compound **3** under UV light (16 × 7.2 W low pressure mercury lamps, λ = 254 nm) at 100 ℃ for 2 hours, and no side products were formed.

For the synthesis of precursor P1, monomer 2,2'-(4-tetradecyl-[1,1'-biphenyl]-2,6-diyl)bis(4,4,5,5-tetramethyl-1,3,2-dioxaborolane) was synthesized according to a previously reported procedure,[132] which underwent Suzuki-Miyaura polymerization with 1,4-dichloro-2,5-diiodobenzene using the $Pd_2(dba)_3$/SPhos catalyst system to afford P1 in 89% yield. As for the precursor P2, starting from commercially available 1,2-dibromobenzene, a bromine directed *ortho* silylation was performed to access 1,4-disilane, a subsequent Suzuki-Miyaura coupling using $PdCl_2$(dppf) as the catalyst provided compound **5** in 95% yield, which was subjected to bromination with Br_2 to afford compound **6** (74%).[145] Then, a palladium-catalyzed double borylation using 4,4,5,5-tetramethyl-1,3,2-dioxaborolane gave monomer **7** in 81% yield. Finally, a Suzuki-Miyaura polymerization with 2,3-dichloro-1,4-diiodobenzene using $Pd_2(dba)_3$ as the catalyst and XPhos as the ligand provided P2 in 88% yield.

For the synthesis of GNR1 and GNR2, P1 and P2 were dissolved in anhydrous decalin at a concentration of 0.002 M in an oven-dried quartz flask and irradiated under UV light (16 × 7.2

W low pressure mercury lamps, λ = 254 nm) for 96 hours at 100 ℃ under a continuous flow of argon (to remove oxygen and the hydrochloric acid formed during the CDHC reaction). Upon irradiation, the solution of P1 went from colorless to yellow brown with green-yellow fluorescence, and the P2 solution turned from colorless to dark orange with a strong pinkish white fluorescence, indicating a significant change of the π-conjugation along the polymer chains. After purification (see Supporting Information), GNR1 was obtained as a brown solid in 92% yield and GNR2 as an orange solid in 95% yield.

1.4.2. Size-exclusion chromatography (SEC) analysis

High temperature size-exclusion chromatography (SEC) was employed to determine the molecular weight of the precursors and GNRs using polystyrene as standard and 1,2,4-trichlorobenzene as eluent. As shown in Figure 1.1, P1 and P2 exhibited a unimodal molecular weight distribution with a number-average molecular weight ($\overline{Mn}$) value of 17.1 kg mol^{-1} (corresponding to a degree of polymerization (DP) of 34 repeat units) and 14.1 kg mol^{-1} (corresponding to a DP of 20 repeat units), respectively. Upon irradiation, both GNR1 ($\overline{Mn}$ = 19.0 kg mol^{-1}) and GNR2 ($\overline{Mn}$ = 16.6 kg mol^{-1}) showed larger $\overline{Mn}$ value than its precursor, which is attributed to the increased planarity of the polymer chain after CDHC reaction, and this results in a higher hydrodynamic radius and higher molecular weight distribution.[87]

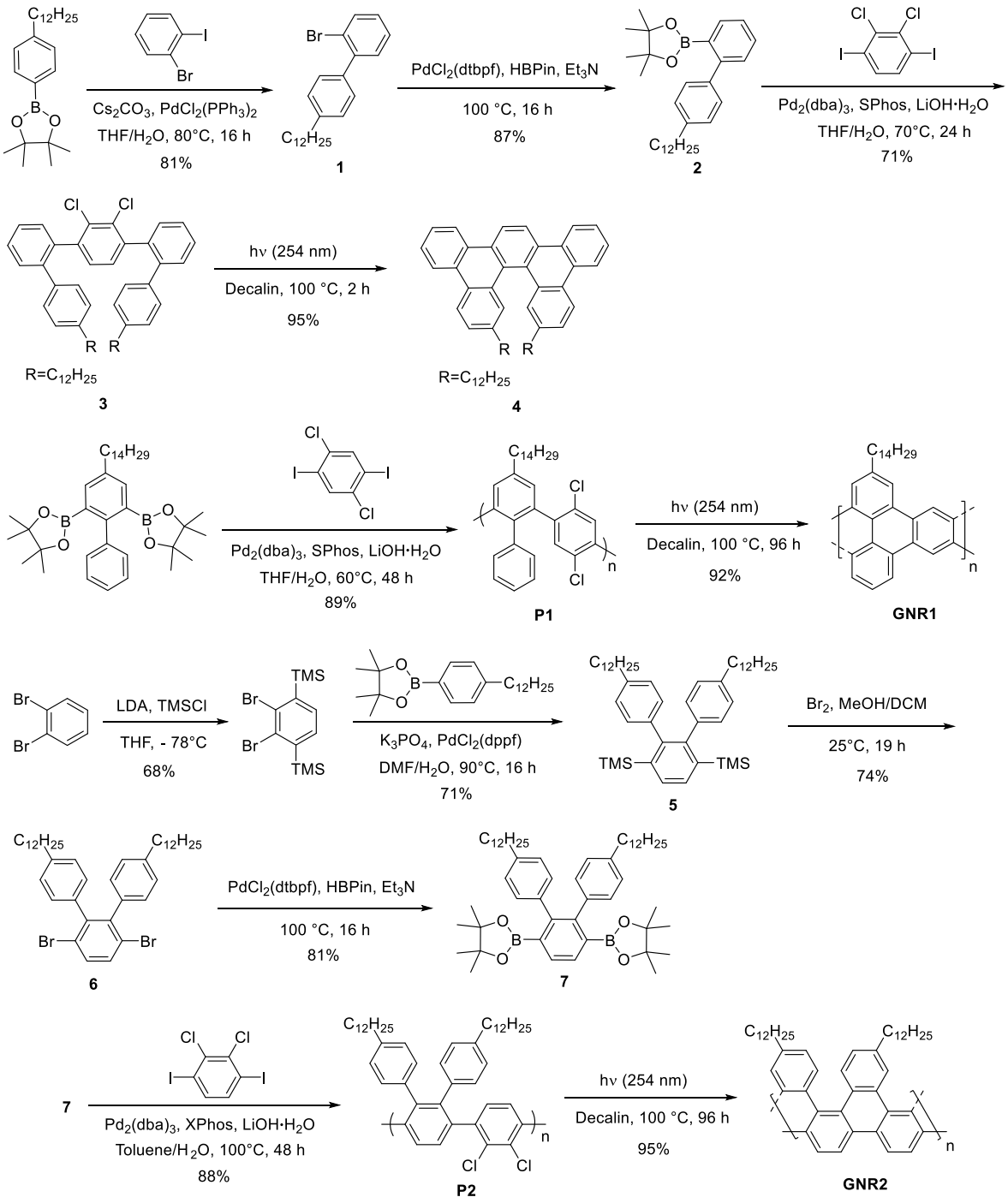

Scheme 1.2. Synthesis of model compound **4**, GNR1 and GNR2.

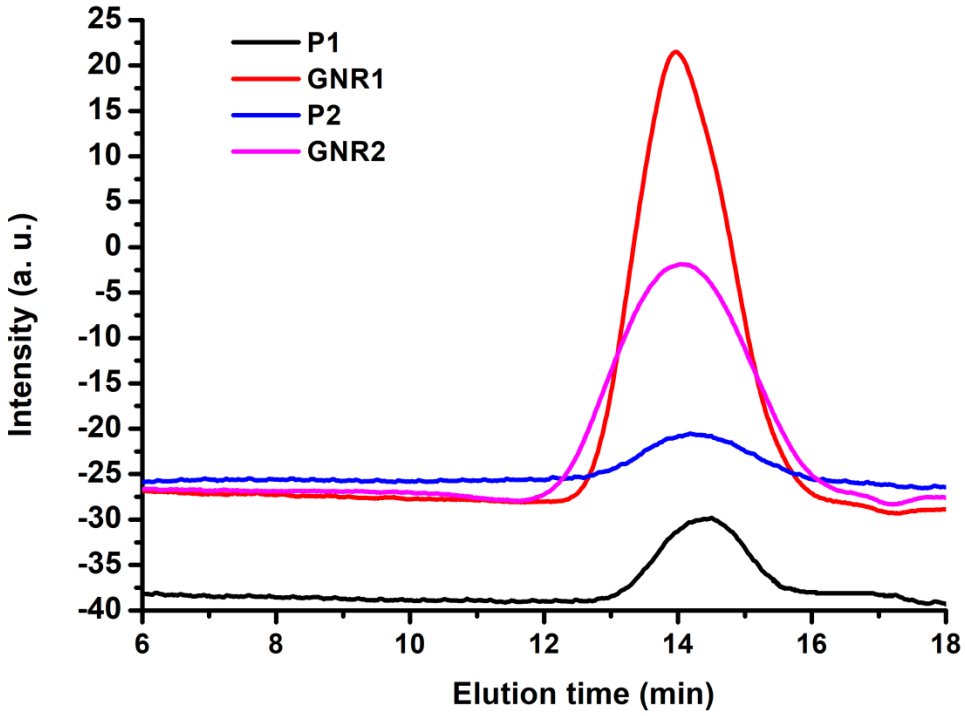

Figure 1.1. Size exclusion chromatography traces for P1 ($\overline{Mn}$: 17.1 kg mol^{-1}, $\overline{Mw}$: 22.8 kg mol^{-1}, dispersity index ($Đ$): 1.3, X_n: 34, black trace), GNR1 ($\overline{Mn}$ = 19.0 kg mol^{-1}, $\overline{Mw}$ = 31.7 kg mol^{-1}, dispersity index ($Đ$): 1.7, red trace), P2 ($\overline{Mn}$: 14.1 kg mol^{-1}, $\overline{Mw}$: 28.0 kg mol^{-1}, dispersity index ($Đ$): 1.9, X_n: 20, blue trace), and GNR2 ($\overline{Mn}$ = 16.6 kg mol^{-1}, $\overline{Mw}$ = 38.5 kg mol^{-1}, dispersity index ($Đ$): 2.3, pink trace).

1.4.3. ^{1}H NMR analysis

The ^{1}H NMR analysis of P1, P2, GNR1 and GNR2 were conducted in tetrachloroethane-d_2 (TCE-d_2) at 383 K and the results are shown in Figure 1.2. P1 exhibits broad peak centered at δ = 6.81 ppm which is associated with proton H_b. The undefined broad peaks between δ = 6.96 and 7.12 ppm can be ascribed to the protons H_a, H_c, H_d and H_e. After irradiation, a flatter ^{1}H NMR spectrum with the peaks broadened and downfield shifted was obtained, especially the peaks located in the aromatic region, due to a more rigid structure.[66,151] The peaks centered at δ = 8.67 ppm can be ascribed to the bay region protons H_a', while the peaks at 7.27 ppm are attributed to the protons H_b', H_d' and H_e', similar behavior was previously reported for

hexabenzocoronenes[152] and hexabenzotriphenylene motifs.[78] These results strongly indicate that the CDHC reaction went to near completion. Similar behaviors are observed for P2 and GNR2. Compared to P2, the spectrum for GNR2 flattens and shifts downfield as a rigid and more conjugated structure is obtained. Also, the bay region protons H_a' generate peaks at δ = 8.76 ppm, suggesting again that the CDHC reaction went to near completion.

1.4.4. FT-IR analysis

The completeness of the CDHC reaction upon irradiation of P1 and P2 can be attested by Fourier-transform infrared spectroscopy (FT-IR) analysis (see Figure 1.3 and Figure 1.23). As is shown in Figure 1.3, the band at 4054 cm^{-1}, which is associated with the rotation of free phenyl rings,[153] disappeared completely after irradiation, indicating that the CDHC reaction went to near completion. Moreover, the bands at 3085, 3050 and 3026 cm^{-1}, attributed to the aromatic C-H stretching vibrations,[145] almost diminished completely, and the out-of-plane (*opla*) aromatic C-H deformation bands at 699, 762, 826 and 900 cm^{-1} from mono-, and di-substituted benzene rings,[66,147] almost completely vanished after the CDHC reaction, which strongly indicate the loss of HCl molecules and the formation of GNR2. Similar behavior is observed for P1 and GNR1 (Figure 1.23).

1.4.5. XPS analysis

The X-ray photoelectron spectroscopy (XPS) analysis was performed to further attest the completeness of the photochemical CDHC reactions upon irradiation of P1 and P2 (see Figure 1.24-1.27). For P1 and P2, the peak at 200 eV corresponds to the Cl 2p, indicating the presence of chlorine atoms in P1 and P2. As for GNR1 and GNR2, the spectra show no trace of this peak, meaning that the chlorine atoms have disappeared completely and no chlorine-containing side products were formed during the CDHC reaction. These results further confirm that the photochemical CDHC reaction is complete.

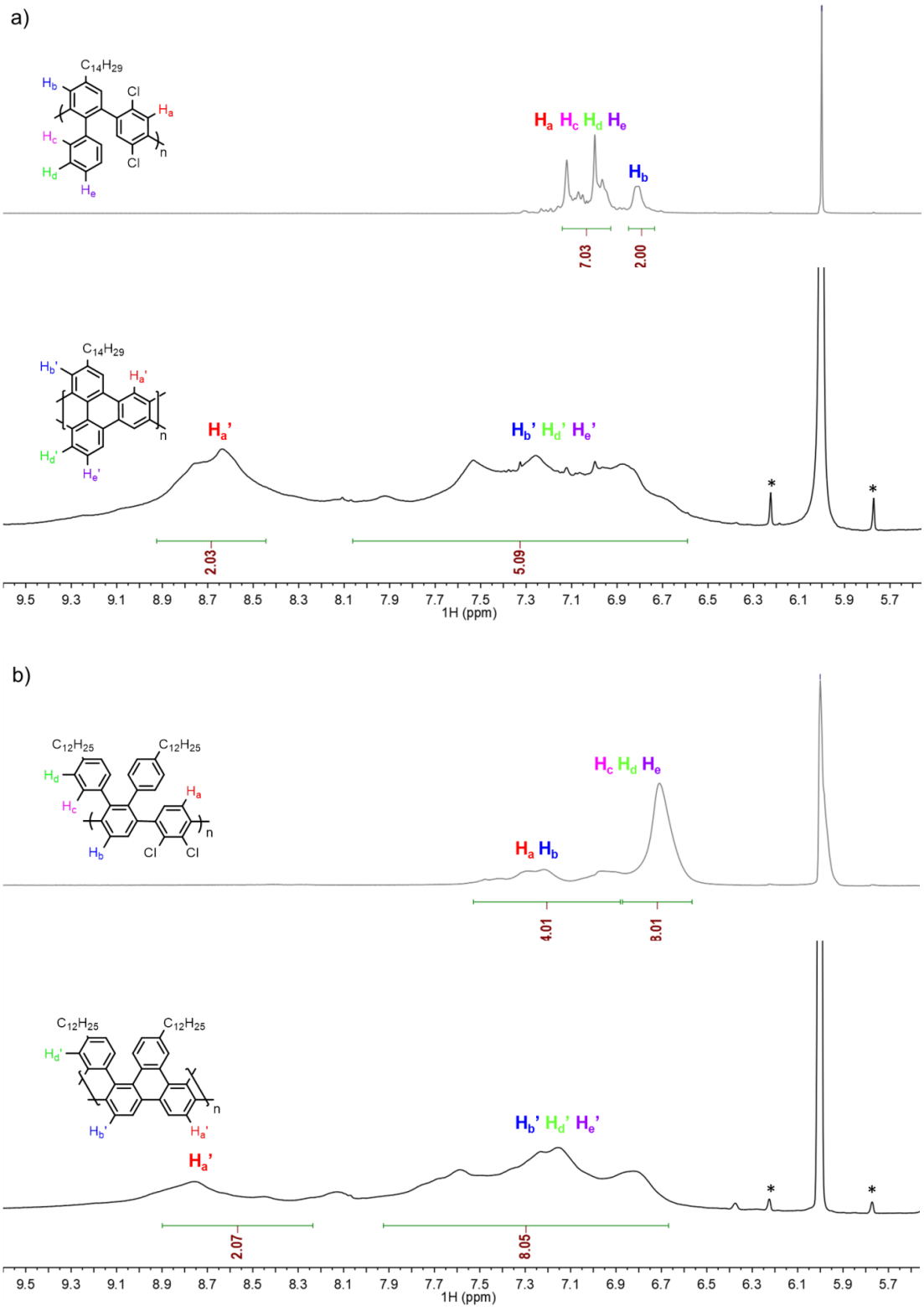

Figure 1.2. a) ^{1}H NMR spectra of precursor P1 (top) and GNR1 (bottom) in TCE-d_2 at 383 K. b) ^{1}H NMR spectra of precursor P2 (top) and GNR2 (bottom) in TCE-d_2 at 383 K.

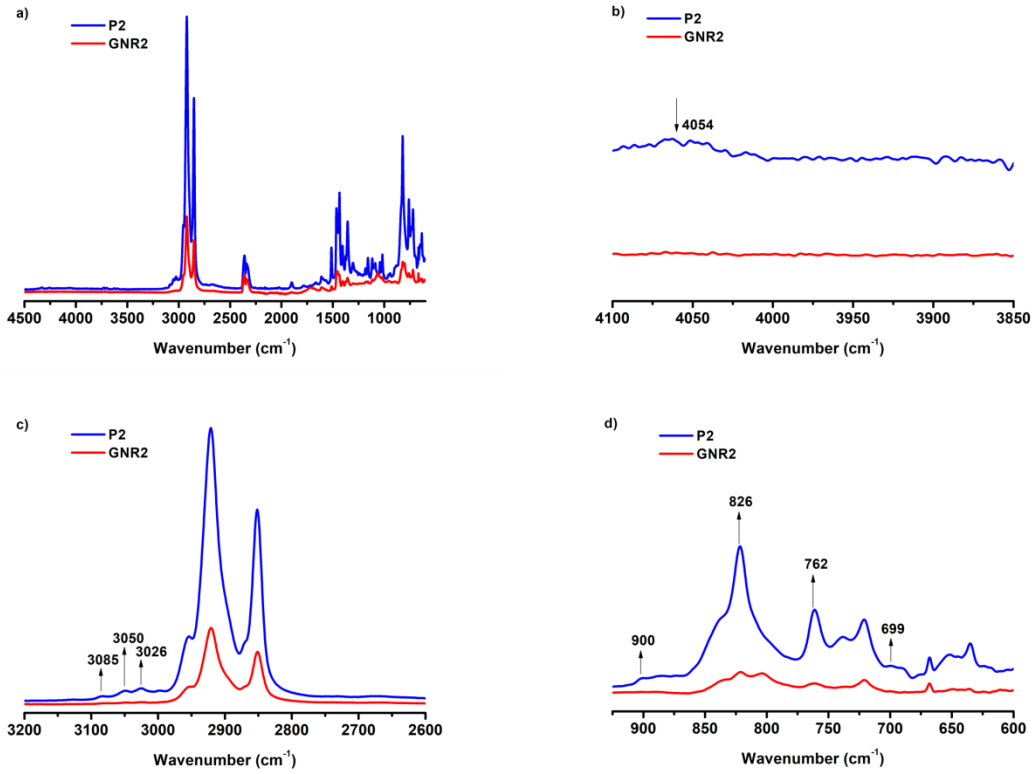

Figure 1.3. a) FT-IR spectrum of precursor P2 (blue lines) and GNR2 (red lines). b), c), d) FT-IR spectrum of P2 (blue lines) and GNR2 (red lines) zoomed.

1.4.6. UV-vis and photoluminescence analysis

The optical and electronic properties of GNR1 and GNR2 were investigated by UV-vis and photoluminescence spectroscopy and the results are shown in Figure 1.4. P1 and P2 showed featureless absorption below 300 nm, which indicates a non-rigid, less conjugated structure. In contrast, GNR1 exhibits absorption between 270 to 400 nm with the absorption maxima at 280, 298, and 320 nm, and GNR2 absorbs between 280 to 500 nm with the absorption maxima at 300 and 335 nm, indicating that the rigid and more π-conjugated structures were formed upon irradiation. For both GNR1 and GNR2, the solid-state absorption spectrum is only slightly red-shifted compared to that in solution, suggesting that there are very weak intermolecular interactions in the solid state, and GNR1 and GNR2 possess similar conformation in both solution and solid state, which is consistent with a highly rigid π-conjugated backbone.[154]

Optical bandgaps measured from the absorption band onset is 3.10 eV for GNR1 and 2.70 eV for GNR2, such high bandgaps have been reported for conjugated ladder polymers poly-*m*-carbazoles[154] and thiophene-edged graphene nanoribbons.[88] In contrast with P1 and P2, GNR1 and GNR2 also exhibited strong photoluminescence properties in solution with emission band peaking at 504 and 503 nm, respectively. Notably, the fluorescence excitation spectra of GNR1 and GNR2 were also recorded and they match well with the UV-vis absorption spectra (see Figure 1.28 and 1.29), indicating that the fluorescence emission were originating from the GNRs themselves.[155]

1.5. Conclusion

In conclusion, we successfully synthesized the laterally symmetrical and unsymmetrical GNRs from polychlorinated polyphenylene precursors by the photochemical cyclodehydrochlorination (CDHC) reaction, which demonstrates the regioselectivity, edge configuration control, and efficiency of the CDHC reaction. ^{1}H NMR, FT-IR, and XPS confirmed the structures of the GNRs. The optical and electronic properties of the GNRs were carefully studied by UV-vis and photoluminescence analysis. The laterally symmetrical and unsymmetrical GNRs have rather large bandgaps and are highly emissive both in solution and solid state. The regioselectivity, better edge control and high efficiency of the CDHC reaction enable us to synthesize well-defined, larger lateral width GNRs with lower bandgap in the future.

1.6. Acknowledgements

This work was supported by NSERC (Natural Sciences and Engineering Research Council of Canada) through a Discovery Grant. D.M. thanks the China Scholarship Council (CSC) for a PhD scholarship. The authors thank Pascale Chevallier for her help for the XPS analysis.

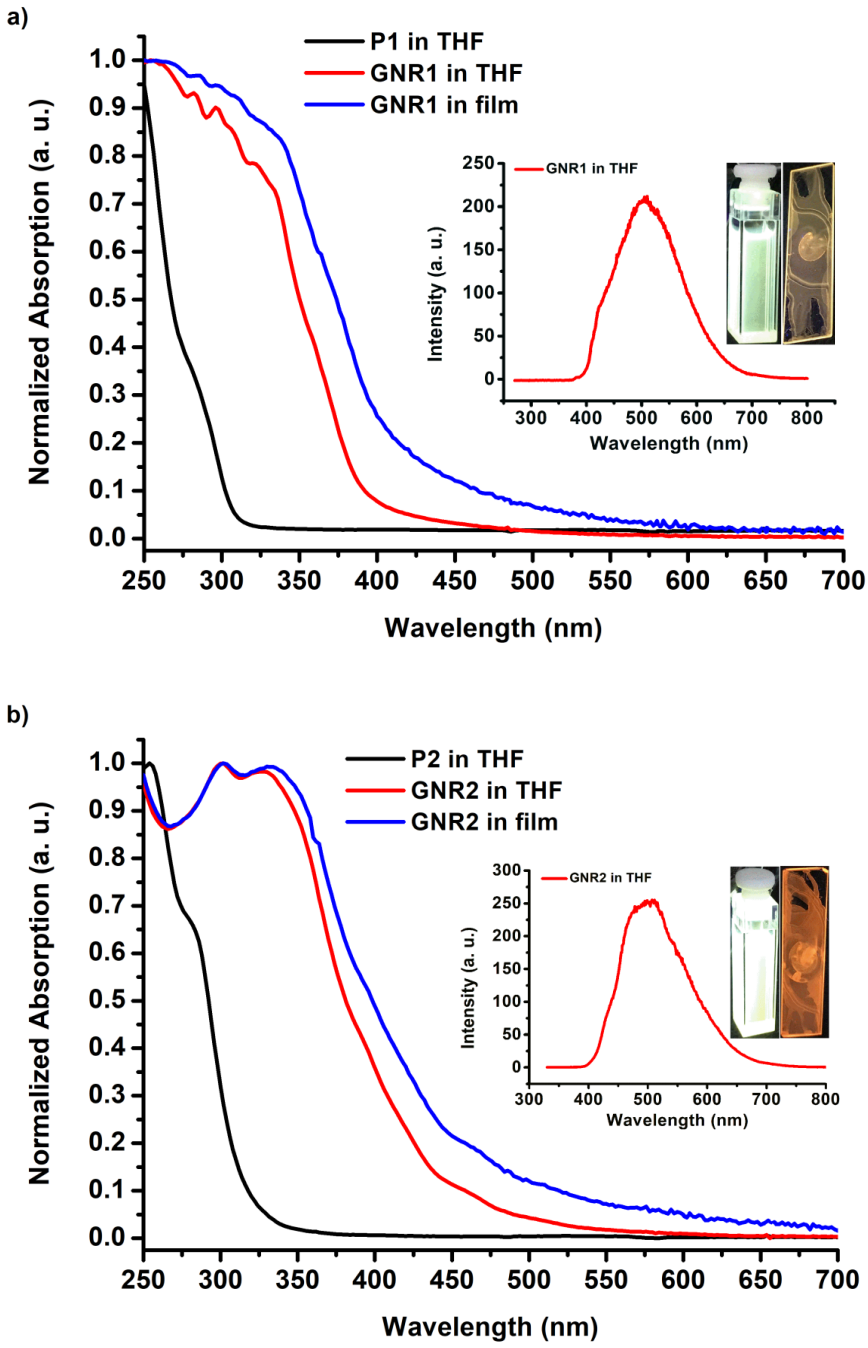

Figure 1.4. UV-vis absorption spectra of a) P1 and GNR1 and b) P2 and GNR2 in both THF and thin films. Insets: Photoluminescence spectra of a) GNR1 and b) GNR2 in THF solution (λ_{ex} = 300 nm); dilute solution (left) and spin-cast film (right) of a) GNR1 and b) GNR2 in THF under UV light (λ = 365 nm).

1.7. Supporting Information

1.7.1. Materials and Methods

Chemical reagents were purchased from Sigma-Aldrich Co. Canada, Alfa Aesar Co., TCI America Co. or Oakwood Products Inc. and used as received. Solvents used for organic synthesis were purchased from Fisher Chemical Co., EMD Millipore Co. and CFS Chemical Co. as HPLC grade. These solvents were degassed, dried and purified using a solvent purifier system (SPS) (Vacuum Atmosphere Co., Hawthorne, USA). Anhydrous decahydronaphthalene (mixture of *cis* + *trans*) was used as received for photochemical reactions and other anhydrous solvents were bought from Sigma-Aldrich Co. Canada. All anhydrous and air sensitive reactions were performed in oven-dried glassware purchased from Synthware™ under positive nitrogen stream. Analytical thin-layer chromatography was performed with silica gel 60 F254, 0.25 mm pre-coated thin layer chromatography (TLC) plates (Silicycle, Québec, Canada). Compounds were revealed by a 254 nm and/or 365 nm UV wavelength and/or aqueous K_2CO_3 and NaOH solution of potassium permanganate. Flash column chromatography was performed with 230-400 mesh silica gel R10030B (Silicycle, Québec, Canada). 2-(4-dodecylphenyl)-4,4,5,5-tetramethyl-1,3,2-dioxaborolane was synthesized according to literature procedures.[147] 2,3-dichloro-1,4-diiodobenzene and 1,4-dichloro-2,5-diiodobenzene were synthesized according to literature procedures[131] and further purified by recrystallization in isopropanol. 2,2'-(4-tetradecyl-[1,1'-biphenyl]-2,6-diyl)bis-(4,4,5,5-tetramethyl-1,3,2-dioxaborolane) was synthesized according to literature procedures.[132]

1.7.2. Apparatus

Photochemical reactions were performed in a CCP-ICH2 Luzchem® photochemical reactor equipped with a thermostat and a heating mantle. Photochemical reactions were performed in a 100 mL quartz round-bottom flask bought from Chemglass®. Nuclear magnetic resonance (NMR) spectra were recorded on a Varian Inova AS400 spectrometer (Varian, Palo Alto, USA)

at 400 MHz (^{1}H) and 100 MHz (^{13}C). Signals are reported as m (multiplet), s (singlet), d (doublet), t (triplet), and coupling constants are reported in hertz (Hz). Chemical shifts are reported as values ppm (δ) relative to residual solvent peak. High resolution mass spectra (HRMS) were recorded with an Agilent 6210 Time-of-Flight (TOF) liquid chromatography-mass spectrometry (LC-MS) apparatus equipped with an atmospheric pressure photo-ionization (APPI) ion source (Agilent Technologies, Toronto, Canada). Number-average ($\overline{M}$n) and weight-average ($\overline{M}$w) molecular weights were determined by size-exclusion chromatography (SEC) using a Varian Polymer Laboratories GPC220 equipped with an RI detector and a PL BV400 HT Bridge viscometer. The column set consists of 2 PL gel Mixed C (300 × 7.5 mm) columns and a PL gel Mixed C guard column. The flow rate was fixed at 1mL min^{-1} using 1,2,4-trichlorobenzene (TCB) (with 0.0125% BHT w/v) as the eluent. The temperature of the system was set to 110 ℃. All the samples were prepared at a nominal concentration of 1.0 mg mL^{-1} in TCB. Dissolution was performed using a Varian Polymer Laboratories PL-SP 260VC sample preparation system. The sample vials were held at 110 ℃ with shaking for 1 h for complete dissolution. The solutions were filtered through a 2 mm porous stainless steel filter and a 0.40 μm glass filter into a 2 mL chromatography vial. The calibration method used to generate the reported data was the classical polystyrene method using polystyrene narrow standards Easi-Vials PS-M from Varian Polymer Laboratories which were dissolved in TCB. FT-IR spectra were recorded in ATR mode on an infrared spectrometer (Thermo-Nicolet Magna 850) equipped with Golden Gate. UV-visible absorption and photoluminescence spectra were recorded on a UV-vis HP 8452 spectrophotometer and a Varian Cary Eclipse fluorescence spectrofluorimeter, respectively, using 10-mm path length quartz cells. For solid state measurements, the polymer solution (1.0 mg mL^{-1} in THF) was spin coated on quartz plates. Optical bandgaps were calculated from the onset of the absorption band. The chemical composition of P1, P2, GNR1 and GNR2 was investigated by X-ray photoelectron spectroscopy (XPS), using a PHI 5600-ci spectrometer (Physical Electronics, Eden Prairie, MN, USA). The main XPS chamber was maintained at a base pressure of < 1 ×

10^{-8} Torr. A standard aluminium X-ray source (Al kalpha = 1486.6 eV) was used to record survey spectra (1400-0 eV, 10min) with charge neutralization. The detection angle was set at 45 °with respect to the normal of the surface and the analyzed area was 0.125 mm^2.

1.7.3. Synthesis

2-bromo-4'-dodecyl-1,1'-biphenyl (1)

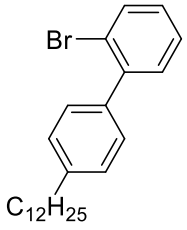

1

A round bottom flask was flushed three times with a vacuum/nitrogen cycle, charged with 2-(4-dodecylphenyl)-4,4,5,5-tetramethyl-1,3,2-dioxaborolane (2.00 g, 5.37 mmol), 1-bromo-2-iodobenzene (1.52 g, 5.37 mmol), cesium carbonate (7.00 g, 21.5 mmol) and flushed three times with a vacuum/nitrogen cycle again. THF (54.0 mL) and H_2O (13.5 mL) was added and the reaction mixture was degassed with a nitrogen stream for 10 mins. $PdCl_2(PPh_3)_2$ (0.377 g, 0.537 mmol) was added and the reaction mixture was degassed with nitrogen for another 5 mins and heated to 80 ℃ for 16 h. Once cooled to room temperature, 20 mL of an aqueous saturated NH_4Cl solution was added and the aqueous layer was extracted with ethyl acetate (3 × 40 mL). The organic layer was dried with Na_2SO_4 and the solvent was removed under reduced pressure. The resulting residue was purified by silica gel chromatography with hexanes to yield compound **1** as a colorless oil (1.75 g, 81 %). ^{1}H NMR (400 MHz, $CDCl_3$): δ 7.78 (d, *J* = 3.96 Hz, 1H), 7.43 (m, 4H), 7.37 (m, 2H), 7.26 (m, 1H), 2.79 (t, *J* = 7.76 Hz, 2H), 1.81 (m, 2H), 1.43 (m, 18H), 1.04 (m, 3H). ^{13}C NMR (100 MHz, $CDCl_3$): δ 142.72, 142.39, 138.48, 133.21, 131.44, 129.35, 128.53, 128.06, 127.38, 122.86, 35.93, 32.12, 31.55, 29.89, 29.86, 29.81, 29.74, 29.63, 29.57, 22.88, 14.31. HRMS (APPI+): calculated for $C_{24}H_{33}Br$ $(M + H)^+$ 400.17656, found 400.18016.

2-(4'-dodecyl-[1,1'-biphenyl]-2-yl)-4,4,5,5-tetramethyl-1,3,2-dioxaborolane (2)

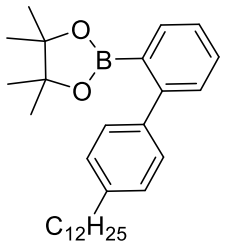

2

An oven-dried round bottom flask was flushed three times with a vacuum/nitrogen cycle. Compound **1** (1.00 g, 2.50 mmol), anhydrous 1,4-dioxane (12.5 mL) and $PdCl_2$(dtbpf) (64.9 mg, 99.6 μmol) were added and the flask was flushed three times again with a vacuum/nitrogen cycle. Triethylamine (1.56 mL, 11.2 mmol) was degassed with a nitrogen stream for 10 mins and then added into the reaction flask. 4,4,5,5-Tetramethyl-1,2,3-dioxaborolane (1.08 mL, 7.50 mmol) was filtered through a 0.45 μm syringe filter and added dropwise to the reaction mixture. The flask was flushed three times with a vacuum/nitrogen cycle and heated at 100 ℃ for 16 h. Once cooled to room temperature, 20 mL of a saturated aqueous solution of NH_4Cl was added and the aqueous layer was extracted with ethyl acetate (3 × 40 mL). The organic layer was dried with Na_2SO_4 and the solvent was removed under reduced pressure. The crude product was purified by silica gel chromatography (5% Et_2O/hexanes) to yield compound **2** as a colorless solid (0.970 g, 87%). ^{1}H NMR (400 MHz, $CDCl_3$): δ 7.72 (d, *J* = 3.70 Hz, 1H), 7.45 (m, 2H), 7.34 (m, 3H), 7.21 (d, *J* = 4.01 Hz, 2H), 2.67 (t, *J* = 7.60 Hz, 2H), 1.67 (m, 2H), 1.29 (m, 18H), 1.23 (s, 12H), 0.91 (t, *J* = 6.89 Hz, 3H). ^{13}C NMR (100 MHz, $CDCl_3$): δ 147.61, 141.61, 140.70, 134.41, 130.10, 129.08, 128.97, 128.01, 126.15, 83.79, 35.76, 32.08, 31.74, 29.84, 29.81, 29.79, 29.73, 29.51, 29.37, 24.75, 22.84, 14.27. HRMS (APPI+): calculated for $C_{30}H_{45}BO_2$ $(M + H)^+$ 447.35489, found 447.36133.

2'',3''-dichloro-4,4''''-didodecyl-1,1':2',1'':4'',1''':2''',1''''-quinquephenyl (3)

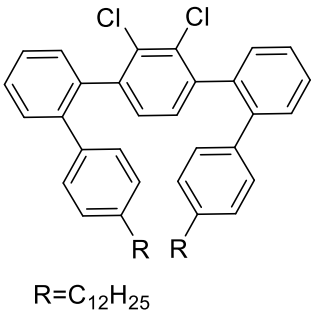

$R=C_{12}H_{25}$

3

A round bottom flask under nitrogen was charged with compound **2** (0.618 g, 1.38 mmol), 2,3-dichloro-1,4-diiodobenzene (0.250 g, 0.600 mmol), $LiOH \bullet H_2O$ (0.210 g, 5.00 mmol), THF (3.10 mL) and H_2O (0.800 mL), flushed three times with a vacuum/nitrogen cycle and degassed with a nitrogen stream for 10 mins. $Pd_2(dba)_3$ (28.7 mg, 30.0 μmol) and SPhos (51.4 mg, 0.120 mmol) were added and the reaction flask was degassed with nitrogen for another 5 mins. The reaction mixture was heated to 70 ℃ for 24 h. Once cooled down to room temperature, 15 mL of a saturated aqueous solution of NH_4Cl was added and the aqueous layer was extracted with ethyl acetate (3 × 20 mL). The organic layer was dried with Na_2SO_4 and the solvent was removed under reduced pressure. The resulting residue was purified by silica gel chromatography (5% CH_2Cl_2/hexanes) to obtain compound **3** as a white solid (0.350 g, 71%). ^{1}H NMR (400 MHz, $CDCl_3$): δ 7.49 (m, 8H), 7.07 (m, 8H), 6.97 (s, 1H), 6.83 (s, 1H), 2.68 (m, 4H), 1.69 (m, 4H), 1.29 (m, 36H), 0.92 (t, J = 6.82 Hz, 6H). ^{13}C NMR (100 MHz, $CDCl_3$): δ 141.54, 141.42, 141.37, 141.36, 141.27, 141.40, 138.19, 138.01, 137.87, 132.52, 132.31, 131.57, 130.88, 130.82, 130.58, 130.34, 130.23, 129.86, 129.42, 129.39, 129.27, 129.21, 128.48, 128.40, 128.13, 128.05, 128.01, 127.83, 126.85, 126.77, 36.01, 35.69, 32.09, 31.70, 31.41, 29.88, 29.86, 29.82, 29.80, 29.78, 29.70, 29.53, 29.41, 22.86, 14.29. HRMS (APPI+): calculated for $C_{54}H_{68}Cl_2$ $(M + H)^+$ 786.46981, found 786.46885.

7,10-didodecyldibenzo[*f,j*]picene (4)

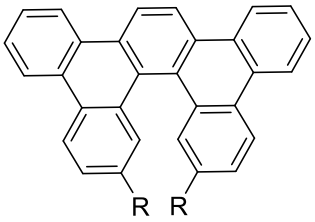

4

An oven-dried quartz flask was flushed three times with a vacuum/nitrogen cycle and charged with compound **3** (0.142 g, 0.180 mmol) and anhydrous decahydronaphthalene (50.0 mL). The flask was degassed with a nitrogen stream for 10 mins and the reaction solution was irradiated at 254 nm at 100 ℃ for 2 hours under a continuous flow of argon. Once cooled down to room temperature, the solvent was removed by vacuum distillation and the resulting residue was further purified by silica gel chromatography (25% CH_2Cl_2/hexanes) to yield compound **4** as a light yellow solid (0.122 g, 95%). ^{1}H NMR (400 MHz, $CDCl_3$): δ 8.64 (m, 6H), 8.49 (d, *J* = 4.24 Hz, 2H), 8.05 (s, 2H), 7.72 (m, 4H), 7.36 (d, *J* = 4.11 Hz, 2H), 2.45 (m, 4H), 1.38 (m, 4H), 1.26 (m, 36H), 0.89 (t, *J* = 6.84 Hz, 6H). ^{13}C NMR (100 MHz, $CDCl_3$): δ 139.92, 131.15, 130.63, 130.42, 130.39, 129.46, 127.93, 127.87, 127.82, 127.28, 127.09, 123.82, 123.42, 123.11, 121.74, 36.05, 32.10, 31.38, 29.86, 29.83, 29.67, 29.65, 29.58, 29.54, 22.86, 14.29. HRMS (APPI+): calculated for $C_{54}H_{66}$ $(M + H)^+$ 714.52042, found 714.51645.

(4,4''-didodecyl-[1,1':2',1''-terphenyl]-3',6'-diyl)bis(trimethylsilane) (5)

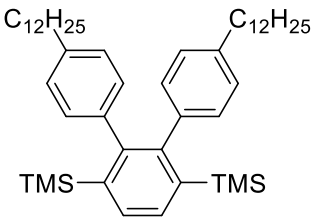

5

A round bottom flask under nitrogen was charged with (2,3-dibromo-1,4-phenylene)bis(trimethylsilane) (2.00 g, 5.30 mmol), 2-(4-dodecylphenyl)-4,4,5,5-tetramethyl-1,3,2-dioxaborolane (5.88 g, 15.8 mmol), K_3PO_4 (6.70 g, 31.6 mmol), Pd(dppf)Cl_2 (0.430 g, 0.530 mmol), DMF (16.8 mL) and H_2O (3.40 mL), flushed three times with a vacuum/nitrogen cycle and degassed with a nitrogen stream for 10 mins. The reaction mixture was heated to 90 ℃ for 16 h. Once cooled down to room temperature, 20 mL of water was added and the aqueous layer was extracted with ethyl acetate (3 × 40 mL). The organic layer was dried with Na_2SO_4 and the solvent was removed under reduced pressure. The resulting residue was purified by silica gel chromatography with hexanes to obtain compound **5** as a colorless solid (3.55 g, 95%). ^{1}H NMR (400 MHz, $CDCl_3$): δ 7.70 (s, 2H), 6.93 (m, 8H), 2.56 (t, *J* = 7.51 Hz, 4H), 1.58 (m, 4H), 1.35 (m, 36H), 0.97 (t, *J* = 6.82 Hz, 6H), 0.03 (s, 18H). ^{13}C NMR (100 MHz, $CDCl_3$): δ 147.72, 140.58, 140.21, 139.84, 132.66, 130.96, 126.87, 35.64, 32.16, 31.58, 29.95, 29.92, 29.90, 29.71, 29.60, 29.08, 22.91, 14.32, 0.67. HRMS (APPI+): calculated for $C_{48}H_{78}Si_2$ $(M + H)^+$ 710.56421, found 710.56413.

3',6'-dibromo-4,4''-didodecyl-1,1':2',1''-terphenyl (6)

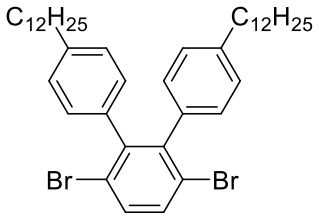

6

To a solution of dichloromethane (8.80 mL) and methnol (8.80 mL) in a round bottom flask was added compound **5** (2.50 g, 3.50 mmol) at room temperature. After the solid was dissolved, Br_2 (1.69 g, 10.5 mmol) was added dropwise and the mixture was stirred at room temperature for 19 h. 30 mL of a saturated aqueous solution of Na_2SO_3 was added and the aqueous layer was extracted with dichloromethane (3 × 50 mL). The organic layer was dried with Na_2SO_4 and

the solvent was removed under reduced pressure. The resulting residue was purified by silica gel chromatography with hexanes to obtain compound **6** as a white solid (1.88 g, 74%). ^{1}H NMR (400 MHz, $CDCl_3$): δ 7.52 (s, 2H), 6.96 (d, *J* = 4.03 Hz, 4H), 6.87 (d, *J* = 4.03 Hz, 4H), 2.51 (t, *J* = 7.65 Hz, 4H), 1.53 (m, 4H), 1.29 (m, 36H), 0.91 (t, *J* = 6.76 Hz, 6H). ^{13}C NMR (100 MHz, $CDCl_3$): δ 144.00, 141.34, 137.16, 132.33, 129.50, 127.18, 123.17, 35.39, 31.78, 31.00, 29.57, 29.53, 29.50, 29.35, 29.23, 28.95, 22.55, 13.97. HRMS (APPI+): calculated for $C_{42}H_{60}Br_2$ $(M + H)^+$ 722.30618, found 722.30478.

2,2'-(4,4''-didodecyl-[1,1':2',1''-terphenyl]-3',6'-diyl)bis(4,4,5,5-tetramethyl-1,3,2-dioxabor-olane) (7)

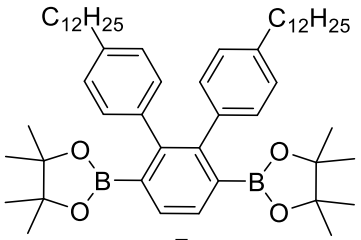

7

A round bottom flask was oven-dried and flushed three times with a vacuum/nitrogen cycle. Compound **6** (1.50 g, 2.00 mmol), anhydrous 1,4-dioxane (10.3 mL), $PdCl_2$(dtbpf) (80.9 mg, 0.120 mmol) were added and the flask was flushed three times with a vacuum/nitrogen cycle. Triethylamine (2.60 mL, 18.6 mmol) was degassed with a nitrogen stream for 10 minutes and then added into the reaction flask using a syringe. 4,4,5,5-Tetramethyl-1,2,3-dioxaborolane (1.80 mL, 12.4 mmol) was filtered through a 0.45 μm filter syringe and added dropwise. The reaction mixture was flushed three times with a vacuum/nitrogen cycle and heated at 100 ℃ for 16 h. Once cooled to room temperature, 20 mL of a saturated aqueous solution of NH_4Cl was added and the aqueous layer was extracted with ethyl acetate (3 × 40 mL). The organic layer was dried with Na_2SO_4 and the solvent was removed under reduced pressure. The resulting residue was purified by silica gel chromatography (10% Et_2O/hexanes) to yield compound **7** as

a white solid (1.37 g, 81%). ^{1}H NMR (400 MHz, $CDCl_3$): δ 7.56 (s, 2H), 6.87 (s, 8H), 2.49 (t, *J* = 7.45 Hz, 4H), 1.51 (m, 4H), 1.25 (m, 36H), 1.09 (s, 24H), 0.88 (m, 6H). ^{13}C NMR (100 MHz, $CDCl_3$): δ 145.24, 140.29, 139.77, 131.42, 130.40, 127.11, 83.60, 35.69, 32.07, 31.77, 29.86, 29.85, 29.82, 29.79, 29.73, 29.52, 29.22, 24.65, 22.84, 14.27. HRMS (APPI+): calculated for $C_{54}H_{84}B_2O_4$ $(M + H)^+$ 816.66284, found 816.66284.

Polymerization procedure for the precursor P1

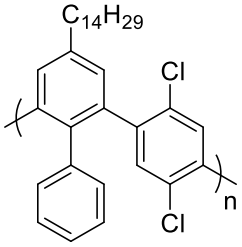

P1

2,2'-(4-tetradecyl-[1,1'-biphenyl]-2,6-diyl)bis(4,4,5,5-tetramethyl-1,3,2-dioxaborolane) was polymerized with 1,4-dichloro-2,5-diiodobenzene by a palladium-catalyzed Suzuki-Miyaura polymerization to afford the precursor P1. A flask under nitrogen was charged with 2,2'-(4-tetradecyl-[1,1'-biphenyl]-2,6-diyl)bis(4,4,5,5-tetramethyl-1,3,2-dioxaborolane) (0.250 g, 0.415 mmol), 1,4-dichloro-2,5-diiodobenzene (0.165 g, 0.415 mmol.), $LiOH{\bullet}H_2O$ (0.139 g, 3.32 mmol), THF (4.15 mL) and H_2O (0.520 mL). The flask was flushed three times with a vacuum/nitrogen cycle and degassed with a continuous flow of nitrogen for 10 mins. $Pd_2(dba)_3$ (3.80 mg, 4.15 μmol) and SPhos (13.6 mg, 33.2 μmol) were added and the reaction flask was flushed three times with a vacuum/nitrogen cycle and the reaction mixture was heated at 60 ℃ for 48 h. Once cooled to room temperature, the reaction mixture was precipitated in cold methanol under strong stirring and filtered through a 0.45 μm nylon filter. The residue was purified by Soxhlet extraction in acetone for 24 hours and recovered with hexanes through the extraction thimble. The solvent was removed under reduced pressure with the exclusion of light

and the solid was dissolved in a minimum amount of hexanes, precipitated in methanol, filtered through a 0.45 μm nylon filter and thoroughly dried under vacuum to obtain precursor P1 ($\overline{Mn}$ = 17.1 kg mol^{-1}, $\overline{Mw}$ = 22.8 kg mol^{-1}, dispersity index ($Đ$): 1.3) as a light grey solid (0.182 g, 89%).

Polymerization procedure for the precursor P2

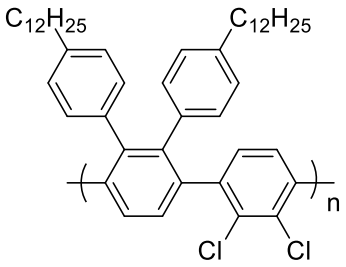

P2

Compound **7** was polymerized with 2,3-dichloro-1,4-diiodobenzene by a palladium-catalyzed Suzuki-Miyaura polymerization to afford the precursor P2. A flask under nitrogen was charged with compound **7** (0.250 g, 0.305 mmol), 1,4-dichloro-2,5-diiodobenzene (0.122 g, 0.305 mmol.), LiOH•H_2O (0.154 g, 3.66 mmol), toluene (3.10 mL) and H_2O (0.380 mL). The flask was flushed three times with a vacuum/nitrogen cycle and degassed with a continuous flow of nitrogen for 10 mins. $Pd_2(dba)_3$ (14.0 mg, 15.3 μmol) and XPhos (29.1 mg, 61.1 μmol) were added and the reaction flask was flushed three times with a vacuum/nitrogen cycle and the reaction mixture was heated at 100 ℃ for 48 h. Once cooled to room temperature, the reaction mixture was precipitated in cold methanol under strong stirring and filtered through a 0.45 μm nylon filter. The residue was purified by Soxhlet extraction in acetone for 24 hours and recovered with hexanes through the extraction thimble. The solvent was removed under reduced pressure with the exclusion of light and the solid was dissolved in a minimum amount of hexanes, precipitated in methanol, filtered through a 0.45 μm nylon filter and thoroughly dried under vacuum to obtain precursor P2 ($\overline{Mn}$ = 14.1 kg mol^{-1}, $\overline{Mw}$ = 28.0 kg mol^{-1},

dispersity index (*Đ*): 1.9) as a light yellow solid (0.191 g, 88%).

Photochemical procedure for the synthesis of GNR1 and GNR2

The precursor (P1, P2) was dissolved in anhydrous decahydronaphthalene (0.002 M) in an oven-dried quartz flask under argon. The solution was degassed with a continuous flow of argon for 10 minutes. The solution was heated to 100 ℃ and irradiated with 16 × 7.2 W low pressure mercury lamps at λ = 254 nm for 96 hours while maintaining a continuous flow of argon. Once cooled down to room temperature, the solvent was removed by vacuum distillation and the solid was dissolved in a minimum amount of THF, precipitated in cold methanol, filtered through a 0.45 µm nylon filter. The residue was purified by Soxhlet extraction in hexanes for 24 hours and recovered with THF. Once concentrated to a minimum amount of solvent, the polymer was precipitated in methanol, filtered and thoroughly dried under vacuum.

GNR1

P1 (99.0 mg) was subjected to the procedure described above to obtain GNR1 ($\overline{Mn}$ = 19.0 kg mol^{-1}, $\overline{Mw}$ = 31.7 kg mol^{-1}, dispersity index (*Đ*): 1.7) as a brown solid (78.0 mg, 92%).

GNR2

P2 (0.142 g) was subjected to the procedure described above to obtain GNR2 ($\overline{Mn}$ = 16.6 kg mol^{-1}, $\overline{Mw}$ = 38.5 kg mol^{-1}, dispersity index (*Đ*): 2.3) as an orange solid (0.121 g, 95%).

1.7.4. NMR Spectra

Compound 1

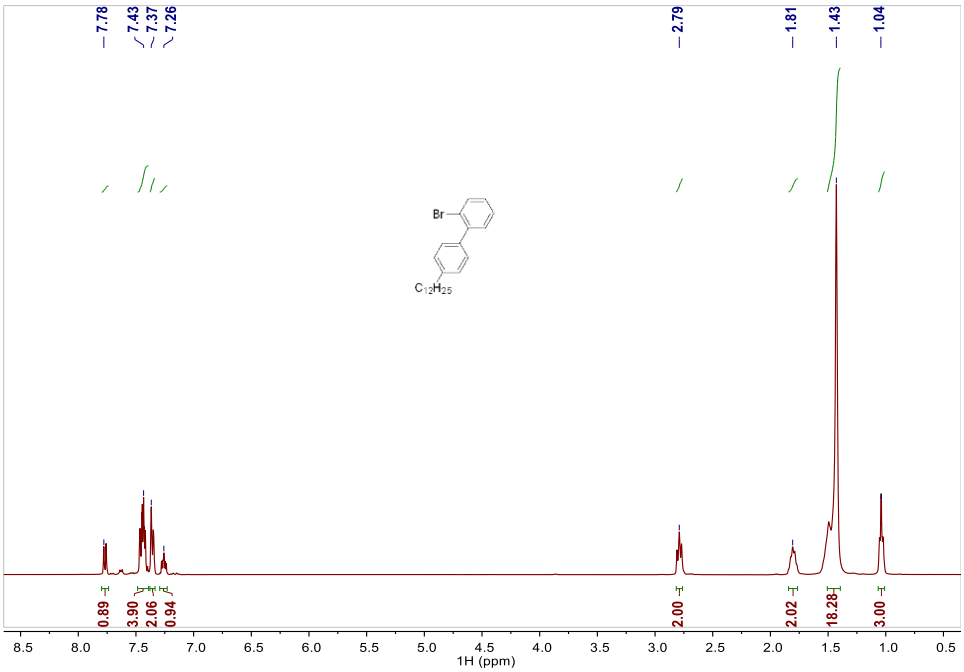

Figure 1.5. ^{1}H NMR spectrum of compound **1** in $CDCl_3$.

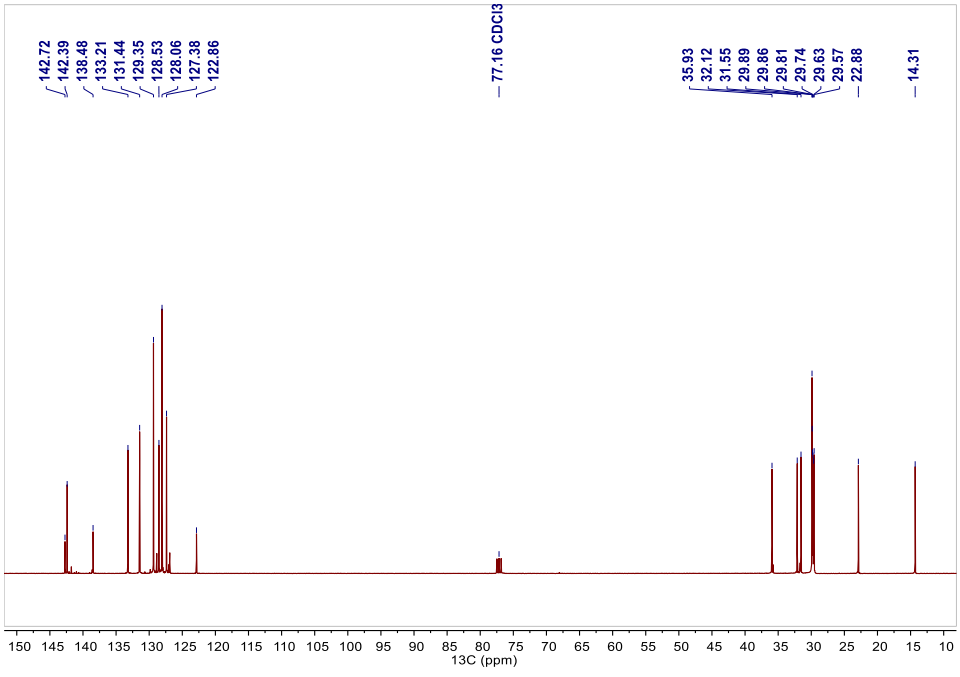

Figure 1.6. ^{13}C NMR spectrum of compound **1** in $CDCl_3$.

Compound 2

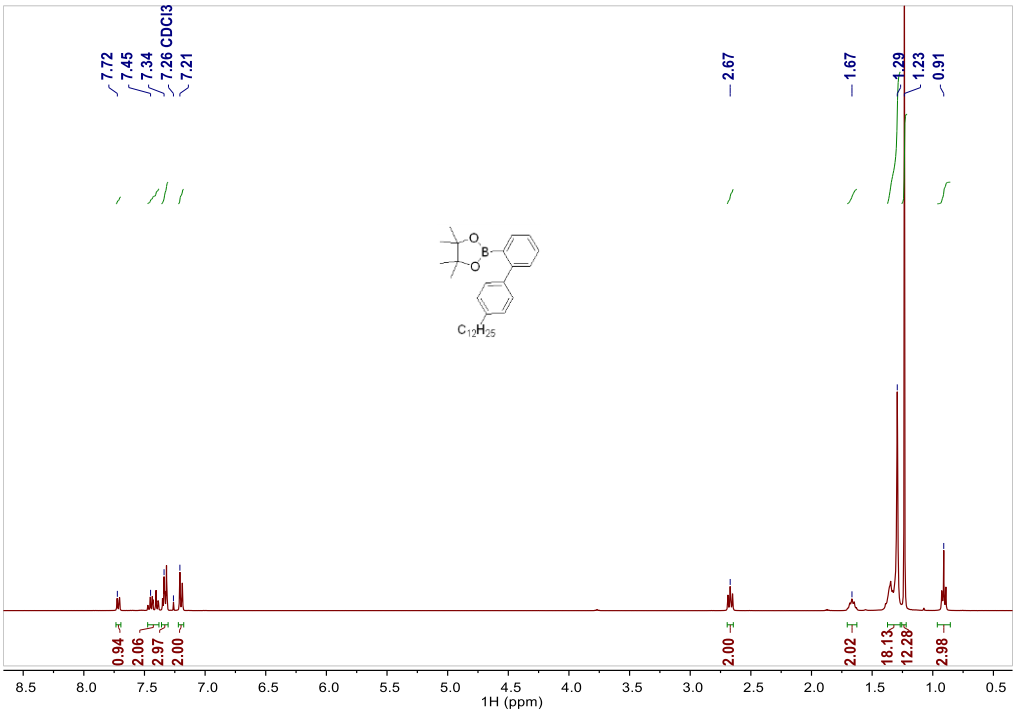

Figure 1.7. ^{1}H NMR spectrum of compound **2** in $CDCl_3$.

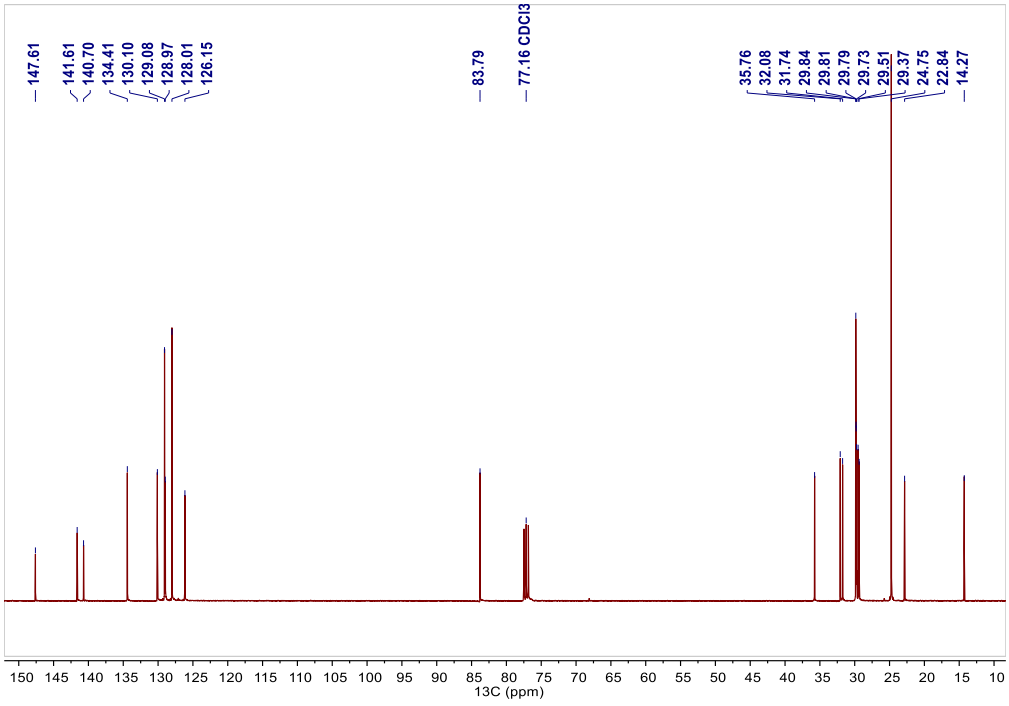

Figure 1.8. ^{13}C NMR spectrum of compound **2** in $CDCl_3$.

Compound 3

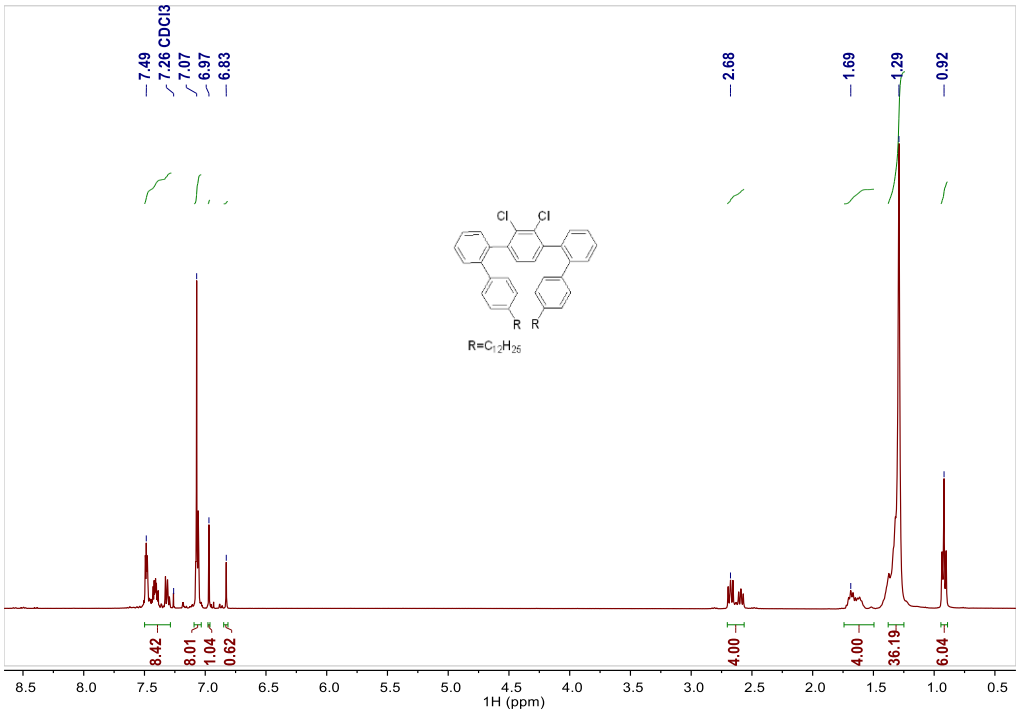

Figure 1.9. ^{1}H NMR spectrum of compound **3** in $CDCl_3$.

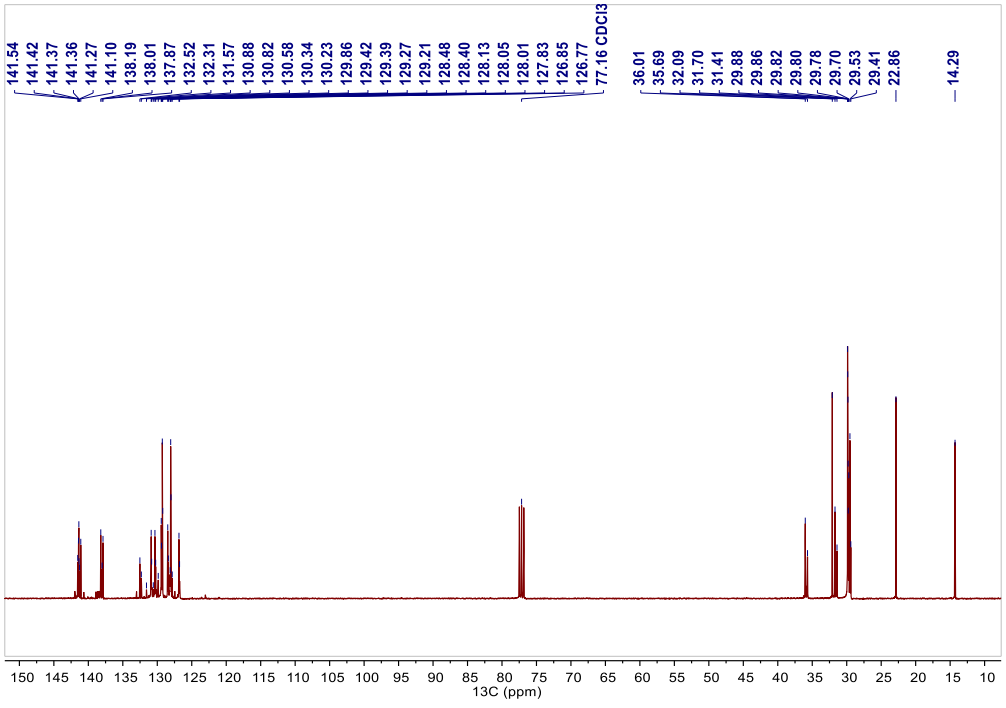

Figure 1.10. ^{13}C NMR spectrum of compound **3** in $CDCl_3$.

Compound 4

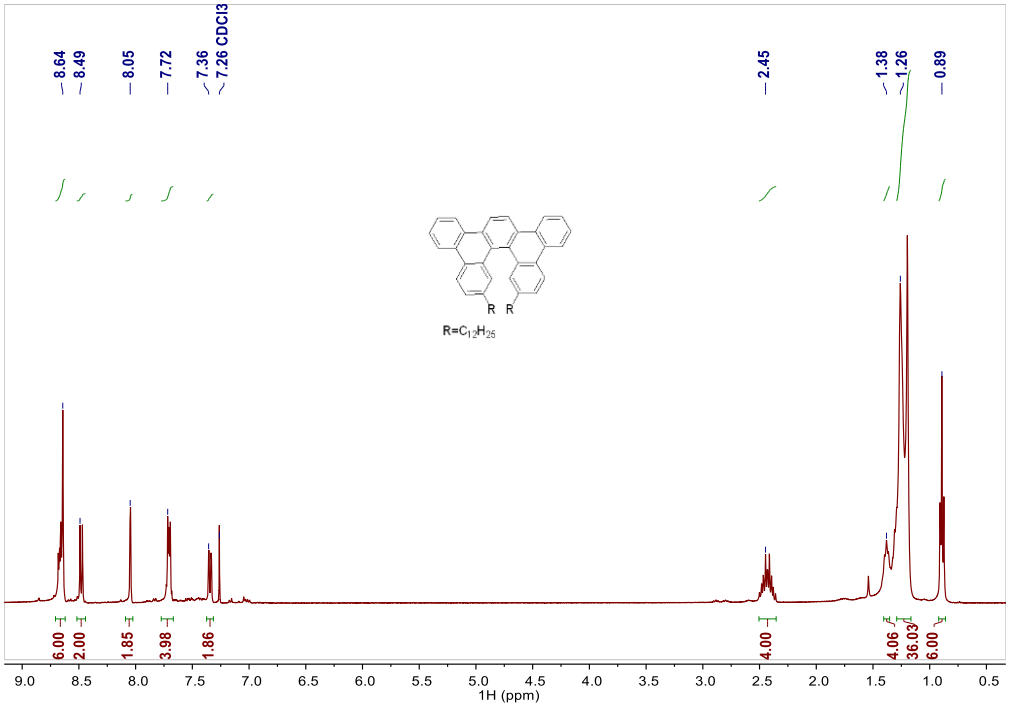

Figure 1.11. ^{1}H NMR spectrum of compound **4** in $CDCl_3$.

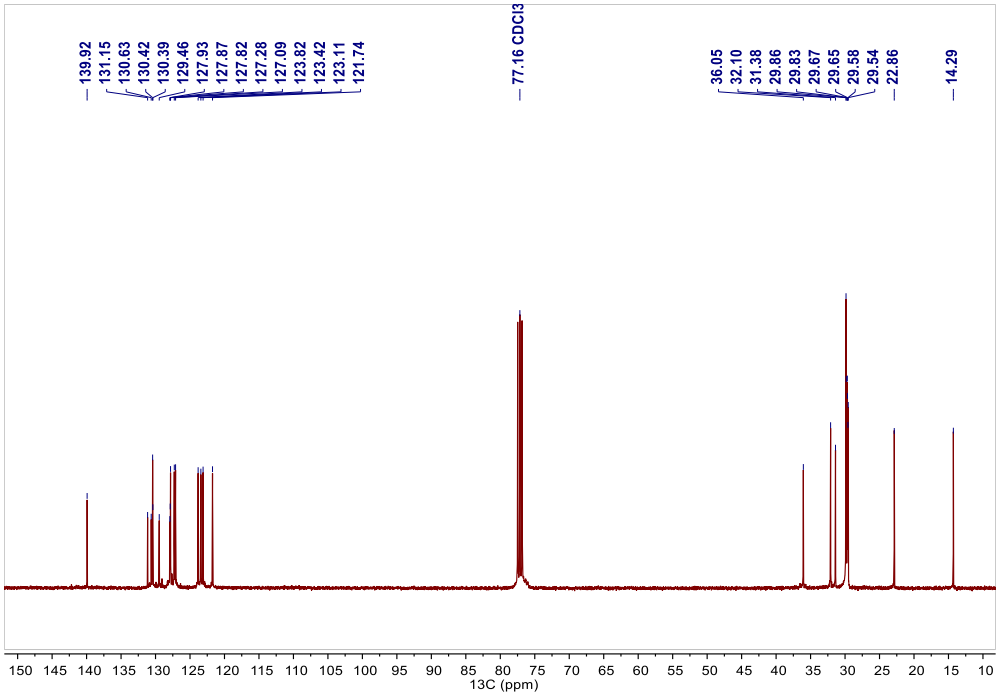

Figure 1.12. ^{13}C NMR spectrum of compound **4** in $CDCl_3$.

Compound 5

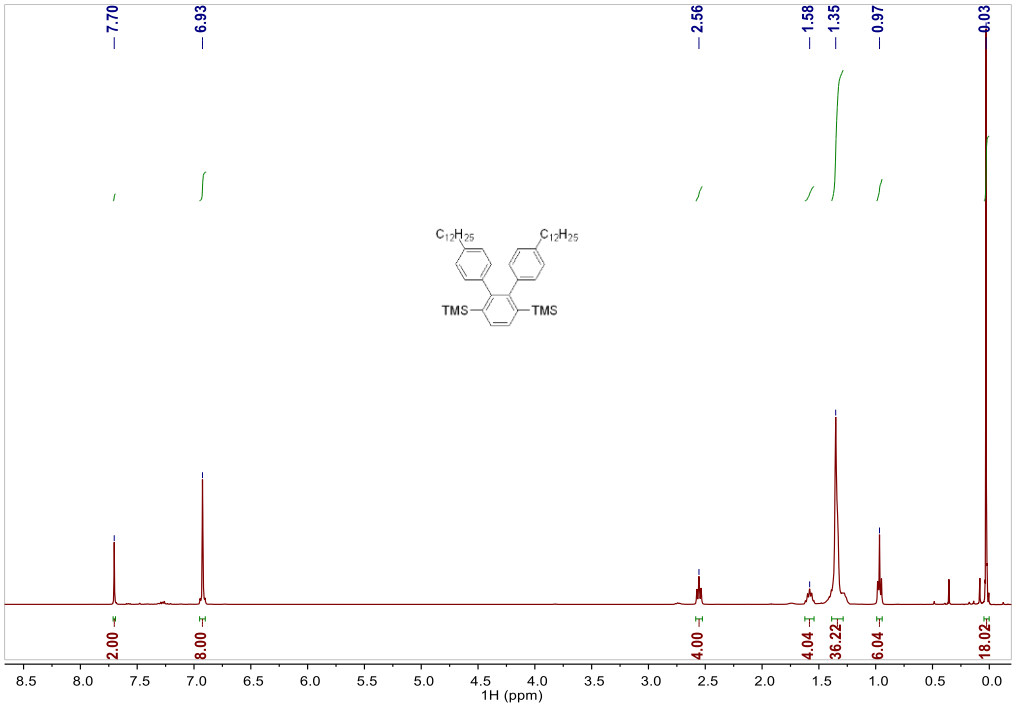

Figure 1.13. ^{1}H NMR spectrum of compound **5** in $CDCl_3$.

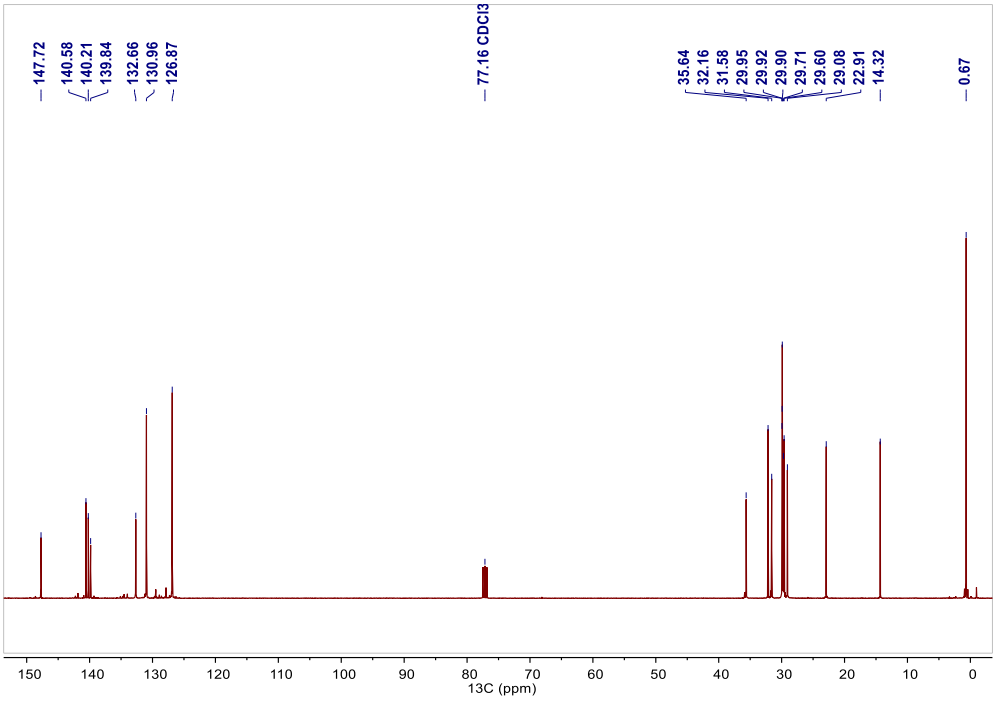

Figure 1.14. ^{13}C NMR spectrum of compound **5** in $CDCl_3$.

Compound 6

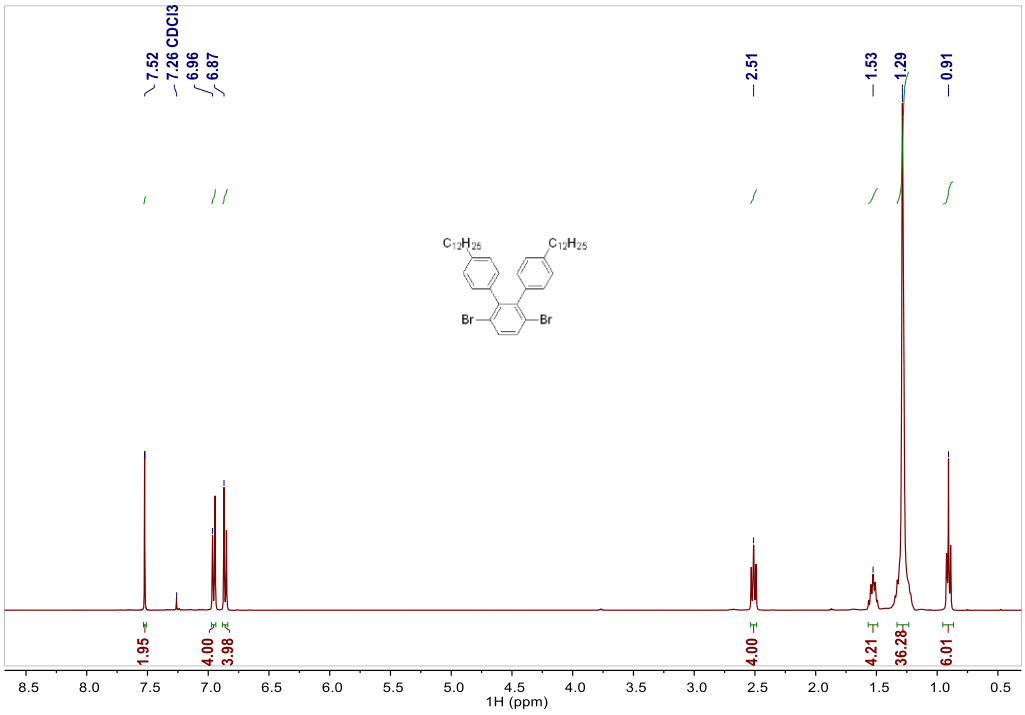

Figure 1.15. ^{1}H NMR spectrum of compound **6** in $CDCl_3$.

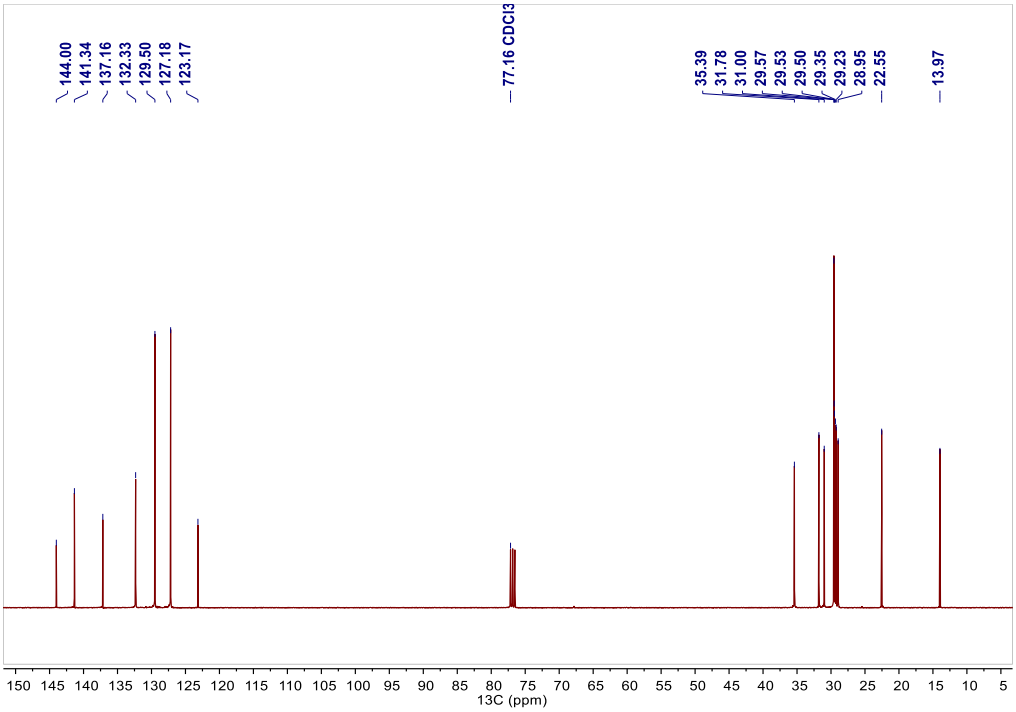

Figure 1.16. ^{13}C NMR spectrum of compound **6** in $CDCl_3$.

Compound 7

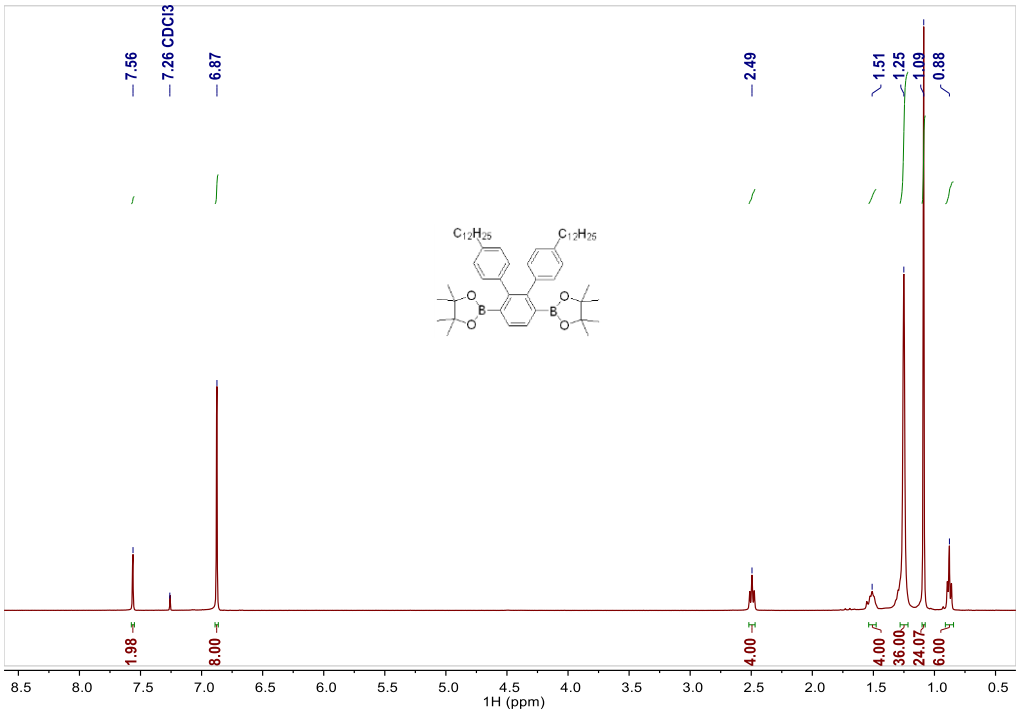

Figure 1.17. ^{1}H NMR spectrum of compound **7** in $CDCl_3$.

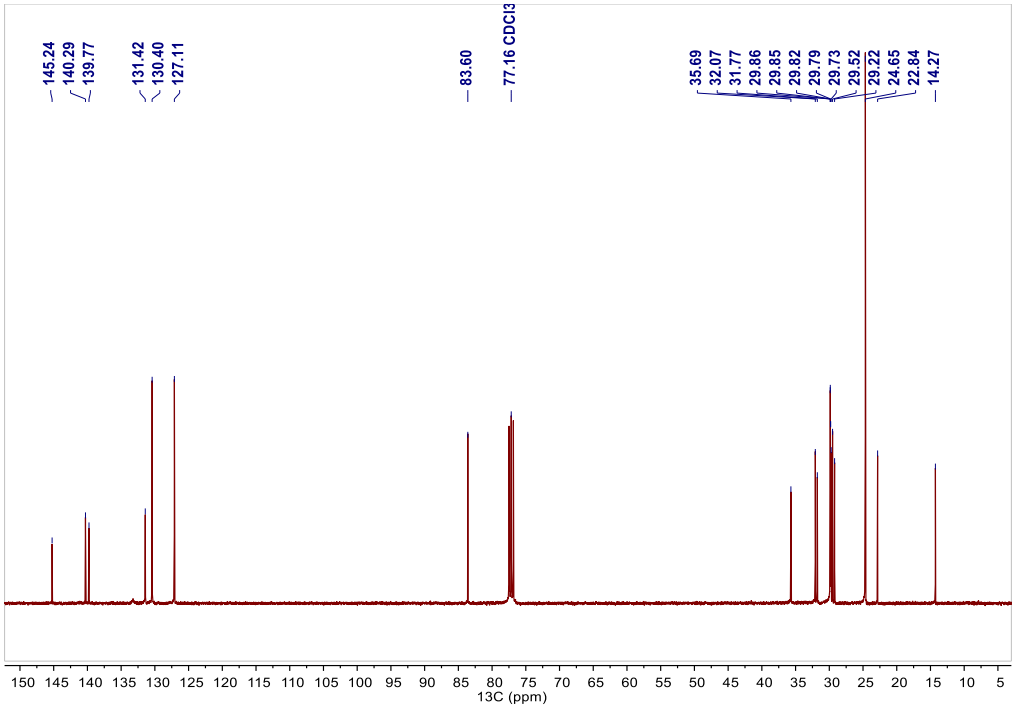

Figure 1.18. ^{13}C NMR spectrum of compound **7** in $CDCl_3$.

Precursor P1

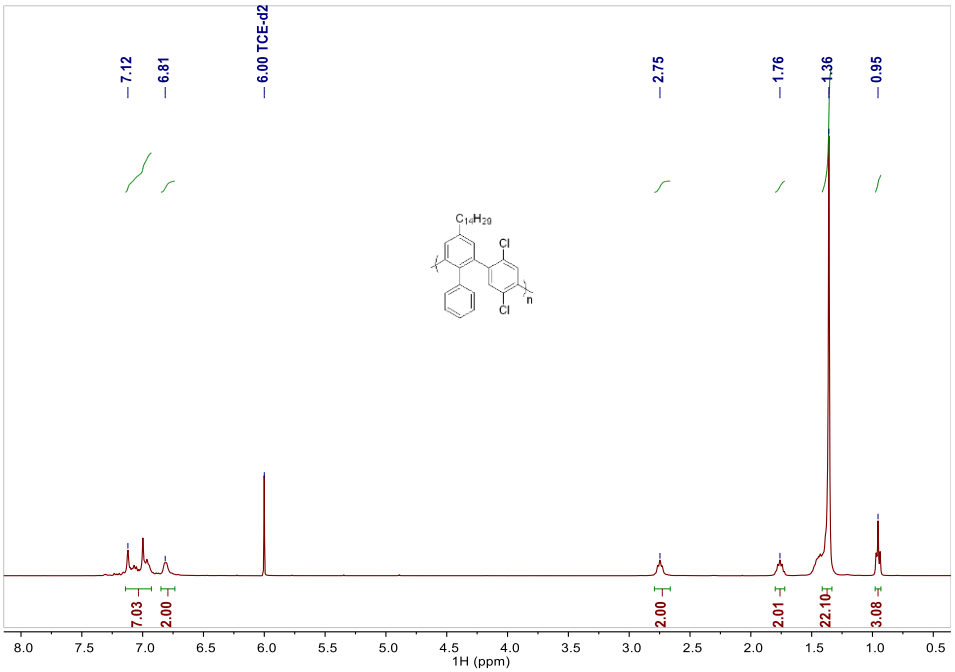

Figure 1.19. ^{1}H NMR spectrum of P1 in TCE-d_2 at 383 K.

GNR1

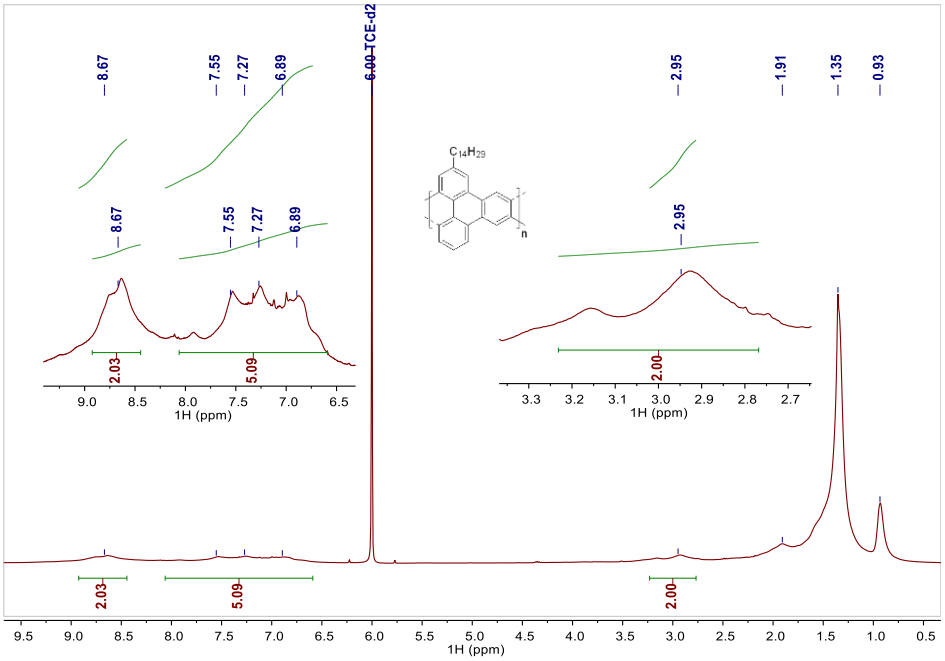

Figure 1.20. ^{1}H NMR spectrum of GNR1 in TCE-d_2 at 383 K.

Precursor P2

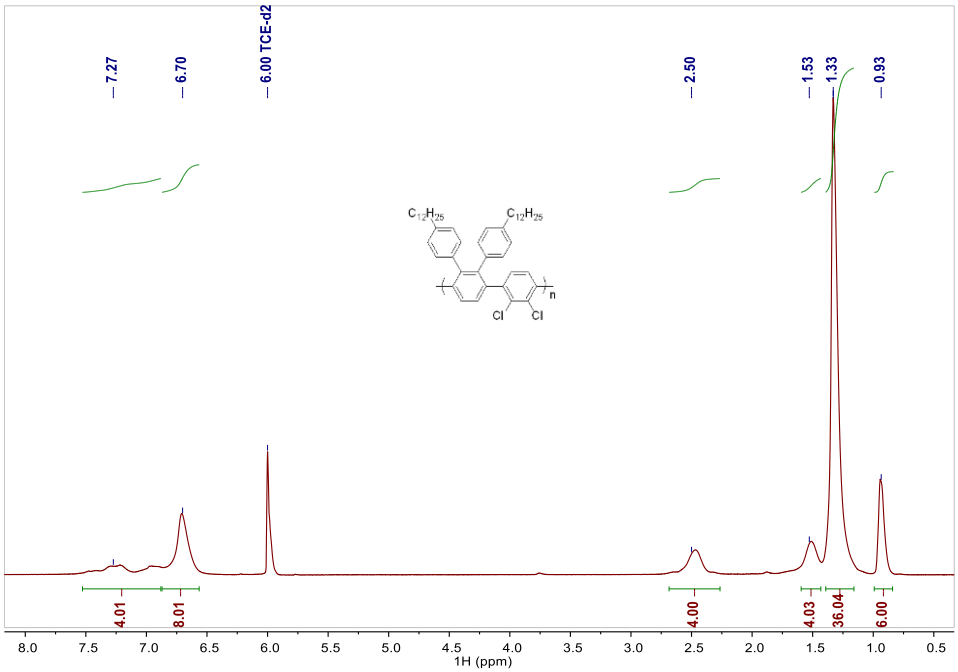

Figure 1.21. ^{1}H NMR spectrum of P2 in TCE-d_2 at 383 K.

GNR2

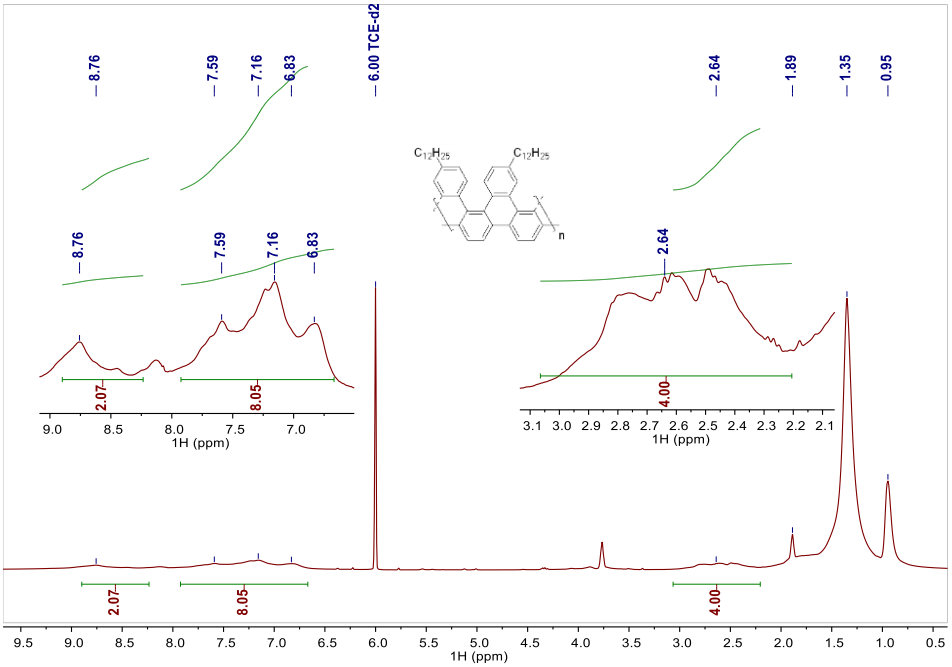

Figure 1.22. ^{1}H NMR spectrum of GNR2 in TCE-d_2 at 383 K.

1.7.5. FT-IR analysis

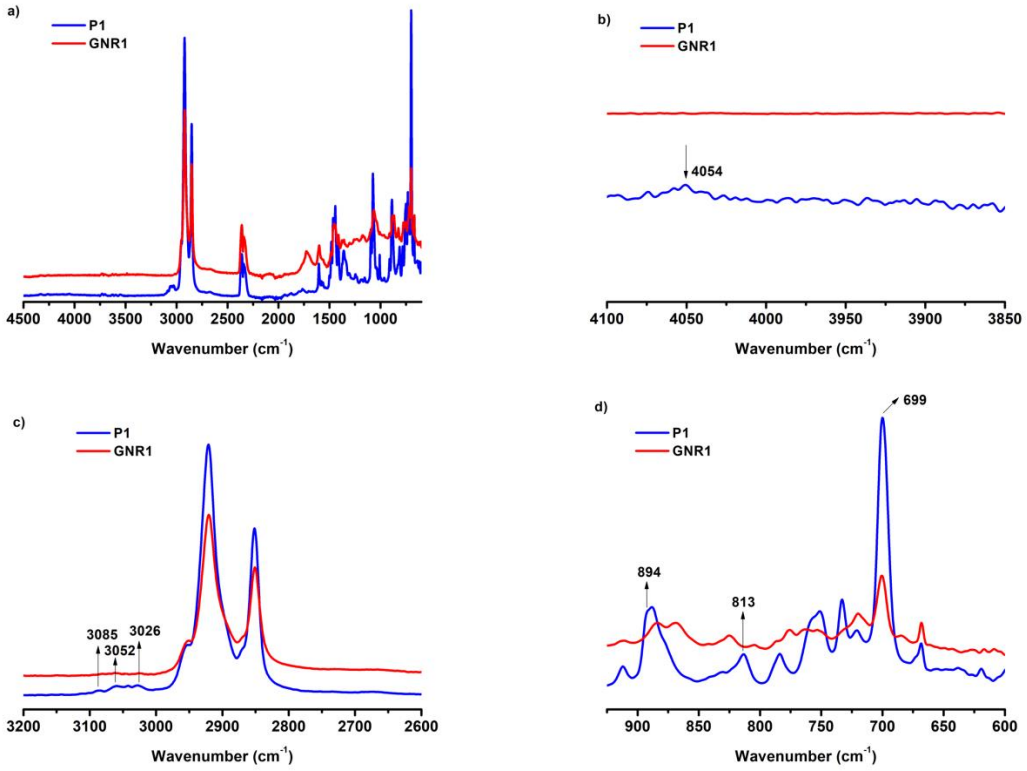

Figure 1.23. a) FT-IR spectrum of precursor P1 (blue lines) and GNR1 (red lines). b), c), d) FT-IR spectrum of P1 (blue lines) and GNR2 (red lines) zoomed.

1.7.6. XPS analysis

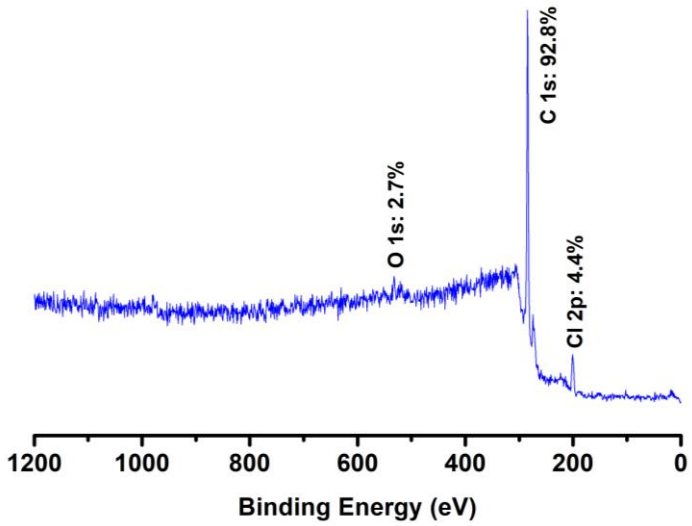

Figure 1.24. XPS spectrum of P1. The presence of oxygen is due to the sample holder being made of a silicon-based polymer.

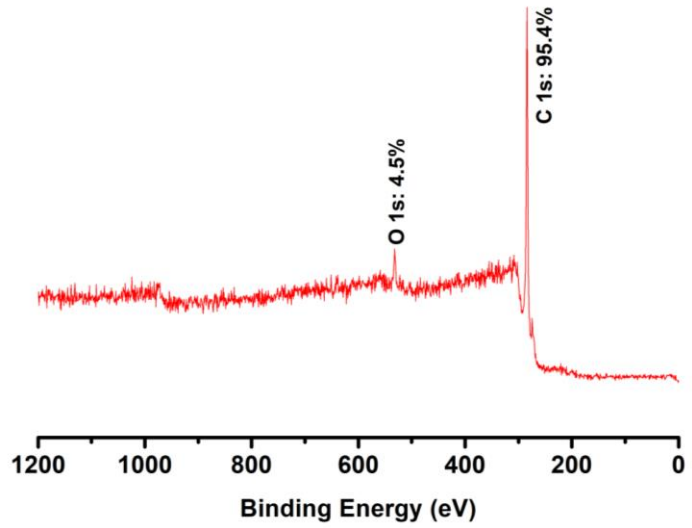

Figure 1.25. XPS spectrum of GNR1. The presence of oxygen is due to the sample holder being made of a silicon-based polymer.

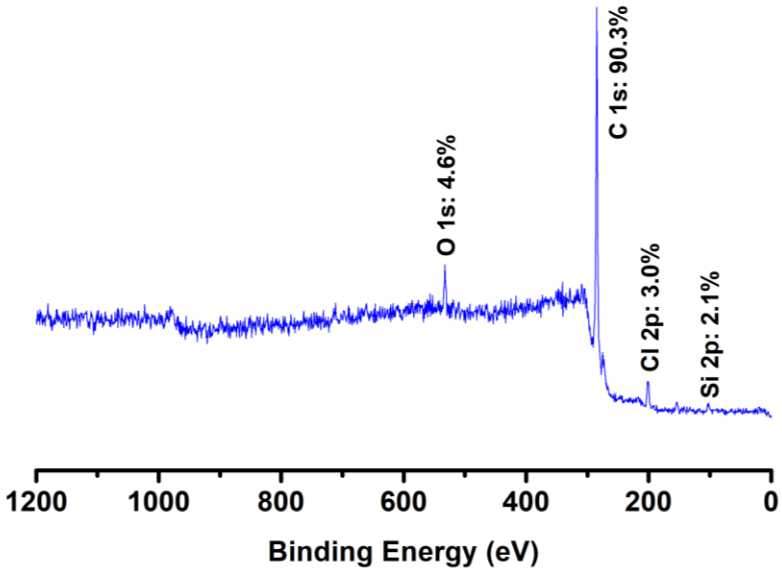

Figure 1.26. XPS spectrum of P2. The presence of silicon and oxygen is due to the sample holder being made of a silicon-based polymer.

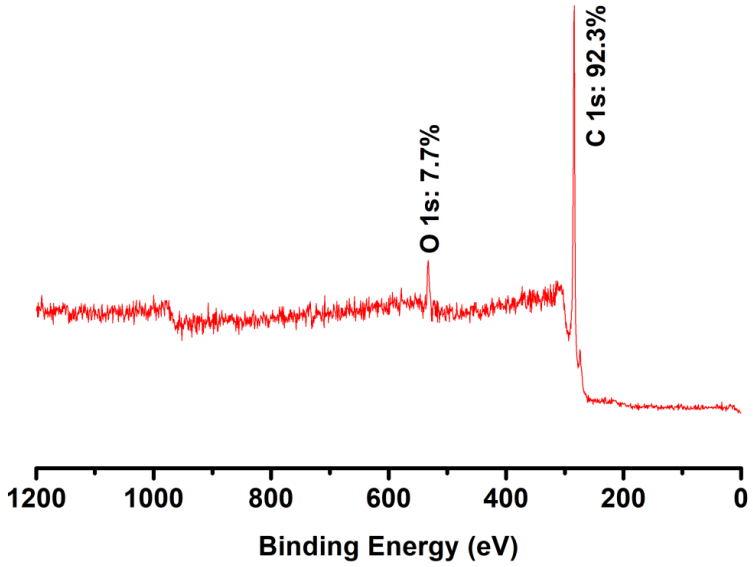

Figure 1.27. XPS spectrum of GNR2. The presence of oxygen is due to the sample holder being made of a silicon-based polymer.

1.7.7. UV-vis and photoluminescence analysis

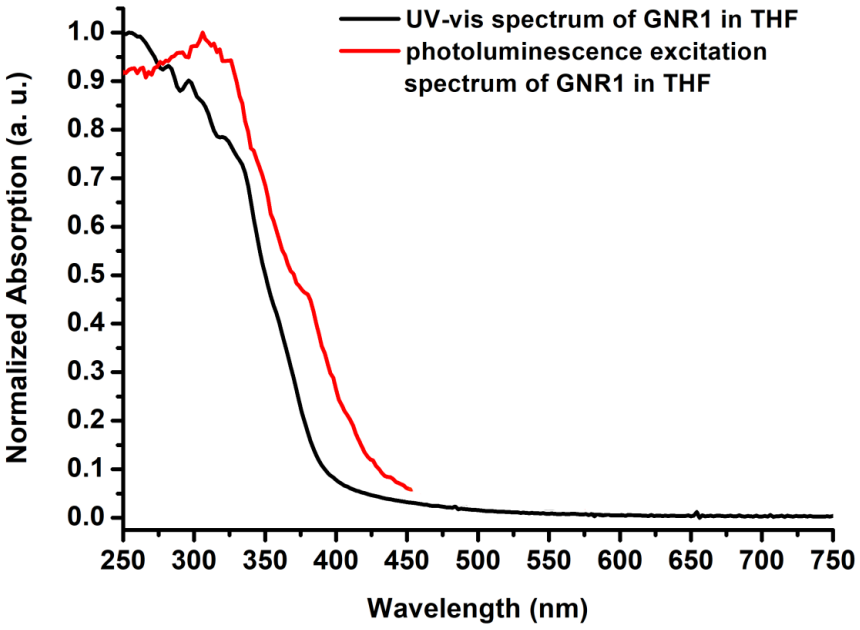

Figure 1.28. UV-vis absorption (black) and photoluminescence excitation (red, monitored at λ_{em} = 500 nm) spectra of GNR1 in THF solution.

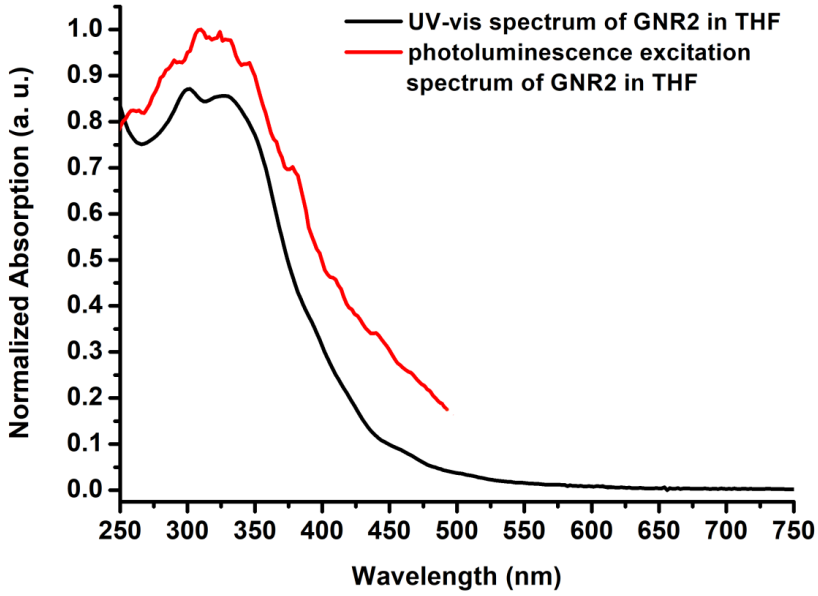

Figure 1.29. UV-vis absorption (black) and photoluminescence excitation (red, monitored at λ_{em} = 500 nm) spectra of GNR2 in THF solution.

Chapter 2. **Toward Thiophene-Annulated Graphene Nanoribbons**

Dandan Miao[a], Maxime Daigle[a], Andrea Lucotti[b], Joël Boismenu-Lavoie[a], Matteo Tommasini [b], and Jean-François Morin*[a]

a) Département de Chimie et Centre de Recherche sur les Materiaux Avancés (CERMA), Université Laval, Pavillon A.-Vachon, 1045 Ave de la Médecine, Québec QC, Canada G1V 0A6

b) Dipartimento di Chimica, Materiali e Ingegneria Chimica "G. Natta", Politecnico di Milano, Piazza Leonardo da Vinci, 32, 20133 Milano (Italy)

Accepted manuscript online on February 06, 2018.

Published in *Angewandte Chemie International Edition*, **2018**, *57*, 3588-3592.

2.1. Résumé

Des nanorubans de graphène (GNR) à base de thiophène ont été préparés à partir de poly (*p*-phénylène) polychlorés contenant du thiophène en utilisant la réaction de cyclodéhydrochloration (CDHC) photochimique sans métal. Les spectroscopies RMN ^{1}H et Raman ont confirmé les structures des GNR. La régiosélectivité de la réaction CDHC permet la préparation de GNR symétriques latéralement et asymétriques et, par conséquent, la modulation de leurs propriétés optiques et électroniques.

2.2. Abstract

Narrow thiophene-edged graphene nanoribbons (GNRs) were prepared from polychlorinated thiophene-containing poly(*p*-phenylene)s using the photochemical, metal-free cyclodehydrochlorination (CDHC) reaction. ^{1}H NMR and Raman spectroscopy confirmed the structures of the GNRs. The regioselectivity of the CDHC reaction allows the preparation of both laterally symmetrical and unsymmetrical GNRs and, consequently, the modulation of their optical and electronic properties.

2.3. Introduction

The bottom-up, solution-phase approach has been increasingly popular to prepare structurally well-defined graphene nanoribbons (GNRs) with customized electronic properties. Unlike top-down approaches, the bottom-up strategy allows a strict control over the width and edge configuration of GNRs. In the most commonly used strategy, a polyphenylene precursor undergoes a cycloaromatization reaction, called the Scholl reaction, using an oxidant-like iron (III) chloride in a polar solvent.[63,66,68,144-148] Although the Scholl reaction proved to be useful to prepare a large variety of GNRs, it can suffer from poor regioselectivity and can lead to rearrangement reactions, which are mostly due to the harsh conditions often required.[77,80,149,150] The introduction of oxidation-sensitive functional groups and electron-rich heterocycles is thus

difficult to achieve, limiting the scope and versatility of this reaction. Therefore, only electron-poor and chemically robust pyridine, pyrimidine, naphthalene monoimide, and perylene monoimide moieties can be used as edge units to modulate the electronic properties of GNRs.[85,86] Other methods, including alkyne benzannulation[89,92,101] and thermal polydiacetylene aromatization,[110,156] have been reported lately in the aim to circumvent some of the drawbacks of the Scholl reaction, but all of them have been used to prepare all-phenyl GNRs only. A milder method to prepare GNRs that will allow the introduction of a large variety of functional groups and heterocycles, both electron-poor and electron-rich, is thus highly desirable.

As a supplement to the Scholl reaction, our group recently used the photochemical intramolecular cyclodehydrochlorination (CDHC) reaction on polychlorinated polyphenylene precursors.[87,131,132] As this reaction is achieved without metal catalyst and oxidant in mild conditions, it is well-suited for the synthesis of GNRs. Moreover, it possesses excellent regioselectivity and provides nanographenes and GNRs in very good yield with minimal formation of side-products.[132]

Herein, we report the synthesis of two narrow GNRs (*o*T-GNR and *p*T-GNR), using the CDHC reaction from polychlorinated poly(*p*-phenylene) copolymers. Both structures consist of a "ladderized" poly(*p*-phenylene) polymer backbone (in blue, Figure 2.1) annulated with [2,3]thiophene units (in red, Figure 2.1). The synthesis of *o*T-GNR and *p*T-GNR shows the possibility of obtaining a laterally unsymmetrical structure, which gives rise to a permanent dipole within the GNR. This feature could be exploited to improve molecular organization by driving the dipoles to arrange in an antiparallel fashion in the solid state.[157,158] Structures and properties of *o*T-GNR and *p*T-GNR were characterized using ^{1}H NMR, UV-vis, fluorescence, and Raman spectroscopy. Density functional theory (DFT) calculations were also used to determine the most stable conformation adopted by the GNRs as well as to predict their Raman signatures theoretically.

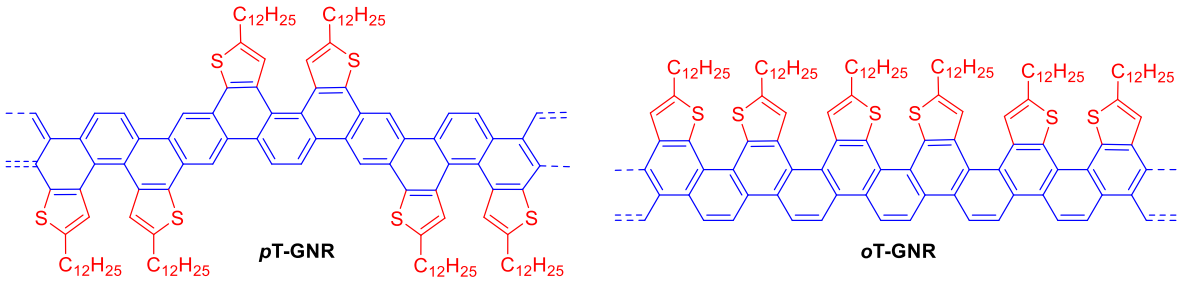

Figure 2.1. Structures of *p*T-GNR and *o*T-GNR.

2.4. Results and Discussion

2.4.1. Synthesis

Prior to the synthesis of the thiophene-edged GNRs, we undertook the synthesis of model compounds **4** and **8** to optimize the CDHC reaction conditions (Scheme 2.1). In our latest study, decahydronaphthalene (decalin) was employed for the CDHC reaction as it is stable upon UV irradiation and allows higher temperatures to be reached to overcome solubility issues, especially in case of polymers.[132] Fortunately, compound **4** was obtained in 97% yield after 40 minutes of irradiation of compound **3** (16 × 7.2 W low pressure mercury lamps, λ = 300 nm) at 100 ℃. More importantly, no side reactions were detected, even when the reaction time was extended to 48 hours to mimic the conditions used for the synthesis of the GNRs. As a comparison, we performed the reaction in benzene and acetone at room temperature, in these cases, yields of 84% and 70% were obtained, respectively. To test the reaction even further before attempting it on P2, the synthesis of an oligomer (compound **8**) from a tetrachlorinated precursor (compound **7**) was accomplished. While the reaction was slower than that for compound **4**, it went to completion after 48 hours of irradiation at 300 nm and no side-products were detected. The slow rate of formation for oligomer **8** compared to model compound **4** might be attributed to a less efficient photochemical reaction (lower quantum yield) owing to the lower band gap of oligomer **8**. Although this did not prevent us in successfully preparing different GNRs, it might be an issue for the synthesis of low band-gap materials.

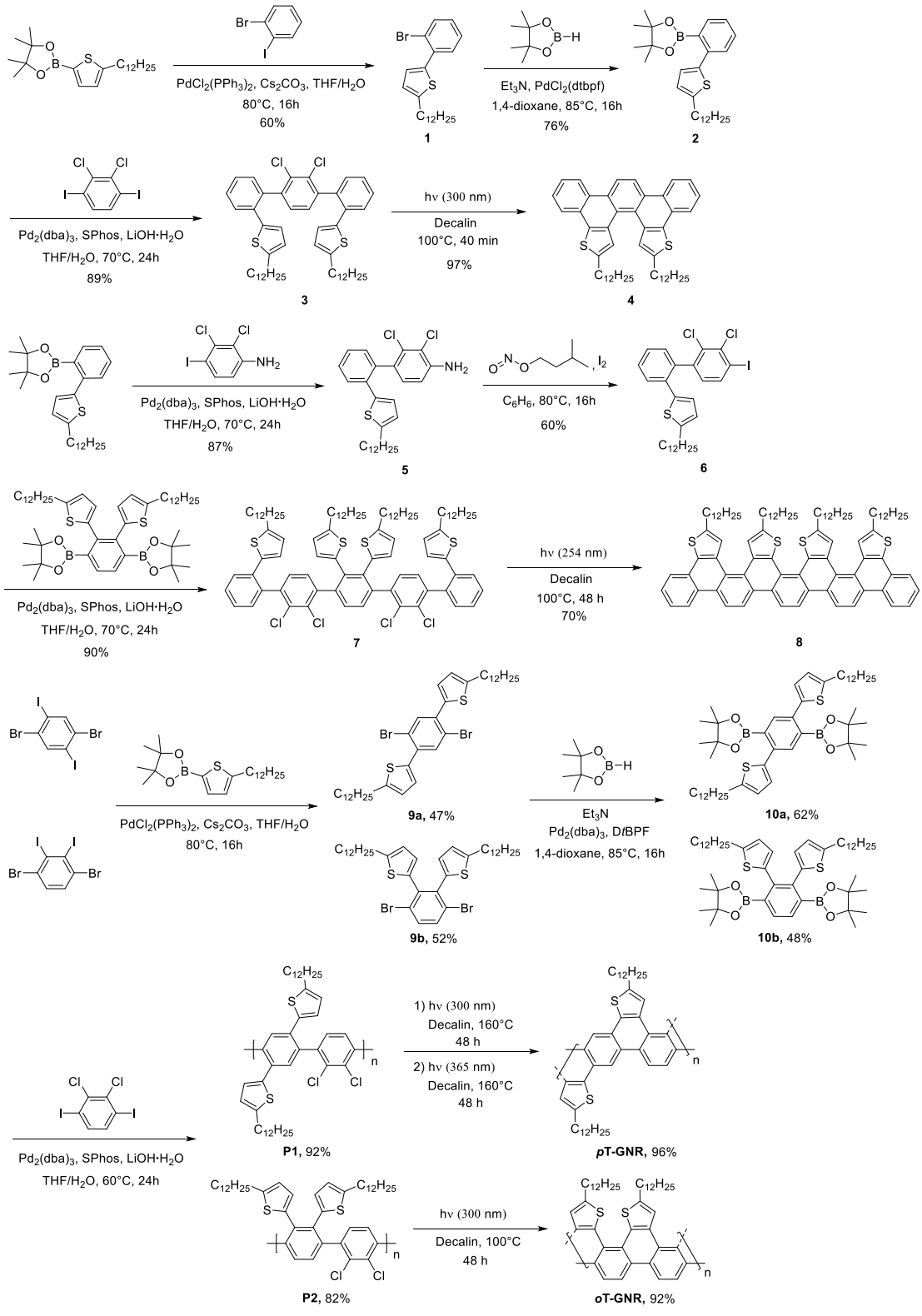

Scheme 2.1. Synthesis of piceno[5,6-b:8,7-b']dithiophene model compound **4**, oligomer **8**, *p*T-GNR, and *o*T-GNR.

Both *o*T-GNR and *p*T-GNR were prepared using a copolymer strategy as shown in Scheme 3.1. 5-Dodecylthiophene-2-boronic acid pinacol ester[159] was coupled to 1,4-dibromo-2,5-diiodobenzene[160] and 1,4-dibromo-2,3-diiodobenzene[161-163] to give compounds **9a** (47%) and **9b** (52%), respectively. Palladium-catalyzed borylation using 4,4,5,5-tetramethyl-1,3,2-dioxaborolane provided monomers **10a** (62%) and **10b** (48%), which were coupled to 1,4-diiodo-2,3-dichlorobenzene[164] in Suzuki–Miyaura conditions to afford P1 (92%) and P2 (82%). The Pd_2dba_3/SPhos catalyst system was used in both cases as it leads to low amount of defects when used for the polymerization of *meta*-linked polyphenylene.[165] P1 and P2 were purified by precipitation in methanol followed by a Soxhlet extraction with acetone to remove the low-molecular-weight fractions and catalyst residues.

For the synthesis of *p*T-GNR and *o*T-GNR, the precursors were dissolved in decalin at a concentration of 0.002 M and irradiated using UV light (16 × 7.2 W low pressure mercury lamps, λ = 300 nm) for 48 hours under a stream of argon at 160 and 100 ℃, respectively. During irradiation, the P1 solution turned brown and became fluorescent yellow. At this stage, ^{1}H NMR analysis of the resulting polymer suggested that the CDHC reaction was not complete. Thus, the resulting polymer was placed back again in the photoreactor and irradiated with the λ = 365 nm lamps (16 × 7.2 W low pressure mercury lamps) at 160 ℃ for an additional 48 hours. Fortunately, this additional time under a lower-energy wavelength allowed to complete the CDHC reaction, as observed by ^{1}H NMR spectroscopy (see below). In the case of P2, the solution turned from pale yellow to orange with green-yellow fluorescence upon irradiation at 300 nm, indicating a decrease of the band gap as expected upon planarization. In this case, the CDHC reaction was complete after irradiation for 48 hours at 300 nm. After the removal of a large volume of decalin, both *p*T-GNR and *o*T-GNR were precipitated and washed with hexanes using a Soxhlet apparatus to provide black and brownish solid, respectively, that can be readily solubilized in $CHCl_3$ and THF.

2.4.2. Size-exclusion chromatography (SEC) analysis

Size-exclusion chromatography (SEC) was used to determine the molecular weight of the GNRs and their precursors. Polystyrene and 1,2,4-trichlorobenzene were used as standard and eluent, respectively. As is shown in Figure 2.2, for P1 and P2, number-average molecular weight ($\overline{M}$n) values of 9700 and 9500 g mol^{-1} were measured, respectively, corresponding to 13 repeating units in each case. Upon irradiation, both $\overline{M}$n values increased significantly to 20 800 and 27 700 g mol^{-1}, which is attributed to the stiffening of the main chain after CDHC reaction and a dramatic change of the hydrodynamic radius. Such an increase in $\overline{M}$n values has been previously reported for GNRs and ladder conjugated polymers obtained from polyphenylene precursors.[90,143]

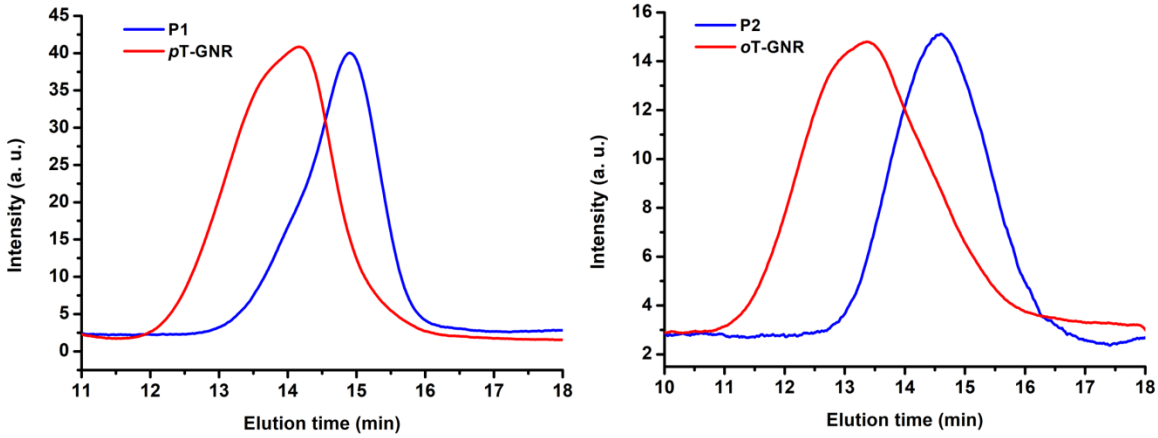

Figure 2.2. Size exclusion chromatography traces for P1 ($\overline{M}$n: 9 700 g mol^{-1}, $\overline{M}$w: 13 900 g mol^{-1}, dispersity index ($Đ$): 1.4, X_n: 13), *p*T-GNR ($\overline{M}$n = 20 800 g mol^{-1}, $\overline{M}$w = 38 200 g mol^{-1}, dispersity index ($Đ$): 1.8), P2 ($\overline{M}$n: 9 500 g mol^{-1}, $\overline{M}$w: 17 100 g mol^{-1}, dispersity index ($Đ$): 1.8, X_n: 13), and *o*T-GNR ($\overline{M}$n = 27 700 g mol^{-1}, $\overline{M}$w = 81 700 g mol^{-1}, dispersity index ($Đ$): 2.9).

2.4.3. ^{1}H NMR analysis

The ^{1}H NMR analysis of *o*T-GNR and *p*T-GNR and their precursors (P2 and P1) have been conducted and the results are shown in Figure 2.3. As expected for rigid polymers, P2 exhibits broad, undefined peaks compared to its monomeric units. The two protons H_a and H_b attached

to thiophene produce peaks between δ = 6.1 and 6.5 ppm, while phenyl protons H_c and H_d give peaks at δ = 6.9 and 7.3 ppm, respectively. After the CDHC reaction, which produce a more rigid *o*T-GNR, all the peaks of the ^{1}H NMR spectrum broadened and shifted downfield, especially the peaks located in the aromatic region, as previously observed for other types of GNRs.[66] Also, the peaks in the δ = 6.1-6.5 ppm region completely disappeared, suggesting a nearly complete CDHC conversion. Interestingly, the resonances of H_c' and H_d' in *o*T-GNR are significantly shielded (δ = 7.5-8.0 ppm) compared to the bay region protons (armchair edge) of other molecules reported (δ > 8.8 ppm).[78,152,166] This difference can be ascribed to the highly contorted conformation of *o*T-GNR, resulting in a decreased steric repulsion between both protons of the bay region and, consequently, to a weaker dispersion interaction. This phenomenon has been reported before for other contorted and curved molecules in which the protons of the bay region are not facing each other in the same plane ($\theta_{dihedral} > 0$).[167] For *p*T-GNR, similar behavior was observed upon CDHC reaction on P1. All of the aromatic protons shifted downfield to give four broadened peaks between 6.8 and 9.0 ppm. No peak attributed to P1 can be found in the spectrum of *p*T-GNR, meaning that the reaction went to near completion.

2.4.4. UV-vis and photoluminescence analysis

The optical properties of model compounds **4** and **8**, *p*T-GNR and *o*T-GNR were determined using UV-vis and fluorescence spectroscopy and the results are summarized in Figure 2.4 and the Supporting Information, Figures 2.34-2.37. In solution, *o*T-GNR exhibits a very sharp absorption band with a maximum (λ_{max}) at 294 nm, which is red-shifted compared to the oligomer **8** (λ_{max} = 260 nm; Supporting Information, Figure 2.36). The absorption profile of *o*T-GNR is very comparable to that reported by Swager et al. for a similar ladder poly(*p*-phenylene).[90] The band gap value for *o*T-GNR (2.91 eV), measured at the low-energy onset of the absorption band, is quite high compared to other ladder-type polymers or GNRs, but lower than those observed for very narrow unsubstituted [*n*]phenacene derivatives (*ca*. 3.0

eV).[168] The slightly lower band gap of *o*T-GNR can be attributed to the presence of electron-rich thiophene units on the edge of the [*n*]phenacene backbone. Remarkably, the solid-state absorption spectrum is only slightly broader than that in solution, meaning that very weak intermolecular π interactions take place in the solid state. UV-vis analysis in solution showed that the spectrum of *o*T-GNR is concentration-independent, ruling out the possibility of aggregation in solution to explain such a similarity between the two spectra. The similar UV-vis spectrum in both states also suggests that very few conformational changes occurred upon aggregation, which is consistent with a highly rigid backbone. Similar behavior has been observed recently for carbazole-based conjugated ladder polymers.[154] Interestingly, *p*T-GNR possesses a much broader absorption band with a λ_{max} value of 390 nm and a band gap of 2.61 eV. The lower band gap of *p*T-GNR compared to *o*T-GNR can be attributed to a better electronic communication between the thiophene units (*para* versus *ortho*) and the presence of an acene moiety (anthracene) within the backbone. Similar to *o*T-GNR, the solid-state spectrum is very comparable to that in solution, proving the rigid nature of *p*T-GNR. Both *o*T-GNR and *p*T-GNR are photoluminescent in solution and exhibit featureless emission band peaking at 500 and 560 nm, respectively (Figure 2.4, insets) with quantum yield (ϕ_F) of 3 and 6 %, respectively. Time-resolved photoluminescence spectroscopy have been performed and fluorescence lifetime values of 1.1 and 1.7 ns have been measured for *o*T-GNR and *p*T-GNR, respectively, which is in the same order of magnitude as that measured for all-phenyl GNRs (Supporting Information, Figures 2.38 and 2.39).[155] The Stokes shift in solution for both *o*T-GNR and *p*T-GNR are relatively large (206 and 170 nm, respectively) and in the same range as that observed for ladder conjugated polymers with a poly(*para*-phenylene) backbone.[90] Notably, the fluorescence excitation spectrum of both *p*T-GNR and *o*T-GNR matches well with the absorption spectra, meaning that the emission originated from the GNRs (Supporting Information, Figures 2.34 and 2.35).[155]

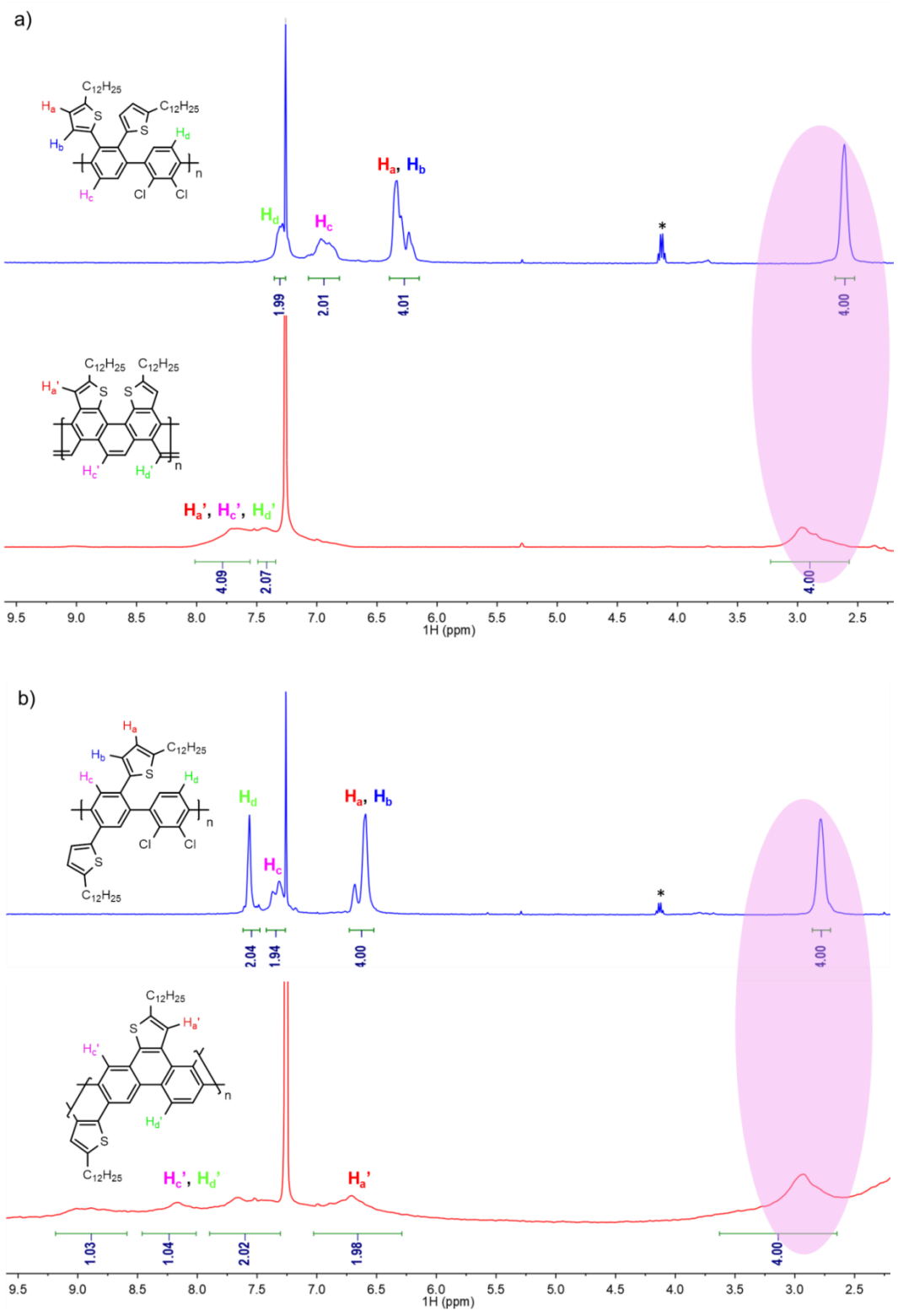

Figure 2.3. a) ^{1}H NMR spectra of precursor P2 (top) and *o*T-GNR (bottom) in $CDCl_3$ at 60 ℃. b) ^{1}H NMR spectra of precursor P1 (top) and *p*T-GNR (bottom) in $CDCl_3$ at 60 ℃.

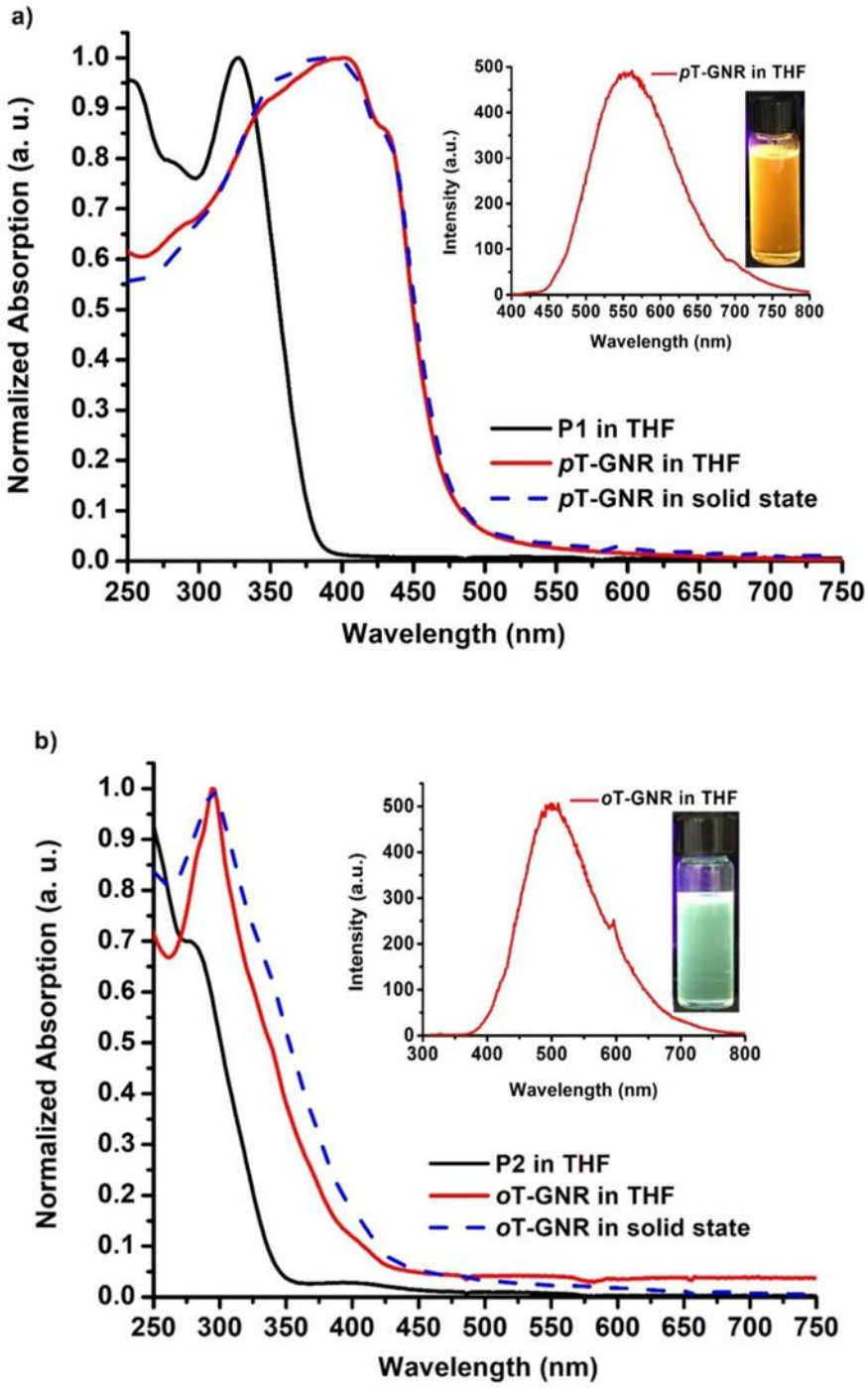

Figure 2.4. UV-vis absorption spectra of a) P1 and *p*T-GNR and b) P2 and *o*T-GNR in both solution (THF, solid lines) and solid state (dashed lines). Insets: Photoluminescence spectra of a) *p*T-GNR (λ_{ex} = 400 nm) and b) *o*T-GNR (λ_{ex} = 300 nm) in THF solution.

2.4.5. DFT calculations

Both *o*T-GNR and *p*T-GNR have a contorted structure and can adopt different conformations. To study the different conformers and their relative energy, DFT calculations have been performed. Calculations suggest that *p*T-GNR adopts a very rigid geometry due to the steric congestion at the thiophene H-contorted region (Supporting Information, Figure 2.40) for which the inversion into the other isomer is not possible. On the contrary, *o*T-GNR may adopt several geometries. As shown on Figure 2.5, steric congestion in the S-contorted region of the polymer forces whether a helical (C1) or an alternated (C5) conformation occurs. According to calculations, alternated C5 is predicted to be more stable (ΔG = -13.2 kcal mol^{-1}) than its fully twisted counterpart. Moreover, QST3 calculations have been conducted to investigate the activation energy of the system to rotate a thiophene moiety from one side of the polymer plan to the other, eventually leading to the twisted C1. Transition-state energies of 7.2 and 9.4 kcal mol^{-1} for C2 (TS1) and C4 (TS2) were obtained, respectively (Figure 2.5). These results suggest that *o*T-GNR and oligomer **8** can undergo a conformational change in solution at room temperature, contributing to some extent to the line broadening of the ^{1}H NMR spectrum of both compounds.

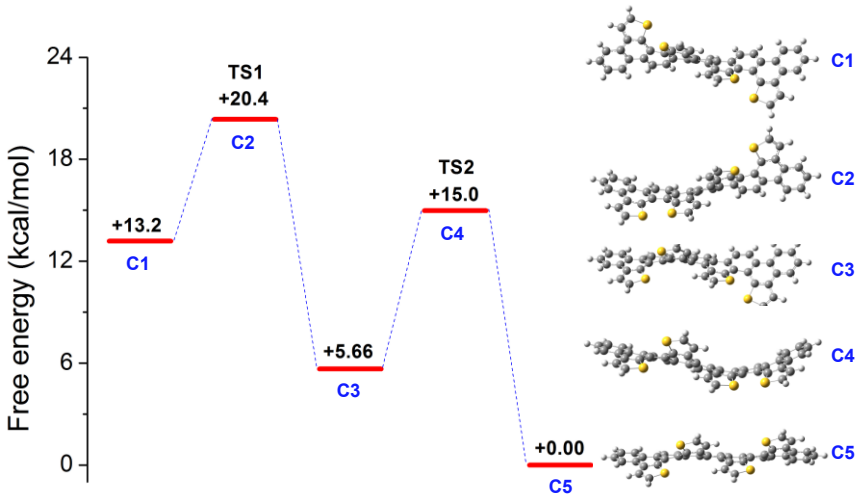

Figure 2.5. Free energy of different conformers of *o*T-GNR and their transition states as determined by DFT calculations.

2.4.6. Raman analysis and DFT calculations

*o*T-GNR and *p*T-GNR have been characterized with Raman spectroscopy and DFT calculations aimed at the interpretation of the main observed lines. The results are shown in Figure 2.6, where the FT-Raman spectra of *o*T-GNR and *p*T-GNR are compared to the corresponding spectra simulated by DFT on selected model oligomers. The signatures expected for graphene nanoribbons over the G and D region are clearly observed for both *o*T-GNR (G: 1591 cm^{-1}; D: 1360 cm^{-1}) and *p*T-GNR (G: 1610 cm^{-1}; D: 1368 cm^{-1}). These Raman lines match well with the results from DFT calculations, and an inspection of the associated nuclear displacement patterns (Supporting Information, Figures 2.41-2.43) supports the assignment of these Raman lines to the G and D features of *o*T-GNR and *p*T-GNR. The observed Raman spectra and their very good match against DFT calculations on suitable molecular models support the successful synthesis of *o*T-GNR and *p*T-GNR.

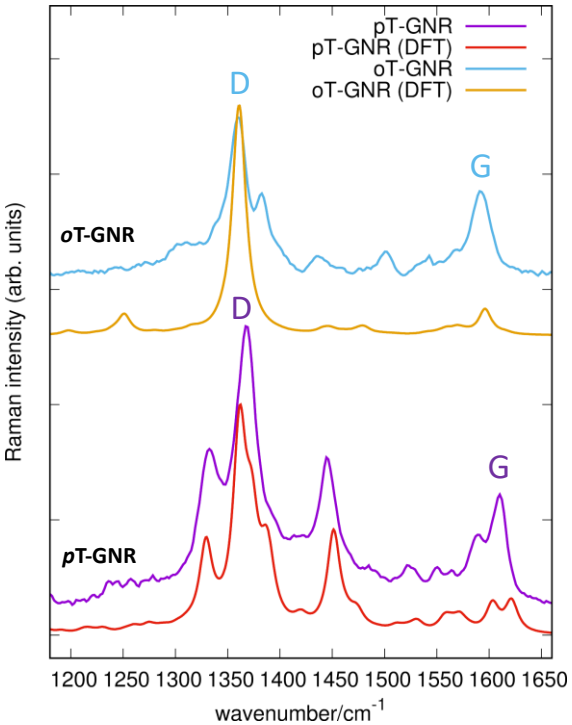

Figure 2.6. FT-Raman spectra of *o*T-GNR and *p*T-GNR compared with results from DFT calculations. The G and D features characteristic of graphene nanoribbons are identified.

2.5. Conclusion

In conclusion, we showed that the cyclodehydrochlorination reaction (CDHC) can be used to prepare well-defined thiophene-edge graphene nanoribbons regioselectively from thiophene-containing polychlorinated poly(*p*-phenylene) precursors. ^{1}H NMR analysis shows that the CDHC reaction went to near completion and Raman spectroscopy corroborates the structural integrity of both GNRs. Also, optical characterization showed that the position of the thiophene units on the edge of the nanoribbons plays a critical role in the electronic properties of the GNR. The synthesis of wider thiophene-edge graphene nanoribbons is now underway to test the efficiency of the CDHC reaction for the preparation of low band-gap GNRs.

2.6. Acknowledgements

This work was supported by NSERC through a Discovery Grant. D.M. thanks the China Scholarship Council (CSC) for a PhD scholarship. The authors thank Prof. Claudine Allen (Centre d'Optique Photonique et Laser, Université Laval) for her precious help for the measurements of quantum yields and Yannick Ledemi, Samuel Ouellet and Prof. Denis Boudreau (Département de chimie, Université Laval) for their gracious help for time-resolved photoluminescence spectroscopy measurements.

2.7. Supporting Information

2.7.1. Materials and Methods

Chemical reagents were purchased from Sigma-Aldrich Co. Canada, Alfa Aesar Co., TCI America Co. or Oakwood Products Inc. and used as received, unless mentioned. Solvents used for organic synthesis were purchased from Fisher Chemical Co., EMD Millipore Co. and CFS Chemical Co. as HPLC grade. These solvents were degassed, dried and purified using a Solvent Purifier System (SPS) (Vacuum Atmosphere Co., Hawthorne, USA). Anhydrous decahydronaphthalene (mixture of *cis* + *trans*) was used as received for photochemical reactions and other anhydrous solvents were bought from Sigma-Aldrich Co. Canada. All anhydrous and air sensitive reactions were performed in oven-dried glassware purchased from Synthware™ under positive nitrogen stream. Analytical thin-layer chromatographies were performed with silica gel 60 F254, 0.25 mm pre-coated TLC plates (Silicycle, Québec, Canada). Compounds were revealed by a 254 nm and/or 365 nm UV wavelength and/or aqueous K_2CO_3 and NaOH solution of potassium permanganate. Flash column chromatographies were performed with 230-400 mesh silica gel R10030B (Silicycle, Québec, Canada). 5-dodecylthiophene-2-boronic acid pinacol ester, 1,4-dibromo-2,5-diiodobenzene, 1,4-dibromo-2,3-diiodobenzene and 1,4-diiodo-2,3-dichlorobenzene were synthesized according to literature procedures.[159-164]

2.7.2. Apparatus

Photochemical reactions were performed in a CCP-ICH2 Luzchem® photochemical reactor equipped with a thermostat and a heating mantle. Photochemical reactions were performed in a 100 mL quartz round-bottom flask bought from Chemglass®. Nuclear magnetic resonance (NMR) spectra were recorded on a Varian Inova AS400 spectrometer (Varian, Palo Alto, USA) at 400 MHz (^{1}H) and 100 MHz (^{13}C). Signals are reported as m (multiplet), s (singlet), d (doublet), t (triplet), and coupling constants are reported in hertz (Hz). Chemical shifts are

reported as values ppm (δ) relative to residual solvent peak. High resolution mass spectra (HRMS) were recorded with an Agilent 6210 Time-of-Flight (TOF) LC-MS apparatus equipped with an APPI ion source (Agilent Technologies, Toronto, Canada). Number-average ($\overline{Mn}$) and weight-average ($\overline{Mw}$) molecular weights were determined by size-exclusion chromatography (SEC) using a Varian Polymer Laboratories GPC220 equipped with an RI detector and a PL BV400 HT Bridge Viscometer. The column set consists of 2 PL gel Mixed C (300 × 7.5 mm) columns and a PL gel Mixed C guard column. The flow rate was fixed at 1mL min^{-1} using 1,2,4-trichlorobenzene (TCB) (with 0.0125% BHT w/v) as the eluent. The temperature of the system was set to 110 ℃. All the samples were prepared at a nominal concentration of 1.0 mg mL^{-1} in TCB. Dissolution was performed using a Varian Polymer Laboratories PL-SP 260VC sample preparation system. The sample vials were held at 110 ℃ with shaking for 1 h for complete dissolution. The solutions were filtered through a 2 mm porous stainless steel filter and a 0.40 μm glass filter into a 2 mL chromatography vial. The calibration method used to generate the reported data was the classical polystyrene method using polystyrene narrow standards Easi-Vials PS-M from Varian Polymer Laboratories which were dissolved in TCB. UV-visible absorption and photoluminescence spectra were recorded on a UV-vis HP 8452 spectrophotometer and a Varian Cary Eclipse Fluorescence Spectrofluorimeter, respectively, using 10-mm path length quartz cells. For solid state measurements, the polymer solution (1.0 mg mL^{-1} in THF) was spin coated on quartz plates. Optical bandgaps were calculated from the onset of the absorption band. Quantum yields values were determined using an integration sphere (QE-CA-10309 (Spectraflect coating) by SphereOptics) equipped with a 405 nm laser diode as the excitation source. FT-Raman spectra were recorded using a Nicolet NXR 9650 instrument equipped with Nd-VO4 laser (1064 nm), and a InGaAs detector. The FT-Raman spectra were recorded using unpolarized light in the backscattering geometry. The resolution is 4 cm^{-1} for all reported spectra. With reference to the spectra of solid powders reported in Figure 3.6, power at the sample was on the order of 140 mW for *o*T-GNR and 72 mW for *p*T-GNR on a laser spot diameter of approximately 50 μm; 2048 (4096) scans were accumulated for

*o*T-GNR (*p*T-GNR).

2.7.3. Synthesis

2-(2-bromophenyl)-5-dodecylthiophene (1)

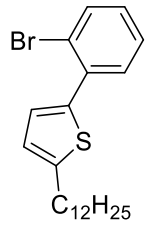

1

A round bottom flask was flushed three times with a vacuum/nitrogen cycle, charged with 2-(5-dodecyl-2-thienyl)-4,4,5,5-tetramethyl-1,3,2-dioxaborolane (1.50 g, 4.00 mmol), 1-bromo-2-iodobenzene (1.12 g, 4.00 mmol), cesium carbonate (5.16 g, 15.8 mmol), THF (40.0 mL) and H_2O (10.0 mL). The reaction mixture was flushed three times with a vacuum/nitrogen cycle again and degassed with a nitrogen stream for 10 mins. Bis(triphenylphosphine)palladium(II) dichloride (0.278 g, 0.400 mmol) was added to the reaction mixture and further degassed with nitrogen for another 5 mins. The mixture was heated to 80 ℃ for 16 h. Once cooled to room temperature, 15 mL of an aqueous saturated NH_4Cl solution was added and the aqueous layer was extracted with ethyl acetate (3 × 30 mL). The organic layer was dried with Na_2SO_4 and the solvent was removed under reduced pressure. The resulting residue was purified by silica gel chromatography with hexanes to yield compound **1** as a colorless oil (0.966 g, 60 %). ^{1}H NMR (400 MHz, $CDCl_3$): δ 7.70 (d, *J* = 3.69 Hz, 1H), 7.52 (d, *J* = 3.92 Hz, 1H), 7.34 (t, *J* = 7.65 Hz, 1H), 7.21 (d, *J* = 1.62 Hz, 1H), 7.17 (t, *J* = 7.38 Hz, 1H), 6.83 (d, *J* = 1.69 Hz, 1H), 2.88 (t, *J* = 7.68 Hz, 2H), 1.77 (m, 2H), 1.36 (m, 18H), 0.97 (t, *J* = 7.04 Hz, 3H). ^{13}C NMR (100 MHz, $CDCl_3$): δ 146.84, 138.99, 135.63, 133.68, 131.64, 128.43, 127.51, 127.26, 123.92, 122.53, 77.16, 32.06, 31.64, 30.24, 29.79, 29.50, 29.25, 22.75, 14.24. HRMS (APPI+): calculated for $C_{22}H_{31}BrS$ $(M)^+$ 406.13298, found 406.13130.

2-(2-(5-dodecylthiophen-2-yl)phenyl)-4,4,5,5-tetramethyl-1,3,2-dioxaborolane (2)

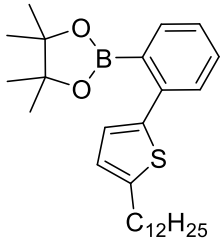

2

An oven-dried round bottom flask was flushed three times with a vacuum/nitrogen cycle. Compound **1** (0.611 g, 1.50 mmol), anhydrous 1,4-dioxane (7.50 mL) and 1,1'-bis(di-*t*-butylphosphino)ferrocene palladium dichloride (39.1 mg, 60.0 μmol) were added and the flask was flushed three times again with a vacuum/nitrogen cycle. Triethylamine (0.840 mL, 6.00 mmol) was degassed with a nitrogen stream for 10 mins and then added into the reaction flask. 4,4,5,5-Tetramethyl-1,2,3-dioxaborolane (0.435 mL, 3.00 mmol) was filtered through a 0.45 μm syringe filter and added dropwise to the reaction mixture. The flask was flushed three times with a vacuum/nitrogen cycle and heated at 85 ℃ for 16 h. Once cooled to room temperature, 10 mL of a saturated aqueous solution of NH_4Cl was added and the aqueous layer was extracted with ethyl acetate (3 × 20 mL). The organic layer was dried with Na_2SO_4 and the solvent was removed under reduced pressure. The crude product was purified by silica gel chromatography (5% Et_2O/hexanes) to yield compound **2** as a white solid (0.515 g, 76%). ^{1}H NMR (400 MHz, $CDCl_3$): δ 7.62 (d, 1H, *J* = 3.67 Hz), 7.42 (d, 1H, *J* = 3.76 Hz), 7.39 (t, 1H, *J* = 7.43 Hz), 7.28 (t, 1H, *J* = 7.24 Hz), 6.90 (d, 1H, *J* = 1.72 Hz), 6.70 (d, 1H, *J* = 1.65 Hz), 2.82 (t, 2H, *J* = 7.56 Hz), 1.70 (m, 2H), 1.29 (m, 30H), 0.89 (t, 3H, *J* = 7.04 Hz). ^{13}C NMR (100 MHz, $CDCl_3$): δ 146.48, 142.81, 140.17, 134.69, 130.40, 129.65, 126.96, 126.09, 124.55, 84.27, 77.16, 32.39, 32.29, 30.69, 30.15, 30.14, 30.11, 30.06, 29.88, 29.83, 29.58, 25.15, 23.16, 14.60. HRMS (APPI+): calculated for $C_{28}H_{43}BO_2S$ $(M + H)^+$ 453.30932, found 453.31131.

5,5'-(2',3'-dichloro-[1,1':4',1''-terphenyl]-2,2''-diyl)bis(2-dodecylthiophene) (3)

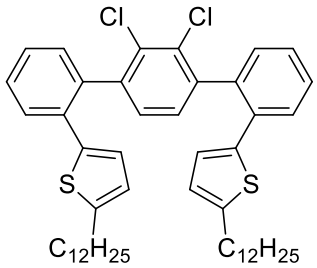

3

A round bottom flask under nitrogen was charged with compound **2** (0.400 g, 0.900 mmol), 2,3-dichloro-1,4-diiodobenzene (0.160 g, 0.400 mmol), LiOH•H_2O (0.134 g, 3.20 mmol), THF (2.00 mL) and H_2O (0.500 mL), flushed three times with a vacuum/nitrogen cycle and degassed with a nitrogen stream for 10 mins. $Pd_2(dba)_3$ (20.7 mg, 19.0 μmol) and SPhos (32.8 mg, 80.0 μmol) were added and the reaction flask was degassed with nitrogen for another 5 mins. The reaction mixture was heated to 70 ℃ for 24 h. Once cooled down to room temperature, 10 mL of a saturated aqueous solution of NH_4Cl was added and the aqueous layer was extracted with ethyl acetate (3 × 20 mL). The organic layer was dried with Na_2SO_4 and the solvent was removed under reduced pressure. The resulting residue was purified by silica gel chromatography (5% CH_2Cl_2/hexanes) to obtain compound **3** as a light yellow solid (0.280 g, 89%). ^{1}H NMR (400 MHz, $CDCl_3$): δ 7.60 (m, 2H), 7.43 (m, 2H), 7.35 (m, 2H), 7.29 (m, 2H), 7.15 (s, 1H), 7.11 (s, 1H), 6.58 (m, 3H), 6.46 (d, *J* = 1.68 Hz, 1H), 2.78 (m, 4H), 1.68 (m, 4H), 1.26 (m, 36H), 0.91 (t, *J* = 7.12 Hz, 6H). ^{13}C NMR (100 MHz, $CDCl_3$): δ 147.08, 146.58, 142.11, 140.10, 140.07, 137.74, 137.67, 134.46, 134.25, 133.38, 133.34, 131.30, 131.24, 130.10, 129.92, 129.75, 129.72, 128.92, 128.89, 127.34, 127.29, 126.71, 126.45, 124.62, 124.55, 77.16, 32.40, 32.11, 32.09, 30.67, 30.55, 30.17, 30.14, 30.09, 30.05, 29.91, 29.87, 29.85, 29.84, 29.69, 29.55, 23.17, 14.61. HRMS (APPI+): calculated for $C_{50}H_{64}Cl_2S_2$ $(M + H)^+$ 798.38265, found 798.37965.

6,9-didodecylpiceno[5,6-b:8,7-b']dithiophene (4)

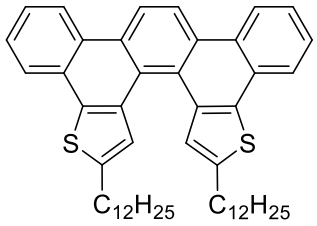

4

An oven-dried quartz flask was flushed three times with a vacuum/nitrogen cycle and charged with compound **3** (80.0 mg, 0.100 mmol) and anhydrous decahydronaphthalene (50.0 mL). The flask was degassed with a nitrogen stream for 10 mins and the reaction solution was irradiated at 300 nm at 100 ℃ for 40 minutes with a constant stream of argon. Once cooled down to room temperature, the solvent was removed by vacuum distillation and the resulting residue was further purified by silica gel chromatography (25% CH_2Cl_2/hexanes) to yield compound **4** as a yellow solid (68.9 mg, 97%). ^{1}H NMR (400 MHz, $CDCl_3$): δ 8.72 (m, 4H), 8.17 (m, 2H), 7.66 (m, 4H), 7.57 (s, 2H), 2.90 (t, *J* = 7.50 Hz, 4H), 1.76 (m, 4H), 1.25 (m, 36H), 0.88 (t, *J* = 6.68 Hz, 6H). ^{13}C NMR (100 MHz, $CDCl_3$): δ 143.66, 136.70, 135.22, 129.16, 129.12, 128.44, 127.60, 126.47, 126.43, 125.66, 124.65, 124.21, 121.62, 77.16, 32.43, 32.33, 31.26, 30.21, 30.16, 30.09, 30.02, 29.87, 29.72, 23.19, 14.62. HRMS (APPI+): calculated for $C_{50}H_{62}S_2$ $(M + H)^+$ 726.42929, found 726.43100.

2,3-dichloro-2'-(5-dodecylthiophen-2-yl)-[1,1'-biphenyl]-4-amine (5)

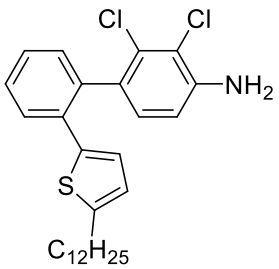

5

A round bottom flask under nitrogen was charged with compound **2** (1.47 g, 3.00 mmol), 2,3-dichloro-4-iodoaniline (0.850 g, 3.00 mmol), $LiOH \cdot H_2O$ (0.991 g, 23.0 mmol), THF (15.0 mL) and H_2O (3.70 mL), flushed three times with a vacuum/nitrogen cycle and degassed with a nitrogen stream for 10 mins. $Pd_2(dba)_3$ (0.135 g, 14.7 mmol) and SPhos (0.242 g, 59.0 mmol) were added and the reaction flask was degassed with nitrogen for another 5 mins. The reaction mixture was heated to 70 ℃ for 24 h. Once cooled down to room temperature, 30 mL of a saturated aqueous solution of NH_4Cl was added and the aqueous layer was extracted with ethyl acetate (3 × 50 mL). The organic layer was dried with Na_2SO_4 and the solvent was removed under reduced pressure. The resulting residue was purified by silica gel chromatography (15% EtOAc/hexanes) to obtain compound **5** as a dark brown oil (1.25 g, 87%). ^{1}H NMR (400 MHz, $CDCl_3$): δ 7.61 (d, *J* = 7.71 Hz, 1H), 7.41 (t, *J* = 7.56 Hz, 1H), 7.33 (t, *J* = 7.41 Hz, 1H), 7.27 (d, *J* = 7.72 Hz, 1H), 6.96 (d, *J* = 8.20 Hz, 1H), 6.67 (d, *J* = 8.30 Hz, 1H), 6.60 (d, *J* = 3.54 Hz, 1H), 6.57 (d, *J* = 3.59 Hz, 1H), 4.21 (s, 2H), 2.74 (t, *J* = 7.85 Hz, 2H), 1.64 (m, 2H), 1.31 (m, 18H), 0.94 (t, *J* = 7.80 Hz, 3H). ^{13}C NMR (100 MHz, $CDCl_3$): δ 146.34, 143.76, 140.06, 137.52, 134.42, 132.76, 131.52, 131.45, 129.85, 129.30, 128.12, 126.83, 125.87, 124.12, 117.84, 113.48, 77.16, 32.04, 31.62, 30.11, 29.80, 29.77, 29.69, 29.48, 29.16, 22.84, 14.26. HRMS (APPI+): calculated for $C_{28}H_{35}Cl_2NS$ $(M + H)^+$ 487.18673, found 487.19127.

2-(2',3'-dichloro-4'-iodo-[1,1'-biphenyl]-2-yl)-5-dodecylthiophene (6)

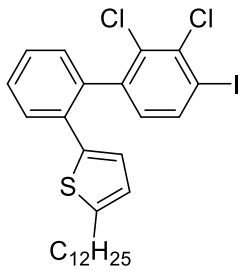

6

A two-necked round bottom flask equipped with a reflux condenser under nitrogen was charged

with compound **5** (1.02 g, 2.00 mmol) and benzene (14.7 mL) and was flushed three times with a vacuum/nitrogen cycle. The solution was degassed using a continuous flow of nitrogen for 10 mins before iodine (2.64 g, 10.0 mmol) was added. Iso-amylnitrite (0.340 mL, 2.40 mmol) was added dropwise and the flask was flushed three times with a vacuum/nitrogen cycle and heated at 80 ℃ for 16 h. Once cooled, the reaction mixture was diluted with chloroform (50 mL), treated with sodium bisulfite (50 mL), washed with water (3 × 30 mL) and brine (50 mL). The aqueous layer was extracted three times with chloroform and the organic phases were combined and dried over Na_2SO_4. The solvent was evaporated under reduced pressure and the crude product was purified by silica gel chromatography using hexanes as the eluent to afford compound **6** as a colorless oil (0.726 g, 60%). ^{1}H NMR (400 MHz, $CDCl_3$): δ 7.75 (d, *J* = 8.23 Hz, 1H), 7.61 (d, *J* = 8.13 Hz, 1H), 7.44 (t, *J* = 7.83 Hz, 1H), 7.36 (t, *J* = 7.54 Hz, 1H), 7.24 (d, *J* = 7.64 Hz, 1H), 6.89 (d, *J* = 7.80 Hz, 1H), 6.57 (d, *J* =3.57 Hz, 1H), 6.55 (d, *J* = 3.30 Hz, 1H), 2.75 (t, *J* = 7.68 Hz, 2H), 1.65 (m, 2H), 1.33 (m, 18H), 0.94 (t, *J* = 6.72 Hz, 3H). ^{13}C NMR (100 MHz, $CDCl_3$): δ 146.44, 142.44, 139.03, 137.39, 137.00, 136.39, 133.61, 132.33, 130.56, 130.14, 129.41, 128.43, 126.74, 125.91, 124.01, 97.51, 77.16, 31.75, 31.30, 29.81, 29.51, 29.49, 29.39, 29.20, 29.19, 28.82, 22.53, 13.99. HRMS (APPI+): calculated for $C_{28}H_{33}Cl_2IS$ $(M + H)^+$ 598.07247, found 598.06937.

5,5',5'',5'''-(2',2''',3',3'''-tetrachloro-[1,1':4',1'':4'',1''':4''',1''''-quinquephenyl]-2,2'',2'''',3''-tetrayl)tetrakis(2-dodecylthiophene) (7)

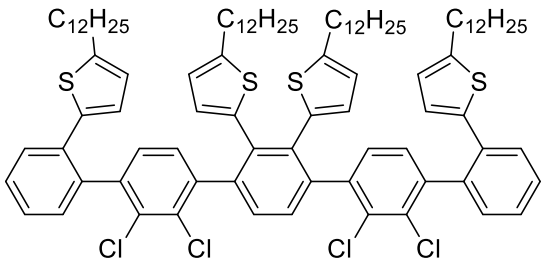

7

A round bottom flask under nitrogen was charged with compound **6** (0.307 g, 0.500 mmol), compound **10b** (0.170 g, 0.200 mmol), $LiOH \cdot H_2O$ (68.7 mg, 1.60 mmol), THF (2.00 mL) and H_2O (0.260 mL), flushed three times with a vacuum/nitrogen cycle and degassed with a nitrogen stream for 10 mins. $Pd_2(dba)_3$ (9.40 mg, 10.0 μmol) and SPhos (16.8 mg, 40.0 μmol) were added and the reaction flask was degassed with nitrogen for another 5 mins. The reaction mixture was heated to 70 ℃ for 24 h. Once cooled down to room temperature, 20 mL of a saturated aqueous solution of NH_4Cl was added and the aqueous layer was extracted with ethyl acetate (3 × 30 mL). The organic layer was dried with Na_2SO_4 and the solvent was removed under reduced pressure. The resulting residue was purified by silica gel chromatography (15% CH_2Cl_2/hexanes) to obtain compound **7** as a light yellow solid (0.280 g, 90%). ^{1}H NMR (400 MHz, $CDCl_3$): δ 7.59 (d, *J* = 6.99 Hz, 2H), 7.42 (m, 4H), 7.33 (d, *J* = 7.33 Hz, 2H), 7.08 (m, 6H), 6.56 (d, *J* = 3.74 Hz, 2H), 6.41 (m, 5H), 6.13(m, 1H), 2.75 (m, 8H), 1.69 (m, 8H), 1.26 (m, 72H), 0.89 (m, 12H). ^{13}C NMR (100 MHz, $CDCl_3$): δ 147.21, 147.16, 147.07, 147.02, 146.93, 146.85, 146.70, 146.66, 145.87, 141.80, 141.74, 141.60, 141.36, 141.31, 141.23, 141.09, 140.28, 140.12, 139.76, 137.56, 137.53, 137.39, 137.34, 137.14, 137.10, 135.56, 135.44, 135.37, 135.33, 134.12, 133.84, 132.58, 132.41, 130.93, 129.47, 128.71, 128.60, 128.50, 126.89, 126.16, 126.08, 124.59, 124.54, 124.21, 123.25, 122.99, 77.16, 32.40, 32.11, 32.09, 30.67, 30.55, 30.17, 30.14, 30.09, 30.05, 29.91, 29.87, 29.85, 29.84, 29.69, 29.55, 23.17, 14.61. HRMS (APPI+): calculated for $C_{94}H_{122}Cl_4S_4$ $(M + H)^+$ 1518.72306, found 1518.71835.

Oligomer 8

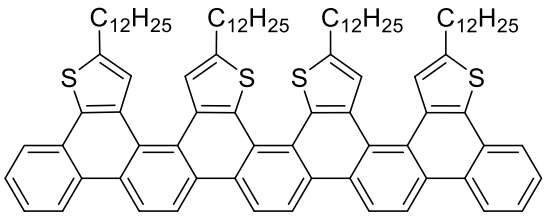

8

A quartz flask was oven-dried and flushed three times with a vacuum/nitrogen cycle. Compound **7** (30.4 mg, 20.0 μmol) was added into the flask and then anhydrous decahydronaphthalene (100 mL) was added to the flask and degassed with argon for 10 minutes. The solution was then irradiated at 300 nm at 100 ℃ for 48 h under a continuous flow of argon. After cooling down to room temperature, the solvent was removed by vacuum distillation and the resulting residue was purified by silica gel chromatography (from 15% CH_2Cl_2/hexanes, gradually increased to 100% CH_2Cl_2 to take all the product out) to obtain compound **8** as a brownish thick oil (19.2 mg, 70%) (Some product lost in the column). ^{1}H NMR (400 MHz, $CDCl_3$): δ 7.60 (m, 2H), 7.43 (m, 2H), 7.35 (m, 2H), 7.29 (m, 2H), 7.15 (s, 1H), 7.11 (s, 1H), 6.58 (m, 3H), 6.46 (d, *J* = 1.68 Hz, 1H), 2.78 (m, 4H), 1.68 (m, 4H), 1.26 (m, 36H), 0.91 (t, *J* = 7.12 Hz, 6H). HRMS (APPI+): calculated for $C_{94}H_{118}S_4$ $(M + H)^+$ 1374.81164, found 1374.81277.

5,5'-(2,5-dibromo-1,4-phenylene)bis(2-dodecylthiophene) (9a)

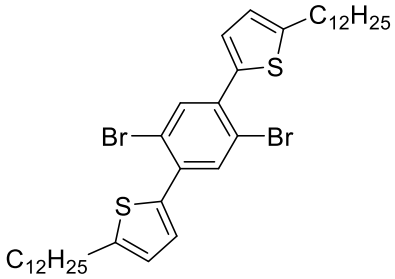

9a

A round bottom flask was flushed three times with a vacuum/nitrogen cycle, charged with 2-(5-dodecyl-2-thienyl)-4,4,5,5-tetramethyl-1,3,2-dioxaborolane (3.07 g, 8.12 mmol), 1,4-dibromo-2,5-diiodobenzene (1.80 g, 3.69 mmol), cesium carbonate (10.6 g, 32.5 mmol), THF (36.9 mL) and H_2O (9.23 mL). Then, the flask was flushed three times with a vacuum/nitrogen cycle and degassed with a nitrogen stream for 10 minutes. Bis(triphenylphosphine)palladium(II) dichloride (0.259 g, 0.369 mmol) was added, further

degassed with nitrogen for 5 minutes and heated at 80 ℃ for 16 h. After cooling to room temperature, 15 mL of a saturated aqueous solution of NH_4Cl was added and the aqueous phase was extracted with ethyl acetate (3 × 30 mL). The organic phase was dried with Na_2SO_4 and the solvent was removed under reduced pressure. The resulting residue was purified by silica gel chromatography with hexanes to yield compound **9a** as a white solid (1.27 g, 47%). ^{1}H NMR (400 MHz, $CDCl_3$): δ 7.75 (s, 2H), 7.18 (d, *J* = 3.97 Hz, 2H), 6.78 (d, *J* = 4.31 Hz, 2H), 2.83 (t, *J* = 7.68 Hz, 4H), 1.71 (m, 4H), 1.39-1.26 (m, 36H), 0.88 (t, *J* = 6.42 Hz, 6H). ^{13}C NMR (100 MHz, $CDCl_3$): δ 148.06, 137.13, 135.89, 135.71, 128.21, 124.36, 120.97, 77.16, 32.08, 31.77, 30.31, 29.83, 29.81, 29.71, 29.52, 29.33, 22.86, 14.29. HRMS (APPI+): calculated for $C_{38}H_{56}Br_2S_2$ $(M)^+$ 734.21902, found 734.21818.

5,5'-(3,6-dibromo-1,2-phenylene)bis(2-dodecylthiophene) (9b)

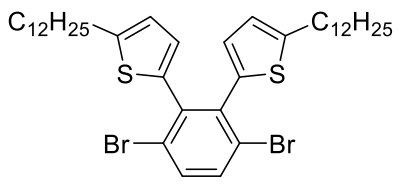

9b

A round bottom flask was flushed three times with a vacuum/nitrogen cycle, charged with 2-(5-dodecyl-2-thienyl)-4,4,5,5-tetramethyl-1,3,2-dioxaborolane (3.41 g, 9.00 mmol), 1,4-dibromo-2,3-diiodobenzene (2.00 g, 4.10 mmol), cesium carbonate (11.8 g, 36.1 mmol), THF (41.0 mL) and H_2O (10.0 mL). Then, the reaction mixture was flushed three times with a vacuum/nitrogen cycle and degassed with a nitrogen stream for 10 minutes. Bis(triphenylphosphine)palladium(II) dichloride (0.287 g, 0.410 mmol) was added and the reaction mixture was degassed with a nitrogen stream for another 5 minutes and heated at 80 ℃ for 16 h. After cooling down to room temperature, 20 mL of a saturated aqueous solution of NH_4Cl was added and the aqueous phase was extracted with ethyl acetate (3 × 40 mL). The

organic phase was dried with Na_2SO_4 and the solvent was removed under reduced pressure. The crude product was purified by silica gel chromatography with hexanes to yield compound **9b** as a white solid (1.57 g, 52%). ^{1}H NMR (400 MHz, $CDCl_3$): δ 7.51 (s, 2H), 6.57 (d, *J* = 1.57 Hz, 2H), 6.54 (d, *J* = 1.74 Hz, 2H), 2.71 (t, *J* = 7.54 Hz, 4H), 1.26 (s, 36H), 0.88 (t, *J* = 6.94 Hz, 6H). ^{13}C NMR (100 MHz, $CDCl_3$): δ 147.57, 139.41, 137.98, 133.71, 129.02, 125.37, 123.45, 77.16, 32.41, 32.07, 30.38, 30.19, 30.18, 30.16, 30.10, 29.86, 29.84, 29.36, 23.03, 14.72. HRMS (APPI+): calculated for $C_{38}H_{56}Br_2S_2$ $(M + H)^+$ 734.21902, found 734.21448.

2,2'-(2,5-bis(5-dodecylthiophen-2-yl)-1,4-phenylene)bis(4,4,5,5-tetramethyl-1,3,2-dioxabor-olane) (10a)

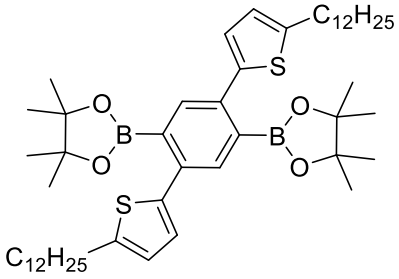

10a

A round bottom flask was oven-dried and flushed three times with a vacuum/nitrogen cycle. Compound **9a** (0.770 g, 1.00 mmol), anhydrous 1,4-dioxane (5.00 mL), $Pd_2(dba)_3$ (19.1 mg, 20.9 μmol) and 1,1'-bis(di-*tert*-butylphosphino)ferrocene (19.8 mg, 41.8 μmol) were added and the flask was flushed three times with a vacuum/nitrogen cycle. Triethylamine (0.874 mL, 6.30 mmol) was degassed with a nitrogen stream for 10 minutes and then added into the reaction flask using a syringe. 4,4,5,5-Tetramethyl-1,2,3-dioxaborolane (0.610 mL, 4.20 mmol) was filtered through a 0.45 μm filter syringe and added dropwise. The reaction mixture was flushed three times with a vacuum/nitrogen cycle and heated at 85 ℃ for 16 h. Once cooled to room temperature, 10 mL of a saturated aqueous solution of NH_4Cl was added and the aqueous layer was extracted with ethyl acetate (3 × 20 mL). The organic layer was dried with Na_2SO_4 and the

solvent was removed under reduced pressure. The resulting residue was purified by silica gel chromatography (5% Et_2O/hexanes) to yield compound **10a** as a colorless solid (0.532 g, 62%). ^{1}H NMR (400 MHz, $CDCl_3$): δ 7.65 (s, 2H), 6.91 (d, *J* = 1.76 Hz, 2H), 6.69 (d, *J* = 1.70 Hz, 2H), 2.81 (t, *J* = 7.38 Hz, 4H), 1.69 (m, 4H), 1.37-1.26 (m, 60H), 0.88 (t, *J* = 6.94 Hz, 6H). ^{13}C NMR (100 MHz, $CDCl_3$): δ 146.14, 142.22, 137.91, 135.04, 125.85, 124.20, 84.03, 77.16, 32.08, 30.40, 29.84, 29.79, 29.75, 29.57, 29.52, 29.29, 24.84, 22.85, 14.28. HRMS (APPI+): calculated for $C_{50}H_{80}B_2O_4S_2$ $(M + H)^+$ 828.57568, found 828.57630.

2,2'-(2,3-bis(5-dodecylthiophen-2-yl)-1,4-phenylene)bis(4,4,5,5-tetramethyl-1,3,2-dioxabor-olane) (10b)

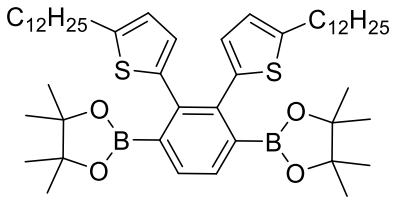

10b

A round bottom flask was flushed three times with a vacuum/nitrogen cycle and charged with compound **9b** (1.00 g, 1.36 mmol), anhydrous 1,4-dioxane (6.80 mL), $Pd_2(dba)_3$ (24.9 mg, 27.0 μmol) and 1,1'-bis(di-*tert*-butylphosphino)ferrocene (25.8 mg, 54.3 μmol), and flushed three times again with a vacuum/nitrogen cycle. Triethylamine (1.14 mL, 8.10 mmol) was degassed with a nitrogen stream for 10 minutes and added into the reaction flask. 4,4,5,5-Tetramethyl-1,2,3-dioxaborolane (0.790 mL, 5.43 mmol) was filtered through a 0.45 μm syringe filter and added dropwise. The reaction mixture was flushed three times with a vacuum/nitrogen cycle and heated at 85 ℃ for 16 h. Once cooled to room temperature, 15 mL of a saturated aqueous solution of NH_4Cl was added and the aqueous layer was extracted with ethyl acetate (3 × 30 mL). The organic layer was dried with Na_2SO_4 and the solvent was removed under reduced pressure. The resulting residue was purified by silica gel

chromatography (5% Et_2O/hexanes) to yield compound **10b** as a light yellow solid (0.537 g, 48%). ^{1}H NMR (400 MHz, $CDCl_3$): δ 7.52 (s, 2H), 6.55 (d, *J* = 1.64 Hz, 2H), 6.52 (d, *J* = 1.72 Hz, 2H), 2.69 (t, *J* = 7.41 Hz, 4H), 1.57 (m, 4H), 1.26 (m, 36H), 1.17 (s, 24H), 0.88 (t, *J* = 6.86 Hz, 6H). ^{13}C NMR (100 MHz, $CDCl_3$): δ 146.58, 140.93, 139.62, 132.33, 128.12, 123.34, 84.11, 77.16, 32.40, 30.47, 30.18, 30.13, 30.11, 29.91, 29.84, 29.42, 25.05, 23.16, 14.56. HRMS (APPI+): $C_{50}H_{80}B_2O_4S_2$ $(M + H)^+$ 828.57568, found 828.57068.

Polymerization procedure for the precursors P1, P2

Compound **10a** and Compound **10b** was polymerized with 1,4-diiodo-2,3-dichlorobenzene by a palladium-catalyzed Suzuki-Miyaura polymerization to afford the precursors P1 and P2, respectively. A flask under nitrogen was charged with compound **10a** (1 equiv.) or compound **10b** (1 equiv.), 1,4-diiodo-2,3-dichlorobenzene (1.05 equiv.), LiOH•H_2O (8 equiv.), THF (0.1 M) and H_2O (0.8 M). The flask was flushed three times with a vacuum/nitrogen cycle and degassed with a continuous flow of nitrogen for 10 minutes. $Pd_2(dba)_3$ (0.05 equiv.) and SPhos (0.2 equiv.) were added and the reaction flask was flushed three times using a vacuum/nitrogen cycle and the reaction mixture was heated at 60 ℃ for 24 hours. Once cooled to room temperature, the reaction mixture was precipitated in cold methanol under strong stirring and filtered through a 0.45 µm nylon filter. The residue was purified by Soxhlet extraction in acetone for 24 hours and recovered with THF through the extraction thimble. The solvent was removed under reduced pressure with the exclusion of light and the solid was dissolved in a minimum amount of THF, precipitated in methanol, filtered through a 0.45 µm nylon filter and thoroughly dried under vacuum.

Polymer P1

Compound **10a** (0.300 g, 0.361 mmol) was polymerized with 1,4-diiodo-2,3-dichlorobenzene (0.151 g, 0.379 mmol) according to the procedure described above. Polymer P1 ($\overline{Mn}$ = 9 700 g

mol^{-1}, $\overline{Mw}$ = 13 900 g mol^{-1}, dispersity index ($Đ$): 1.4) was obtained as a brown solid (0.238 g, 92%).

Polymer P2

Compound **10b** (0.300 g, 0.361 mmol) was polymerized with 1,4-diiodo-2,3-dichlorobenzene (0.151 g, 0.379 mmol) according to the procedure described above. Polymer P2 ($\overline{Mn}$ = 9 500 g mol^{-1}, $\overline{Mw}$ = 17 100 g mol^{-1}, dispersity index ($Đ$): 1.8) was obtained as a light yellow solid (0.214 g, 82%).

Photochemical procedure for the synthesis of *p*T-GNR and *o*T-GNR

Precursor (P1, P2) was dissolved in anhydrous decahydronaphthalene (0.002 M) in an oven-dried quartz flask under argon. The solution was degassed with a continuous flow of argon for 10 minutes. The P1 solution was heated to 160 °C and irradiated with 16 × 7.2 W low pressure mercury lamps at λ = 300 nm for 48 hours, and then irradiated for an additional 48 hours under λ = 365 nm at 160 °C, while maintaining a continuous flow of argon. And the P2 solution was heated to 100 °C and irradiated with 16 × 7.2 W low pressure mercury lamps at λ = 300 nm for 48 hours under a continuous flow of argon. Once cooled down to room temperature, the solvent was removed by vacuum distillation and the solid was dissolved in a minimum amount of THF, precipitated in cold methanol, filtered through a 0.45 µm nylon filter. The residue was purified by Soxhlet extraction in hexanes for 24 hours and recovered with THF. Once concentrated to a minimum amount of solvent, the polymer was precipitated in methanol, filtered and thoroughly dried under vacuum.

***p*T-GNR**

P1 (72.2 mg, 0.100 mmol) was subjected to the procedure described above to obtain *p*T-GNR ($\overline{M}$n = 20 800 g mol^{-1}, $\overline{M}$w = 38 200 g mol^{-1}, dispersity index (*Đ*): 1.8) as a black solid (62.0 mg, 96%).

***o*T-GNR**

P2 (72.2 mg, 0.100 mmol) was subjected to the procedure described above to obtain *o*T-GNR ($\overline{M}$n = 27 700 g mol^{-1}, $\overline{M}$w = 81 700 g mol^{-1}, dispersity index (*Đ*): 2.9) as a dark brown solid (60.0 mg, 92%).

2.7.4. NMR Spectra

Compound 1

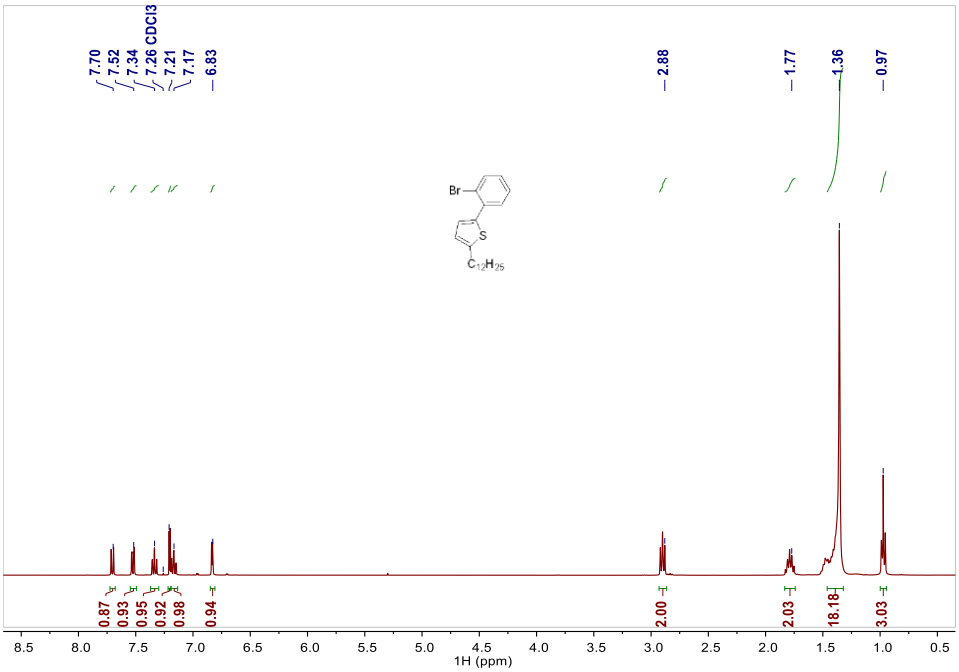

Figure 2.7. ^{1}H NMR spectrum of compound **1** in $CDCl_3$.

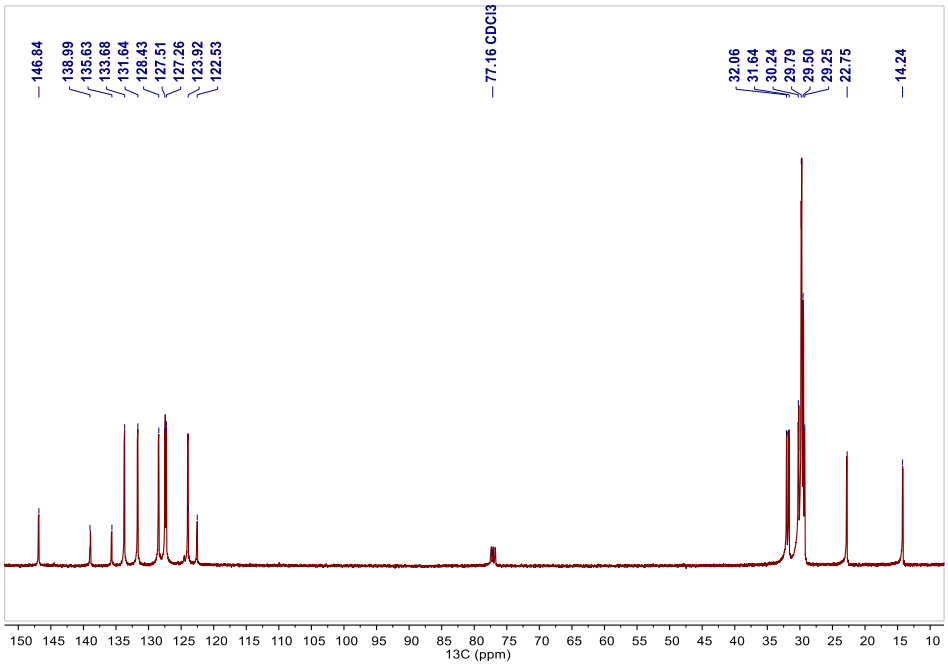

Figure 2.8. ^{13}C NMR spectrum of compound **1** in $CDCl_3$.

Compound 2

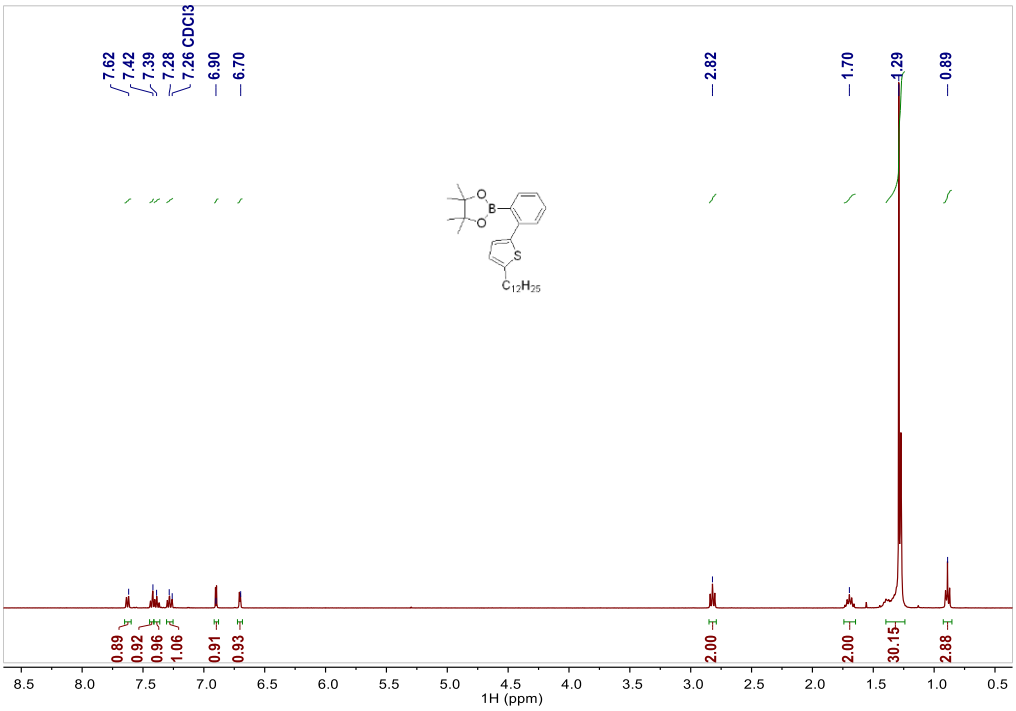

Figure 2.9. ^{1}H NMR spectrum of compound **2** in $CDCl_3$.

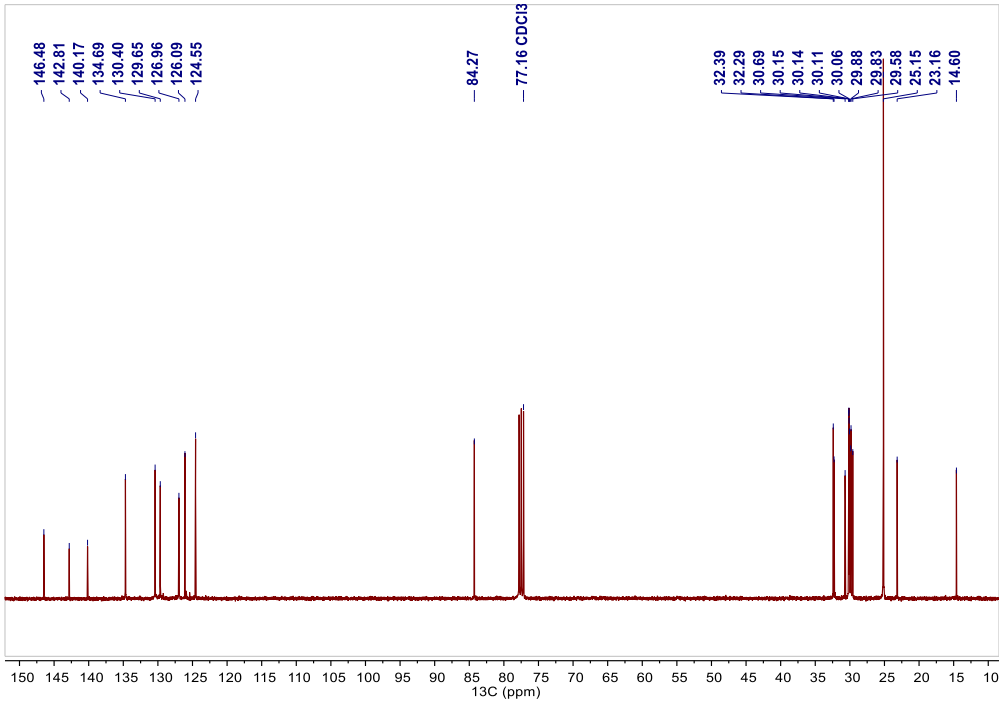

Figure 2.10. ^{13}C NMR spectrum of compound **2** in $CDCl_3$.

Compound 3

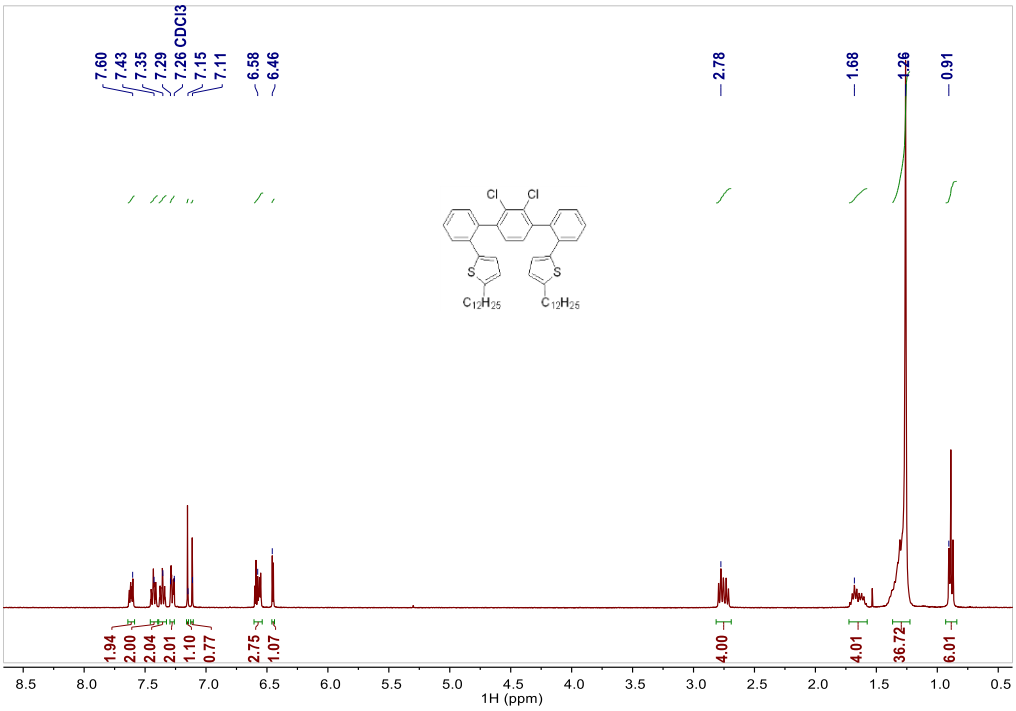

Figure 2.11. ^{1}H NMR spectrum of compound **3** in $CDCl_3$.

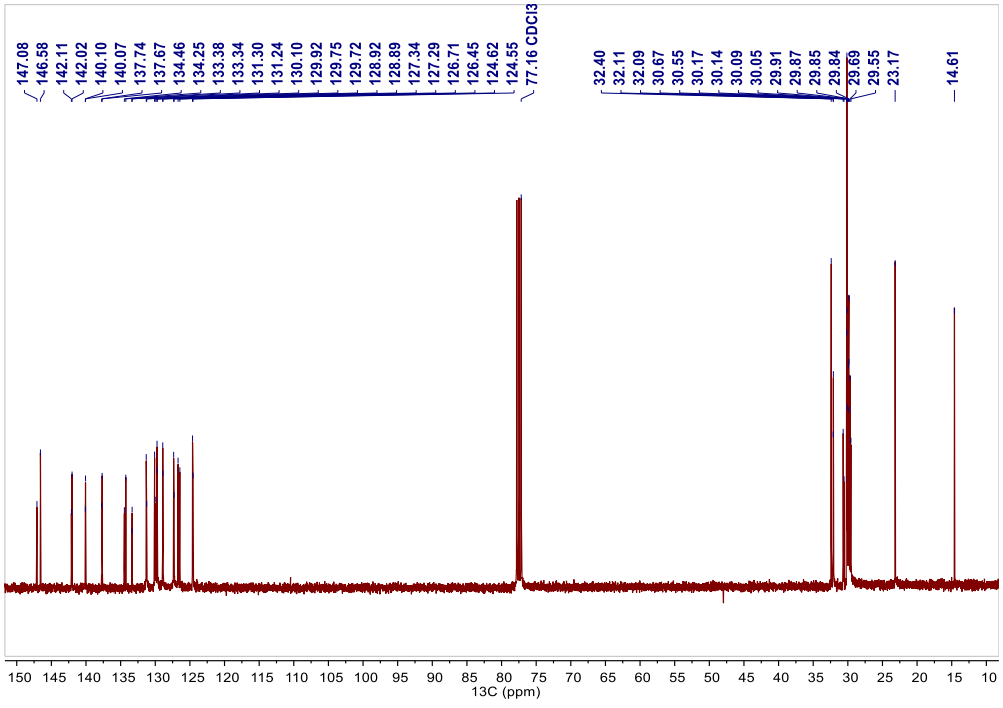

Figure 2.12. ^{13}C NMR spectrum of compound **3** in $CDCl_3$.

Compound 4

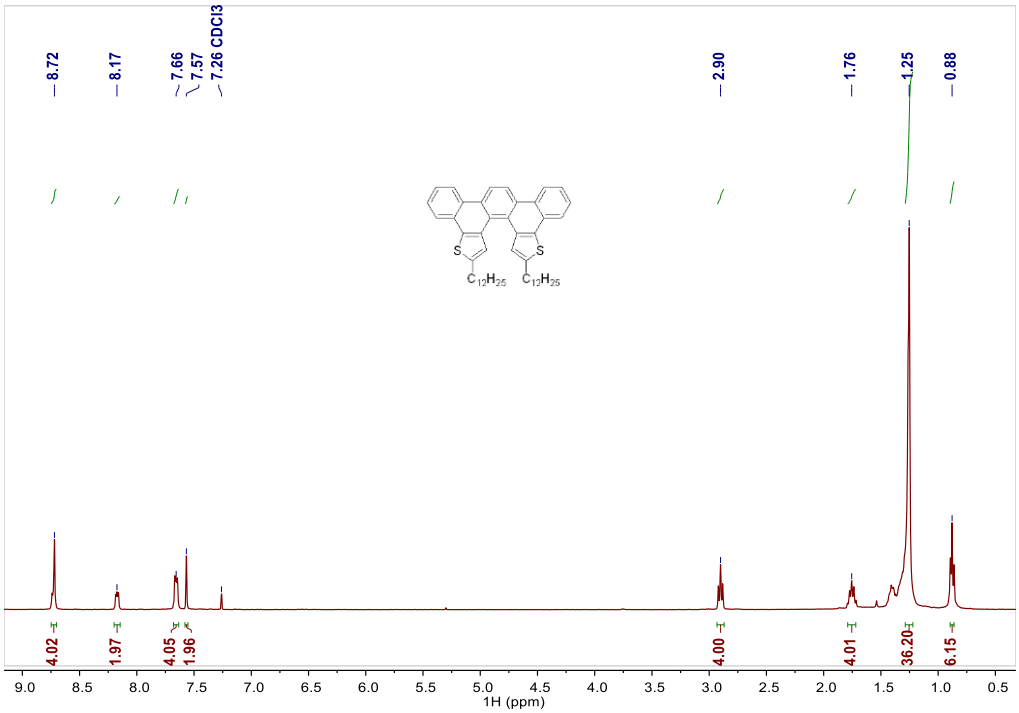

Figure 2.13. ^{1}H NMR spectrum of compound **4** in $CDCl_3$.

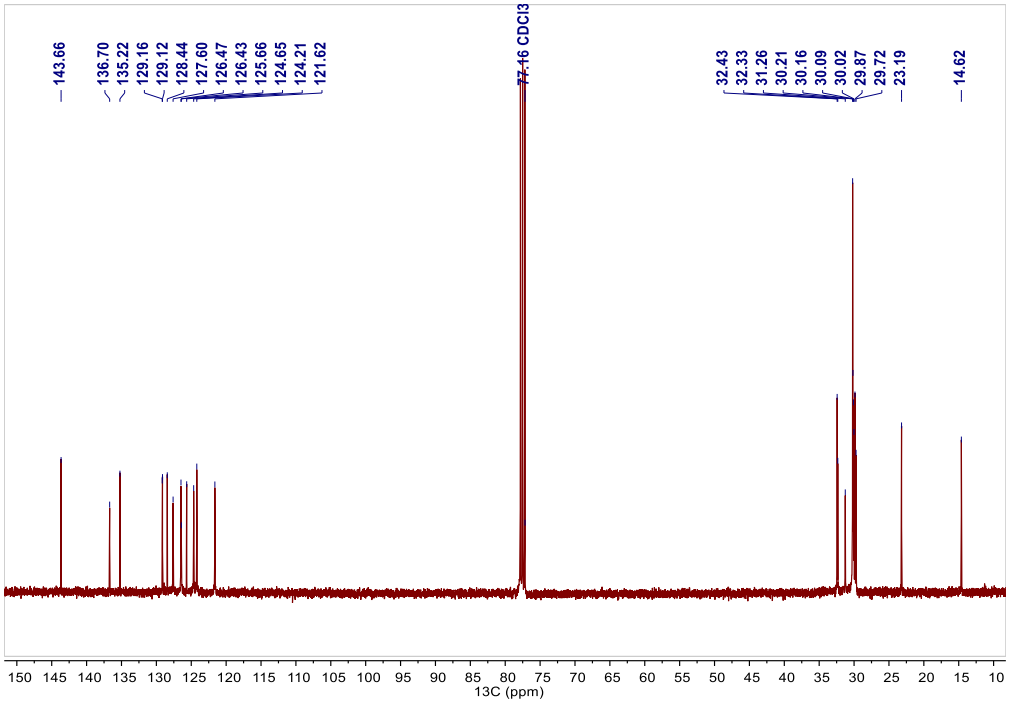

Figure 2.14. ^{13}C NMR spectrum of compound **4** in $CDCl_3$.

Compound 5

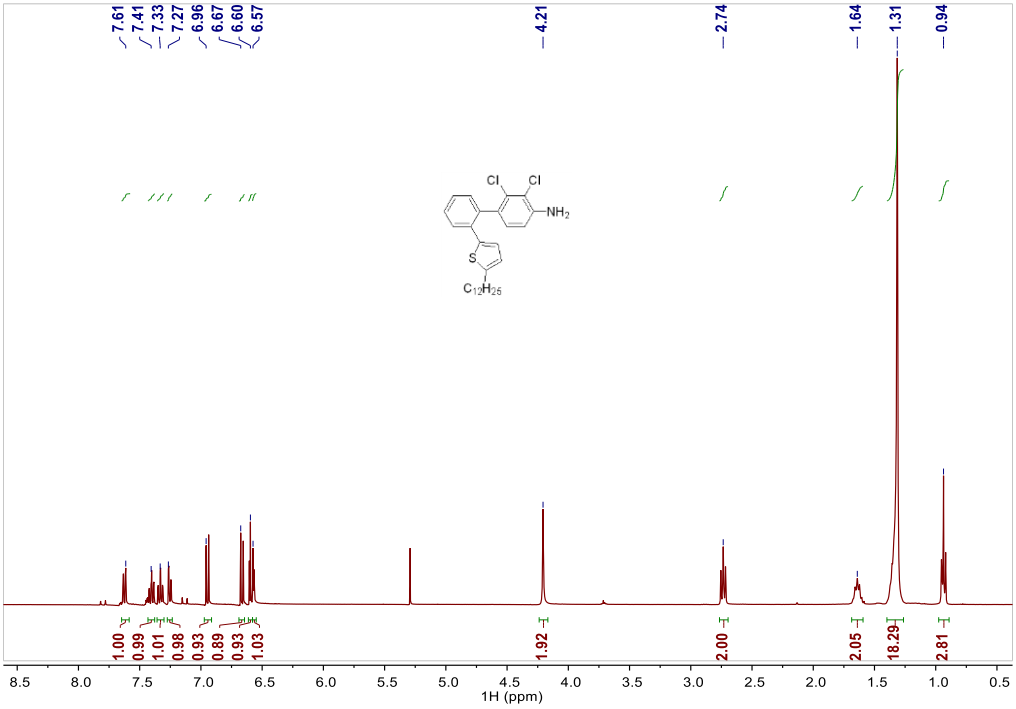

Figure 2.15. ^{1}H NMR spectrum of compound **5** in $CDCl_3$.

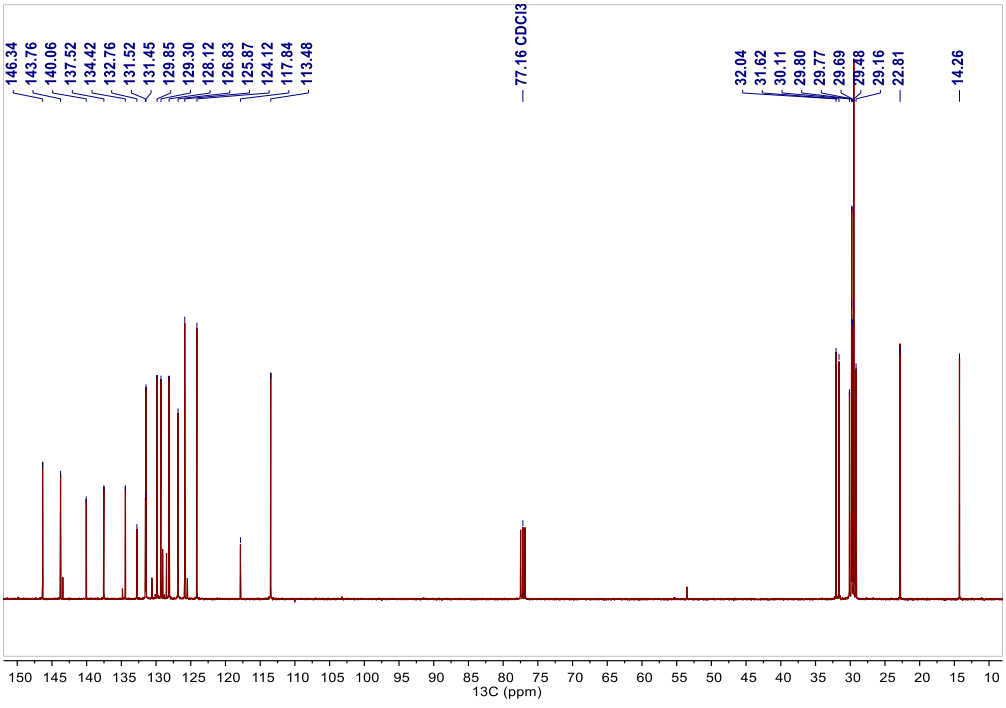

Figure 2.16. ^{13}C NMR spectrum of compound **5** in $CDCl_3$.

Compound 6

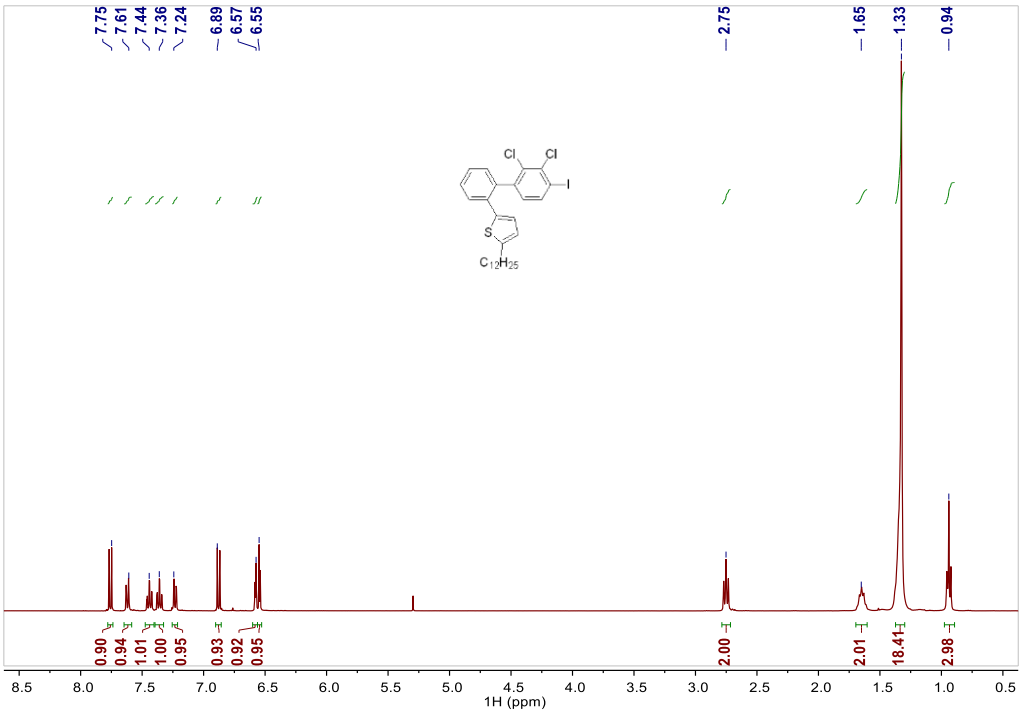

Figure 2.17. ^{1}H NMR spectrum of compound **6** in $CDCl_3$.

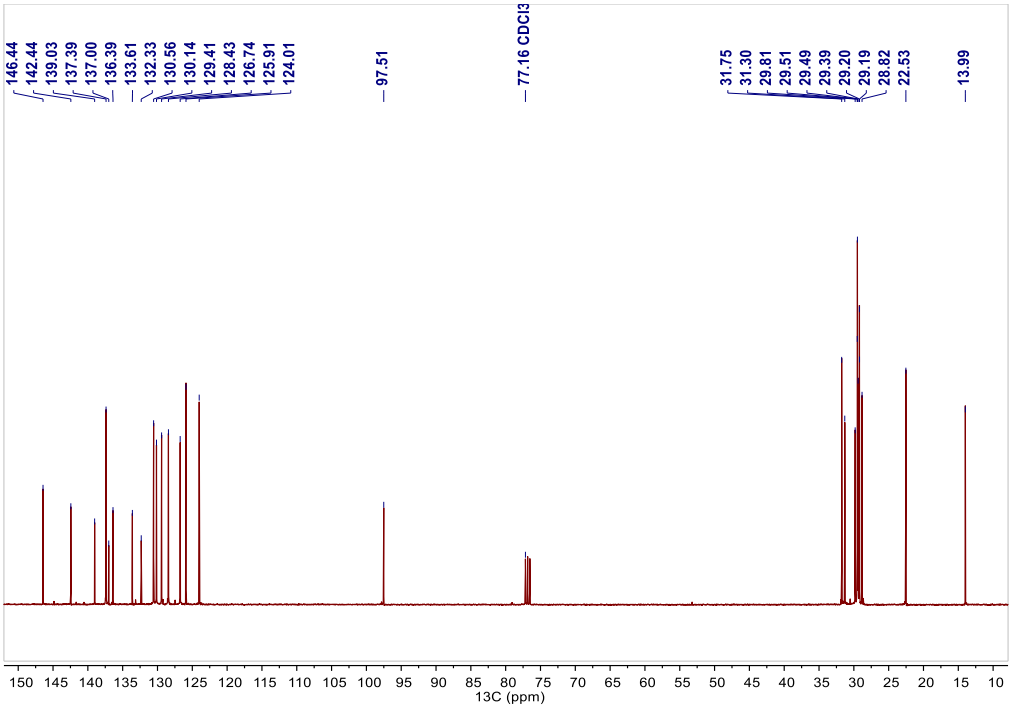

Figure 2.18. ^{13}C NMR spectrum of compound **6** in $CDCl_3$.

Compound 7

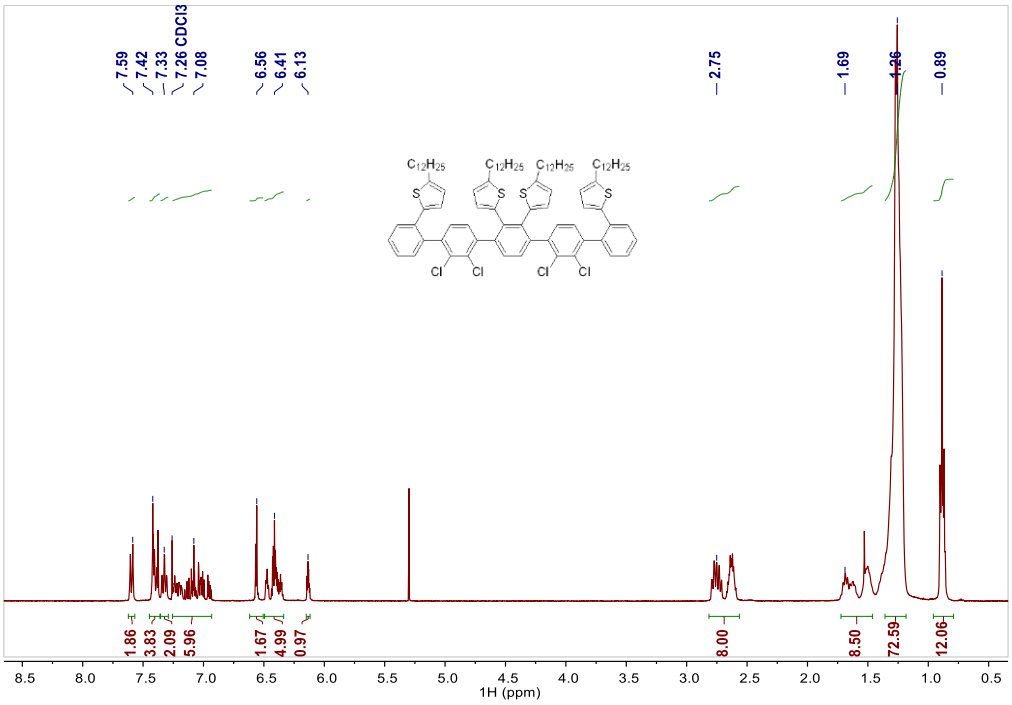

Figure 2.19. ^{1}H NMR spectrum of compound **7** in $CDCl_3$.

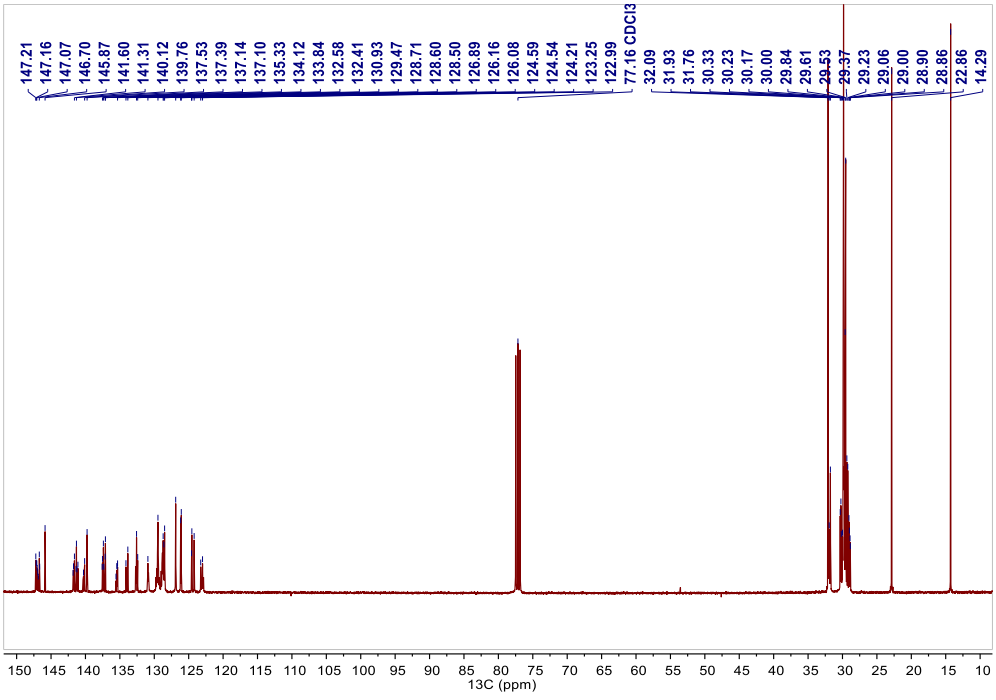

Figure 2.20. ^{13}C NMR spectrum of compound **7** in $CDCl_3$.

Compound 8

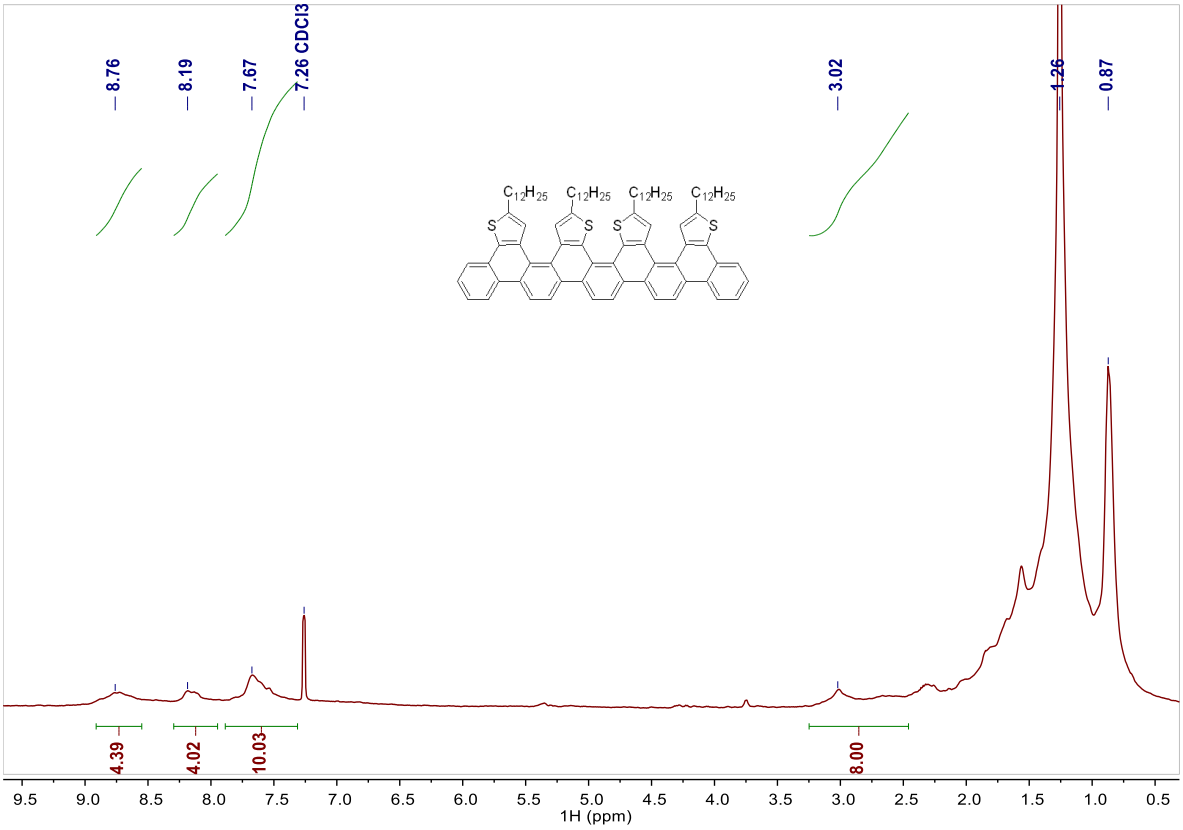

Figure 2.21. ^{1}H NMR spectrum of compound **8** in $CDCl_3$.

Compound 9a

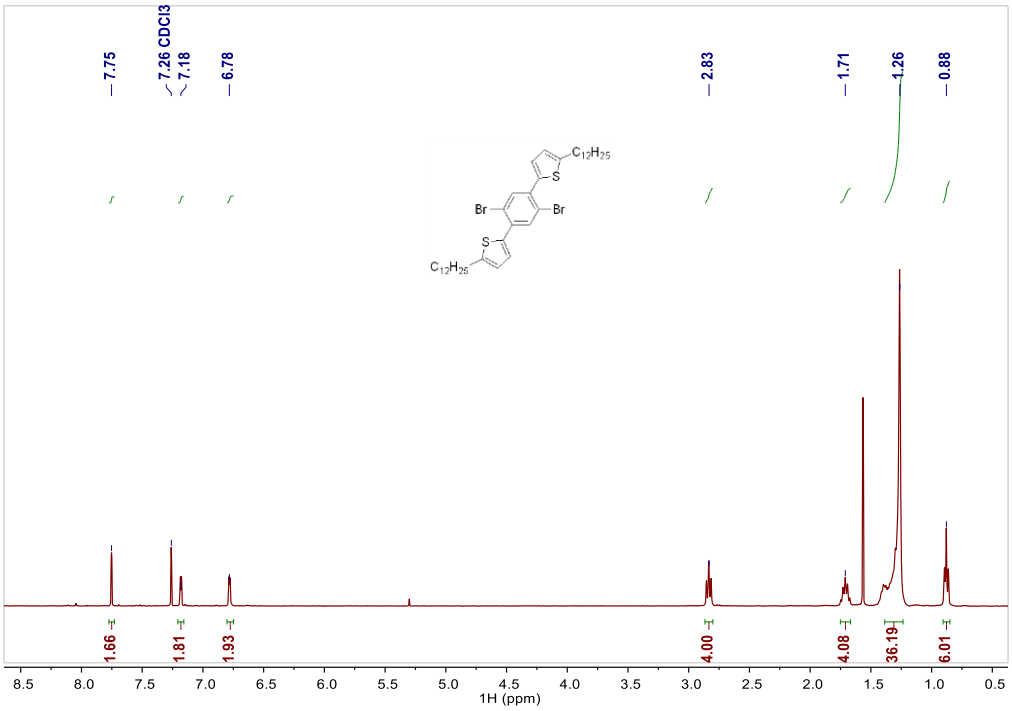

Figure 2.22. ^{1}H NMR spectrum of compound **9a** in $CDCl_3$.

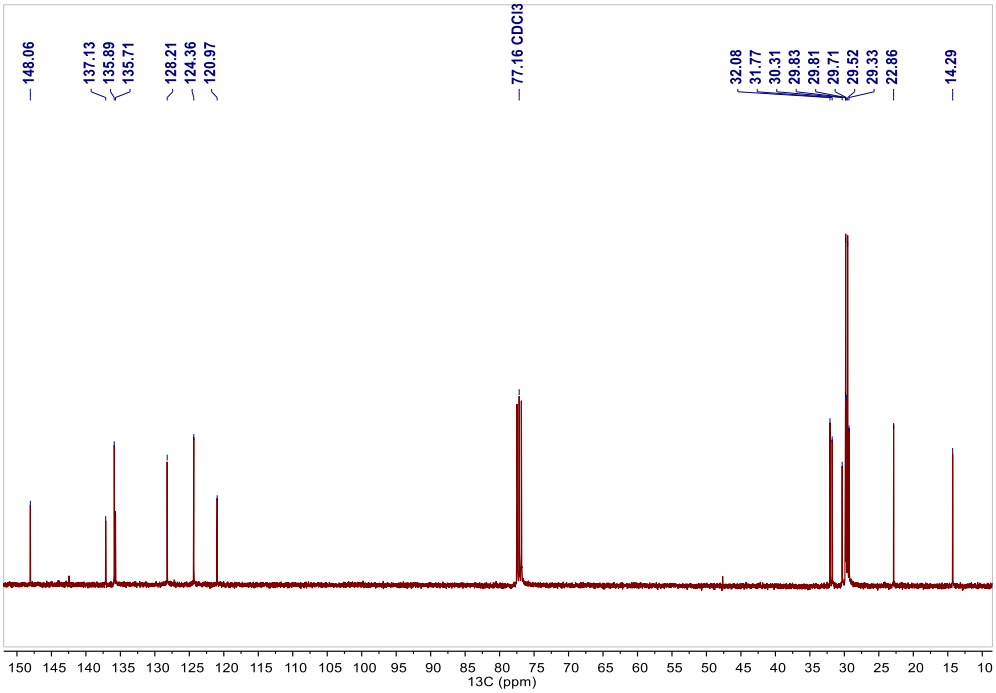

Figure 2.23. ^{13}C NMR spectrum of compound **9a** in $CDCl_3$.

Compound 9b

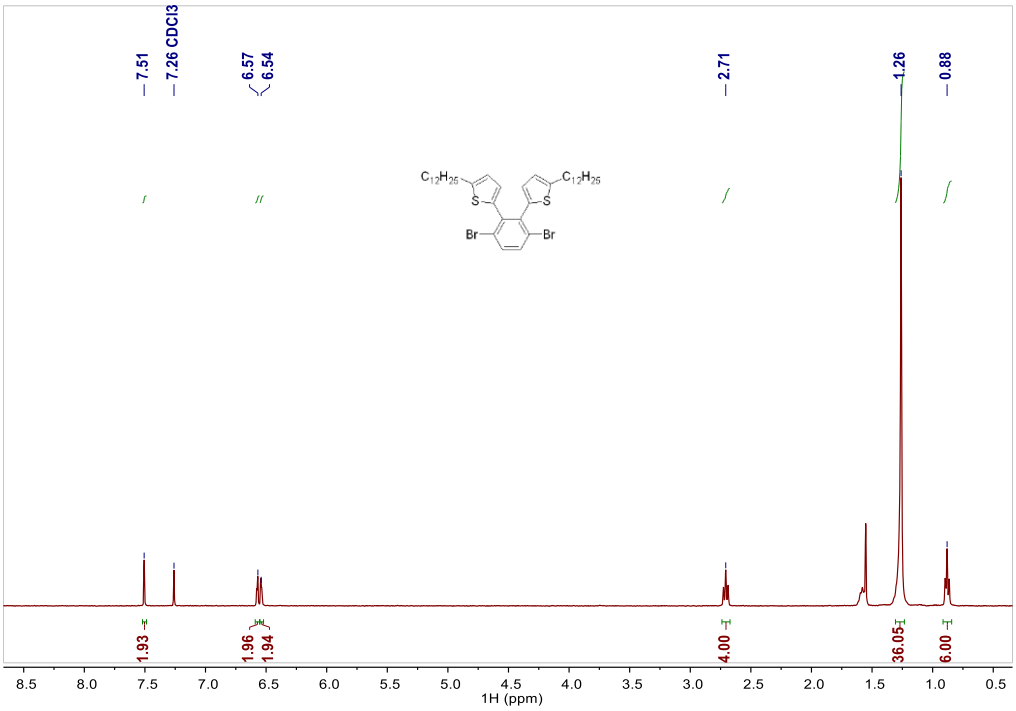

Figure 2.24. ^{1}H NMR spectrum of compound **9b** in $CDCl_3$.

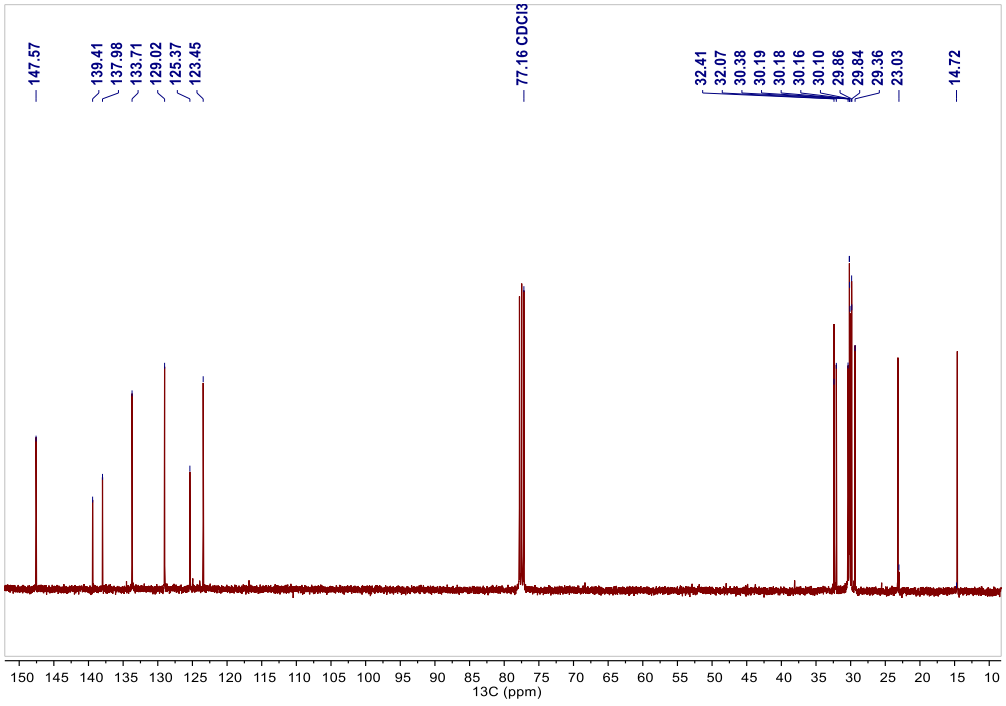

Figure 2.25. ^{13}C NMR spectrum of compound **9b** in $CDCl_3$.

Compound 10a

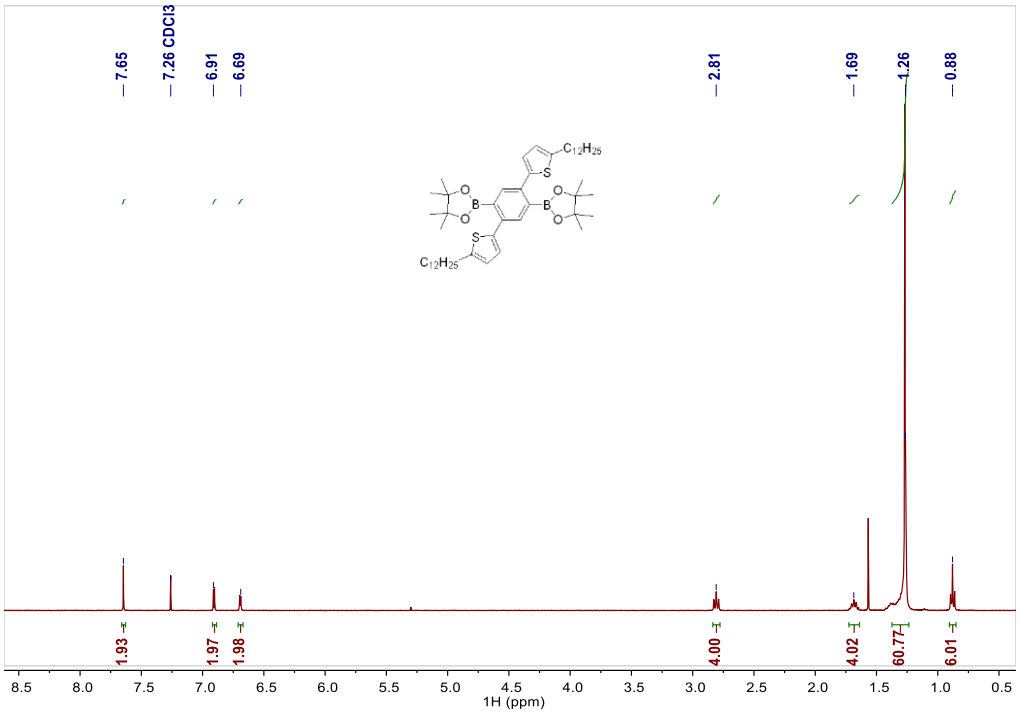

Figure 2.26. ^{1}H NMR spectrum of compound **10a** in $CDCl_3$.

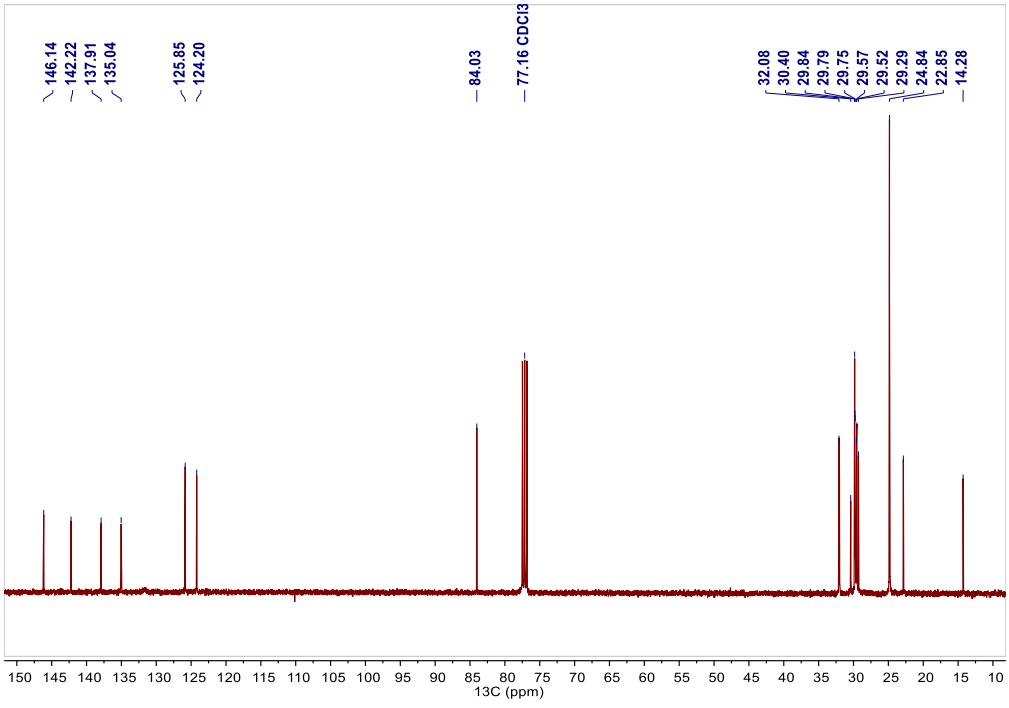

Figure 2.27. ^{13}C NMR spectrum of compound **10a** in $CDCl_3$.

Compound 10b

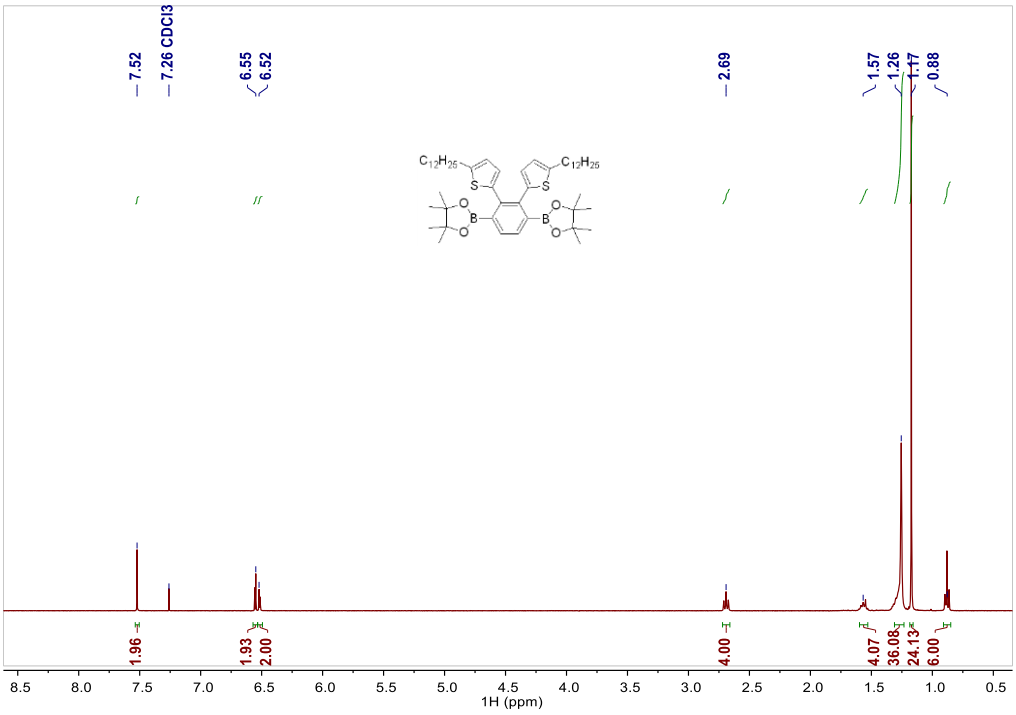

Figure 2.28. ^{1}H NMR spectrum of compound **10b** in $CDCl_3$.

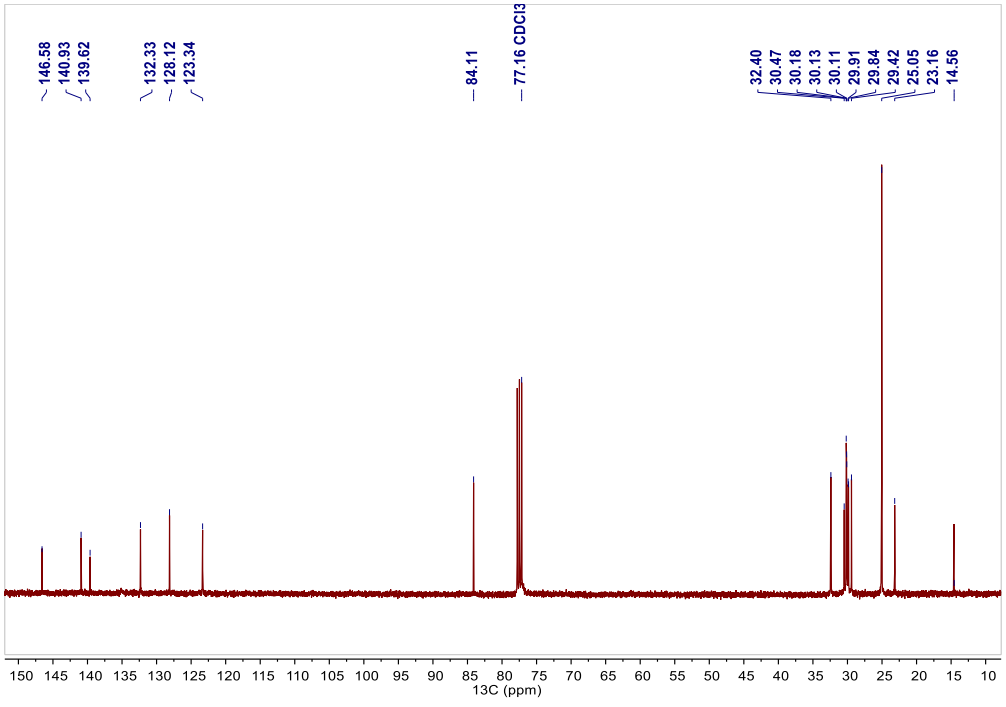

Figure 2.29. ^{13}C NMR spectrum of compound **10b** in $CDCl_3$.

Precursor P1

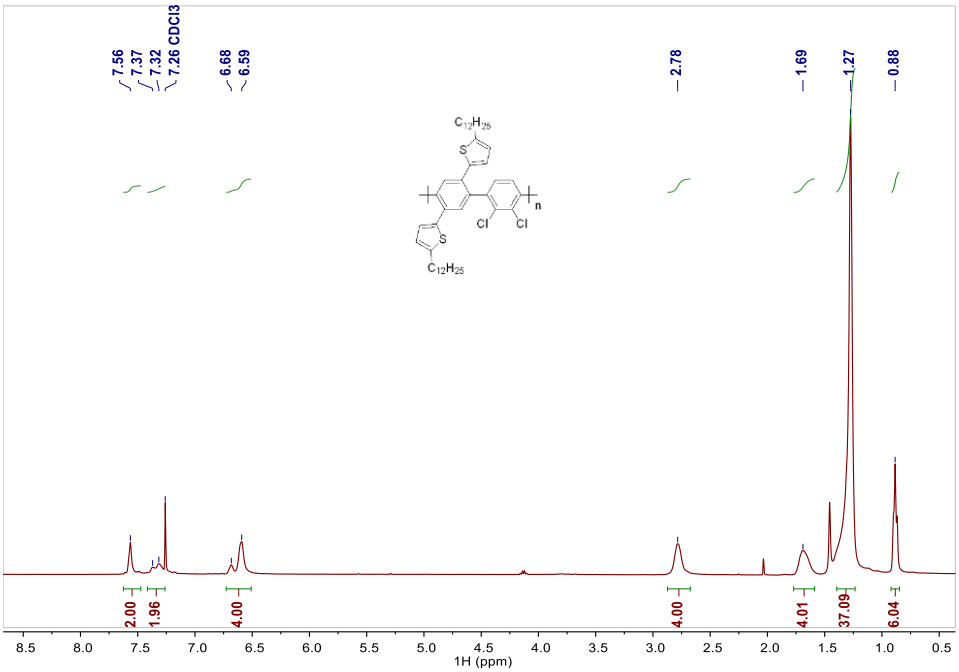

Figure 2.30. ^{1}H NMR spectrum of Precursor P1 in $CDCl_3$ at 60 ℃.

***p*T-GNR**

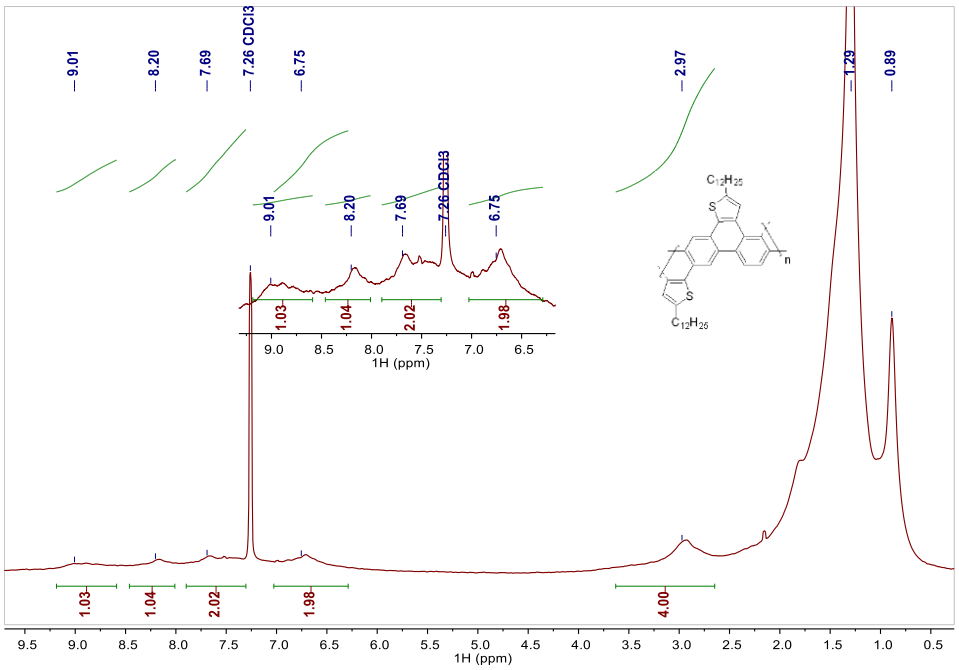

Figure 2.31. ^{1}H NMR spectrum of *p*T-GNR in $CDCl_3$ at 60 ℃.

Precursor P2

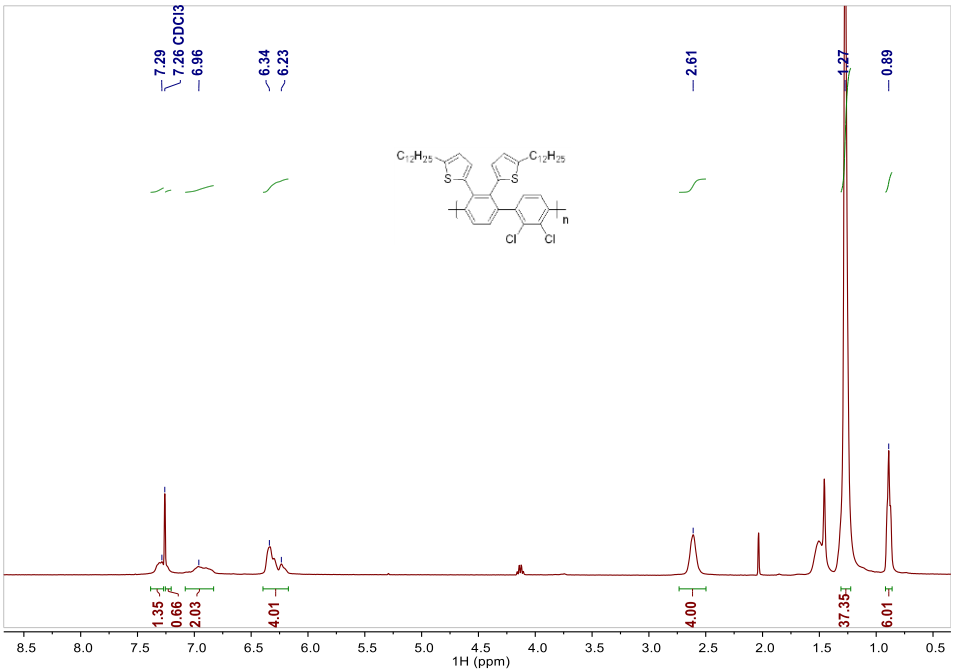

Figure 2.32. ^{1}H NMR spectrum of Precursor P2 in $CDCl_3$ at 60 ℃.

***o*T-GNR**

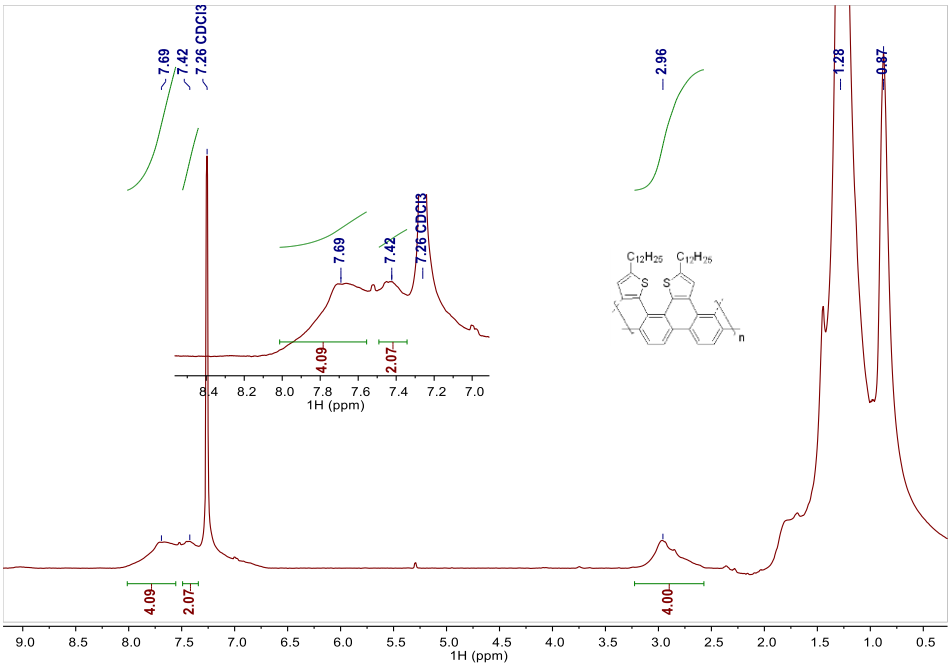

Figure 2.33. ^{1}H NMR spectrum of *o*T-GNR in $CDCl_3$ at 60 ℃.

2.7.5. UV-visible and photoluminescence analysis

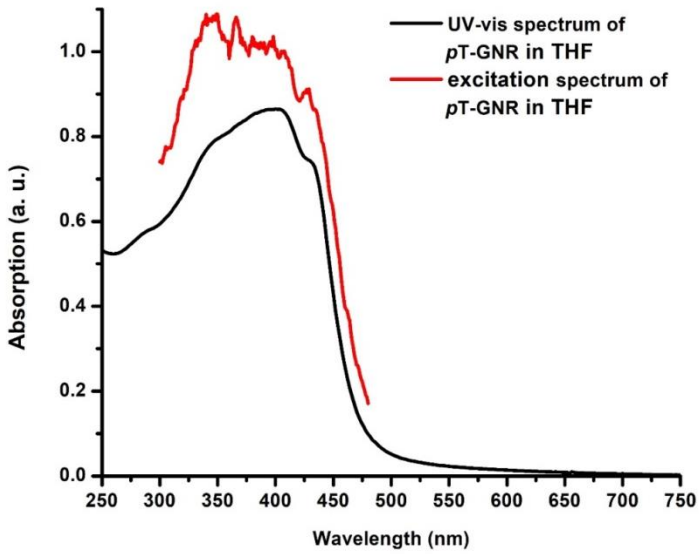

Figure 2.34. UV-visible (black) and photoluminescence excitation (red, monitored at λ_{em} = 550 nm) spectra of *p*T-GNR in THF solution. The intensity scale of the excitation spectrum is arbitrary.

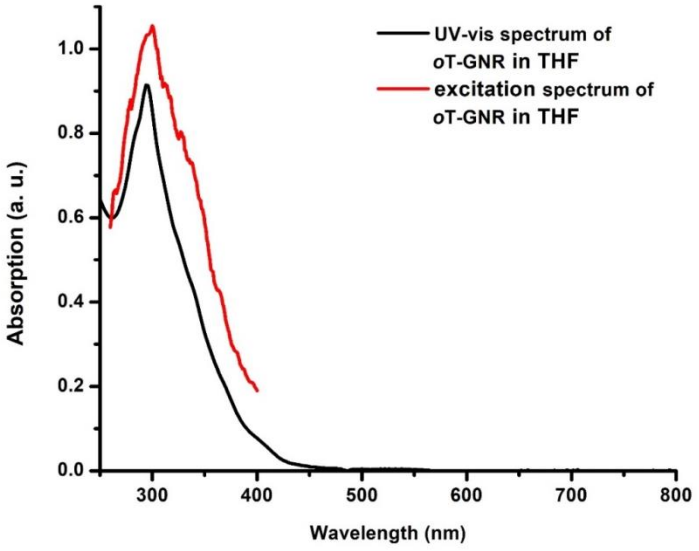

Figure 2.35. UV-visible (black) and photoluminescence excitation (red, monitored at λ_{em} = 500 nm) spectra of *o*T-GNR in THF solution. The intensity scale of the excitation spectrum is arbitrary.

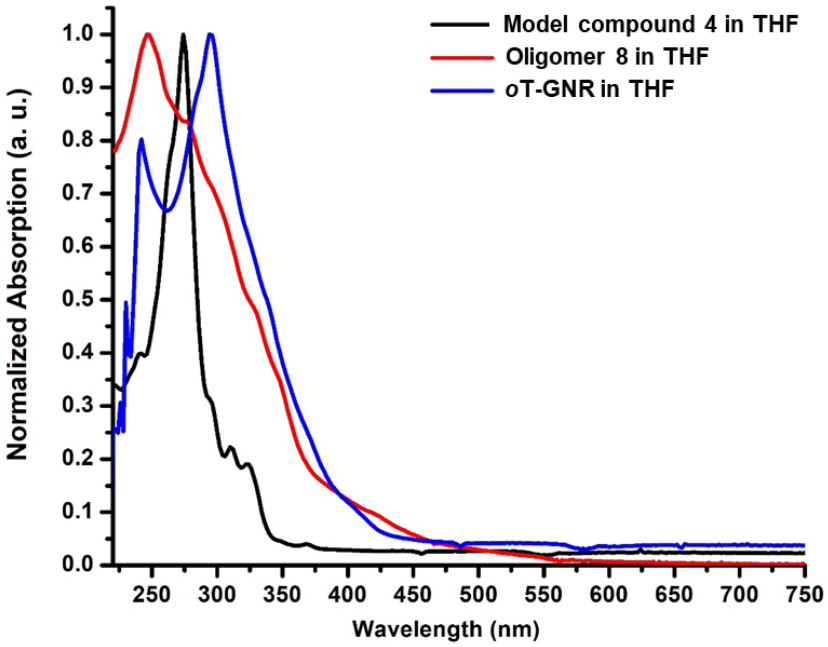

Figure 2.36. UV-vis absorption spectra of model compound **4**, oligomer **8** and *o*T-GNR in THF solution.

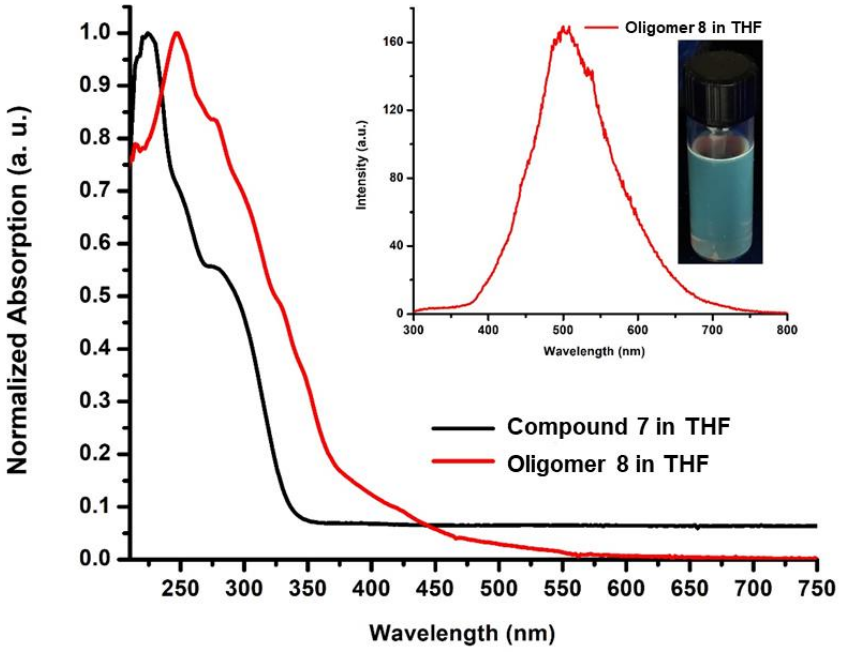

Figure 2.37. UV-vis absorption spectra of compound **7** and oligomer **8** in THF, insert is the photoluminescence spectrum of oligomer **8** in THF (λ_{ex} = 250 nm).

2.7.6. Lifetime measurements

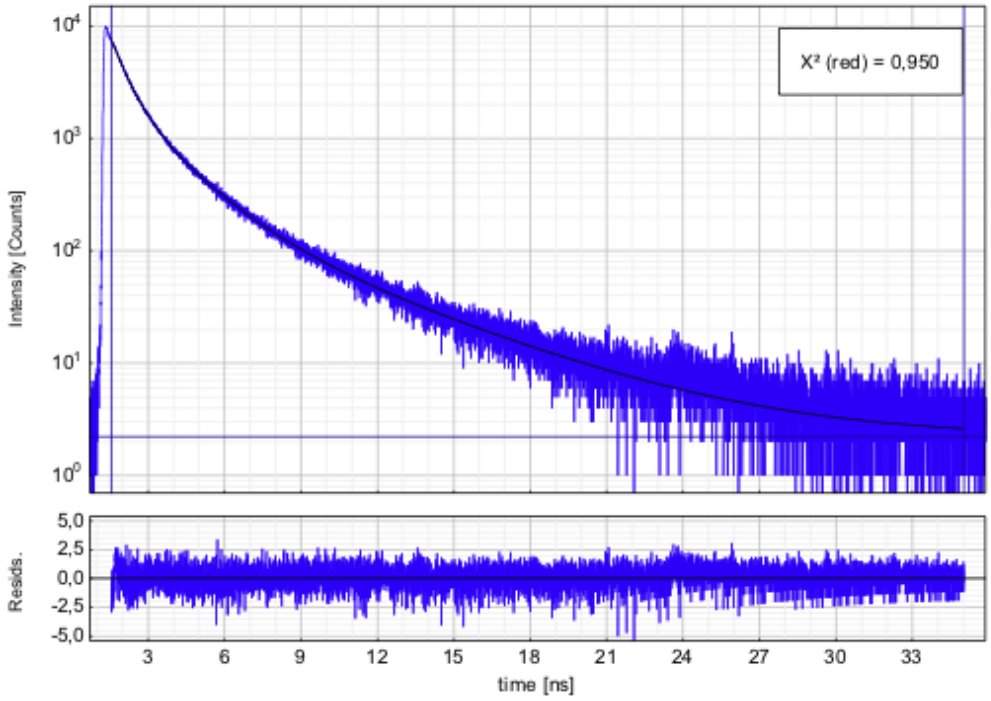

$$I(t) = \sum_{i=1}^{n} A_i \, e^{-\frac{t}{\tau_i}}$$

Parameter	Value	Conf. Lower	Conf. Upper	Conf. Estimation
A_1 [Cnts]	318,6	-11,5	+11,5	Fitting
τ_1 [ns]	4,991	-0,197	+0,251	Support Plane
A_2 [Cnts]	2172,2	-44,8	+44,8	Fitting
τ_2 [ns]	1,7298	-0,0729	+0,0836	Support Plane
A_3 [Cnts]	5101	-117	+117	Fitting
τ_3 [ns]	0,5783	-0,0143	+0,0151	Support Plane
Bkgr. Dec [Cnts]	2,227	-0,509	+0,509	Fitting

Figure 2.38. Lifetime data for *o*T-GNR.

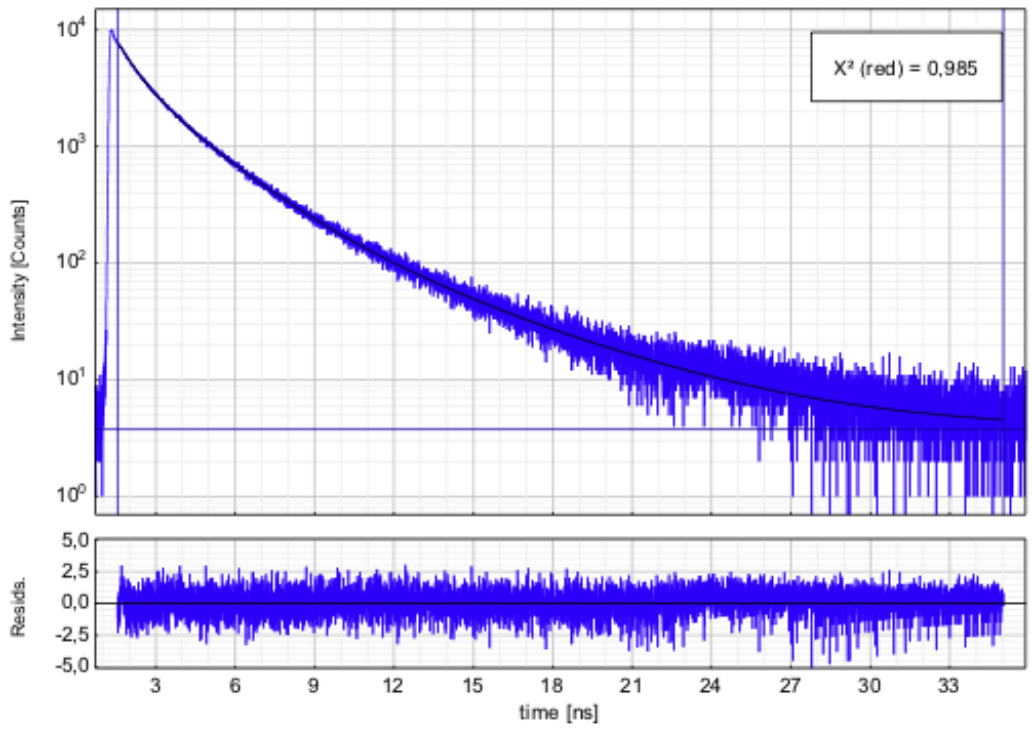

$$I(t) = \sum_{i=1}^{n} A_i \, e^{-\frac{t}{\tau_i}}$$

Parameter	Value	Conf. Lower	Conf. Upper	Conf. Estimation
A_1 [Cnts]	550,5	-16,4	+16,4	Fitting
τ_1 [ns]	5,111	-0,248	+0,322	Support Plane
A_2 [Cnts]	3863,8	-49,4	+49,4	Fitting
τ_2 [ns]	2,0810	-0,0838	+0,0929	Support Plane
A_3 [Cnts]	3399	-115	+115	Fitting
τ_3 [ns]	0,7127	-0,0341	+0,0354	Support Plane
Bkgr. Dec [Cnts]	3,761	-0,666	+0,666	Fitting

Figure 2.39. Lifetime data for *p*T-GNR.

2.7.7. Computational methods for structures, isomers, transition states and energies of *p*T-GNR and *o*T-GNR

DFT calculations for the geometry optimization as well as frequency optimization of both *p*T-GNR and *o*T-GNR were carried out with Gaussian 09 suites at the B3LYP/6-31G(d,p) level of theory. As one may observe in Figure 3.40, *p*T-GNR has no isomerization possible. However, *o*T-GNR may adopt many configurations in solution as described in Figure 3.5 as multiple isomerization is possible. Transitions state conformations and energies have been calculated at the same level of theory using QST3 method. QST3 calculation requires three coordinates of three molecules which are the reactant, the product and a suggested conformation of the molecule in the transition state. For a complete discussion about *o*T-GNR possible conformations, please refer to the manuscript.

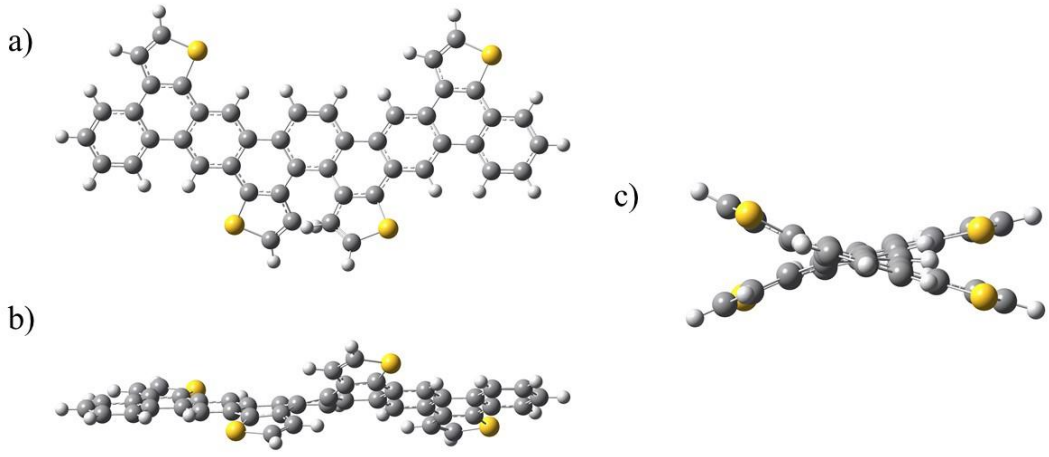

Figure 2.40. Optimized geometry of *p*T-GNR displayed according to different angle.

2.7.8. Computational methods for simulation of Raman spectra

DFT calculations aimed at the simulation of Raman spectra have been carried out at the B3LYP/6-31G(d,p) level, which constitutes a good compromise between accuracy and computational cost, and provides a good description of the Raman spectra of several polycyclic aromatic hydrocarbons and GNRs. We adopted the oligomer approach to the simulation of the Raman spectra and we considered tetramers of *p*T-GNR and *o*T-GNR as the longest oligomer affordable with the available hardware (20 Intel E5-2690 CPU cores, 3.00 GHz, 196 Gb RAM, 400 Gb solid state drive for fast scratch). We constructed the tetramer models by adopting the most stable molecular conformations determined in the calculation of the potential energy surface described above. To avoid spurious effects in the simulated Raman spectra, which arise from vibrational coupling with the end-groups of the models, we considered heavy mass end-groups. As customary, we adopted a uniform wavenumber scale factor of 0.98 to ease the comparison of the simulated Raman spectra *vs*. the corresponding experimental data.

2.7.9. DFT models for simulating the Raman spectra of *p*T-GNR and *o*T-GNR

Early analysis of the simulated Raman spectra of *p*T-GNR showed a few discrepancies with the experiment, while in the case of *o*T-GNR the agreement was good. Notably, in the region around 1450 cm^{-1}, where the simulated spectrum exhibits two peaks, only one Raman line is observed (compare for instance the experimental spectrum of *p*T-GNR in Figure 2.6 with the simulated spectrum shown in magenta in Figure 2.41). Also, the relative intensities in the D region were not correctly accounted for by the model. By tracing the normal modes associated to these discrepancies, we uncovered end-group coupling effects, which are of course due to the finiteness of the molecular model we are using (tetramers). Hence, to fully settle this issue, we simulated the Raman spectra again, based on the same Hessian and polarizability derivatives, but considering heavy masses (100 amu) on the terminal C and H atoms (see Figure 2.41 for the definition of the terminal atoms). The resulting simulated Raman spectrum of *p*T-GNR turns out to provide a much-improved match *vs*. experiment (see Figure 2.6 and Figure 2.41).

Interestingly *o*T-GNR is less sensitive to end-group effects: the spectrum simulated with heavy end-groups is rather close to that simulated with regular masses, and they are both close to the experimental Raman spectrum (Figure 2.6 and Figure 2.41). This explains our early observation of the good agreement between theory and Raman experiments in the case of *o*T-GNR.

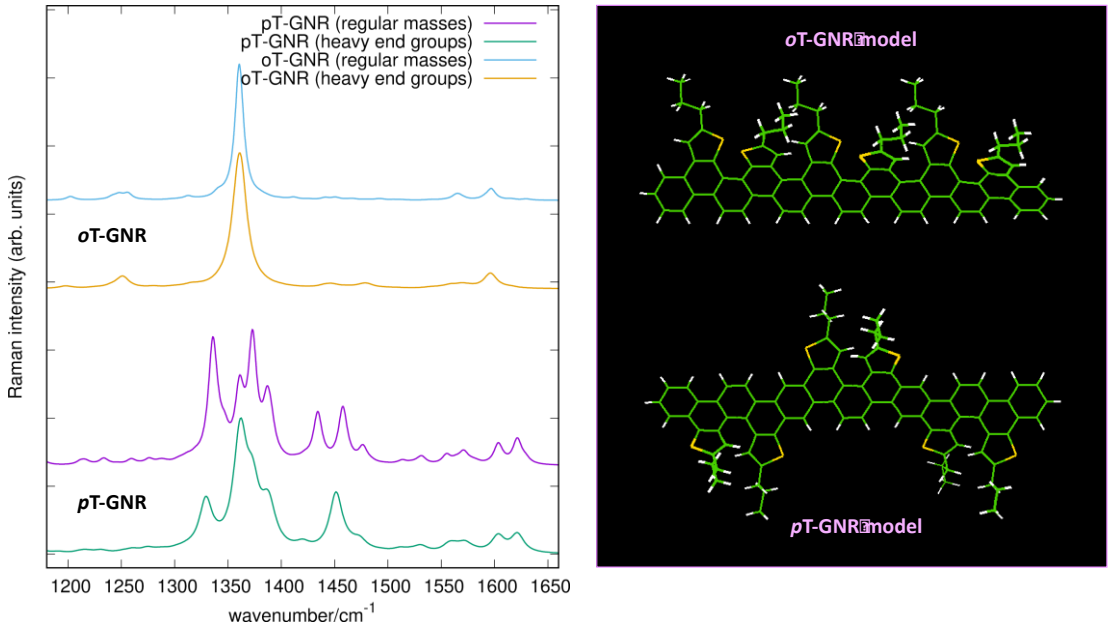

Figure 2.41. Simulated Raman spectra (left panel) of *p*T-GNR and *o*T-GNR based on the tetramer molecular models shown in the right panel. The C and H atoms, which assume a mass of 100 amu in the "heavy end-groups" models are highlighted in light magenta.

2.7.10. Assignment of the D and G modes of *o*T-GNR and *p*T-GNR

We report in Figure 2.42 and 2.43 the sketch of the nuclear displacements associated to the most intense peaks computed in the D and G regions (Figure 2.6). By inspecting the vibrational motion of the rings across the backbone of the polymer, one can easily recognize the expected patterns found in graphene. Sometimes the correspondence with graphene pattern is very good, some other times the pattern is perturbed because of the intrinsic structure of the ribbons, which obviously differs from that of highly symmetric graphene. This is particularly evident in *p*T-GNR.

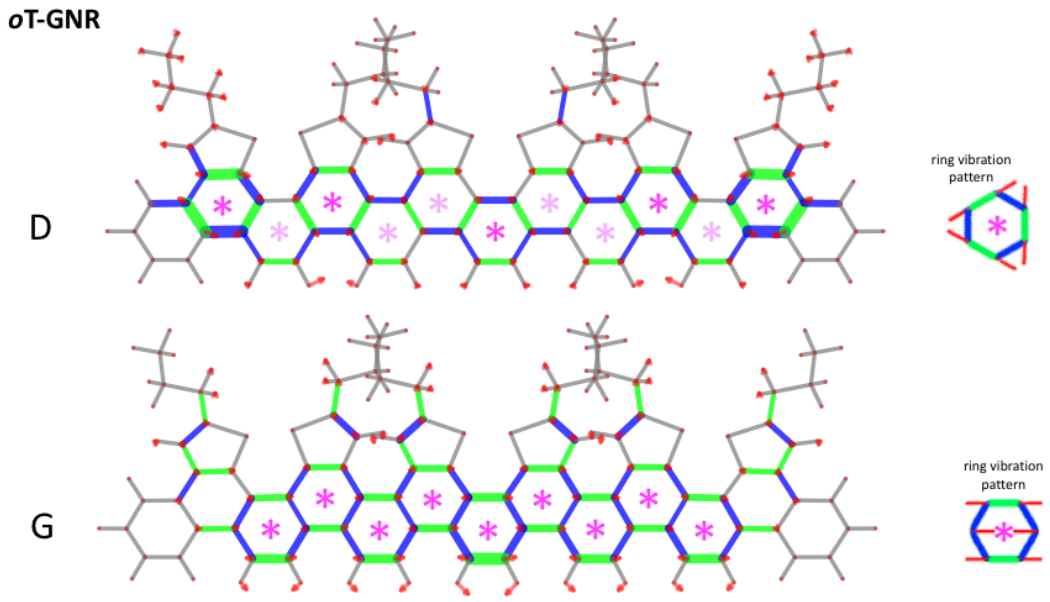

Figure 2.42. Analysis of the D and G normal modes of the *o*T-GNR model (heavy end-groups). Red arrows represent displacement vectors; CC bonds are represented as green and blue lines of different thicknesses according to their relative stretching (shrinking). Rings are starred which undergo the same vibrational pattern expected for G and D modes in graphene. Lighter color stars denote rings for which the match of the expected vibrational pattern is perturbed.

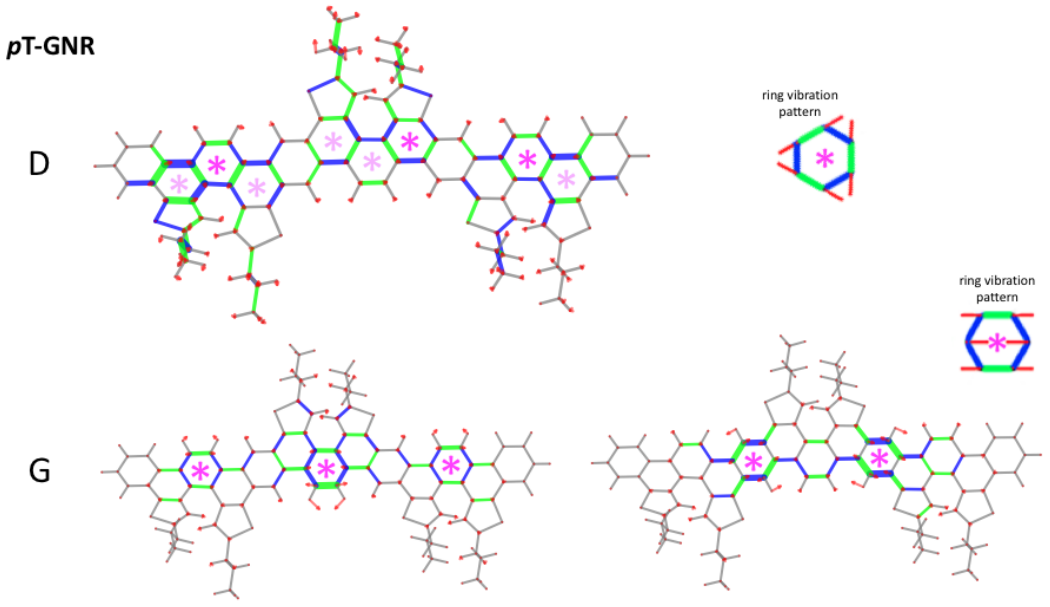

Figure 2.43. Analysis of the D and G normal modes of the ***p*T-GNR** model (heavy end-groups).

The two G modes are associated to the doublet which is observed also in the experiment (1590 cm^{-1}, 1610 cm^{-1}, Figure 2.6). The G mode in the left panel is longitudinal with respect to the polymer chain axis and it is computed at lower wavenumber (1636 cm^{-1}, unscaled) than the other G mode (1654 cm^{-1}, unscaled). Red arrows represent displacement vectors; CC bonds are represented as green and blue lines of different thicknesses according to their relative stretching (shrinking). Rings are starred which undergo the same vibrational pattern expected for G and D modes in graphene. Lighter color stars denote rings for which the match of the expected vibrational pattern is perturbed.

Chapter 3. **Photochemical Synthesis of Conjugated Ladder Polymers Containing Pyrrole Units**

Dandan Miao[a] and Jean-François Morin*[a]

a) Département de Chimie et Centre de Recherche sur les Materiaux Avancés (CERMA), Université Laval, Pavillon A.-Vachon, 1045 Ave de la Médecine, Québec QC, Canada G1V 0A6

In preparation.

3.1. Résumé

Des polymères conjugués linéaires et hélicoïdaux (L-CLP et H-CLP) de type échelle portant des unités pyrrole riches en électrons ont été synthétisés en utilisant la réaction de cyclodéhydrochloration chlorhydrique (CDHC). Les analyses RMN ^{1}H et XPS ont confirmé les structures des CLP. Les unités pyrrole dans le squelette du polymère rendent le polymère très riche en électrons avec des bandes interdites modérées et des taux de HOMO relativement élevés. Un titrage chimique des CLP a été effectué et les CLP riches en électrons ont été facilement oxydé en cations radicalaires avec un oxydant du commerce.

3.2. Abstract

Linear and helical conjugated ladder polymers (L-CLP and H-CLP) bearing electron-rich pyrrole units have been synthesized using the photochemical cyclodehydrochlorination (CDHC) reaction. ^{1}H NMR and XPS analysis confirmed the CLPs structures. The pyrrole units in the polymer backbone make the polymer very electron-rich with moderate bandgaps and relatively high HOMO levels. Chemical titration of the CLPs was performed and the electron-rich CLPs were easily oxidized into radical cations with a commercial oxidant.

3.3. Introduction

Conjugated ladder polymers (CLPs) are a kind of ladder polymers in which all the fused units on the polymer backbone are π-conjugated.[169] With a rigid, planar, and π-conjugated backbone structure, CLPs can be viewed as analogous to graphene nanoribbons (GNRs), which exhibit excellent thermal and mechanical stability,[154,170,171] as well as excellent optical and electronic properties,[170,172,173] making them promising materials in various optical and electronic devices applications, such as organic light emitting diodes (OLEDs)[174-176] and organic field effect transistors (OFETs) .[177-180]

The widely employed synthetic approach towards CLPs is the two-step approach: polymerization followed by "ladderization". For ideal CLPs, the structures should be defect-free, and possess the largest degree of π-electron delocalization possible. However, there are not a lot of efficient "ladderization" reactions can be used on a polymer precursor to achieve a defect-free structure. The "ladderization" (cyclization) reactions, including Friedel-Crafts reaction,[181-183] carbonyl olefination,[184] electrophile-induced cyclization,[90] photocyclization,[185] and thermodynamically controlled imine polycondensation,[186] have been reported to prepare CLPs. More recently, Fang *et al*[154] reported the synthesis of a carbazole-based ladder polymer with good solubility and less defects by an efficient thermodynamically controlled olefin metathesis (RCM) method. Although a lot of CLPs with few defects have been prepared by these methods, the harsh reaction conditions and the need for special functional groups installed on the monomers are still challenges in these methods. Therefore, new and efficient quantitative ladderization reactions need to be developed for the synthesis of CLPs without structural defects, with improved solubility, as well as incorporation of heteroatoms (nitrogen, sulfur) to increase their performance in optoelectronic devices.

Herein, we report the synthesis of linear and helical conjugated ladder polymers (L-CLP and H-CLP) bearing electron-rich pyrrole units using the photochemical cyclodehydrochlorination (CDHC) reaction (Figure 3.1). The photochemical CDHC reaction is conducted under very mild conditions without acid, base or metal catalyst. It is really convenient to synthesize CLPs using this method since there is no need to design complicated monomers with various functional groups, only simple chlorinated monomers are needed. The CDHC reaction proved to be efficient to synthesize various nanographenes (NGs), graphene nanoribbons (GNRs), heterocycles fused GNRs, and CLPs without structural defects and side products.[87,88,131,132] The structures of L-CLP and H-CLP have been confirmed by ^{1}H NMR and XPS analysis. The strong electron-donating pyrrole units in the polymer backbone make the polymer very electron-rich with moderate bandgaps and relatively high HOMO levels. Chemical titration of the CLPs was performed and the electron-rich CLPs were easily oxidized into radical cations

with a commercial oxidant.

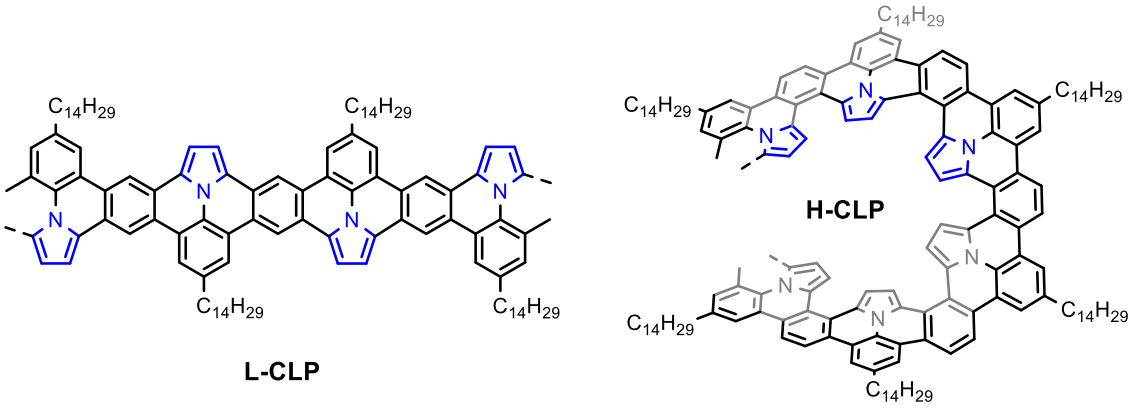

Figure 3.1. Structures of the conjugated ladder polymers L-CLP and H-CLP.

3.4. Results and Discussion

3.4.1. Synthesis

Prior to the synthesis of the CLPs, a model compound **2** was synthesized to test the efficiency of the photochemical CDHC reaction. Using the conditions that we previously reported for GNRs, compound **2** was obtained in 96% yield with no formation of side products after the irradiation of compound **1** under UV light (16 × 7.2 W low pressure mercury lamps, λ = 254 nm) at 100 ℃ for 2 hours. The synthesis of the CLPs is shown in Scheme 3.1. The 1-(4-tetradecyl-2,6-bis(4,4,5,5-tetramethyl-1,3,2-dioxaborolan-2-yl)phenyl)-1*H*-pyrrole was synthesized according to the reported procedure[187] and underwent a Suzuki-Miyaura polymerization with 1,4-dichloro-2,5-diiodobenzene[131] and 2,3-dichloro-1,4-diiodobenzene[131] using the $Pd_2(dba)_3$/SPhos catalyst system to afford polychlorinated precursors P1 and P2 in 86% and 88% yield, respectively. This catalyst system proved to be highly selective for the C-I bond and effective to synthesize poly(*m*-phenylene)s with few defects.[165,188]

For the synthesis of L-CLP and H-CLP, P1 and P2 were dissolved in anhydrous decahydronaphthalene (decalin) at a concentration of 0.002 M in oven-dried quartz flasks under

argon. The solutions were heated to 100 ℃ and irradiated under UV light (16 × 7.2 W low pressure mercury lamps, λ = 254 nm) for 72 hours under a continuous flow of argon (to remove the hydrochloric acid formed during the CDHC reaction). Upon irradiation, the solution of P1 turned from light yellow to brown, while the fluorescence turned from absent to bright yellow. The P2 solution went from colorless to dark orange with a strong yellow fluorescence, indicating a significant change in the π-conjugated structures. After purification (see Supporting Information), L-CLP and H-CLP were obtained as a dark brown and dark orange solid, respectively.

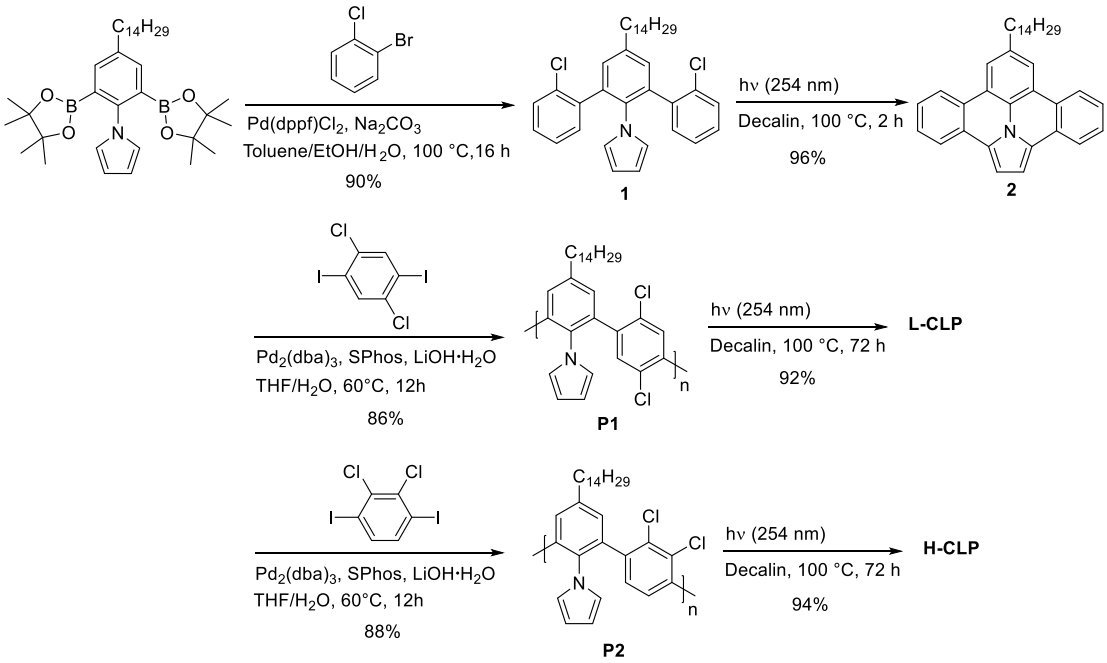

Scheme 3.1. Synthesis of model compound **2**, L-CLP and H-CLP.

3.4.2. Size-exclusion chromatography (SEC) analysis

High temperature size-exclusion chromatography (SEC) at 110 ℃ was employed to determine the molecular weight of the precursors and CLPs using polystyrene as standard and 1,2,4-trichlorobenzene as the eluent. As shown in Figure 3.2, P1 exhibited number-average molecular weight ($\overline{Mn}$) value of 16.6 kg mol^{-1}, corresponding to a degree of polymerization of

34 repeat units. On the other hand, L-CLP showed a higher $\overline{Mn}$ value (18.5 kg mol^{-1}) than its precursor P1. This increase in $\overline{Mn}$ can be attributed to the formation of a more rigid structure after the CDHC reaction, leading to a higher hydrodynamic radius of the polymer in solution.[173] Interestingly, as shown in Figure 3.2, P2 exhibited $\overline{Mn}$ value of 15.8 kg mol^{-1}, corresponding to 32 repeat units, while the corresponding ladderized H-CLP showed a slightly lower $\overline{Mn}$ value of 12.8 kg mol^{-1}. In this case, the formation of a helical structure led to a contraction of the polymer backbone, thus decreasing the hydrodynamic radius in solution compared to the precursor P2. This trend has been observed for other helical GNRs[132] and ladder polymers.[87,189]

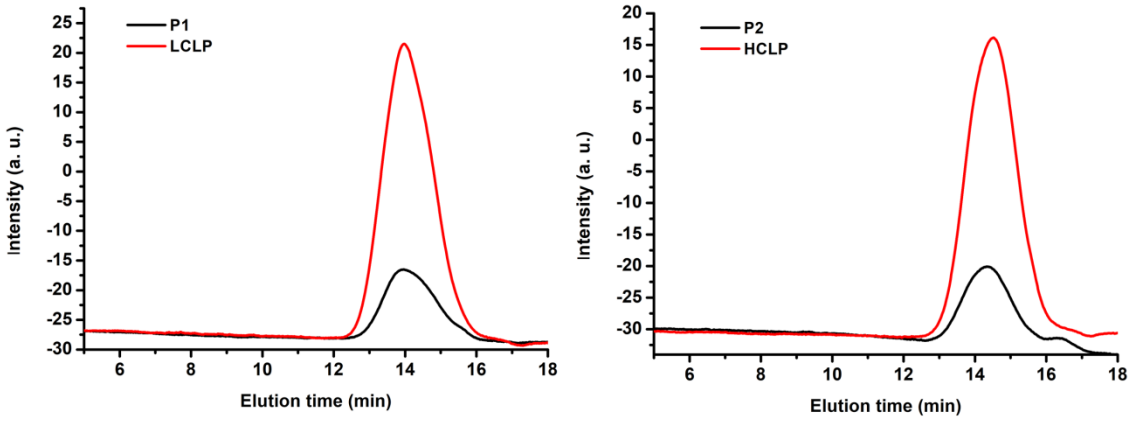

Figure 3.2. Size exclusion chromatography traces for P1 ($\overline{Mn}$: 16.6 kg mol^{-1}, $\overline{Mw}$: 29.4 kg mol^{-1}, dispersity index ($Đ$): 1.8, X_n: 34), L-CLP ($\overline{Mn}$ = 18.5 kg mol^{-1}, $\overline{Mw}$ = 30.7 kg mol^{-1}, dispersity index ($Đ$): 1.7), P2 ($\overline{Mn}$: 15.8 kg mol^{-1}, $\overline{Mw}$: 23.3 kg mol^{-1}, dispersity index ($Đ$): 1.5, X_n: 32), and H-CLP ($\overline{Mn}$ = 12.8 kg mol^{-1}, $\overline{Mw}$ = 20.4 kg mol^{-1}, dispersity index ($Đ$): 1.6, X_n: 31).

3.4.3. ^{1}H NMR analysis

The ^{1}H NMR analysis were conducted in tetrachloroethane-d_2 (TCE-d_2) at 383 K to confirm the chemical structures of P1, P2, L-CLP and H-CLP and the results are shown in Figure 3.3. P1 exhibits two well defined peaks at δ = 5.95 and 6.29 ppm, which can be ascribed to the two protons H_c and H_b attached to pyrrole, respectively, while the two peaks at 7.10 and 7.25 ppm

are associated to the phenyl protons H_a and H_d, respectively. Upon irradiation, a more delocalized π-conjugated structure is obtained, and L-CLP exhibits a flatter ^{1}H NMR spectrum with all the peaks broadened and shifted downfield up to 8.35 ppm.[151] Also, the peaks at δ = 5.95 and 6.29 ppm disappeared completely. These results strongly indicate that the CDHC reaction went to near completion. Similar behaviors are observed for P2 and H-CLP. Compared to P2, the spectrum for H-CLP flattens and shifts downfield as a rigid and more conjugated structure is obtained. Also, the peaks at δ = 5.85 and 6.25 ppm disappeared completely, suggesting again that the CDHC reaction went to near completion.

3.4.4. XPS analysis

X-ray photoelectron spectroscopy (XPS) analysis was performed to further attest the completeness of the photochemical CDHC reactions upon irradiation of P1 and P2 (see Figure 3.14-3.17, Supporting Information). For P1 and P2, the peak at 200 eV corresponds to the Cl 2p, indicating the presence of chlorine atoms in P1 and P2. As for L-CLP and H-CLP, the spectra showed no trace of this peak, meaning that the chlorine atoms have disappeared completely and no chlorine-containing side products were formed during the CDHC reaction. These results further confirm that the photochemical CDHC reaction is complete.

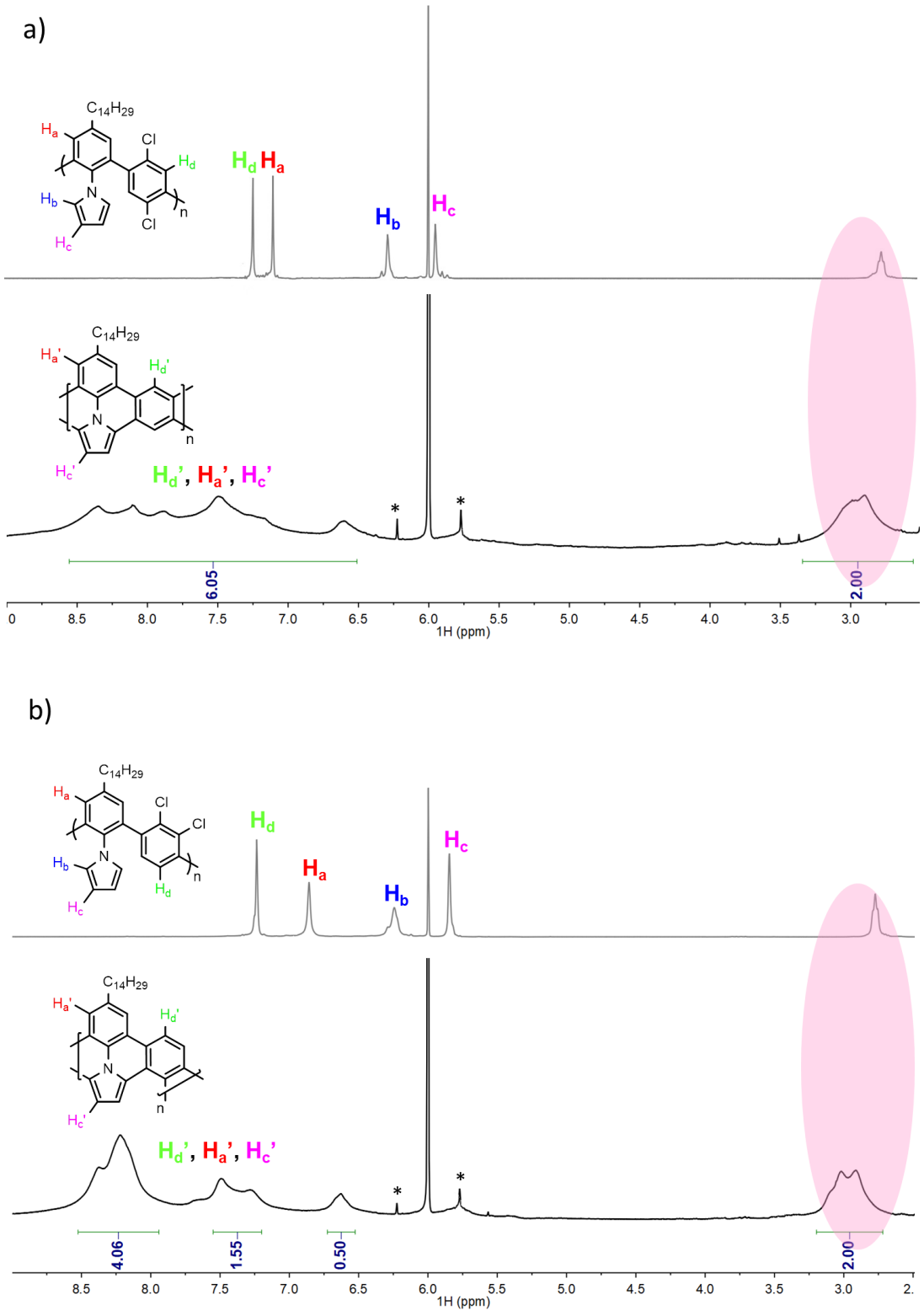

Figure 3.3. a) ^{1}H NMR spectra of precursor P1 (top) and L-CLP (bottom) in TCE-d_2 at 383 K. b) ^{1}H NMR spectra of precursor P2 (top) and H-CLP (bottom) in TCE-d_2 at 383 K.

3.4.5. UV-vis and photoluminescence analysis

The optical properties of L-CLP and H-CLP were investigated by UV-vis and photoluminescence spectroscopy and the results are shown in Figure 3.4. Compared to their precursors P1 and P2, L-CLP exhibits absorption between 280 to 550 nm with the absorption maxima at 295, 377, and 438 nm, and H-CLP absorbs between 280 to 550 nm with the absorption maxima at 292, 341, 375, and 458 nm, indicating that rigid and defined π-conjugated structures were formed upon irradiation. Similar absorption spectra were observed for hexapyrrolohexaazacoronenes.[190-192] The solid state absorption spectra are slightly red-shifted (5 and 9 nm for L-CLP and H-CLP, respectively) compared to that in solution. This result indicates that both L-CLP and H-CLP possess similar conformations in solution and solid state, which is expected for a rigid backbone structure.[87,88,132,154] Optical bandgaps measured from the onset of the absorption spectra in solution are 2.21 eV for L-CLP and 2.20 eV for H-CLP. In contrast with P1 and P2, both L-CLP and H-CLP exhibit strong photoluminescence properties in solution (see the insets of Figure 3.4). The emission maximum is located at 545 and 541 nm for L-CLP and H-CLP, with quite large Stokes shifts of 250 and 249 nm, respectively. Notably, the fluorescence excitation spectra of L-CLP and H-CLP were also recorded and they match well with the UV-vis absorption spectra (Supporting Information, Figure 3.18-3.19), indicating that the fluorescence emission were originated from the L-CLP and H-CLP themselves.

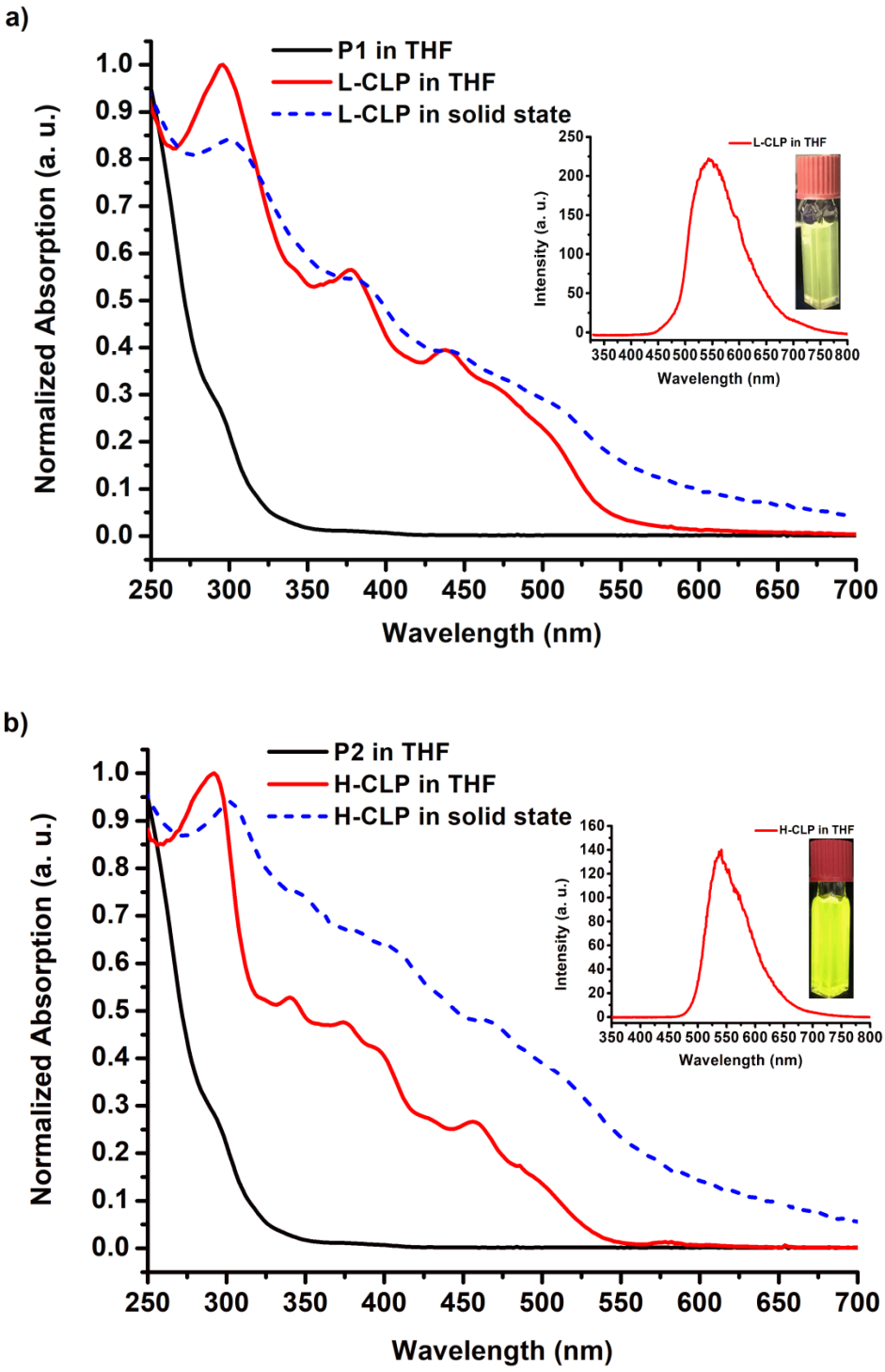

Figure 3.4. UV-vis absorption spectra of a) P1 and L-CLP and b) P2 and H-CLP in both solution (THF, solid lines) and solid state (dashed lines). Insets: Photoluminescence spectrum in THF solution (a) λ_{ex} = 300 nm, b) λ_{ex} = 292 nm).

3.4.6. Electrochemical properties

Thin film cyclic voltammetry (CV) measurements were performed to investigate the electrochemical properties and examine the electron-donating properties of both CLPs, and the results are shown in Figure 3.20-3.21. The estimated HOMO levels for L-CLP and H-CLP are -5.01 and -5.08 eV, respectively. The significantly high HOMO levels of the L-CLP and H-CLP can be attributed to the strong electron-donating property of the pyrrole units in the polymer backbone.[193] However, no reduction peaks have been observed, so the LUMO levels (-2.80 eV for L-CLP and -2.88 eV for H-CLP) were estimated from the optical bandgaps derived from the UV-vis absorption onsets.

3.4.7. Chemical titration

Chemical titration of the L-CLP and H-CLP with tris(4-bromophenyl)ammoniumyl hexachloroantimonate (TBPA) as the one-electron oxidant was conducted and the results are shown in Figures 3.5 and Figure 3.22 (Supporting Information). Upon oxidation of L-CLP with TBPA (gradually from 0 to 1 equivalent), a significant colour change from orange to dark green was observed, indicating that L-CLP is easily oxidized.[192] The oxidized derivatives were investigated by UV-vis-NIR spectroscopy in chloroform. Unlike the neutral L-CLP, which shows the lowest energy transition in the region 400-500 nm, the oxidized form exhibits a broad absorption band between 600-700 nm. Similar behaviour was also observed for H-CLP (see supporting information, Figure 3.22).

3.5. Conclusion

In conclusion, we synthesized linear and helical CLPs bearing electron-rich pyrrole units by the photochemical cyclodehydrochlorination (CDHC) reaction. ^{1}H NMR and XPS analysis confirmed the formation of the structures. The optical and electrochemical properties of both polymers were investigated and quite low bandgaps (2.21 eV for L-CLP, 2.20 eV for H-CLP) and very high HOMO energy levels (-5.01 eV and -5.08 eV) were obtained, indicating the

strong electron-donating property of the pyrrole units in the polymer backbone. And the very electron-rich polymers can be oxidized easily with a commercially available oxidant into stable radical cations. Future work will be focused on the preparation of wider CLPs containing pyrrole units and test their dispersion properties of carbon nanotubes.

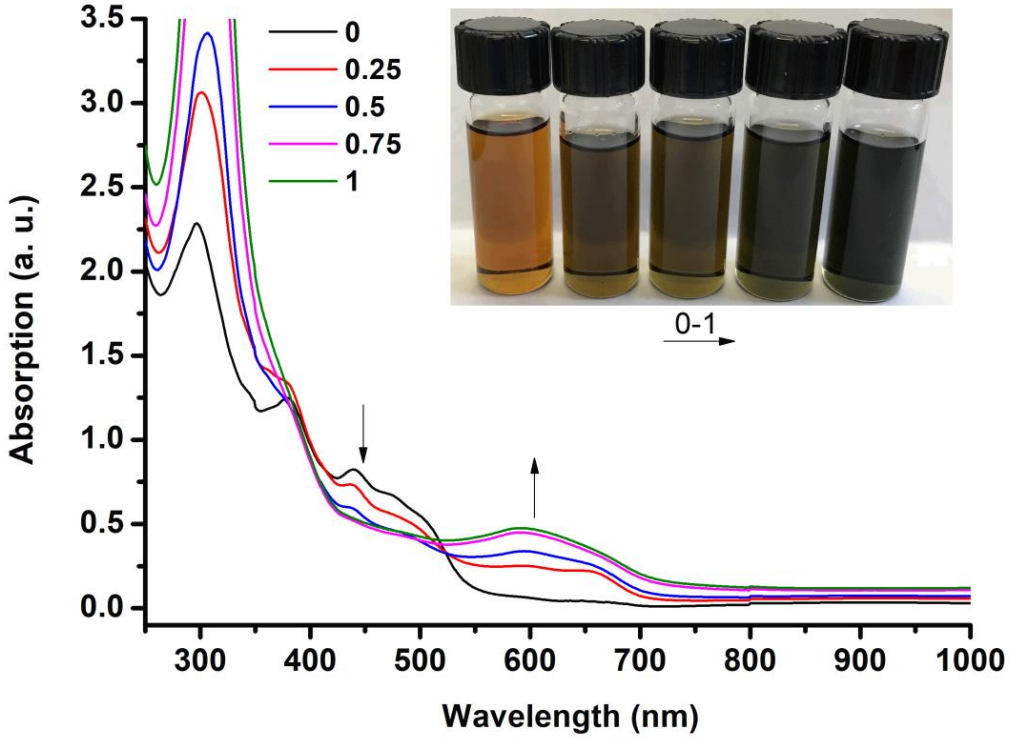

Figure 3.5. Changes of UV-vis-NIR spectra observed during chemical titrations of L-CLP with TBPA. Inset: Color changes (from orange to green) after adding different equivalents of TBPA into the L-CLP solution.

3.6. Acknowledgements

This work was supported by NSERC through a Discovery Grant. D.M. thanks the China Scholarship Council (CSC) for a PhD scholarship.

3.7. Supporting Information

3.7.1. Materials and Methods

Chemical reagents were purchased from Sigma-Aldrich Co. Canada, Alfa Aesar Co., TCI America Co. or Oakwood Products Inc. and used as received, unless mentioned. Solvents used for organic synthesis were purchased from Fisher Chemical Co., EMD Millipore Co. and CFS Chemical Co. as HPLC grade. These solvents were degassed, dried and purified using a Solvent Purifier System (SPS) (Vacuum Atmosphere Co., Hawthorne, USA). Anhydrous decahydronaphthalene (mixture of *cis* + *trans*) was used as received for photochemical reactions and other anhydrous solvents were bought from Sigma-Aldrich Co. Canada. All anhydrous and air sensitive reactions were performed in oven-dried glassware purchased from Synthware™ under positive nitrogen stream. Analytical thin-layer chromatographies were performed with silica gel 60 F254, 0.25 mm pre-coated TLC plates (Silicycle, Québec, Canada). Compounds were revealed by a 254 nm and/or 365 nm UV wavelength and/or aqueous K_2CO_3 and NaOH solution of potassium permanganate. Flash column chromatographies were performed with 230-400 mesh silica gel R10030B (Silicycle, Québec, Canada). 1,4-dichloro-2,5-diiodobenzene and 2,3-dichloro-1,4-diiodobenzene were synthesized according to literature procedures[131] and further purified by recrystallization in isopropanol. 1-(4-tetradecyl-2,6-bis(4,4,5,5-tetramethyl-1,3,2-dioxaborolan-2-yl)phenyl)-1*H*-pyrrole was synthesized according to a previously reported procedure.[187]

3.7.2. Apparatus

Photochemical reactions were performed in a CCP-ICH2 Luzchem® photochemical reactor equipped with a thermostat and a heating mantle. Photochemical reactions were performed in a 100 mL quartz round-bottom flask bought from Chemglass®. Nuclear magnetic resonance (NMR) spectra were recorded on a Varian Inova AS400 spectrometer (Varian, Palo Alto, USA) at 400 MHz (^{1}H) and 100 MHz (^{13}C). Signals are reported as m (multiplet), s (singlet), d

(doublet), t (triplet), and coupling constants are reported in hertz (Hz). Chemical shifts are reported as values ppm (δ) relative to residual solvent peak. High resolution mass spectra (HRMS) were recorded with an Agilent 6210 Time-of-Flight (TOF) LC-MS apparatus equipped with an APPI ion source (Agilent Technologies, Toronto, Canada). Number-average ($\overline{Mn}$) and weight-average ($\overline{Mw}$) molecular weights were determined by size-exclusion chromatography (SEC) using a Varian Polymer Laboratories GPC220 equipped with an RI detector and a PL BV400 HT Bridge Viscometer. The column set consists of 2 PL gel Mixed C (300 × 7.5 mm) columns and a PL gel Mixed C guard column. The flow rate was fixed at 1mL min^{-1} using 1,2,4-trichlorobenzene (TCB) (with 0.0125% BHT w/v) as the eluent. The temperature of the system was set to 110 ℃. All the samples were prepared at a nominal concentration of 1.0 mg mL^{-1} in TCB. Dissolution was performed using a Varian Polymer Laboratories PL-SP 260VC sample preparation system. The sample vials were held at 110 ℃ with shaking for 1 h for complete dissolution. The solutions were filtered through a 2 mm porous stainless steel filter and a 0.40 μm glass filter into a 2 mL chromatography vial. The calibration method used to generate the reported data was the classical polystyrene method using polystyrene narrow standards Easi-Vials PS-M from Varian Polymer Laboratories which were dissolved in TCB. UV-visible absorption and photoluminescence spectra were recorded on UV-vis HP 8452 and Varian Cary Eclipse Fluorescence Spectrofluorimeter, respectively, using 10-mm path length quartz cells. For solid state measurements, the polymer solution (1.0 mg mL^{-1} in THF) was spin coated on quartz plates. Optical bandgaps were calculated from the onset of the absorption band. Cyclic voltammetry (CV) were recorded on a Solartron 1287 potentiostat using platinum wires as the working electrode and counter electrode at a scan rate of 50 mV s^{-1}. The reference electrode was Ag/Ag^+ (0.01 M $AgNO_3$ in acetonitrile) in an anhydrous and argon-saturated solution of 0.1 M tetrabutylammonium hexafluorophosphate (Bu_4NPF_6) in dry acetonitrile. Under these conditions, the oxidation potential of ferrocene was 0.09 V *versus* Ag/Ag^+, whereas the oxidation potential of ferrocene was 0.41 V *versus* the saturated calomel electrode (SCE). The HOMO and LUMO energy levels were determined from the oxidation and reduction onsets

(where the current starts to differ from the baseline) from the cyclic voltammogram assuming that the SCE is -4.71 eV in vacuum, as reported in the literature.[194] The chemical composition of the surface was investigated by X-ray Photoelectron Spectroscopy (XPS), using a PHI 5600-ci spectrometer (Physical Electronics, Eden Prairie, MN, USA). The main XPS chamber was maintained at a base pressure of $< 1 \times 10^{-8}$ Torr. A standard aluminium X-ray source (Al kalpha = 1486.6 eV) was used to record survey spectra (1400-0 eV, 10min) with charge neutralization. The detection angle was set at 45 °with respect to the normal of the surface and the analyzed area was 0.125 mm^2.

3.7.3. Synthesis

1-(2,2''-dichloro-5'-tetradecyl-[1,1':3',1''-terphenyl]-2'-yl)-1*H*-pyrrole) (1)

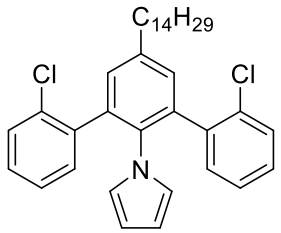

1

A round bottom flask under nitrogen was charged with 1-(4-tetradecyl-2,6-bis(4,4,5,5-tetramethyl-1,3,2-dioxaborolan-2-yl)phenyl)-1*H*-pyrrole (1.00 g, 1.69 mmol), 1-bromo-2-chlorobenzene (0.809 g, 4.23 mmol) and 2 M Na_2CO_3 aqueous solution (8.45 mL, 16.9 mmol) and flushed three times with a vacuum/nitrogen cycle. Toluene (13.5 mL), EtOH (2.10 mL) and H_2O (1.70 mL) was added and the resulting solution was degassed with a nitrogen stream for 10 mins. Pd(dppf)Cl_2 (0.138 g, 0.169 mmol) was added and the reaction flask was flushed three times with a vacuum/nitrogen cycle and heated to 100 ℃ for 16 hours. Once cooled to room temperature, 20 mL of water was added and the aqueous layer was extracted with dichloromethane (3×50 mL). The organic layer was dried with Na_2SO_4 and the solvent was removed under reduced pressure. The resulting residue was purified by silica gel chromatography (25% CH_2Cl_2/hexanes) to obtain compound **1** as a light yellow solid (0.853

g, 90%). ^{1}H NMR (400 MHz, $CDCl_3$): δ 7.28 (m, 10H), 6.37 (s, 2H), 5.79 (s, 2H), 2.75 (m, 2H), 1.74 (m, 2H), 1.29 (m, 22H), 0.91 (t, *J* = 6.8 Hz, 3H). ^{13}C NMR (100 MHz, $CDCl_3$): δ 141.91, 141.56, 138.22, 137.88, 137.14, 136.98, 135.66, 133.96, 133.76, 133.60, 133.27, 131.17, 130.88, 130.76, 130.63, 129.36, 128.80, 126.29, 123.13, 122.49, 108.20, 107.61, 35.56, 32.08, 31.35, 29.85, 29.83, 29.81, 29.74, 29.61, 29.52, 29.36, 22.85, 14.29. HRMS (APPI+): calculated for $C_{36}H_{43}Cl_2N$ $(M + H)^+$ 559.28321, found 559.28796.

8-tetradecylbenzo[7,8]indolizino[6,5,4,3-*def*]phenanthridine (2)

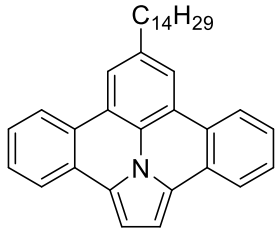

2

A quartz flask was oven-dried and flushed three times with a vacuum/nitrogen cycle. Compound **1** (56.1 mg, 0.100 mmol) and anhydrous decahydronaphthalene (100 mL) were added to the flask and the solution was degassed with a continuous flow of argon for 10 minutes. The solution was then irradiated under 254 nm at 100 ℃ for 2 hours under a continuous flow of argon. After cooling down to room temperature, the solvent was removed by vacuum distillation and the resulting residue was purified by silica gel chromatography (25% CH_2Cl_2/hexanes) to obtain compound **2** as a dark yellow solid (46.9 mg, 96%). ^{1}H NMR (400 MHz, $CDCl_3$): δ 8.34 (d, *J* = 4.0 Hz, 2H), 8.12 (m, 4H), 7.53 (t, *J* = 7.4 Hz, 2H), 7.45 (t, *J* = 7.7 Hz, 2H), 7.29 (s, 2H), 2.92 (t, *J* = 7.8 Hz, 2H), 1.81 (m, 2H), 1.25 (m, 22H), 0.87 (t, *J* = 7.1 Hz, 3H). ^{13}C NMR (100 MHz, $CDCl_3$): δ 138.25, 129.38, 128.48, 126.65, 126.09, 125.52, 125.45, 123.17, 123.04, 122.82, 120.54, 103.53, 36.86, 32.31, 32.08, 29.86, 29.81, 29.79, 29.74, 29.55, 29.52, 22.85, 14.28. HRMS (APPI+): calculated for $C_{36}H_{41}N$ $(M + H)^+$ 487.32390, found 487.33225.

Polymerization procedure for the precursors P1, P2

1-(4-tetradecyl-2,6-bis(4,4,5,5-tetramethyl-1,3,2-dioxaborolan-2-yl)phenyl)-1*H*-pyrrole was polymerized with 1,4-dichloro-2,5-diiodobenzene and 2,3-dichloro-1,4-diiodobenzene by a palladium-catalyzed Suzuki-Miyaura polymerization to afford the precursors P1 and P2, respectively. A flask under nitrogen was charged with 1-(4-tetradecyl-2,6-bis(4,4,5,5-tetramethyl-1,3,2-dioxaborolan-2-yl)phenyl)-1*H*-pyrrole (1 equiv.), 1,4-dichloro-2,5-diiodobenzene or 2,3-dichloro-1,4-diiodobenzene (1 equiv.), $LiOH•H_2O$ (8 equiv.), THF (0.1 M) and H_2O (0.8 M). The flask was flushed three times with a vacuum/nitrogen cycle and degassed with a continuous flow of nitrogen for 10 minutes. $Pd_2(dba)_3$ (0.01 equiv.) and SPhos (0.08 equiv.) were added and the reaction flask was flushed three times using a vacuum/nitrogen cycle and the reaction mixture was heated at 60 ℃ for 12 hours. Once cooled to room temperature, the reaction mixture was precipitated in cold methanol under strong stirring and filtered through a 0.45 μm nylon filter. The residue was purified by Soxhlet extraction in acetone for 24 hours and recovered with hexanes through the extraction thimble. The solvent was removed under reduced pressure with the exclusion of light and the solid was dissolved in a minimum amount of hexanes, precipitated in methanol, filtered through a 0.45 μm nylon filter and thoroughly dried under vacuum.

Polymer P1

1-(4-tetradecyl-2,6-bis(4,4,5,5-tetramethyl-1,3,2-dioxaborolan-2-yl)phenyl)-1*H*-pyrrole (0.250 g, 0.423 mmol) was polymerized with 1,4-dichloro-2,5-diiodobenzene (0.169 g, 0.423 mmol) according to the procedure described above. Polymer P1 ($\overline{Mn}$ = 16.6 kg mol^{-1}, $\overline{Mw}$ = 29.4 kg mol^{-1}, dispersity index ($Đ$): 1.8) was obtained as a yellow powder (0.175 g, 86%).

Polymer P2

1-(4-tetradecyl-2,6-bis(4,4,5,5-tetramethyl-1,3,2-dioxaborolan-2-yl)phenyl)-1*H*-pyrrole (0.250 g, 0.423 mmol) and 2,3-dichloro-1,4-diiodobenzene (0.169 g, 0.423 mmol) was copolymerized

according to the procedure described above. Polymer P2 ($\overline{Mn}$ = 15.8 kg mol^{-1}, $\overline{Mw}$ = 23.3 kg mol^{-1}, dispersity index ($Đ$): 1.5) was obtained as a light yellow powder (0.179 g, 88%).

Photochemical procedure for the synthesis of L-CLP and H-CLP

Precursor (P1, P2) was dissolved in anhydrous decahydronaphthalene (0.002 M) in an oven-dried quartz flask under argon. The solution was degassed with a continuous flow of argon for 10 minutes. The solution was heated to 100 ℃ and irradiated with 16 × 7.2 W low pressure mercury lamps at λ = 254 nm for 72 hours while maintaining a continuous flow of argon. Once cooled down to room temperature, the solvent was removed by vacuum distillation and the solid was dissolved in a minimum amount of THF, precipitated in cold methanol, filtered through a 0.45 μm nylon filter. The residue was purified by Soxhlet extraction in hexanes for 24 hours and recovered with THF. Once concentrated to a minimum amount of solvent, the polymer was precipitated in methanol, filtered and thoroughly dried under vacuum.

L-CLP

P1 (96.0 mg) was subjected to the procedure described above to obtain L-CLP ($\overline{Mn}$ = 18.5 kg mol^{-1}, $\overline{Mw}$ = 30.7 kg mol^{-1}, dispersity index ($Đ$): 1.7) as a dark brown solid (75.0 mg, 92%).

H-CLP

P2 (96.0 mg) was subjected to the procedure described above to obtain H-CLP ($\overline{Mn}$ = 12.8 kg mol^{-1}, $\overline{Mw}$ = 20.4 kg mol^{-1}, dispersity index ($Đ$): 1.6) as a dark orange solid (77.0 mg, 94%).

3.7.4. NMR Spectra

Compound 1

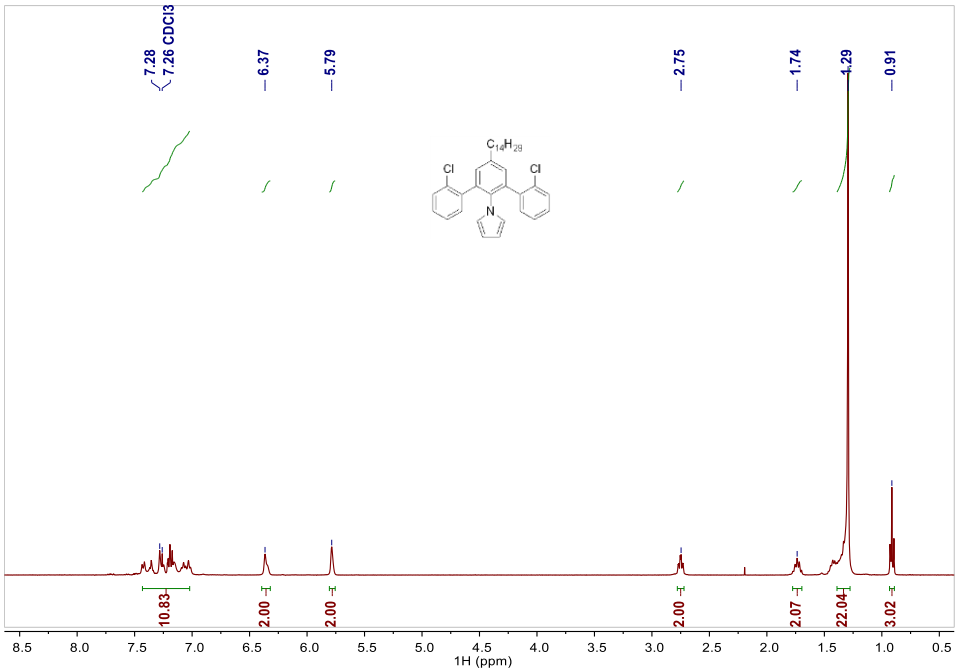

Figure 3.6. ^{1}H NMR spectrum of compound **1** in $CDCl_3$.

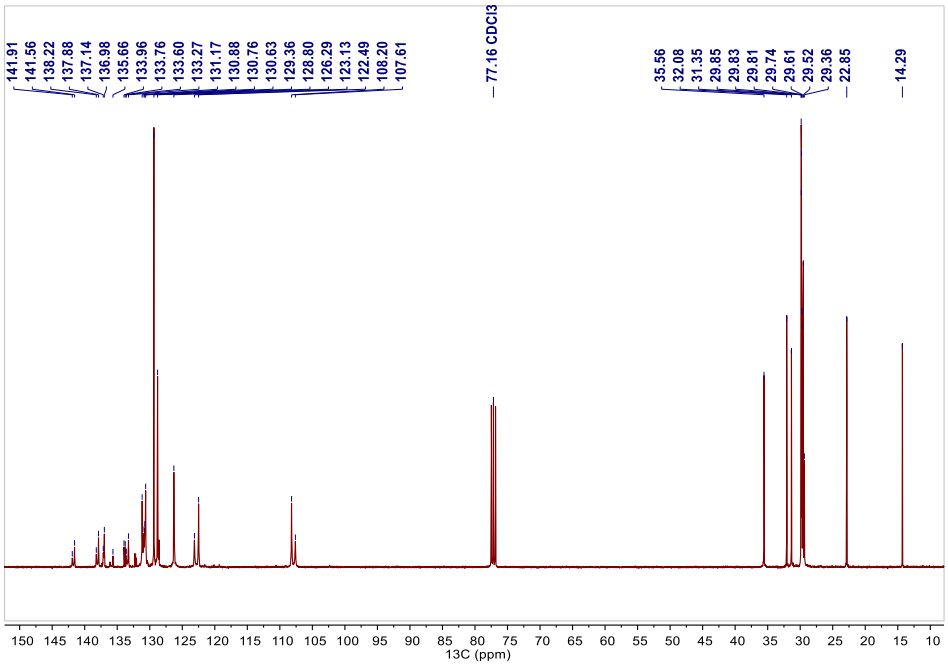

Figure 3.7. ^{13}C NMR spectrum of compound **1** in $CDCl_3$.

Compound 2

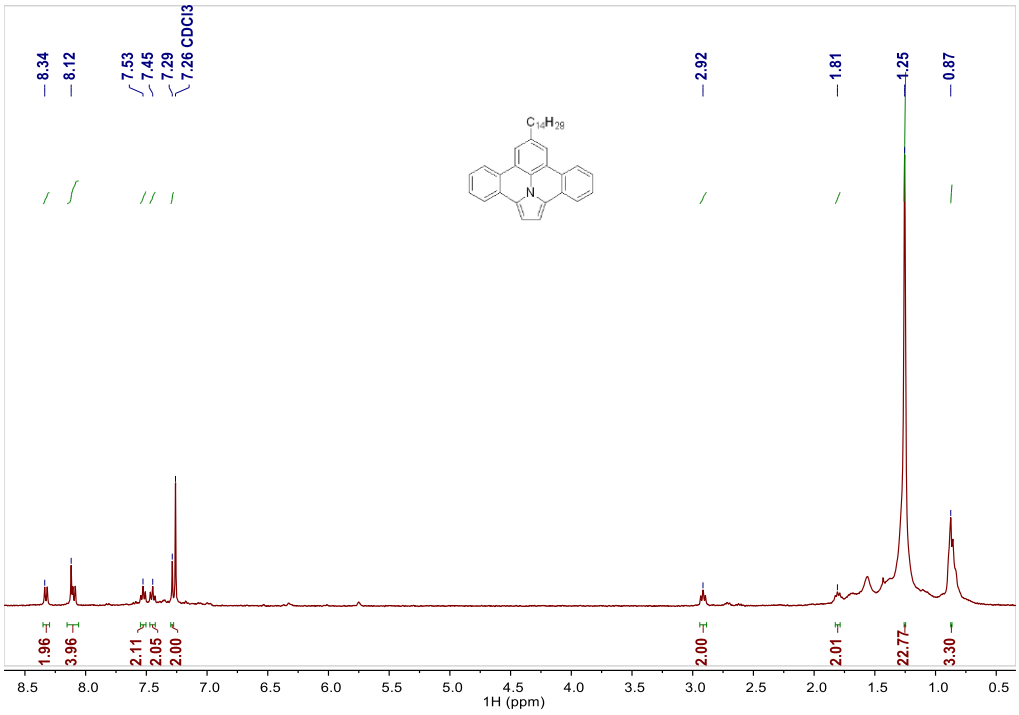

Figure 3.8. ^{1}H NMR spectrum of compound **2** in $CDCl_3$.

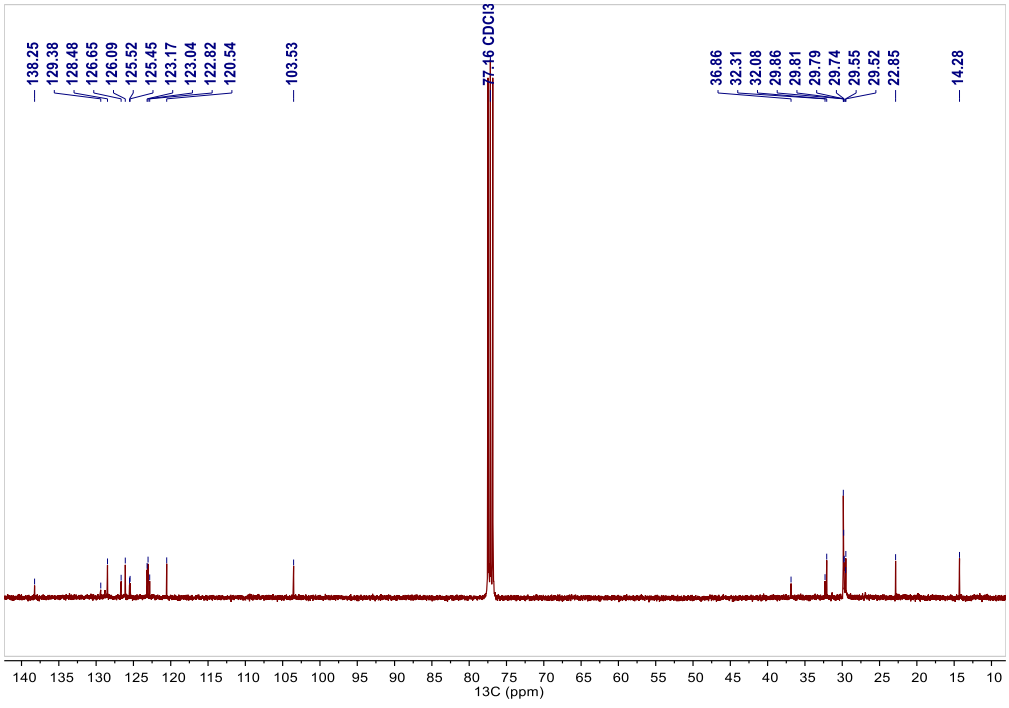

Figure 3.9. ^{13}C NMR spectrum of compound **2** in $CDCl_3$.

Polymer P1

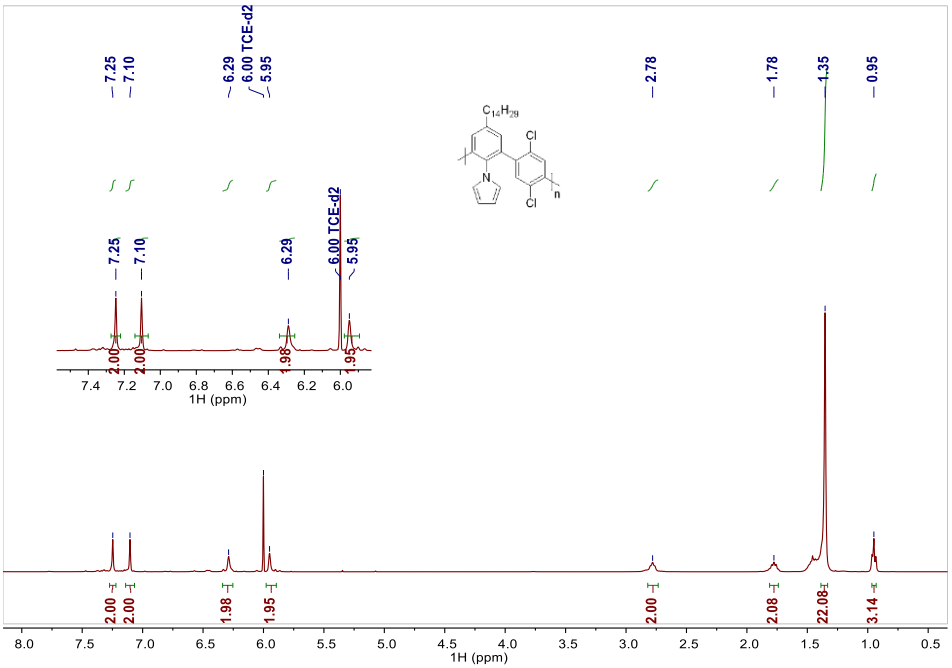

Figure 3.10. ^{1}H NMR spectrum of polymer P1 in TCE-d_2 at 383 K.

L-CLP

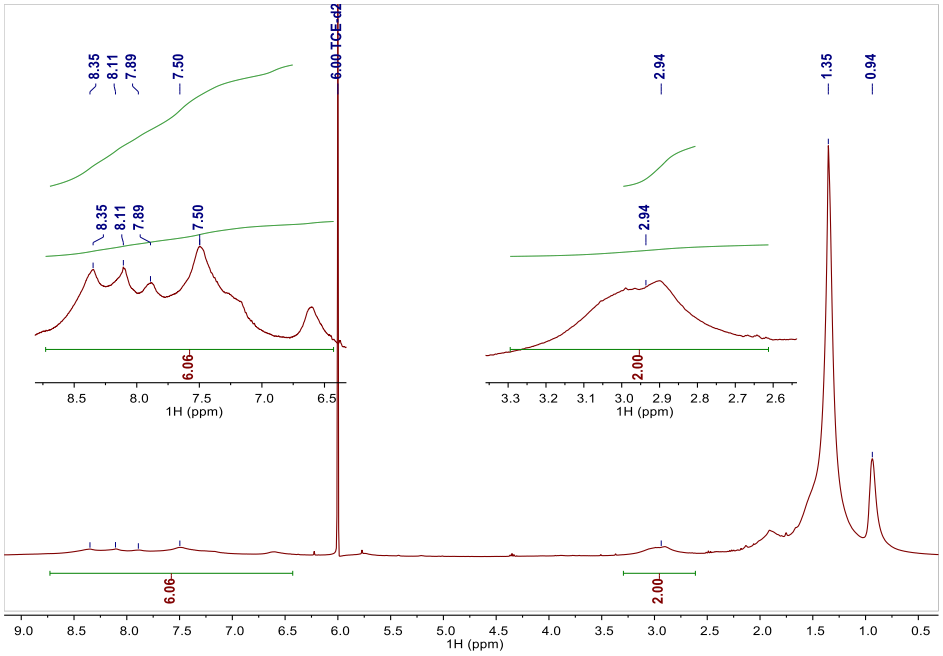

Figure 3.11. ^{1}H NMR spectrum of polymer L-CLP in TCE-d_2 at 383 K.

Polymer P2

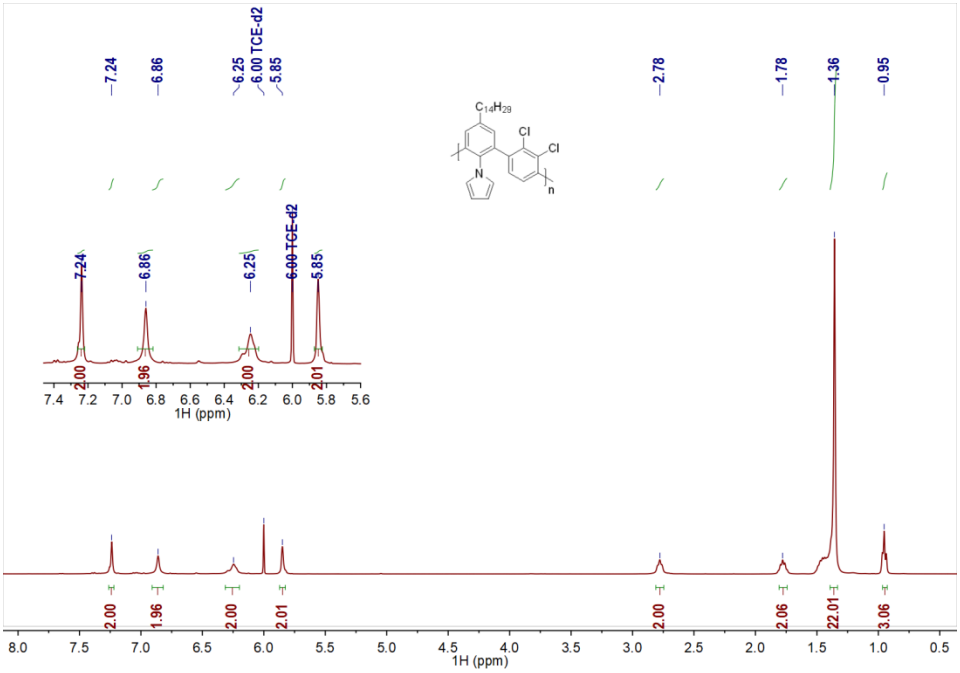

Figure 3.12. ^{1}H NMR spectrum of polymer P2 in TCE-d_2 at 383 K.

H-CLP

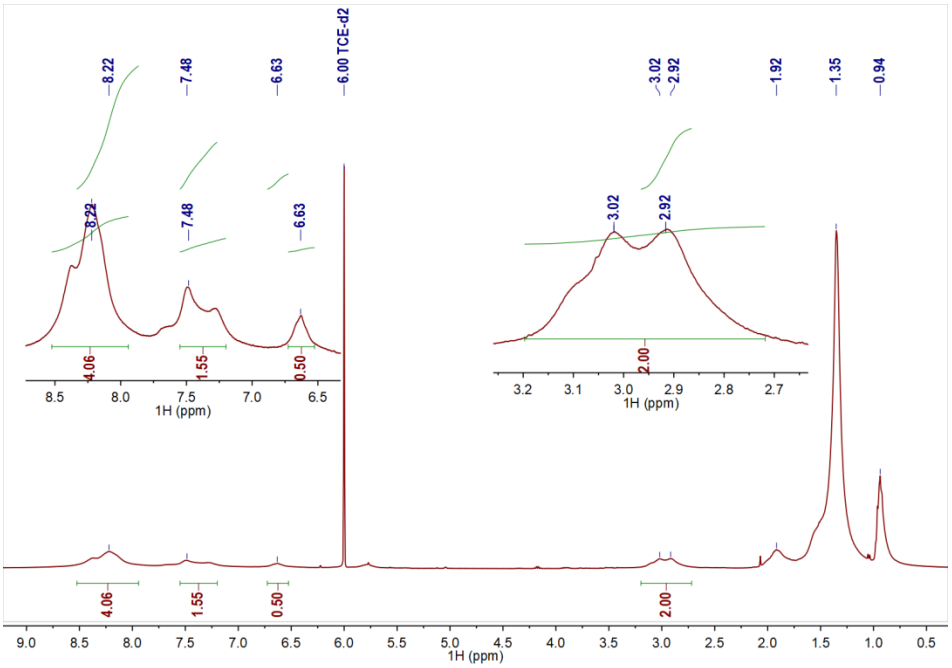

Figure 3.13. ^{1}H NMR spectrum of polymer H-CLP in TCE-d_2 at 383 K.

3.7.5. XPS analysis

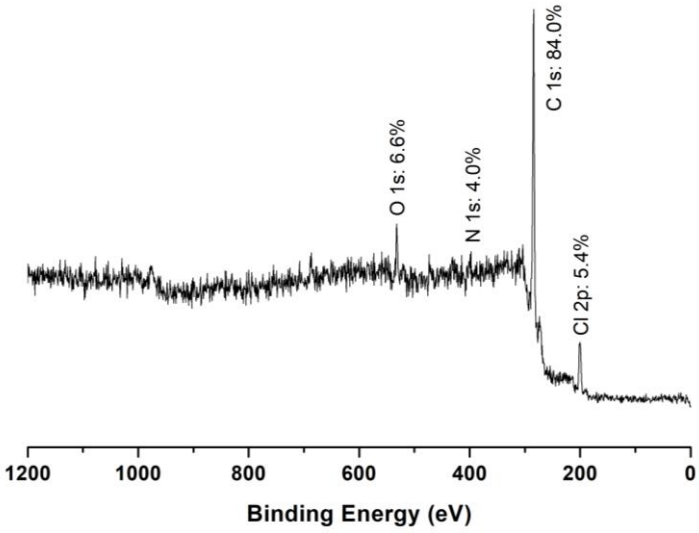

Figure 3.14. XPS spectrum of P1. The presence of oxygen is due to the sample holder made of a silicon-based polymer.

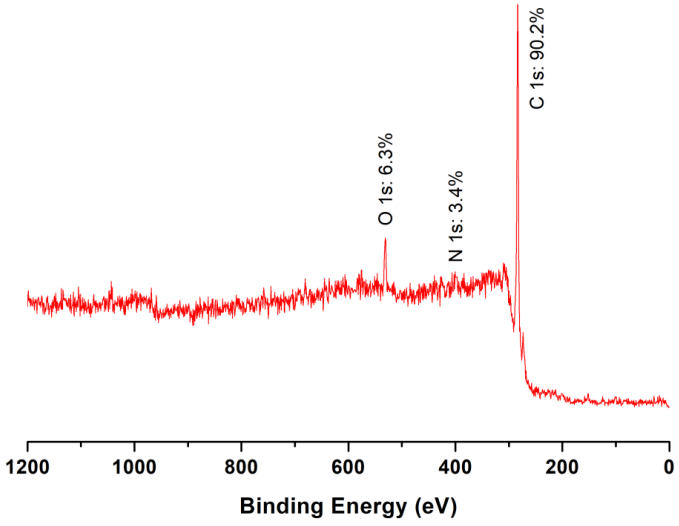

Figure 3.15. XPS spectrum of L-CLP. The presence of oxygen is due to the sample holder made of a silicon-based polymer.

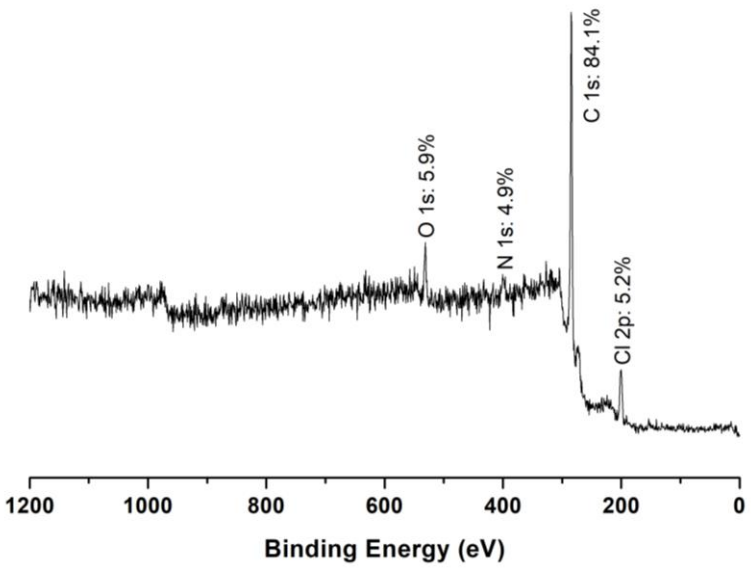

Figure 3.16. XPS spectrum of P2. The presence of oxygen is due to the sample holder made of a silicon-based polymer.

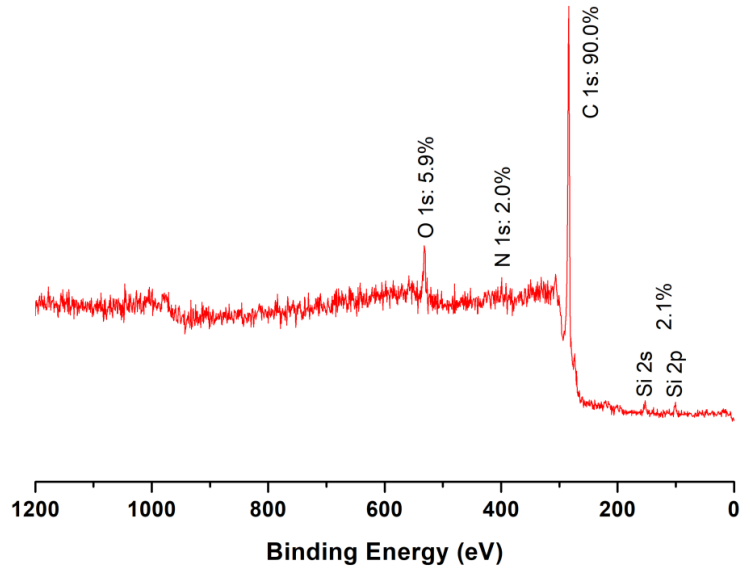

Figure 3.17. XPS spectrum of H-CLP. The presence of oxygen is due to the sample holder made of a silicon-based polymer.

3.7.6. UV-vis and photoluminescence analysis

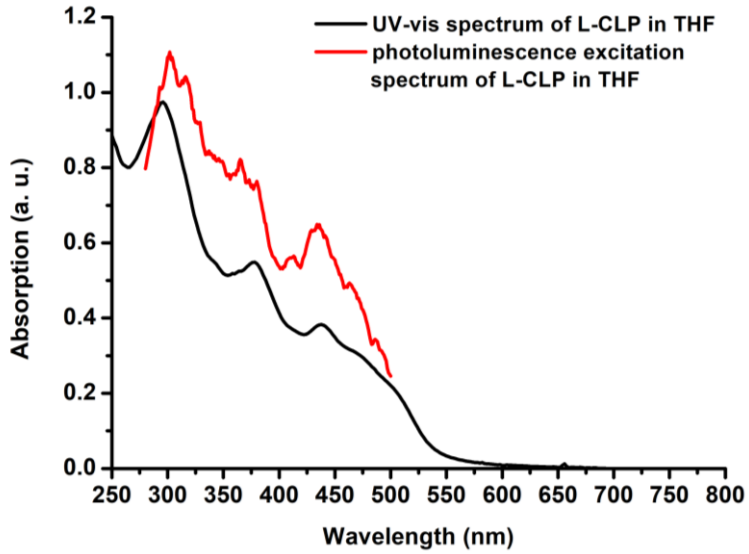

Figure 3.18. UV-vis absorption (black) and photoluminescence excitation (red, monitored at λ_{em} = 540 nm) spectra of L-CLP in THF solution. The intensity scale of the excitation spectrum is arbitrary.

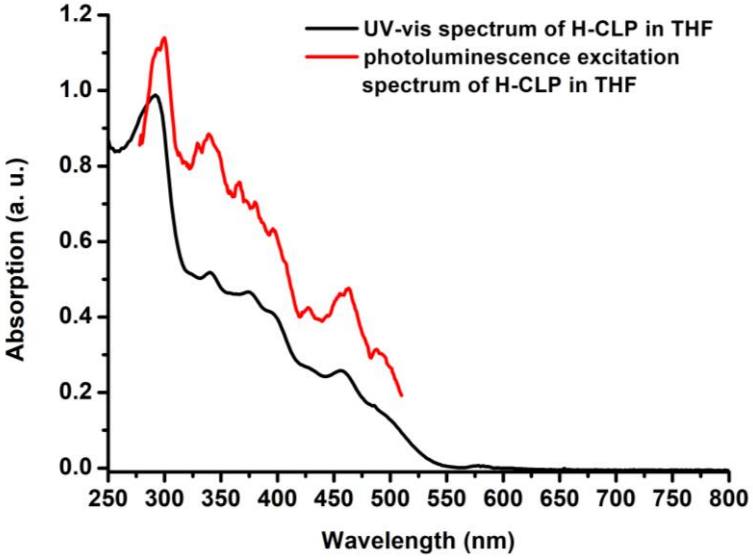

Figure 3.19. UV-vis absorption (black) and photoluminescence excitation (red, monitored at λ_{em} = 540 nm) spectra of H-CLP in THF solution. The intensity scale of the excitation spectrum is arbitrary.

3.7.7. Cyclic voltammetry

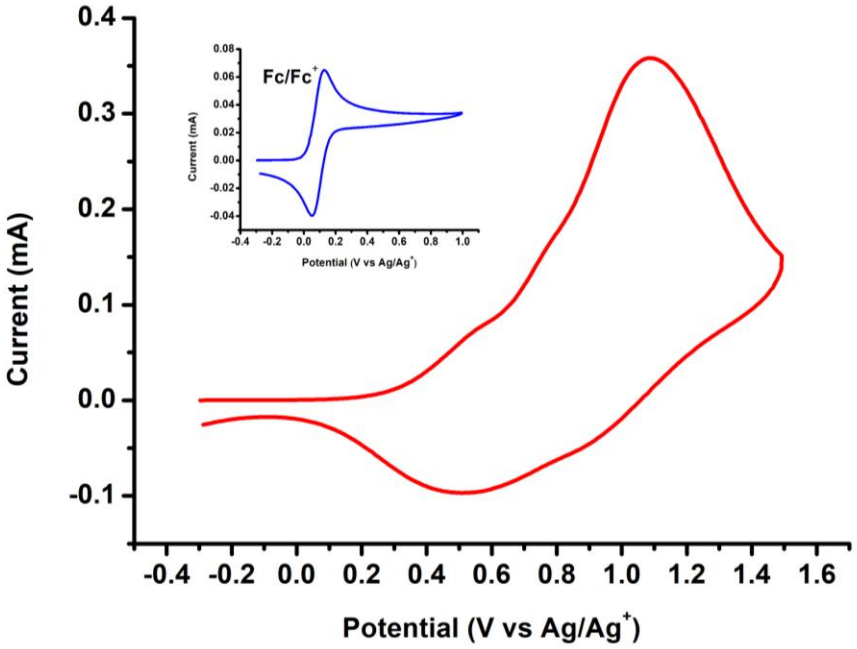

Figure 3.20. Film Cyclic Voltammetry of L-CLP.

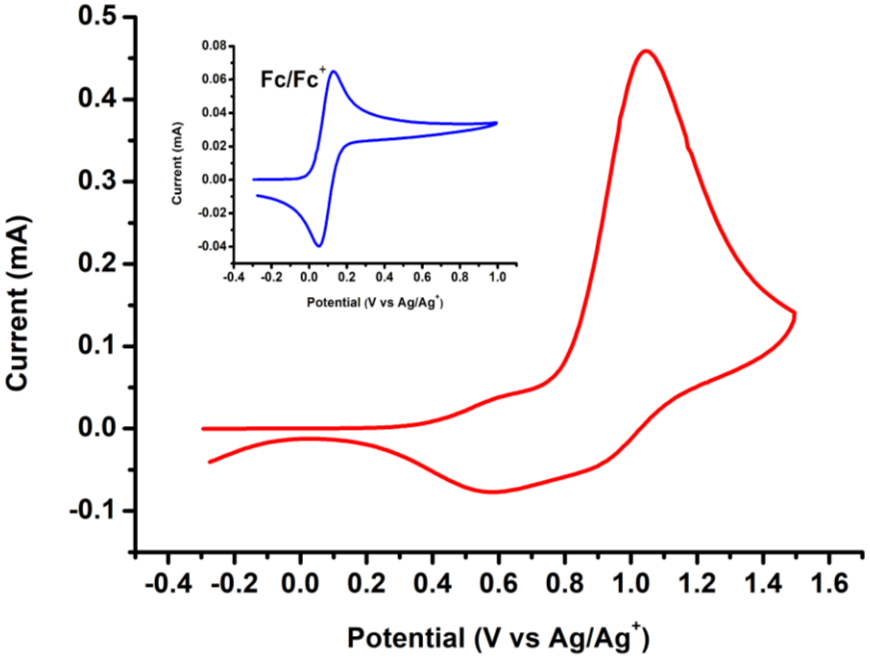

Figure 3.21. Film Cyclic Voltammetry of H-CLP.

3.7.8. Chemical titration of H-CLP

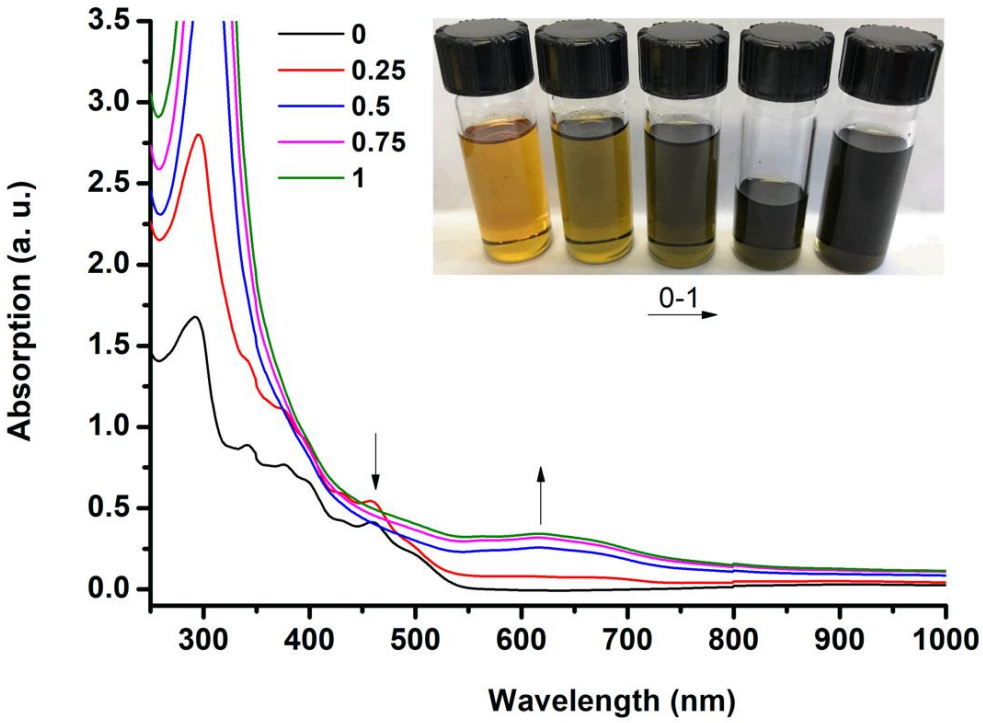

Figure 3.22. Changes of UV-vis-NIR spectra observed during chemical titrations of H-CLP with TBPA. Inset: Color changes (from orange to green) after adding different equivalents of TBPA into the H-CLP solution.

Chapter 4. **Photochemical synthesis of π-extended ullazine derivatives as new electron donors for efficient conjugated D-A polymers**

Dandan Miao[a], Cyril Aumaitre[a], and Jean-François Morin*[a]

a) Département de Chimie et Centre de Recherche sur les Materiaux Avancés (CERMA), Université Laval, Pavillon A.-Vachon, 1045 Ave de la Médecine, Québec QC, Canada G1V 0A6

Received manuscript on October 19, 2018.

Accepted manuscript online on February 11, 2019.

Published in *Journal of Materials Chemistry C*, **2019**, *7*, 3015-3024.

4.1. Résumé

Nous rapportons la synthèse des dérivés ullazine allongés avec prolongés annulés comportant des unités pyridine pauvres en électrons ou des unités thiophènes riches en électrons via une réaction de cyclodéhydrochlorination photochimique (CDHC) sans métal. Le dérivé étant le plus puissant donneur d'électrons, le 7-tétradécylthiéno [3',2':7,8] indolizino [6,5,4,3-*ija*] thiéno [2,3-*c*] quinolone, a été copolymérisé avec de la thiénopyrrolédione déficiente en électrons (DPT), l'isoindigo (IID) et les dérivés de dicétopyrrolopyrrole (DPP) pour fournir trois polymères conjugués donneur-accepteur (CP D-A). Leurs propriétés photophysiques, électrochimiques et photovoltaïques (PV) ont été étudiées. Les polymères présentaient de larges bandes d'absorption UV-vis-NIR avec des valeurs de λ_{max} de 612 nm, 698 nm, 788 nm dans le chloroforme et présentaient une bande interdite optique (E_g^{opt}) de 1.58 eV, 1.41 eV et 1.24 eV, mesurée sous forme de films. Des cellules solaires à polymère hétérojonction en masse inversée (BHJ-PSC) ont été fabriquées en utilisant ces polymères comme matériau hôte et récupérateur de lumière. Le dispositif basé sur les mélanges P3:$PC_{70}BM$ présente le meilleur rendement de conversion de puissance de 2.23% (V_{oc} = 0.55 V, J_{sc} = 7.86 mA cm^{-2}, FF = 52%). Ces résultats prometteurs démontrent que les dérivés ullazine allongés avec peuvent être utilisés comme blocs de construction riches en électrons pour la construction de CP D-A pour des applications efficaces de PSC.

4.2. Abstract

We report the synthesis of π-extended ullazine derivatives annulated with either electron-poor pyridine or electron-rich thiophene units through a metal-free, photochemical cyclodehydrochlorination (CDHC) reaction. The strongest electron-donor derivative, 7-tetradecylthieno[3',2':7,8]indolizino[6,5,4,3-*ija*]thieno[2,3-*c*]quinolone, was copolymerized with electron-deficient thienopyrroledione (TPD), isoindigo (IID), and diketopyrrolopyrrole (DPP) derivatives to provide three donor-acceptor conjugated polymers (D-A CPs). Their

photophysical, electrochemical and photovoltaic (PV) properties were investigated. The polymers showed broad UV-vis-NIR absorption bands with λ_{max} values of 612 nm, 698 nm, 788 nm in chloroform and exhibited optical bandgap (E_g^{opt}) of 1.58 eV, 1.41 eV, 1.24 eV measured as films. Inverted bulk heterojunction polymer solar cells (BHJ-PSCs) were fabricated using these polymers as host and light-harvesting materials. The device based on P3:$PC_{70}BM$ blends shows the best power conversion efficiency (PCE) of 2.23% (V_{oc} = 0.55 V, J_{sc} = 7.86 mA cm^{-2}, FF = 52%). These promising results demonstrate that π-extended ullazine derivatives can be used as electron-rich building blocks for the construction of D-A CPs for efficient PSCs applications.

4.3. Introduction

Ullazine and its π-extended derivatives have recently attracted the attention of the organic electronics community due to their planarity and electron-rich character. The chemical modification with various functional groups and addition of electron-deficient moieties on the periphery of ullazine provide promising opto- and electroactive materials with a wide range of electronic properties.[195,196] With 16 π-electrons, ullazine is isoelectronic to pyrene, but can also be seen as an aromatic, 14 π-electron annulene (outer ring) with a positively charged nitrogen atom resulting from a mesomeric effect.[197] This provides ullazine with the unusual ability to donate electrons while stabilizing the reduced form of the molecule. Ullazine-based molecules have been mostly used as a light-harvesting moiety and electron donor in dye-sensitized solar cells (DSSCs) and an efficiency as high as 8.45% has been obtained.[198] Despite its potential, ullazine has been scarcely used as a building block for organic semiconductors and no example of conjugated polymers incorporating this unit has been reported so far. This might be explained by the difficulty of preparing ullazine derivatives with synthetic handles (Br, I, OTf, $B(OR)_2$, *etc*.) on the alkene units bridging the pyrrole and the phenyl moieties.

Since the first report on the synthesis of ullazine by Balli and Zeller in 1983,[199] several improved methods have been reported, including metal-catalyzed annulation of substituted alkynes,[197,199-205] Friedel-Crafts reaction[206] and [2+3]-cycloaddition reaction on azomethine

ylides.[207,208] Using all these methods, several ullazine derivatives have been prepared, but very few π-extended analogs in the lateral axis have been reported.[209,210] The [2+3]-cycloaddition on azomethine ylides is the only reported strategy so far to provide fused ullazine derivatives and only phenyl-annulated derivatives have been synthesized.

Herein, we report a metal-free, photochemical strategy for the formation of π-extended ullazine derivatives from chlorinated precursors (Scheme 4.1). One of the thiophene-fused derivatives, the 7-tetradecylthieno[3',2':7,8]indolizino[6,5,4,3-*ija*]thieno[2,3-*c*]quinolone, was copolymerized with different electron-deficient moieties and the resulting D-A conjugated polymers were tested in bulkheterojunction solar cells. To the best of our knowledge, this is the first report of conjugated polymers with π-extended ullazine as a comonomer.

4.4. Results and Discussion

4.4.1. Synthesis of ullazine derivatives

Our synthetic approach for the synthesis of π-extended ullazine derivatives involved the photochemical cyclodehydrochlorination (CDHC) reaction as the key step. Our group used this reaction recently for the synthesis of nanographenes[131] and graphene nanoribbons.[87,88,132] The synthetic routes for the ullazine derivatives are shown in Scheme 4.1. Compound **1** was obtained by iodination at the 2 and 6 positions of 4-tetradecylaniline using iodine monochloride in a mixture of H_2O and HCl.[211] Then, the formation of the pyrrole was achieved using the Clauson-Kass reaction between compound **1** and 2,5-dimethoxytetrahydrofuran in the mixture of AcOH and 1,2-dichloroethane.[212] A two-fold borylation reaction using copper iodide (CuI) as the catalyst[213] gave compound **3** that was coupled to 2-bromo-3-chloropyridine and 3-bromo-2-chloropyridine using Pd(dppf)Cl_2 as the catalyst to give compounds **4** (81%) and **6** (88%), respectively. Likewise, compound **3** coupling with 2-bromo-3-chlorothiophene and 3-bromo-2-chlorothiophene using $PdCl_2(PPh_3)_2$ as the catalyst give compounds **8** (89%) and **10** (86%), respectively. It is noteworthy that the conditions had to be optimized for the coupling

with thiophene units as those used for the coupling with pyridine failed to provide the desire products. Compounds **4**, **6**, **8** and **10** were subjected to a photochemical CDHC reaction using conditions that we optimized previously for other substrates:[87,88,131,132] the chlorinated precursors were dissolved in degassed decahydronaphthalene (decalin) at a concentration of 0.001 M and the solutions were irradiated under UV light (16 × 7.2 W low pressure mercury lamps, λ = 254 nm) at 100 ℃ for 2 hours under a continuous flow of argon to obtain the photocyclized compounds **5** (96%), **7** (94%), **9** (92%) and **11** (95%) in excellent yield with no formation of side products. These results demonstrate the versatility of the CDHC reaction to link different heterocycles in an intramolecular fashion.

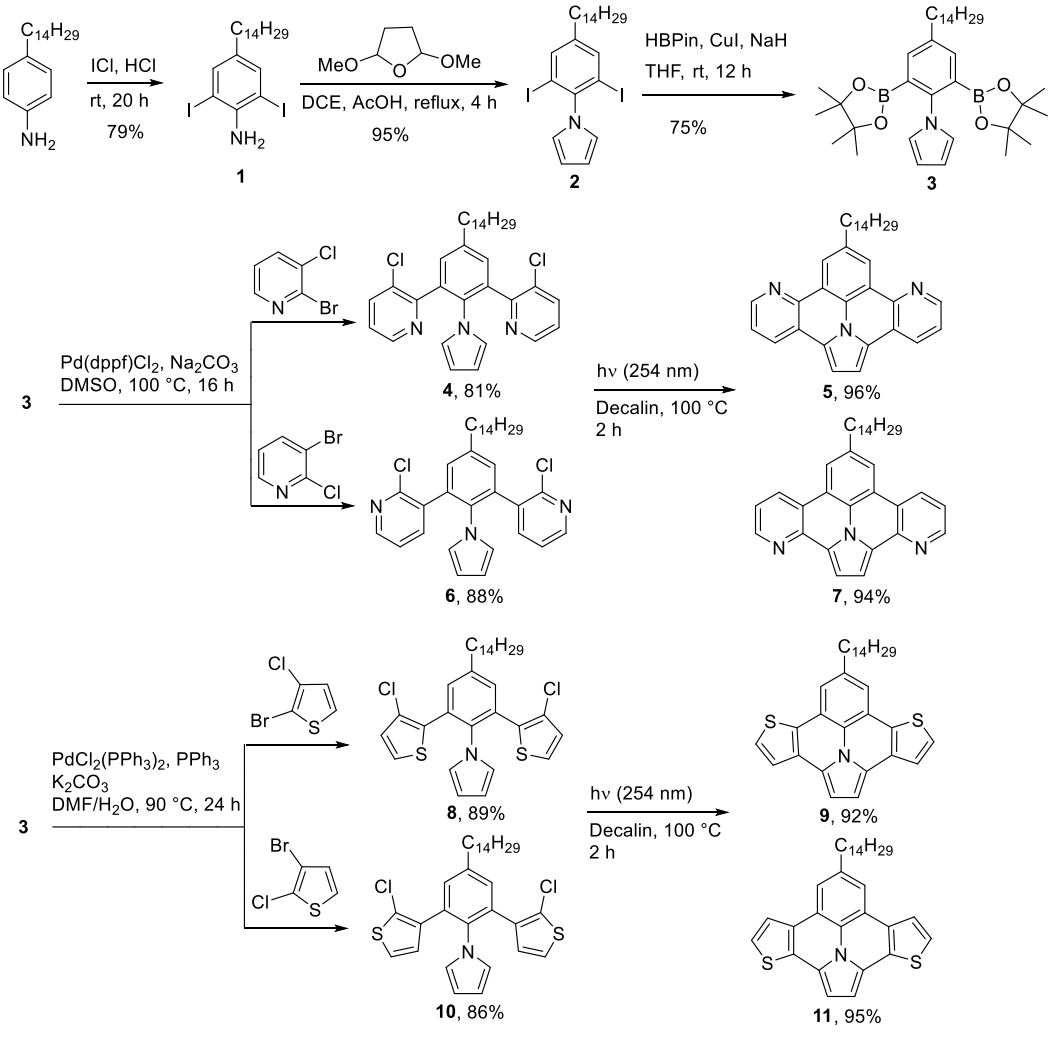

Scheme 4.1. Synthetic routes of the ullazine derivatives.

4.4.2. Optical properties of ullazine derivatives

Figure 4.1 shows the UV-vis absorption spectra of the 4 photocyclized compounds. As shown in Figure 4.1, all π-extended ullazine derivatives exhibit a highly defined vibronic structure, as expected for very rigid structure.[214] Also, compared with their chlorinated precursors, the absorption peaks are all significantly red-shifted (see Supporting Information, Figure 4.32), which confirms that the photocyclization leads to more conjugated structures. Interestingly, the nature of the heterocycle fused at both ends of the ullazine unit does not have a significant influence on the optical properties of the ullazine as all four derivatives have a band gap value of *ca*. 2.8 eV (from the onset of the absorption spectra).

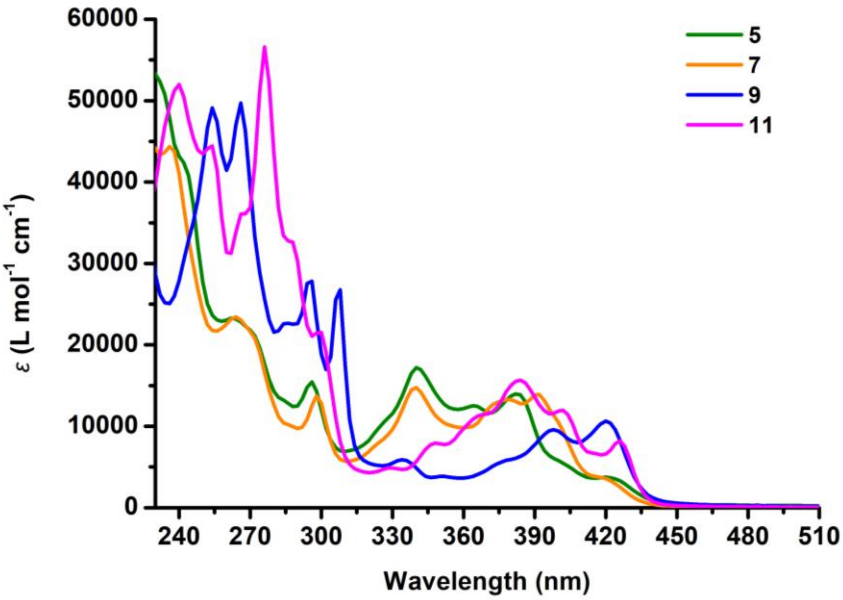

Figure 4.1. UV-vis absorption spectra of compounds **5**, **7**, **9** and **11** in chloroform solution.

4.4.3. Synthesis of polymers

Since 7-tetradecylthieno[3',2':7,8]indolizino[6,5,4,3-*ija*]thieno[2,3-*c*]quinolone (compound **11**) is the most electron-rich and the most conjugated due to its substitution pattern (fused with the pyrrole unit at the 2 position), we undertook the synthesis of D-A conjugated polymers with this unit and three different acceptors. As the first step, we tried the bromination of compound

11 at the 4 and 10 position (α position relative to the sulfur atom), but all our attempts failed. In all the conditions that we have tested, a significant amount of side products, mostly polybrominated compounds, were formed. Decreasing the reaction temperature or adding the bromination agent portion-wise did not improve the yield. Thus, we changed our strategy and synthesized compound **12** that allows the use of Stille coupling with different dibrominated electron-accepting monomers. As shown in Scheme 4.2, compound **12** was obtained in 90% yield by adding *n*-BuLi in THF at -78 ℃ and making the stannylation with tributylchlorostannane.[215] Compound **12** was then copolymerized with three commonly used acceptor monomers, namely 1,3-dibromo-5-(2-hexyldecyl)-4*H*-thieno[3,4-*c*]-pyrrole-4,6(5*H*)-dione (TPD), (*E*)-6, 6'-dibromo-1, 1'-bis(2-hexyldecyl)-[3, 3'-biindolinylidene]-2, 2'-dione (IID), 3,6-bis(5-bromothiophen-2-yl)-2,5-bis(2-octyldodecyl)-2,5-dihydropyrrolo[3,4-*c*]- pyrrole-1,4-dione (DPP)[216-218] by a palladium-catalyzed Stille coupling reaction[219] to afford the three D-A polymers P1, P2 and P3 in 90, 92 and 89% yield, respectively.

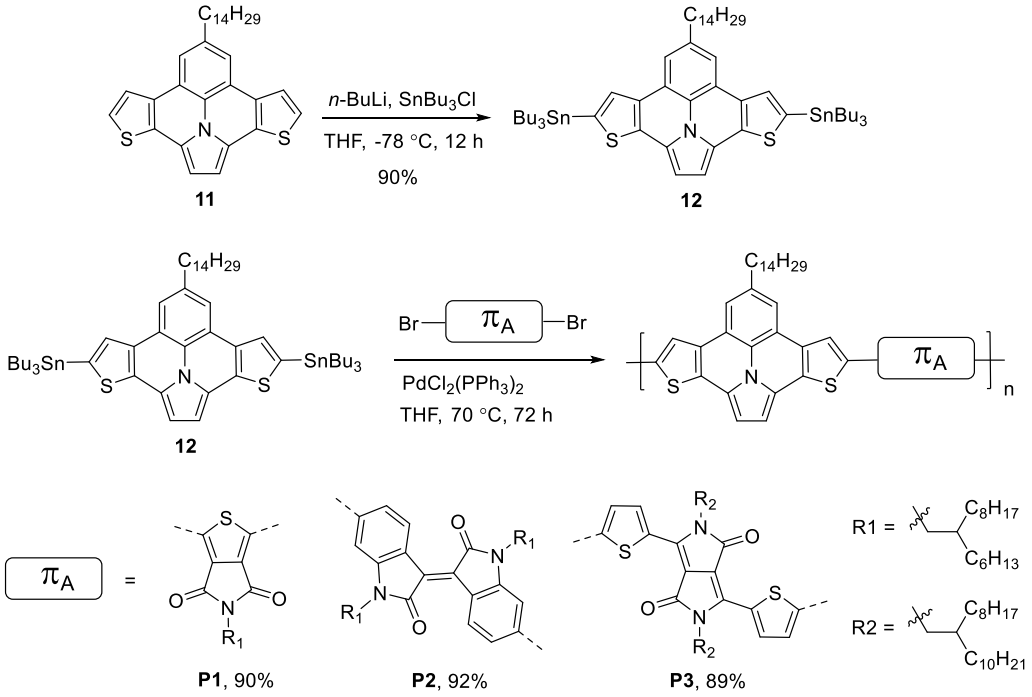

Scheme 4.2. Synthetic routes to the D-A polymers.

4.4.4. Size-exclusion chromatography (SEC) analysis and thermal properties of P1, P2 and P3

Size-exclusion chromatography (SEC) in 1,2,4-trichlorobenzene using polystyrene as standard was performed, and the results are presented in Figure 4.34 (Supporting Information) and Table 4.1. $\overline{Mn}$ values ranging from 12 500 and 21 400 g mol^{-1} were obtained, corresponding to degrees of polymerization between 14 and 16. The thermal properties of P1, P2 and P3 were investigated by thermogravimetric analysis (TGA) and differential scanning calorimetry (DSC) (Supporting Information, Figure 4.35-4.36). The TGA analysis was carried out under nitrogen atmosphere at a heating rate of 10 °C min^{-1}. The polymers showed no degradation up to 425 °C for P1 and P3, and 350 °C for P2, meaning that the π-extended ullazine moiety, despite its electron donating character, is quite robust. DSC studies were also performed to determine the glass transition temperature (T_g) of the polymers. The samples were heated up to 250 °C at a heating rate of 20 °C min^{-1} under nitrogen atmosphere. Unfortunately, the amplitude of the T_g transitions was too weak to measure values reliably, while no melting peaks have been observed. This suggests that all three polymers are amorphous, which can be explained by the presence of long, branched lateral alkyl chains.

Table 4.1. Yields, molecular weights and dispersity indices of polymers P1, P2 and P3

Polymer	Yields (%)	$\overline{Mn}$[a] (kg mol^{-1})	$\overline{Mw}$[a] (kg mol^{-1})	$Đ$[a] ($\overline{Mn}$/ $\overline{Mw}$)
P1	90	12.5	22.5	1.8
P2	92	16.8	47.0	2.8
P3	89	21.4	55.6	2.6

$\overline{Mn}$: the number-average molecular weight. $\overline{Mw}$: the weight-average molecular weight. $Đ$: dispersity index. [a] Molecular weight values and $Đ$ values of P1, P2 and P3 were measured by SEC at 110 °C with 1,2,4-trichlorobenzene as the eluent and polystyrene as standard.

4.4.5. Optical properties of the polymers

The optical properties of the three polymers were investigated both in solution and as thin films by UV-vis-NIR absorption spectroscopy (Figure 4.2). The corresponding photophysical parameters are summarized in Table 4.2. All the polymers showed broad absorption bands in the UV-vis region or the NIR region, matching well with the solar emission spectrum. Each polymer exhibits two characteristic absorption bands with a high-energy band peak at around 400 nm and a low-energy band peak at 612 nm, 698 nm and 788 nm for P1, P2 and P3, respectively (Figure 4.2). The high-energy absorption bands come from the π-π^* transitions of the donor and acceptor units,[220] while the low-energy absorption bands can be attributed to the intramolecular charge transfer (ICT) between the donor and acceptor units in the backbone.[221] Compared to the spectra in the solution state, all the spectra in the solid state were only slightly broadened and redshifted (5-8 nm) (Figure 4.2), which indicates that the polymers have a very similar conformation in both solution and solid states. This behavior is typical of planar polymers with thiophene moiety as the linking unit.[222] The optical bandgaps (E_g^{opt}) estimated from the edges of the absorption spectra in the thin films are 1.58 eV, 1.41 eV and 1.24 eV for P1, P2 and P3, respectively (Table 4.2). Interestingly, the λ_{max} values are larger and the bandgap values lower than most of the D-A copolymers prepared with the same acceptors,[216-218] proving that 7-tetradecylthieno[3',2':7,8]indolizino[6,5,4,3-*ija*]thieno[2,3-*c*]quinolone (compound **11**) is very electron-rich.

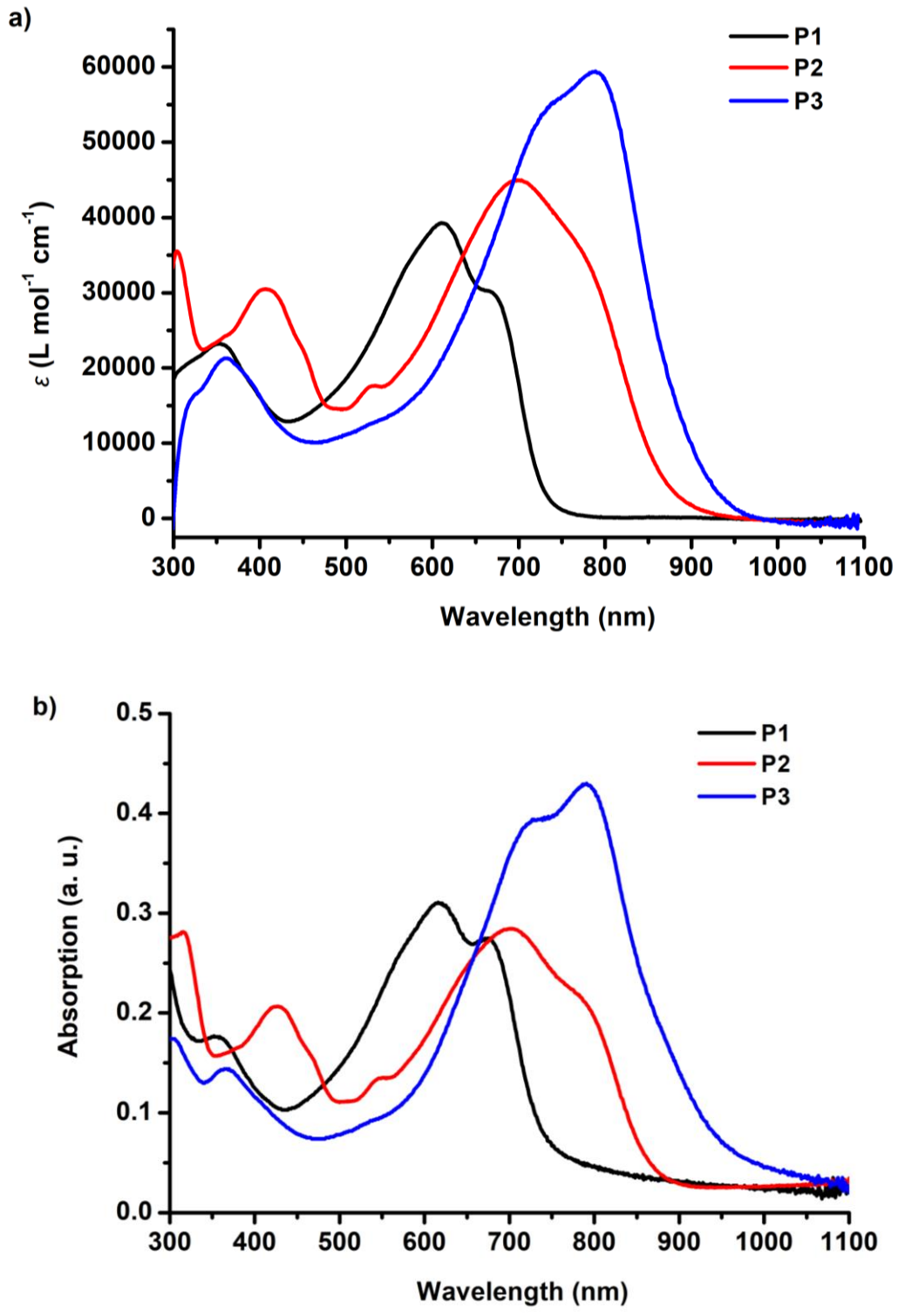

Figure 4.2. UV-vis-NIR absorption spectra of P1, P2, and P3 in a) chloroform solution and b) as thin films.

Table 4.2. Photophysical and electrochemical properties of the polymers

Polymer	λ_{max}^{sol} [a] (nm)	λ_{max}^{film} [b] (nm)	E_g^{opt} [c] (eV)	E_{HOMO} [d] (eV)	E_{LUMO} [d] (eV)	E_g^{elec} (eV)
P1	612	618	1.58	-5.08	-3.49	1.59
P2	698	703	1.41	-4.98	-3.58	1.40
P3	788	796	1.24	-4.97	-3.59	1.38

[a] Solution in chloroform. [b] Spin cast film from chloroform solution. [c] The optical bandgap values were estimated from the edge of the absorption spectra of thin films ($E_g^{opt} = 1240/\lambda_{onset}$). [d] HOMO and LUMO energy levels were calculated the formula $E_{HOMO} = -(4.71 + E_{onset}^{ox})$ eV and $E_{LUMO} = -(4.71 + E_{onset}^{re})$ eV, in which E_{onset}^{ox} and E_{onset}^{re} are the oxidation onset potential (CV thin film) and the reduction onset potential (CV thin film), respectively, *versus* SCE.

4.4.6. Electrochemical properties

Thin-film cyclic voltammetry (CV) measurements were performed to investigate the electrochemical properties and estimate the HOMO and LUMO energy levels of the three polymers. As shown in Figure 4.37-4.39 (Supporting Information), the polymers exhibited quasi reversible processes both in the oxidative and reductive scans. The HOMO and LUMO energy levels were calculated from the oxidation and reduction onset potential,[223] respectively, and the results are summarized in Table 4.2. The HOMO and LUMO energy levels were estimated to be -5.08 and -3.49 eV for P1, -4.98 and -3.58 eV for P2, and -4.97 to -3.59 eV for P3. Correspondingly, the electrochemical bandgap values (E_g^{elec}) were calculated to be 1.59, 1.40 and 1.38 eV for P1, P2 and P3, which are in good agreement with the optical bandgap values. All the polymers showed quite narrow bandgap, which corresponds to near ideal bandgap for solar cells applications.[224] In addition, the LUMO energy levels of these polymers are around -3.5 eV, which is suitable for the electron to transfer from the polymer donors to the acceptor $PC_{70}BM$ or $PC_{60}BM$ (~ -4.0 eV, see Figure 4.3a for the energy level diagram of the organic solar cell device constructed in this work).[222]

4.4.7. Organic photovoltaics properties

The photovoltaic properties of P1, P2, P3 as donor materials were investigated in devices with an inverted configuration of ITO/ZnO/PEI/Active layer/MoO_3/Ag (Figure 4.3a). Several common acceptors ($PC_{60}BM$, $PC_{70}BM$, ITIC) were chosen to evaluate the viability of ullazine moiety in organic solar cell active layers. For the preliminary tests, the three polymers were tested with $PC_{60}BM$ as the acceptor with or without diiodooctane (DIO) as the additive. The *J-V* curves of the best device for each polymer are shown in Figure 4.3b and Table 4.3 summarizes the device parameters including open-circuit voltage (V_{oc}), short-circuit current density (J_{sc}), fill factor (FF) and power conversion efficiency values (PCE). Notably, the first cells show quite low efficiencies for P1 and P2 (respectively 0.36% and 0.26%) and higher value for P3 (1.31%). As expected, these polymers yielded approximately the same V_{oc} (~ 0.55 V, estimated from the difference between the HOMO level of the donor material and the LUMO level of the acceptor material) due to the similar energy of their HOMO levels.

Table 4.3 Photovoltaic device parameters of all the polymer solar cells

Blend	Additive	V_{oc} (V)	J_{sc} (mA cm^{-2})	FF	PCE (best) (%)	PCE (average) (%)
P1:$PC_{60}BM$	--	0.54	1.97	0.33	0.36	0.29
P1:$PC_{60}BM$	1% DIO	0.55	2.16	0.37	0.44	0.40
P2:$PC_{60}BM$	--	0.52	0.91	0.36	0.26	0.19
P2:$PC_{60}BM$	1% DIO	0.59	1.24	0.47	0.34	0.28
P3:$PC_{60}BM$	--	0.55	4.52	0.52	1.31	1.21
P3:$PC_{60}BM$	1% DIO	0.54	6.88	0.46	1.71	1.62
P3:$PC_{70}BM$	1% DIO	0.55	7.86	0.52	2.23	1.98
P3:ITIC	--	0.60	4.73	0.34	0.96	0.89

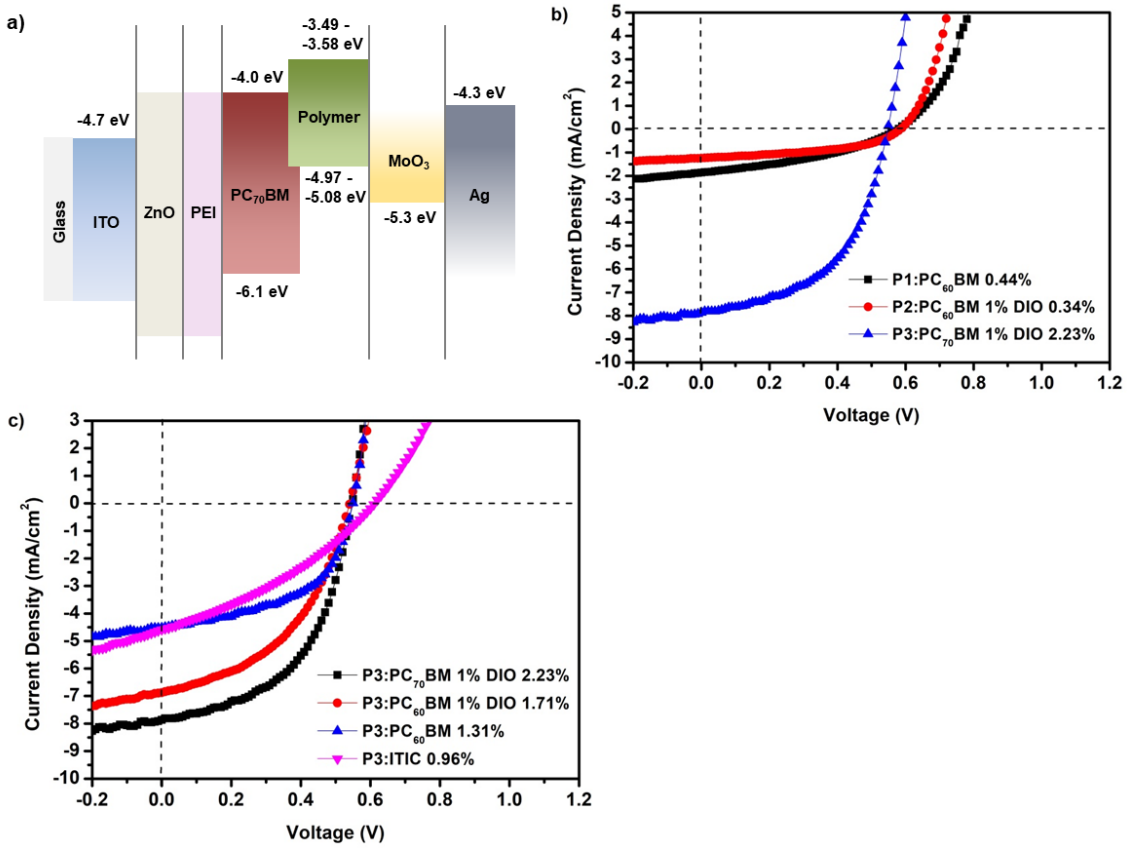

Figure 4.3. a) HOMO/LUMO energy levels of the inverted solar cell architecture ITO/ZnO/PEI/$PC_{70}BM$:polymer/MoO_3/Ag used in this work. b) Current density-voltage (*J*-*V*) curves of P1 (P2, P3):PCBM (C_{60} and C_{70}). c) Current density-voltage (*J*-*V*) curves of P3:($PC_{60}BM$, $PC_{70}BM$ and ITIC).

The morphology of polymer:$PC_{60}BM$ blend films was investigated by tapping mode atomic force microscopy (AFM). The AFM topographic and phase images are shown in Figure 4.40 (Supporting Information). When the polymer blends were processed without additives, the film morphology show aggregated domains, especially in the P2 blend where the nanodomains diameters span from 160 nm to 330 nm. This type of segregation leads to poor current density by an increasing rate of exciton recombination and can explain the poor performances obtained with these blend solutions.[225] As a consequence, we used DIO as a processing additive, which should help to solubilize the fullerene derivatives in the processing solution and enhance the

overall efficiency.[226] The resulting film shows a clear improvement of the segregation phase in the active layer for the three polymer blends, leading to a better organization between the donor and the acceptor materials. These improved morphologies lead to better efficiency but stay non-optimal for high efficiency solar cells.

To pursue our investigations, we focused on the polymer P3 and changed the classical $PC_{60}BM$ for another fullerene derivative ($PC_{70}BM$) and a non-fullerene acceptors (ITIC), that shows better optical absorption properties.[227,228] Notably, the most efficient device was obtained with P3 and $PC_{70}BM$, which showed a PCE of 2.23% with V_{oc} of 0.55 V, J_{sc} of 7.86 mA cm^{-2} and FF of 52% (Figure 4.3c).

We also performed AFM measurements on P3:$PC_{70}BM$ for comparison with P3:$PC_{70}BM$ + DIO blend shown in Figure 4.4. Without additives, nanodomains from 160 nm to 430 nm were observed along with a rough surface of the film (root-mean-square (RMS) roughness value of 9.62 nm), leading not only for poor exciton dissociation but also to rough surfaces decreasing the interface contact with other layers. The addition of DIO strongly influences the blend morphology by suppressing the phase segregation and smoothing the surface roughness to 1.52 nm (RMS), leading to the best efficiency observed for P3 devices.

The ITIC-based device also shows a promising 0.96% PCE with a higher V_{oc} (0.60 V) than PCBM-based devices, which can be ascribed to a higher LUMO level of the acceptor (-3.83 eV *vs*. -4.0 eV) and a homogenous morphology observed with AFM (see Figure 4.41, Supporting Information). Further device optimizations are needed to improve the photovoltaic performances of this series of polymers.

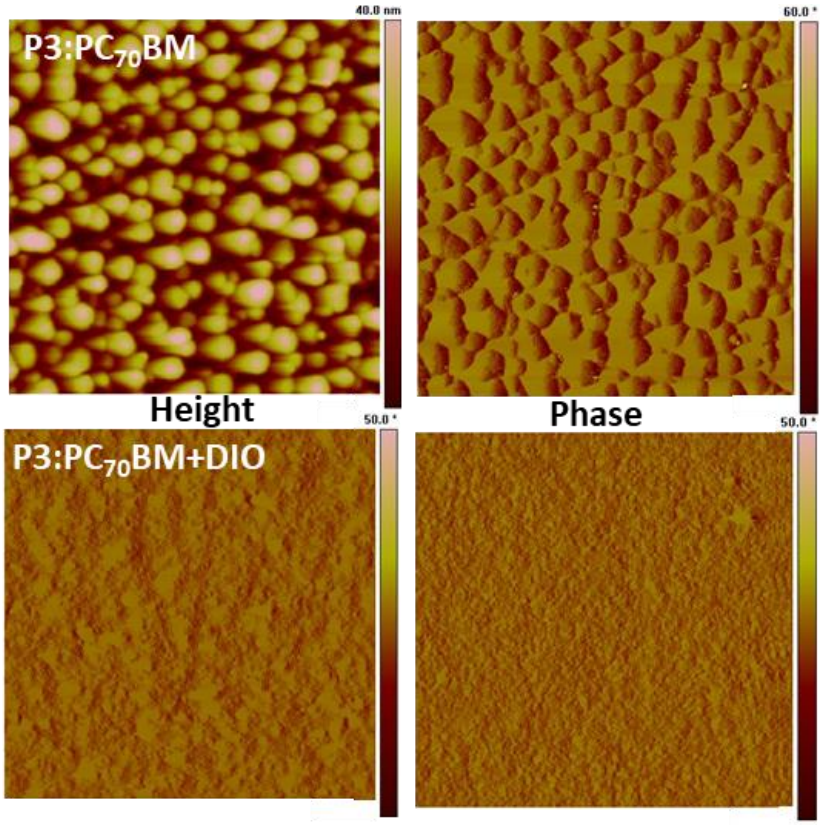

Figure 4.4. AFM images obtained in tapping mode (5×5 μm^2) of P3:PC_{70}BM blend films without DIO (on top) and with DIO (on the bottom).

4.5. Conclusion

In this work, we showed the efficiency and versatility of the photochemical CDHC reaction in synthesizing several π-extended ullazine derivatives containing electron-rich or electron-poor heterocycles. We developed a novel electron donor compound with one pyrrole and two thiophene rings, the 7-tetradecylthieno[3',2':7,8]indolizino[6,5,4,3-*ija*]thieno[2,3-*c*]quinolone, which was successfully employed in the preparation of a series of D-A conjugated polymers whose optical and electrochemical properties were fully investigated. The D-A polymers exhibited strong and broad UV-vis-NIR absorption bands and quite narrow bandgaps (1.24 to 1.58 eV, with the HOMO levels -4.97 to -5.08 eV and LUMO levels -3.49 to -3.59 eV), demonstrating the strong electron-donor property of the ullazine-based monomer. To test the

solar cell performances of these polymers, BHJ-PSCs were fabricated using these polymers as host materials and PCE values as high as 2.23% (V_{oc} = 0.55 V, J_{sc} = 7.86 mA cm^{-2}, FF = 52%) were obtained with $PC_{70}BM$ as the acceptor without any optimization.

4.6. Acknowledgements

This work was supported by NSERC through a Discovery Grant. D.M. thanks the China Scholarship Council (CSC) for a PhD scholarship.

4.7. Supporting Information

4.7.1. Materials and Methods

Chemical reagents were purchased from Sigma-Aldrich Co. Canada, Alfa Aesar Co., TCI America Co. or Oakwood Products Inc. and used as received, unless mentioned. Solvents used for organic synthesis were purchased from Fisher Chemical Co., EMD Millipore Co. and CFS Chemical Co. as HPLC grade. These solvents were degassed, dried and purified using a Solvent Purifier System (SPS) (Vacuum Atmosphere Co., Hawthorne, USA). Anhydrous decahydronaphthalene (mixture of *cis* + *trans*) was used as received for photochemical reactions and other anhydrous solvents were bought from Sigma-Aldrich Co. Canada. All anhydrous and air sensitive reactions were performed in oven-dried glassware purchased from Synthware™ under positive nitrogen stream. Analytical thin-layer chromatographies were performed with silica gel 60 F254, 0.25 mm pre-coated TLC plates (Silicycle, Québec, Canada). Compounds were revealed by a 254 nm and/or 365 nm UV wavelength and/or aqueous K_2CO_3 and NaOH solution of potassium permanganate. Flash column chromatographies were performed with 230-400 mesh silica gel R10030B (Silicycle, Québec, Canada). 1,3-dibromo-5-(2-hexyldecyl)-4*H*-thieno[3,4-*c*]- pyrrole-4,6(5*H*)-dione (TPD) was synthesized according to literature procedures.[229,230] (*E*)-6, 6'-dibromo-1, 1'-bis(2-hexyldecyl)-[3, 3'-biindolinylidene]-2, 2'-dione (IID) was synthesized according to literature procedures.[231] 3,6-bis(5-bromothiophen- 2-yl)-2,5-bis(2-octyldodecyl)-2,5-dihydropyrrolo[3,4-*c*]-pyrrole-1,4-dione (DPP) was synthesized according to literature procedures.[232]

4.7.2. Apparatus

Photochemical reactions were performed in a CCP-ICH2 Luzchem® photochemical reactor equipped with a thermostat and a heating mantle. Photochemical reactions were performed in a 100 mL quartz round-bottom flask bought from Chemglass®. Nuclear magnetic resonance (NMR) spectra were recorded on a Varian Inova AS400 spectrometer (Varian, Palo Alto, USA)

at 400 MHz (^{1}H) and 100 MHz (^{13}C). Signals are reported as m (multiplet), s (singlet), d (doublet), t (triplet), and coupling constants are reported in hertz (Hz). Chemical shifts are reported as values ppm (δ) relative to residual solvent peak. High resolution mass spectra (HRMS) were recorded with an Agilent 6210 Time-of-Flight (TOF) LC-MS apparatus equipped with an APPI ion source (Agilent Technologies, Toronto, Canada). Number-average ($\overline{Mn}$) and weight-average ($\overline{Mw}$) molecular weights were determined by size-exclusion chromatography (SEC) using a Varian Polymer Laboratories GPC220 equipped with an RI detector and a PL BV400 HT Bridge Viscometer. The column set consists of 2 PL gel Mixed C (300 × 7.5 mm) columns and a PL gel Mixed C guard column. The flow rate was fixed at 1mL min^{-1} using 1,2,4-trichlorobenzene (TCB) (with 0.0125% BHT w/v) as the eluent. The temperature of the system was set to 110 ℃. All the samples were prepared at a nominal concentration of 1.0 mg mL^{-1} in TCB. Dissolution was performed using a Varian Polymer Laboratories PL-SP 260VC sample preparation system. The sample vials were held at 110 ℃ with shaking for 1 h for complete dissolution. The solutions were filtered through a 2 mm porous stainless steel filter and a 0.40 μm glass filter into a 2 mL chromatography vial. The calibration method used to generate the reported data was the classical polystyrene method using polystyrene narrow standards Easi-Vials PS-M from Varian Polymer Laboratories which were dissolved in TCB. Thermogravimetric analysis (TGA) was performed with a TGA/SDTA 851e from Metler-Toledo. The acquisitions were recorded under nitrogen atmosphere at a heating rate of 10 ℃ min^{-1}. Differential scanning calorimetry thermal analysis (DSC) was performed with a Perkin-Elmer AED-7 model. The acquisitions were recorded under nitrogen atmosphere at a heating rate of 20 ℃ min^{-1}. UV-vis-NIR absorption spectra were recorded using a Varian Cary 500 UV-vis-NIR spectrophotometer using 1 cm path length quartz cells. For solid state measurements, the polymer solution (1.0 mg mL^{-1} in chloroform) was spin coated on quartz plates. Optical bandgaps were calculated from the onset of the absorption band. Cyclic voltammetry (CV) were recorded on a Solartron 1287 potentiostat using platinum wires as the working electrode and counter electrode at a scan rate of 50 mV s^{-1}. The reference electrode

was Ag/Ag^+ (0.01 M $AgNO_3$ in acetonitrile) in an anhydrous and argon-saturated solution of 0.1M tetrabutylammonium hexafluorophosphate (Bu_4NPF_6) in dry acetonitrile. Under these conditions, the oxidation potential of ferrocene was 0.09 V *versus* Ag/Ag^+, whereas the oxidation potential of ferrocene was 0.41 V *versus* the saturated calomel electrode (SCE). The HOMO and LUMO energy levels were determined from the oxidation and reduction onsets (where the current starts to differ from the baseline) from the cyclic voltammogram assuming that the SCE is -4.71 eV in vacuum, as reported in the literature.[194]

4.7.3. Fabrication and characterization of polymer solar cells

Inverted BHJ solar cells were prepared on a commercial indium tin oxide (ITO) coated glass substrate. The substrates were cleaned sequentially in ultrasonic baths with clean room detergent, deionized (DI) water, acetone and isopropyl alcohol. Prior to the fabrication, the ITO glass substrates were treated in a plasma-oxygen chamber (Spacemaker II sensor, Plasmatic Systems, Inc, USA) for 5 min. First, a 20-30 nm ZnO thin film was made by spin coating a ZnO precursor solution (250 mg of zinc acetate, 69.0 μL of ethanolamine, and 2.91 mL of 2-methoxyethanol) onto the ITO glass at 5000 rpm for 40 s and then annealed at 250 ℃ on a hot plate in air for 1 h. Then, a 0.05 wt % polyethylenimine (PEI) in 2-methoxyethanol solution was spin-coated onto the ZnO layer and dried at 110 ℃ on a hot plate in air for 10 min. The blend solution was spin-coated over the ZnO layer and then dried at 130 ℃ for 90 s to make the active layer. All the blend solutions were prepared by dissolving the polymers (10 mg mL^{-1}) and $PC_{60}BM$ (10 mg mL^{-1}) or $PC_{70}BM$ (10 mg mL^{-1}) or ITIC (10 mg mL^{-1}) in chlorobenzene and stirring the mixtures on a hot plate in air at 60 ℃ overnight. Finally, MoO_3 (8 nm) and Ag anode (100 nm) were sequentially vacuum-deposited onto the active layer through a shadow mask on top of the active layer by thermal evaporation under high vacuum (1×10^{-7} Torr). Current *versus* potential curves (*J-V* characteristics) were measured with a Keithley 2400 Digital Source Meter under a collimated beam. Illumination of the cells was done through the ITO side using light from a 150 W Oriel Instruments Solar Simulator (model 16S, Solar Light

Co., Philadelphia, PA) and a 200 W xenon Lamp Power Supply (Model XPS 200, Solar Light Co., Philadelphia, PA) with an AM 1.5G filter to provide an intensity of 100 mW cm^{-2} calibrated by NREL certified Si photodiode (Model 1787-04, Hamamatsu Photonics K. K., Japan) and a HP4155A semiconductor parameter analyzer (Yokogawa Hewlett-Packard, Japan).

4.7.4. Synthesis

2,6-diiodo-4-tetradecylaniline (1)

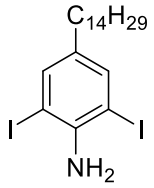

1

To a solution of 37% w/w aq. HCl (24.0 mL, 0.430 M) and water (173 mL, 60.0 mM) in a round-bottom flask was added 4-tetradecylaniline (3.00 g, 10.4 mmol) at room temperature all at once. After the solid was dissolved, ICl (3.36 g, 20.7 mmol) was added all at once and the mixture was stirred at room temperature for 20 hours. The resulting mixture was filtered under vacuum and the solid was washed with water. The crude product was purified by recrystallization in 2-propanol to afford compound **1** as a crystalline brown solid (4.42 g, 79%). ^{1}H NMR (400 MHz, $CDCl_3$): δ 7.45 (s, 2H), 4.45 (s, 2H), 2.40 (t, *J* = 7.8 Hz, 2H), 1.51 (m, 2H), 1.26 (m, 22H), 0.88 (t, *J* = 6.8 Hz, 3H). ^{13}C NMR (100 MHz, $CDCl_3$): δ 144.01, 139.29, 136.44, 81.71, 34.07, 32.08, 31.66, 29.85, 29.84, 29.81, 29.80, 29.70, 29.58, 29.52, 29.26, 22.85, 14.30. HRMS (APPI+): calculated for $C_{20}H_{33}I_2N$ $(M + H)^+$ 541.07024, found 541.07457.

1-(2,6-diiodo-4-tetradecylphenyl)-1*H*-pyrrole (2)

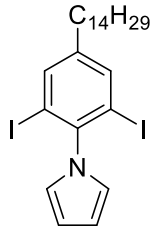

2

A round bottom flask was charged with compound **1** (4.00 g, 7.39 mmol), glacial acetic acid (8.50 mL, 0.870 M), 1,2-dichloroethane (8.50 mL, 0.870 M), and 2,5-dimethoxytetrahydrofuran (2.25 mL, 17.4 mmol). A reflux condenser was installed to the flask and the mixture was heated to reflux for 4 hours. Once cooled to room temperature, the mixture was diluted with CH_2Cl_2, rinsed with H_2O, and the organic layer was washed with saturated aqueous K_2CO_3. The organic phase was dried over Na_2SO_4 and the solvent was removed under reduced pressure. The crude product was purified by silica gel chromatography (20% CH_2Cl_2/hexanes) to yield compound **2** as a light yellow solid (4.15 g, 95%). ^{1}H NMR (400 MHz, $CDCl_3$): δ 7.71 (s, 2H), 6.61 (t, *J* = 2.1 Hz, 2H), 6.37 (t, *J* = 2.1 Hz, 2H), 2.56 (t, *J* = 7.8 Hz, 2H), 1.62 (m, 2H), 1.27 (m, 22H), 0.88 (t, *J* = 6.9 Hz, 3H). ^{13}C NMR (100 MHz, $CDCl_3$): δ 147.19, 143.39, 139.41, 121.12, 109.47, 97.56, 34.65, 32.07, 31.24, 29.85, 29.83, 29.81, 29.79, 29.66, 29.53, 29.51, 29.35, 22.85, 14.29. HRMS (APPI+): calculated for $C_{24}H_{35}I_2N$ $(M + H)^+$ 591.08589, found 591.08988.

1-(4-tetradecyl-2,6-bis(4,4,5,5-tetramethyl-1,3,2-dioxaborolan-2-yl)phenyl)-1*H*-pyrrole (3)

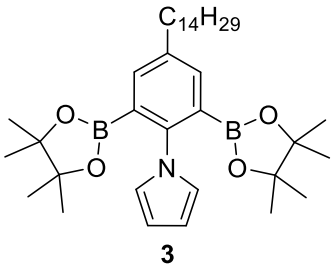

3

An oven-dried round-bottom flask was flushed three times with a vacuum/nitrogen cycle and

charged with compound **2** (3.00 g, 5.07 mmol), copper(I) iodide (0.193 g, 1.02 mmol), sodium hydride (0.365 g, 15.2 mmol) and THF (20.0 mL, 0.250 M). The flask was flushed three times with a vacuum/nitrogen cycle and 4,4,5,5-tetramethyl-1,2,3-dioxaborolane (2.21 mL, 15.2 mmol) was filtered through a 0.45 μm filter syringe and added dropwise. The reaction mixture was stirred at room temperature for 12 hours. The reaction was quenched by adding 10 mL of saturated NH_4Cl aqueous solution and the aqueous layer was extracted with ethyl acetate (3 × 30 mL). The combined organic layers were dried with Na_2SO_4 and the solvent was removed under reduced pressure. The resulting residue was purified by silica gel chromatography (5% EtOAc/hexanes) to obtain compound **3** as a white solid (2.25 g, 75%). ^{1}H NMR (400 MHz, $CDCl_3$): δ 7.46 (s, 2H), 6.72 (m, 2H), 6.14 (m, 2H), 2.61 (t, *J* = 7.8 Hz, 2H), 1.62 (m, 2H), 1.26 (m, 22H), 1.19 (s, 24H), 0.88 (t, *J* = 6.8 Hz, 3H). ^{13}C NMR (100 MHz, $CDCl_3$): δ 147.37, 140.92, 136.21, 123.56, 107.88, 83.90, 35.62, 32.08, 31.79, 29.86, 29.84, 29.81, 29.77, 29.67, 29.66, 29.51, 24.76, 22.84, 14.28. HRMS (APPI+): calculated for $C_{36}H_{59}B_2NO_4$ $(M + H)^+$ 589.47028, found 589.47533.

2,2'-(2-(1*H*-pyrrol-1-yl)-5-tetradecyl-1,3-phenylene)bis(3-chloropyridine) (4)

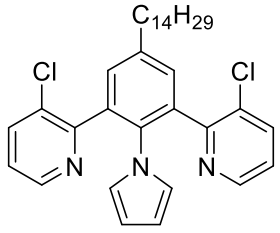

4

A round-bottom flask under nitrogen was charged with compound **3** (0.500 g, 0.845 mmol), 2-bromo-3-chloropyridine (0.407 g, 2.11 mmol), 2 M Na_2CO_3 aqueous solution (4.20 mL, 8.45 mmol) and DMSO (8.45 mL, 0.100 M). The flask was flushed three times with a vacuum/nitrogen cycle and degassed with a nitrogen stream for 10 min. $Pd(dppf)Cl_2$ (61.9 mg, 84.5 μmol) was added and the reaction flask was flushed three times with a vacuum/nitrogen

cycle. The reaction mixture was heated to 100 ℃ for 16 hours. Once cooled to room temperature, 10 mL of water was added and the aqueous layer was extracted with ethyl acetate (3 × 30 mL). The organic layer was dried with Na_2SO_4 and the solvent was removed under reduced pressure. The resulting residue was purified by silica gel chromatography (25% EtOAc/hexanes) to obtain compound **4** as a light grey solid (0.385 g, 81%). ^{1}H NMR (400 MHz, $CDCl_3$): δ 8.46 (d, *J* = 1.6 Hz, 2H), 7.57 (d, *J* = 4.0 Hz, 2H), 7.35 (s, 2H), 7.11 (m, 2H), 6.28 (m, 2H), 5.73 (t, *J* = 2.2 Hz, 2H), 2.73 (t, *J* = 7.8 Hz, 2H), 1.71 (m, 2H), 1.24 (m, 22H), 0.86 (t, *J* = 6.9 Hz, 3H). ^{13}C NMR (100 MHz, $CDCl_3$): δ 155.81, 147.03, 142.22, 136.78, 135.95, 135.92, 131.74, 130.65, 123.42, 107.56, 35.45, 31.93, 31.11, 29.70, 29.69, 29.66, 29.56, 29.47, 29.37, 29.33, 22.70, 14.16. HRMS (APPI+): calculated for $C_{34}H_{41}Cl_2N_3$ $(M + H)^+$ 561.26775, found 561.27596.

2-tetradecylpyrido[3,2-*c*]pyrido[2',3':7,8]indolizino[6,5,4,3-*ija*]quinoline (5)

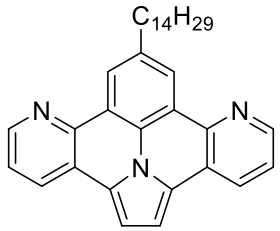

5

A quartz flask was oven-dried and flushed three times with a vacuum/nitrogen cycle. Compound **4** (56.3 mg, 0.100 mmol) and anhydrous decahydronaphthalene (100 mL) were added to the flask and the solution was degassed with argon for 10 minutes. The solution was then irradiated at 254 nm at 100 ℃ for 2 hours under a continuous flow of argon. After cooling down to room temperature, the solvent was removed by vacuum distillation and the resulting residue was purified by silica gel chromatography (25% CH_2Cl_2/hexanes) to obtain compound **5** as a dark yellow solid (47.0 mg, 96%). ^{1}H NMR (400 MHz, $CDCl_3$): δ 8.69 (d, *J* = 2.2 Hz, 2H), 8.64 (s, 2H), 8.20 (d, *J* = 3.9 Hz, 2H), 7.38 (m, 2H), 7.15 (s, 2H), 2.92 (t, *J* = 8.1 Hz, 2H),

1.82 (m, 2H), 1.25 (m, 22H), 0.87 (t, J = 7.1 Hz, 3H). ^{13}C NMR (100 MHz, $CDCl_3$): δ 147.72, 143.36, 139.58, 131.47, 130.19, 124.28, 123.91, 123.16, 123.00, 122.11, 105.17, 36.68, 32.40, 32.08, 29.85, 29.81, 29.79, 29.74, 29.72, 29.52, 22.85, 14.29. HRMS (APPI+): calculated for $C_{34}H_{39}N_3$ $(M + H)^+$ 489.31440, found 489.32261.

3,3'-(2-(1*H*-pyrrol-1-yl)-5-tetradecyl-1,3-phenylene)bis(2-chloropyridine) (6)

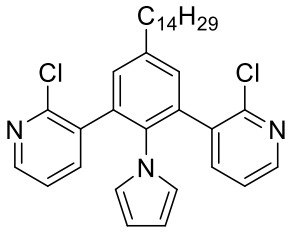

6

A round-bottom flask under nitrogen was charged with compound **3** (0.500 g, 0.845 mmol), 3-bromo-2-chloropyridine (0.407 g, 2.11 mmol), 2 M Na_2CO_3 aqueous solution (4.20 mL, 8.45 mmol), and DMSO (8.45 mL, 0.100 M). The flask was flushed three times with a vacuum/nitrogen cycle and degassed with a nitrogen stream for 10 mins. $Pd(dppf)Cl_2$ (61.9 mg, 84.5 μmol) was added and the reaction flask was flushed three times with a vacuum/nitrogen cycle. The reaction mixture was heated to 100 ℃ for 16 hours. Once cooled to room temperature, 10 mL of water was added and the aqueous layer was extracted with ethyl acetate (3 × 30 mL). The organic layer was dried with Na_2SO_4 and the solvent was removed under reduced pressure. The resulting residue was purified by silica gel chromatography (25% EtOAc/hexanes) to obtain compound **6** as a white solid (0.418 g, 88%). ^{1}H NMR (400 MHz, $CDCl_3$): δ 8.28 (m, 2H), 7.32 (s, 4H), 7.04 (s, 2H), 6.34 (s, 2H), 5.78 (t, J = 2.0 Hz, 2H), 2.74 (t, J = 7.3 Hz, 2H), 1.70 (m, 2H), 1.25 (m, 22H), 0.86 (t, J = 6.8 Hz, 3H). ^{13}C NMR (100 MHz, $CDCl_3$): δ 150.22, 148.89, 142.58, 138.74, 135.51, 133.84, 131.36, 122.21, 121.97, 109.29, 35.48, 32.00, 31.28, 29.78, 29.76, 29.73, 29.67, 29.52, 29.44, 29.24, 22.77, 14.22. HRMS (APPI+): calculated for $C_{34}H_{41}Cl_2N_3$ $(M + H)^+$ 561.26775, found 561.27585.

8-tetradecylpyrido[2,3-*c*]pyrido[3',2':7,8]indolizino[6,5,4,3-*ija*]quinoline (7)

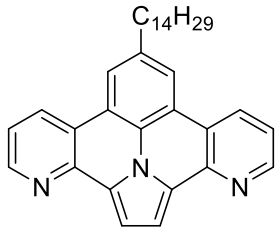

7

An oven-dried quartz flask was flushed three times with a vacuum/nitrogen cycle and charged with compound **6** (56.3 mg, 0.100 mmol) and anhydrous decahydronaphthalene (100 mL) and the flask was degassed with argon for 10 minutes. The solution was then irradiated at 254 nm at 100 ℃ for 2 hours under a continuous flow of argon. After cooling down to room temperature, the solvent was removed by vacuum distillation and the resulting residue was purified by silica gel chromatography (25% CH_2Cl_2/hexanes) to obtain compound **7** as a dark yellow solid (46.0 mg, 94%). ^{1}H NMR (400 MHz, $CDCl_3$): δ 8.64 (d, *J* = 2.4 Hz, 2H), 8.18 (d, *J* = 4.1 Hz, 2H), 7.55 (s, 2H), 7.48 (s, 2H), 7.20 (q, *J* = 6.4 Hz, 2H), 2.60 (t, *J* = 7.7 Hz, 2H), 1.60 (m, 2H), 1.24 (m, 22H), 0.87 (t, *J* = 6.9 Hz, 3H). ^{13}C NMR (100 MHz, $CDCl_3$): δ 150.05, 143.75, 138.55, 130.30, 127.55, 126.74, 121.26, 121.22, 120.90, 120.84, 107.12, 36.41, 32.06, 31.84, 29.84, 29.80, 29.77, 29.70, 29.54, 29.50, 22.83, 14.27. HRMS (APPI+): calculated for $C_{34}H_{39}N_3$ $(M + H)^+$ 489.31440, found 489.32267.

1-(2,6-bis(3-chlorothiophen-2-yl)-4-tetradecylphenyl)-1*H*-pyrrole (8)

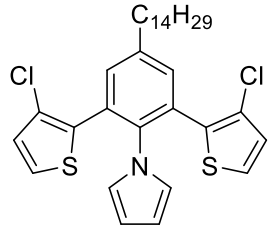

8

A round-bottom flask under nitrogen was charged with compound **3** (0.500 g, 0.845 mmol), 2-bromo-3-chlorothiophene (0.584 g, 2.96 mmol), K_2CO_3 (0.935 g, 6.76 mmol), DMF (4.20 mL, 0.200 M), H_2O (1.00 mL, 0.800 M), and flushed three times with a vacuum/nitrogen cycle and degassed with a nitrogen stream for 10 mins. $PdCl_2(PPh_3)_2$ (59.3 mg, 84.5 μmol) and PPh_3 (55.4 mg, 0.211 mmol) were added and the reaction flask was flushed three times with a vacuum/nitrogen cycle. The reaction mixture was heated to 90 ℃ for 24 hours. Once cooled to room temperature, 10 mL of water was added and the aqueous layer was extracted with dichloromethane (3 × 30 mL). The organic layer was dried with Na_2SO_4 and the solvent was removed under reduced pressure. The resulting residue was purified by silica gel chromatography (20% CH_2Cl_2/hexanes) to obtain compound **8** as a colorless solid (0.431 g, 89%). ^{1}H NMR (400 MHz, $CDCl_3$): δ 7.47 (s, 2H), 7.20 (d, *J* = 2.7 Hz, 2H), 6.92 (d, *J* = 2.6 Hz, 2H), 6.42 (t, *J* = 2.2 Hz, 2H), 6.01 (t, *J* = 2.1 Hz, 2H), 2.75 (t, *J* = 7.7 Hz, 2H), 1.73 (m, 2H), 1.28 (m, 22H), 0.90 (t, *J* = 6.8 Hz, 3H). ^{13}C NMR (100 MHz, $CDCl_3$): δ 142.50, 137.18, 132.90, 132.84, 130.09, 127.36, 125.69, 123.94, 123.18, 109.01, 35.46, 32.07, 31.29, 29.84, 29.82, 29.80, 29.74, 29.60, 29.51, 29.34, 22.84, 14.28. HRMS (APPI+): calculated for $C_{32}H_{39}Cl_2NS_2$ $(M + H)^+$ 571.19010, found 571.19839.

2-tetradecylthieno[2',3':7,8]indolizino[6,5,4,3-*ija*]thieno[3,2-*c*]quinoline (9)

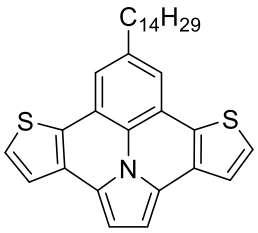

9

A quartz flask was oven-dried and flushed three times with a vacuum/nitrogen cycle. Compound **8** (57.3 mg, 0.100 mmol) and anhydrous decahydronaphthalene (100 mL) were added to the flask and the solution was degassed with argon for 10 minutes. The solution was then irradiated at 254 nm at 100 ℃ for 2 hours under a continuous flow of argon. After cooling down to room temperature, the solvent was removed by vacuum distillation and the resulting residue was purified by silica gel chromatography (25% CH_2Cl_2/hexanes) to obtain compound **9** as a dark yellow solid (46.0 mg, 92%). ^{1}H NMR (400 MHz, $CDCl_3$): δ 7.60 (d, *J* = 2.6 Hz, 2H), 7.52 (d, *J* = 2.6 Hz, 2H), 7.44 (s, 2H), 7.08 (s, 2H), 2.82 (t, *J* = 7.8 Hz, 2H), 1.77 (m, 2H), 1.26 (m, 22H), 0.89 (t, *J* = 6.8 Hz, 3H). ^{13}C NMR (100 MHz, $CDCl_3$): δ 139.03, 130.16, 129.37, 126.51, 125.85, 123.90, 122.87, 121.60, 117.41, 102.11, 36.42, 32.18, 32.09, 29.86, 29.82, 29.73, 29.64, 29.53, 22.86, 14.29. HRMS (APPI+): calculated for $C_{32}H_{37}NS_2$ $(M + H)^+$ 499.23674, found 499.24513.

1-(2,6-bis(2-chlorothiophen-3-yl)-4-tetradecylphenyl)-1*H*-pyrrole (10)

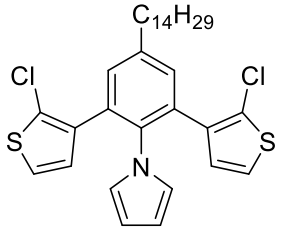

10

A round-bottom flask under nitrogen was charged with compound **3** (2.00 g, 3.38 mmol), 3-bromo-2-chlorothiophene (2.34 g, 11.8 mmol), K_2CO_3 (3.74 g, 27.0 mmol), DMF (17.0 mL,

0.200 M) and H_2O (4.20 mL, 0.800 M). The flask was flushed three times with a vacuum/nitrogen cycle and degassed with a nitrogen stream for 10 mins. $PdCl_2(PPh_3)_2$ (0.237 g, 0.338 mmol) and PPh_3 (0.222 g, 0.845 mmol) were added and the reaction flask was flushed three times with a vacuum/nitrogen cycle. The reaction mixture was heated to 90 ℃ for 24 hours. Once cooled to room temperature, 30 mL of water was added and the aqueous layer was extracted with dichloromethane (3 × 100 mL). The organic layer was dried with Na_2SO_4 and the solvent was removed under reduced pressure. The resulting residue was purified by silica gel chromatography (15% CH_2Cl_2/hexanes) to obtain compound **10** as a light yellow solid (1.66 g, 86%). ^{1}H NMR (400 MHz, $CDCl_3$): δ 7.39 (s, 2H), 6.89 (d, *J* = 3.1 Hz, 2H), 6.33 (m, 4H), 5.98 (m, 2H), 2.74 (t, *J* = 7.6 Hz, 2H), 1.72 (m, 2H), 1.28 (m, 22H), 0.89 (t, *J* = 6.8 Hz, 3H). ^{13}C NMR (100 MHz, $CDCl_3$): δ 142.56, 136.34, 136.28, 132.19, 131.69, 128.12, 126.85, 122.85, 122.53, 109.13, 35.89, 32.40, 31.76, 30.16, 30.13, 30.08, 29.96, 29.83, 29.69, 23.17, 14.61. HRMS (APPI+): calculated for $C_{32}H_{39}Cl_2NS_2$ $(M + H)^+$ 571.19010, found 571.19784.

7-tetradecylthieno[3',2':7,8]indolizino[6,5,4,3-*ija*]thieno[2,3-*c*]quinoline (11)

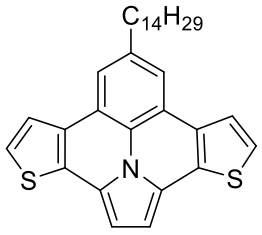

11

A quartz flask was oven-dried and flushed three times with a vacuum/nitrogen cycle. Compound **10** (1.00 g, 1.75 mmol) and anhydrous decahydronaphthalene (250 mL) were added into the flask and the solution was degassed with argon for 10 minutes. The solution was then irradiated at 254 nm at 100 ℃ for 12 hours under a continuous flow of argon. After cooling down to room temperature, the solvent was removed by vacuum distillation and the resulting residue was purified by silica gel chromatography (25% CH_2Cl_2/hexanes) to obtain compound

11 as a yellow solid (82.9 mg, 95%). ^{1}H NMR (400 MHz, $CDCl_3$): δ 7.68 (d, *J* = 2.7 Hz, 2H), 7.63 (s, 2H), 7.38 (d, *J* = 2.6 Hz, 2H), 7.01 (s, 2H), 2.84 (t, *J* = 7.8 Hz, 2H), 1.76 (m, 2H), 1.25 (m, 22H), 0.88 (t, *J* = 6.8 Hz, 3H). ^{13}C NMR (100 MHz, $CDCl_3$): δ 138.69, 130.34, 129.80, 127.81, 123.41, 122.72, 122.63, 122.04, 118.01, 102.59, 36.64, 32.26, 32.08, 29.85, 29.82, 29.80, 29.75, 29.59, 29.52, 22.85, 14.29. HRMS (APPI+): calculated for $C_{32}H_{37}NS_2$ $(M + H)^+$ 499.23674, found 499.24510.

7-tetradecyl-4,10-bis(tributylstannyl)thieno[3',2':7,8]indolizino[6,5,4,3-ija]thieno[2,3-c]qui-noline (12)

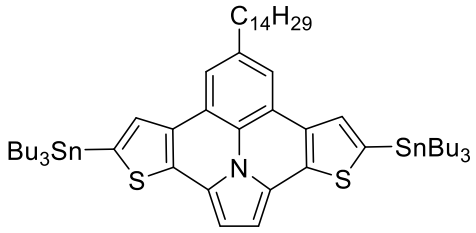

12

An oven-dried round-bottom flask was flushed three times with a vacuum/nitrogen cycle and charged with compound **11** (0.500 g, 1.00 mmol) and anhydrous THF (10.0 mL, 0.100 M). The reaction solution was cooled to -78 ℃ and *n*-BuLi solution (1.50 mL 1.60 M in hexanes, 2.40 mmol) was added dropwise, and the reaction solution was stirred at -78 ℃ for 1 h. Then the reaction mixture was allowed to reach room temperature and stirred at room temperature for 1 h. The reaction mixture was cooled to -78 ℃ and tributyltin chloride (0.684 g, 2.10 mmol) was added dropwise. The reaction mixture was stirred at -78 ℃ for 1 h and then allowed to reach room temperature and stirred at room temperature for 12 hours. 20 mL water was added to quench the reaction and the aqueous layer was extracted with ethyl acetate (3 × 50 mL). The organic layer was dried with Na_2SO_4 and the solvent was removed under reduced pressure. The resulting residue was purified by column chromatography (neutral alumina, 95:5 3% Et_2O/hexanes:triethyl amine) to obtain compound **12** as an orange oil (0.970 g, 90%). ^{1}H NMR

(400 MHz, $CDCl_3$): δ 7.79 (s, 2H), 7.78 (s, 2H), 7.09 (s, 2H), 2.94 (t, *J* = 7.8 Hz, 2H), 1.85 (m, 2H), 1.71 (m, 11H), 1.46 (m, 17H), 1.28 (m, 30H), 0.99 (t, *J* = 7.3 Hz, 18H), 0.91 (t, *J* = 6.9 Hz, 3H). ^{13}C NMR (100 MHz, $CDCl_3$): δ 138.44, 135.61, 135.51, 131.24, 130.51, 127.75, 122.74, 122.04, 117.82, 102.82, 36.83, 32.50, 32.11, 29.89, 29.84, 29.74, 29.55, 29.21, 27.49, 22.88, 14.30, 13.88, 11.16. HRMS (APPI+): $C_{56}H_{89}NS_2Sn_2$ $(M + H)^+$ 1079.44687, found 1079.45362.

General procedure for the synthesis of polymer P1, P2 and P3

Monomer **12** as a donor unit was polymerized with three acceptor monomers TPD, IID, and DPP by a palladium-catalyzed Stille coupling reaction to afford the three D-A polymers P1, P2 and P3, respectively. An oven-dried flask under nitrogen was charged with 1,3-dibromo-5-(2-hexyldecyl)-4*H*-thieno[3,4-*c*]pyrrole-4,6(5*H*)-dione (TPD) (1 equiv.), or (*E*)-6,6'-dibromo-1,1'-bis(2-hexyldecyl)-[3,3'-biindolinylidene]-2,2'- dione (IID) (1 equiv.), or 3,6-bis(5-bromothiophen-2-yl)-2,5-bis(2-octyldodecyl)-2,5-dihydropyrrolo[3,4-*c*]pyrrole-1,4-di one (DPP) (1 equiv.), compound **12** (1 equiv.), and anhydrous THF (0.100 M). The flask was flushed three times with a vacuum/nitrogen cycle and degassed with a nitrogen stream for 10 minutes. $PdCl_2(PPh_3)_2$ (0.05 equiv.) was added and the reaction flask was flushed three times with a vacuum/nitrogen cycle and the reaction mixture was heated at 70 ℃ for 3 days. After cooling down to room temperature, the reaction mixture was precipitated in methanol at 0 ℃ under strong stirring, filtered through a 0.45 μm nylon filter and further purified by Soxhlet extraction in acetone, hexanes and then chloroform. The chloroform fraction was evaporated under reduced pressure to a minimum amount and precipitated again in methanol and the precipitate was filtered through a 0.45 μm nylon filter and thoroughly dried under vacuum.

Polymer P1

Compound **12** (0.200 g, 0.185 mmol) was polymerized with 1,3-dibromo-5-(2-hexyldecyl)-4*H*-thieno[3,4-*c*]pyrrole-4,6(5*H*)-dione (TPD) (99.3 mg, 0.185

mmol) according to the procedure described above. Polymer **P1** ($\overline{Mn}$ = 12.5 kg mol^{-1}, $\overline{Mw}$ = 22.5 kg mol^{-1}, dispersity index (*Đ*): 1.8) was obtained as a dark blue solid (0.146 g, 90%).

Polymer P2

Compound **12** (0.200 g, 0.185 mmol) was polymerized with (*E*)-6,6'-dibromo-1,1'-bis(2-hexyldecyl)-[3,3'-biindolinylidene]-2,2'- dione (IID) (0.161 g, 0.185 mmol) according to the procedure described above. Polymer **P2** ($\overline{Mn}$ = 16.8 kg mol^{-1}, $\overline{Mw}$ = 47.0 kg mol^{-1}, dispersity index (*Đ*): 2.8) was obtained as a dark green solid (0.206 g, 92%).

Polymer P3

Compound **12** (0.200 g, 0.185 mmol) was polymerized with 3,6-bis(5-bromothiophen-2-yl)-2,5-bis(2-octyldodecyl)-2,5-dihydropyrrolo[3,4-*c*]pyrrole-1,4-di one (DPP) (0.151 g, 0.185 mmol) according to the procedure described above. Polymer **P3** ($\overline{Mn}$ = 21.4 kg mol^{-1}, $\overline{Mw}$ = 55.6 kg mol^{-1}, dispersity index (*Đ*): 2.6) was obtained as a dark green solid (0.224 g, 89%).

4.7.5. NMR Spectra

Compound 1

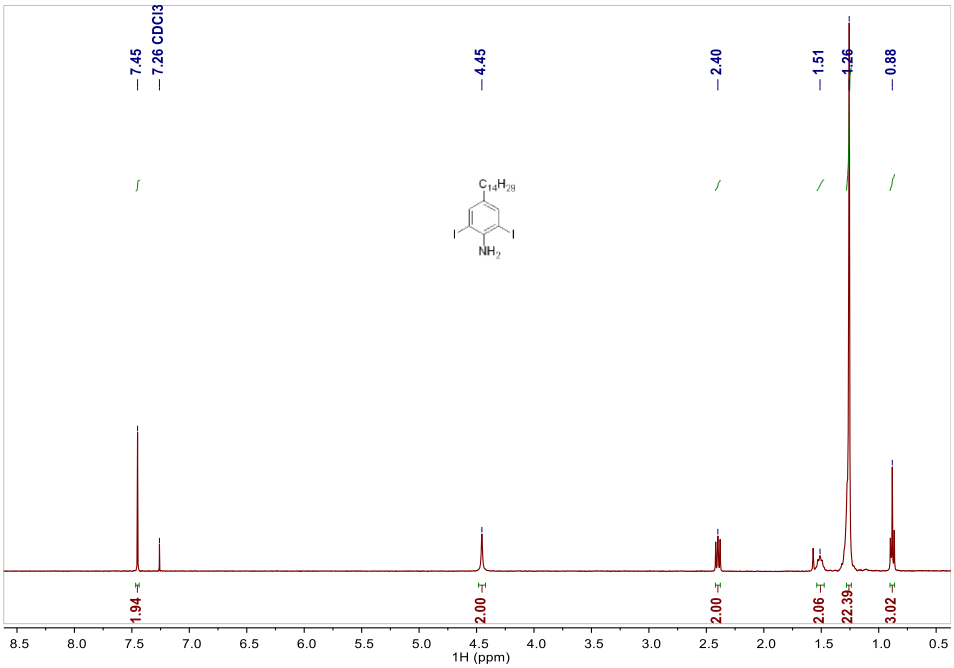

Figure 4.5. ^{1}H NMR spectrum of compound **1** in $CDCl_3$.

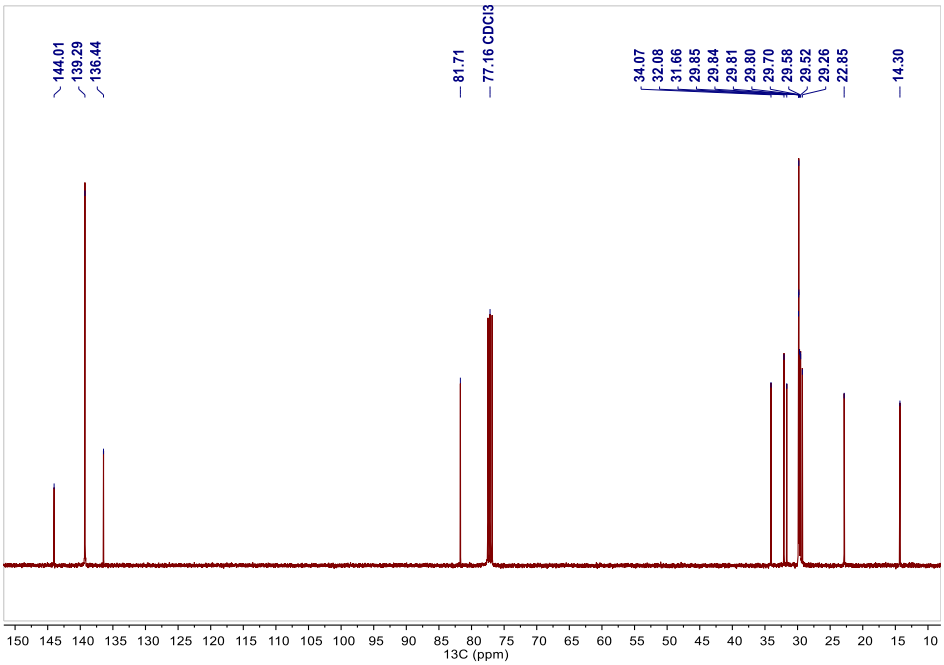

Figure 4.6. ^{13}C NMR spectrum of compound **1** in $CDCl_3$.

Compound 2

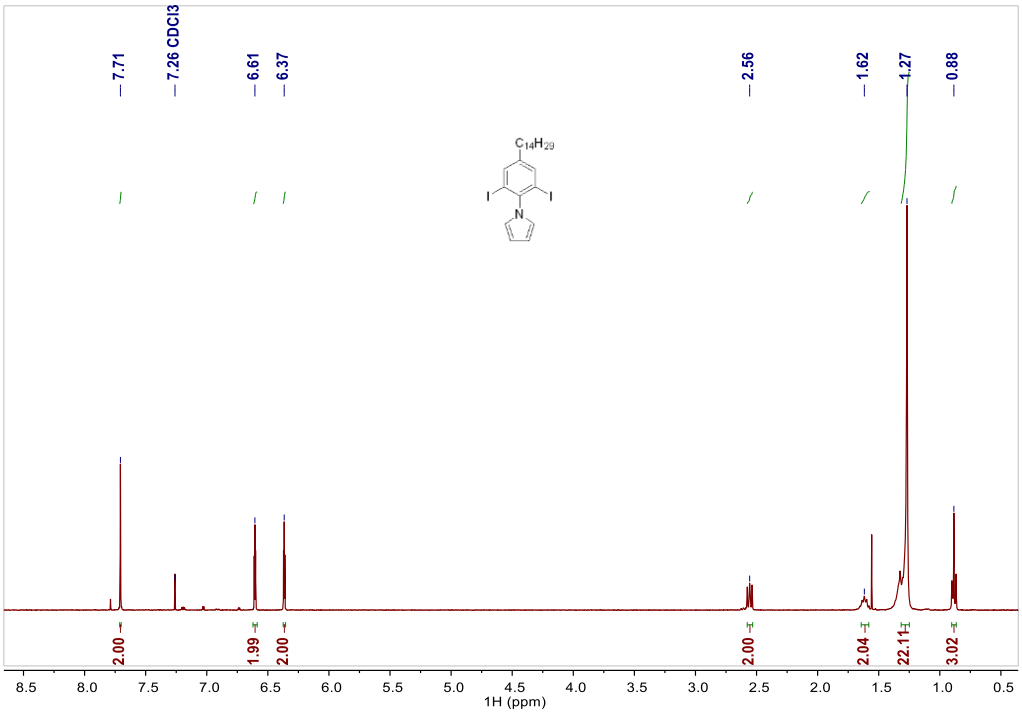

Figure 4.7. ^{1}H NMR spectrum of compound **2** in $CDCl_3$.

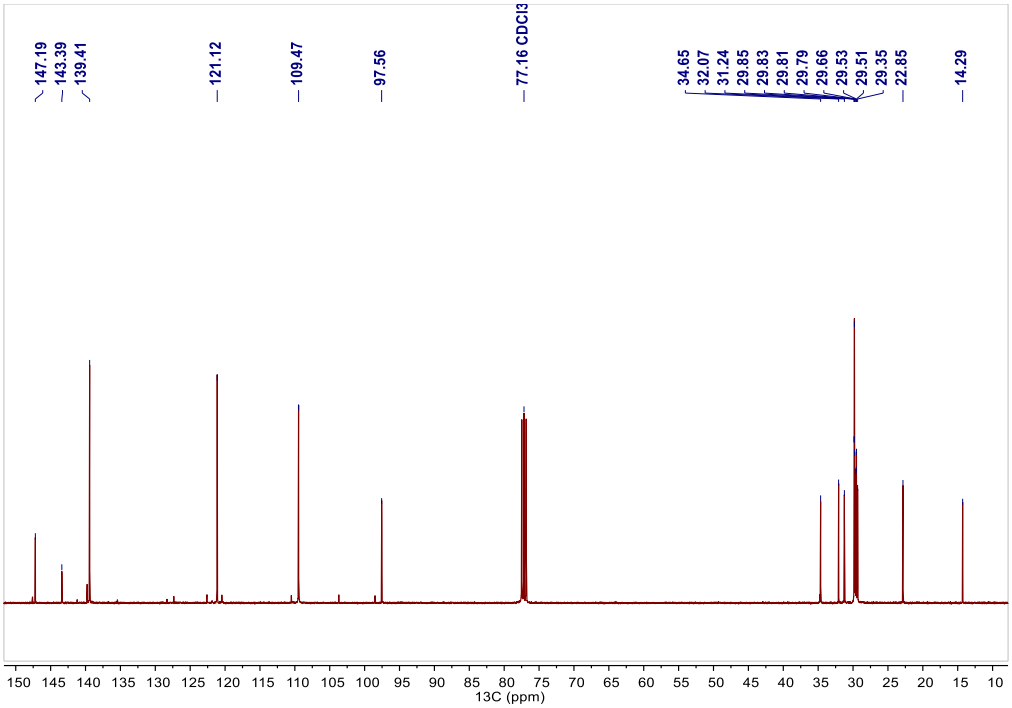

Figure 4.8. ^{13}C NMR spectrum of compound **2** in $CDCl_3$.

Compound 3

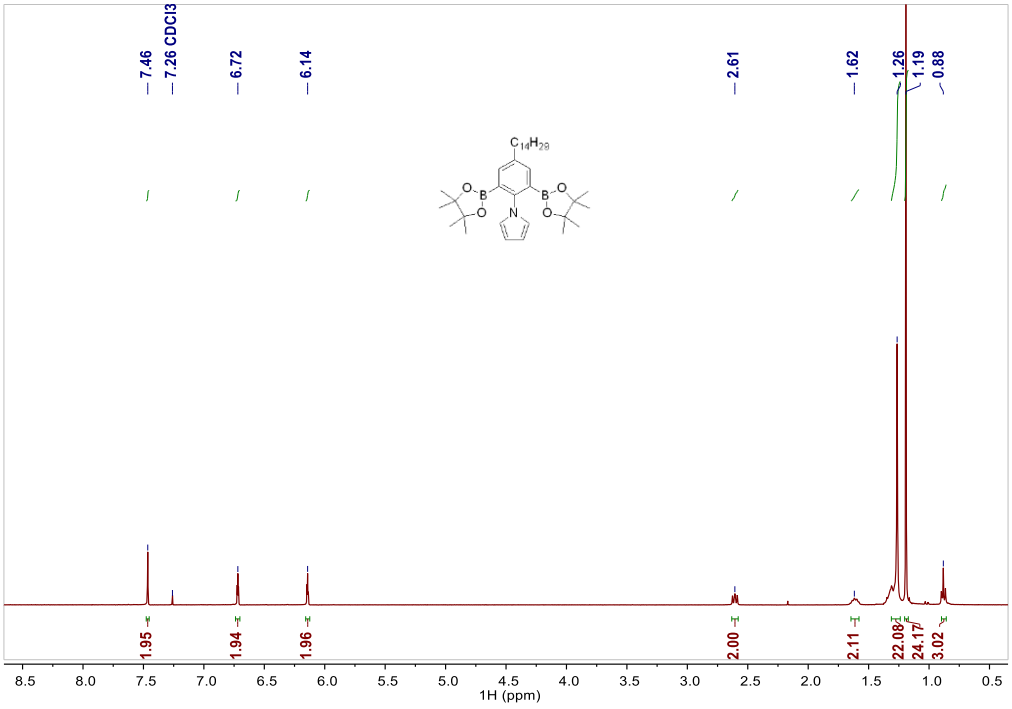

Figure 4.9. ^{1}H NMR spectrum of compound **3** in $CDCl_3$.

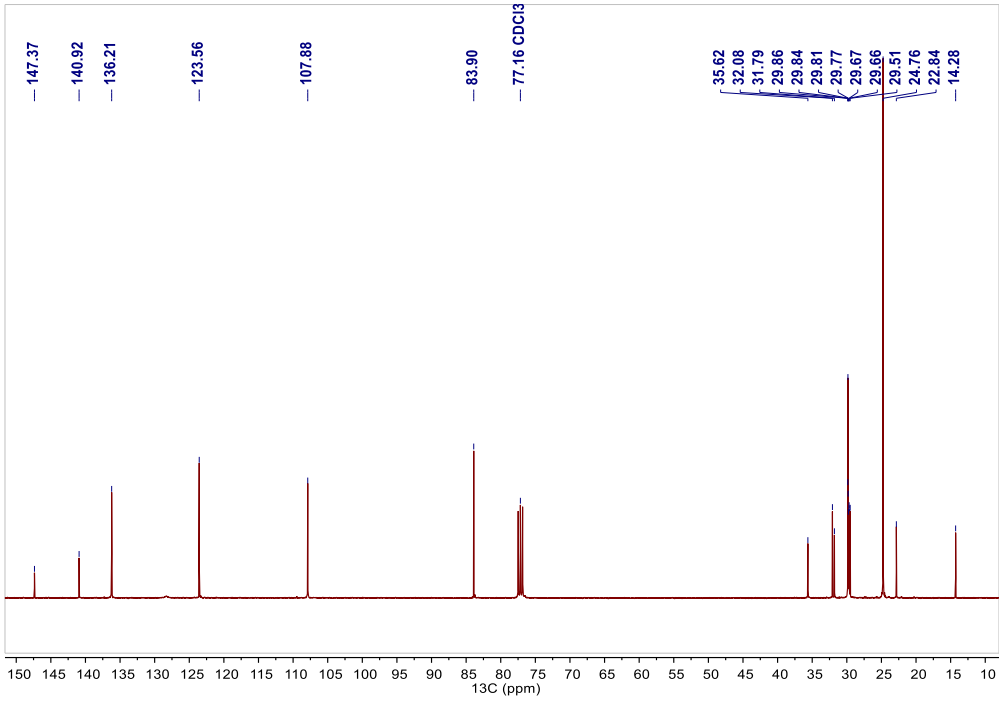

Figure 4.10. ^{13}C NMR spectrum of compound **3** in $CDCl_3$.

Compound 4

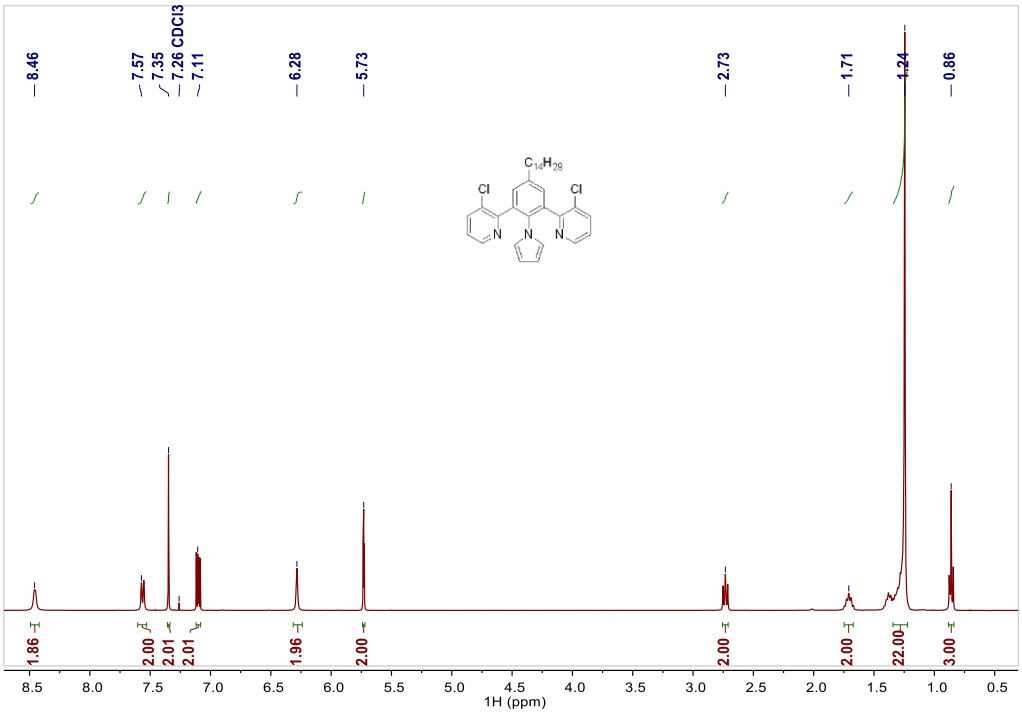

Figure 4.11. ^{1}H NMR spectrum of compound **4** in $CDCl_3$.

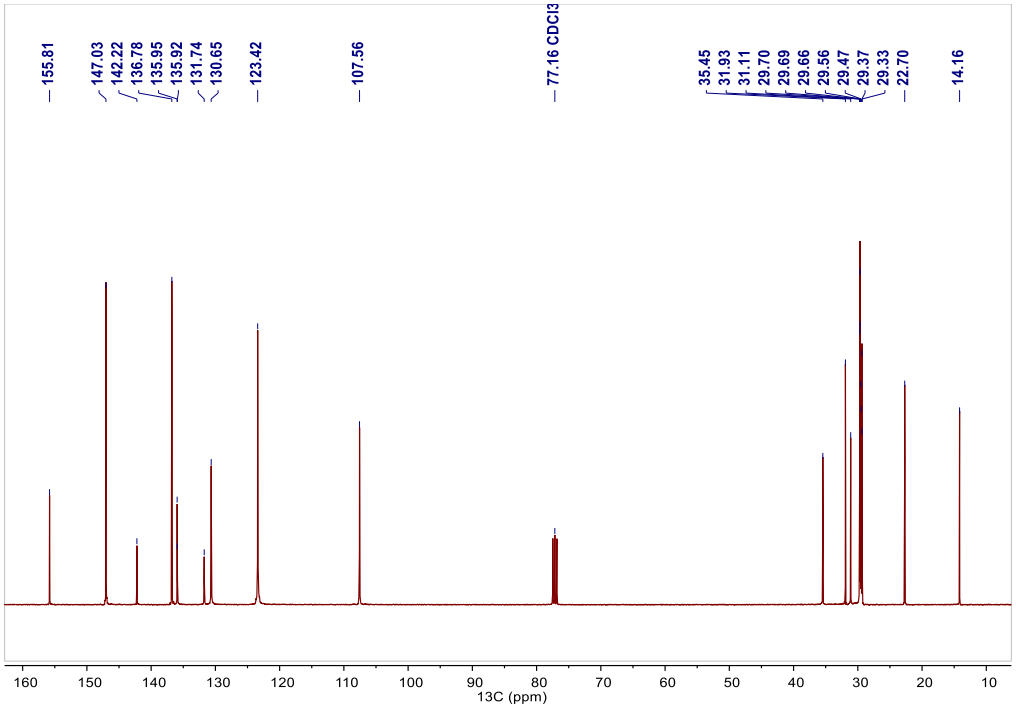

Figure 4.12. ^{13}C NMR spectrum of compound **4** in $CDCl_3$.

Compound 5

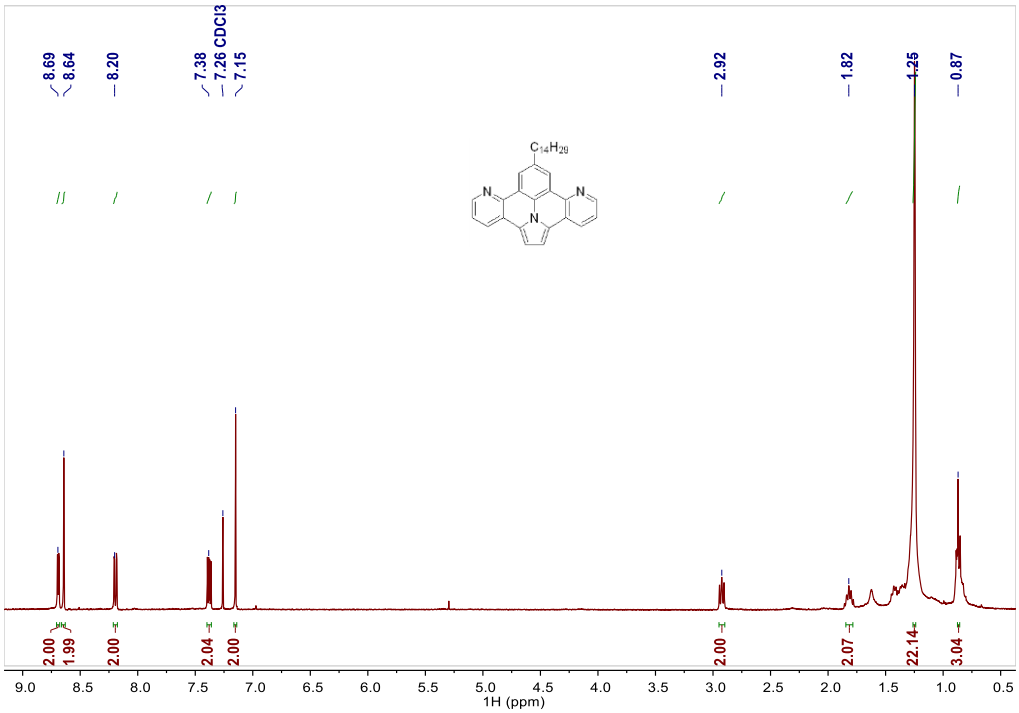

Figure 4.13. ^{1}H NMR spectrum of compound **5** in $CDCl_3$.

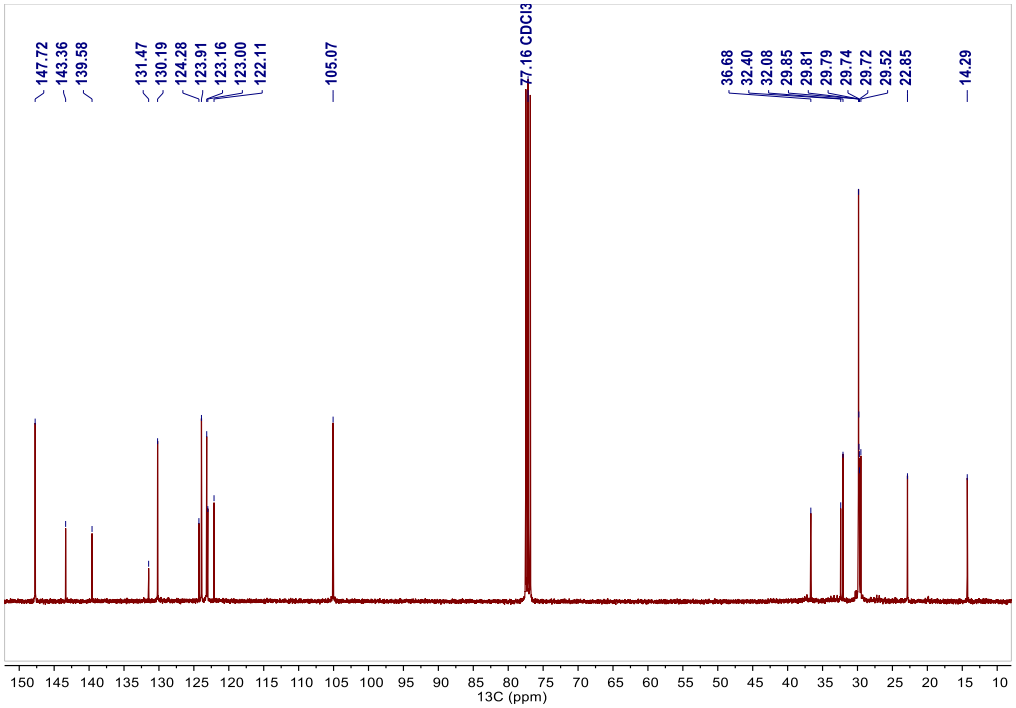

Figure 4.14. ^{13}C NMR spectrum of compound **5** in $CDCl_3$.

Compound 6

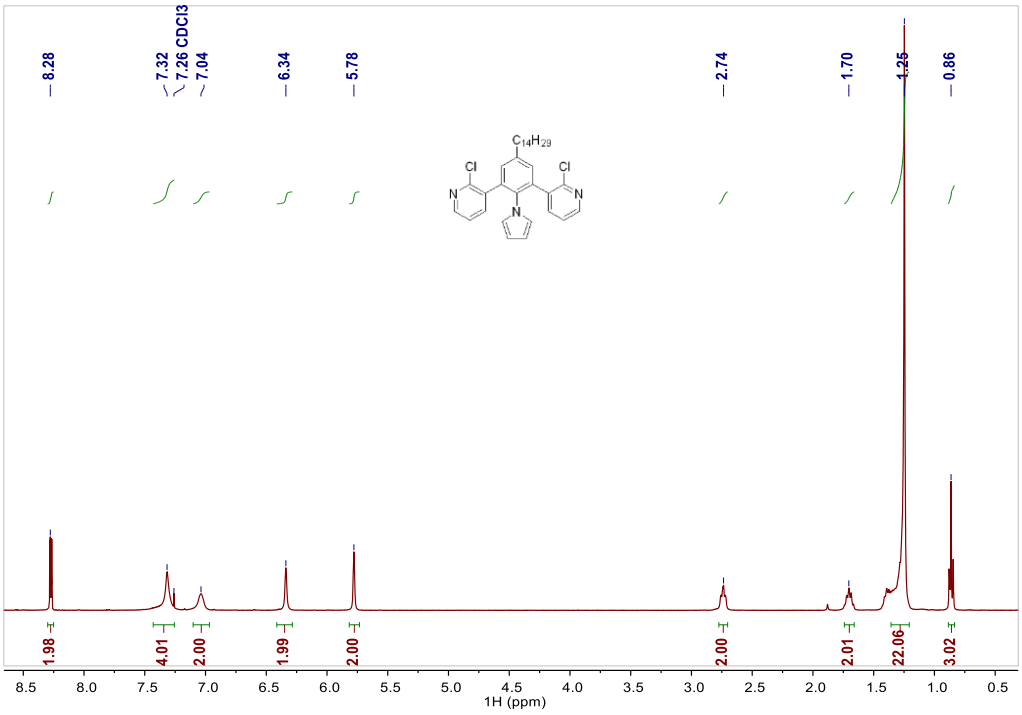

Figure 4.15. ^{1}H NMR spectrum of compound **6** in $CDCl_3$.

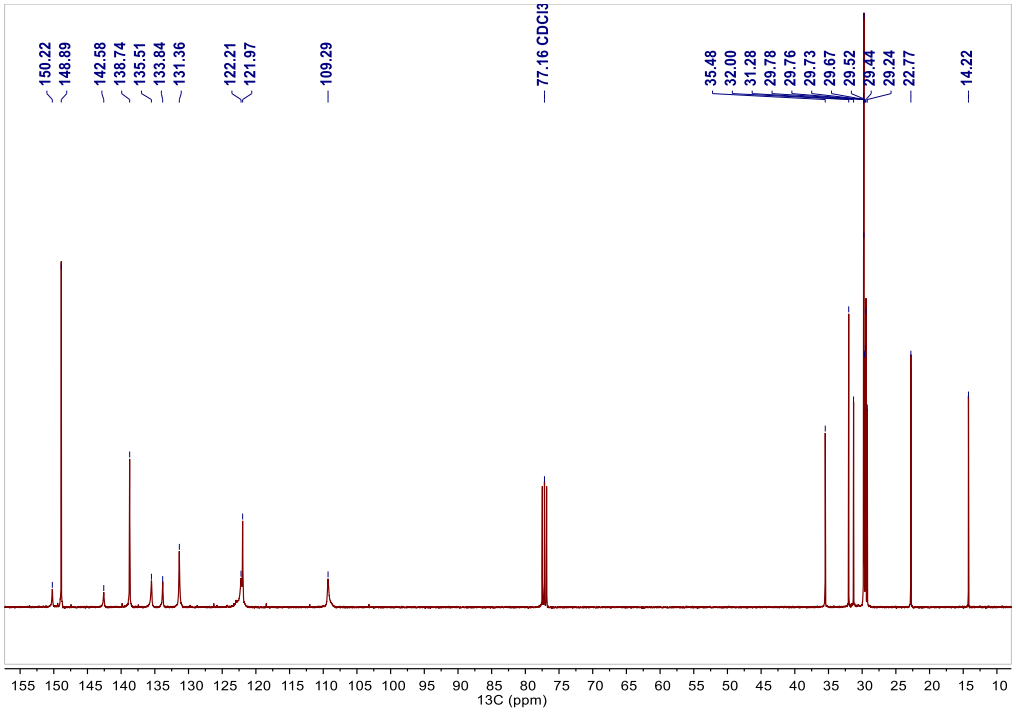

Figure 4.16. ^{13}C NMR spectrum of compound **6** in $CDCl_3$.

Compound 7

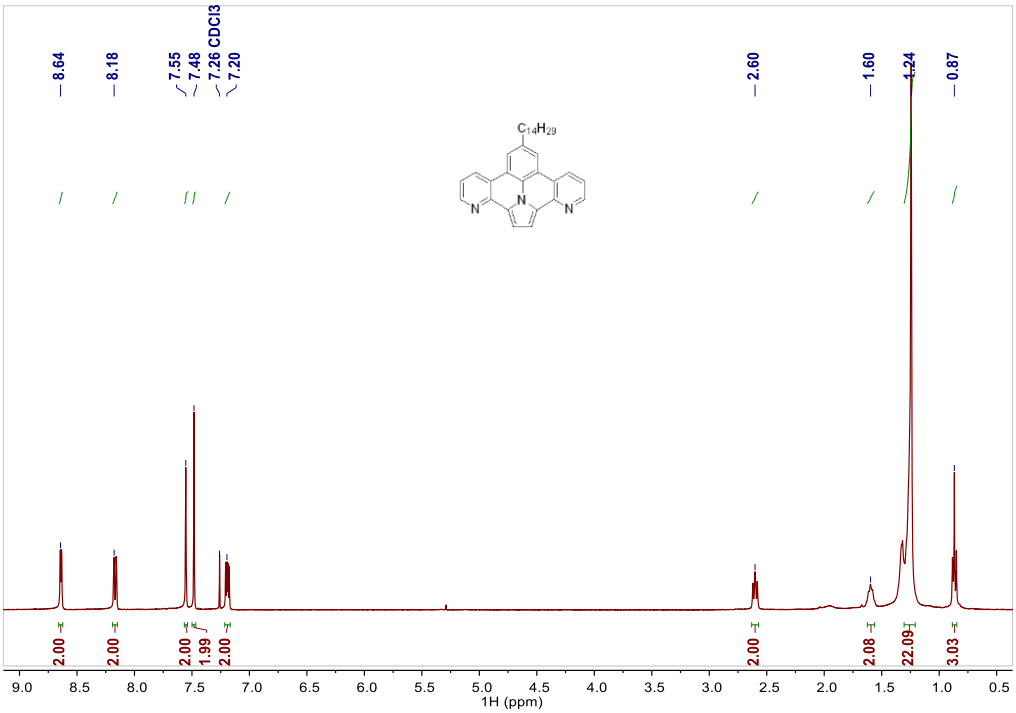

Figure 4.17. ^{1}H NMR spectrum of compound **7** in $CDCl_3$.

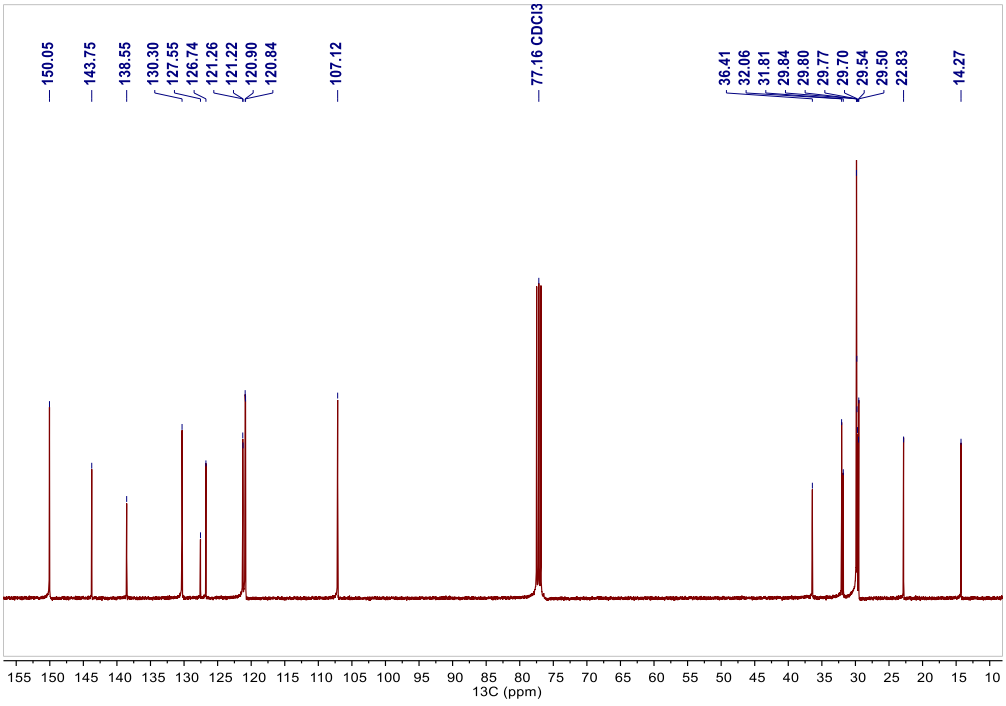

Figure 4.18. ^{13}C NMR spectrum of compound **7** in $CDCl_3$.

Compound 8

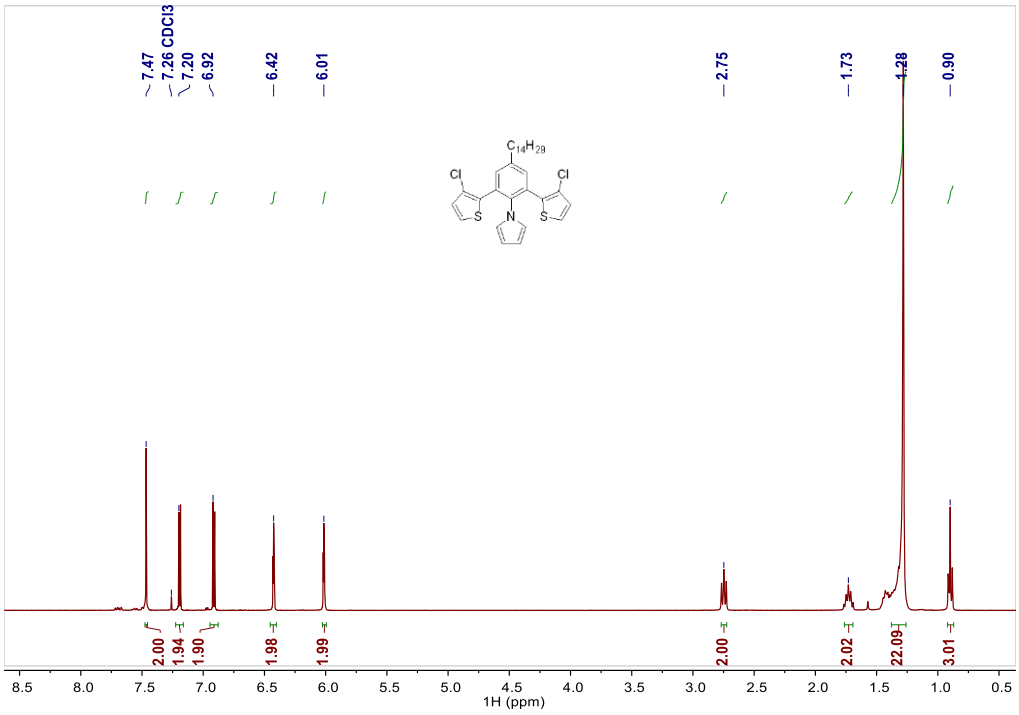

Figure 4.19. ^{1}H NMR spectrum of compound **8** in $CDCl_3$.

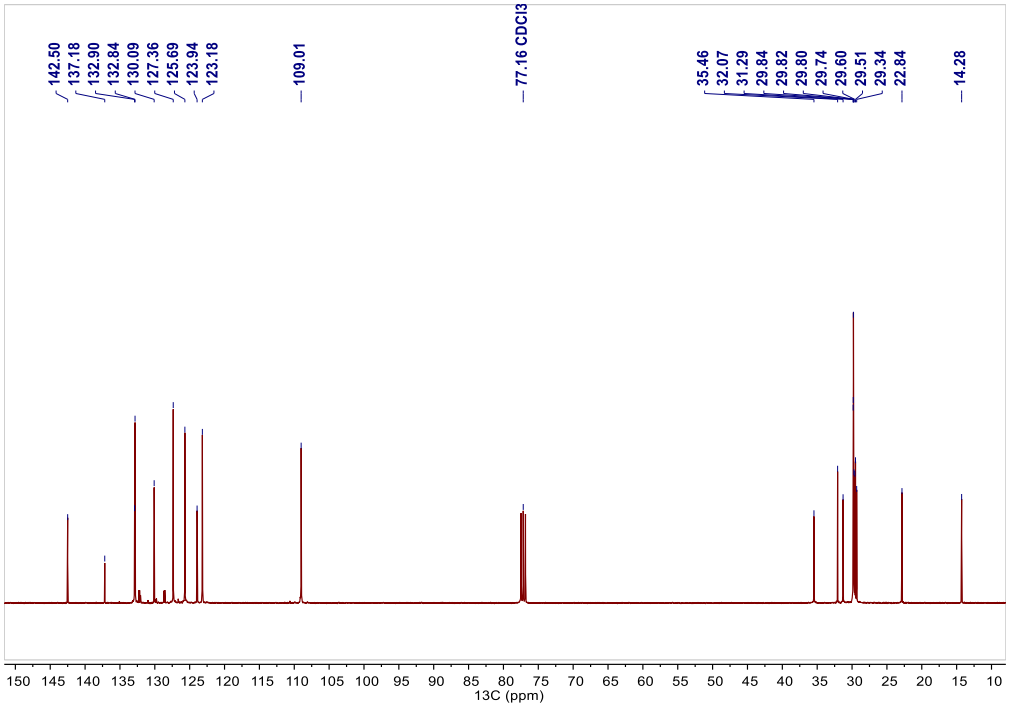

Figure 4.20. ^{13}C NMR spectrum of compound **8** in $CDCl_3$.

Compound 9

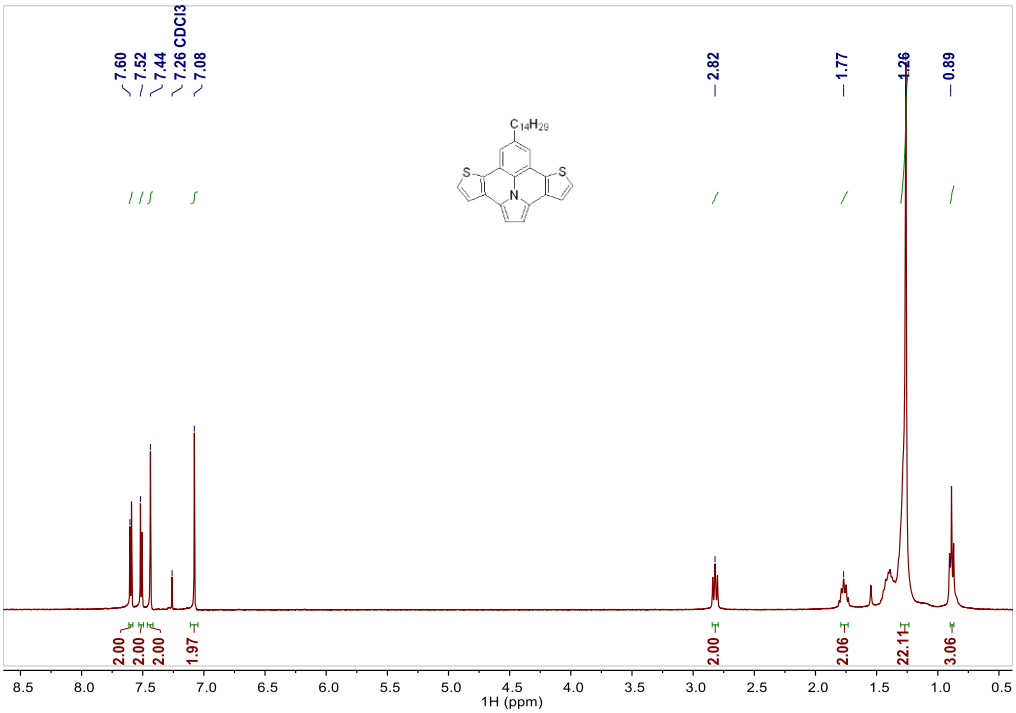

Figure 4.21. ^{1}H NMR spectrum of compound **9** in $CDCl_3$.

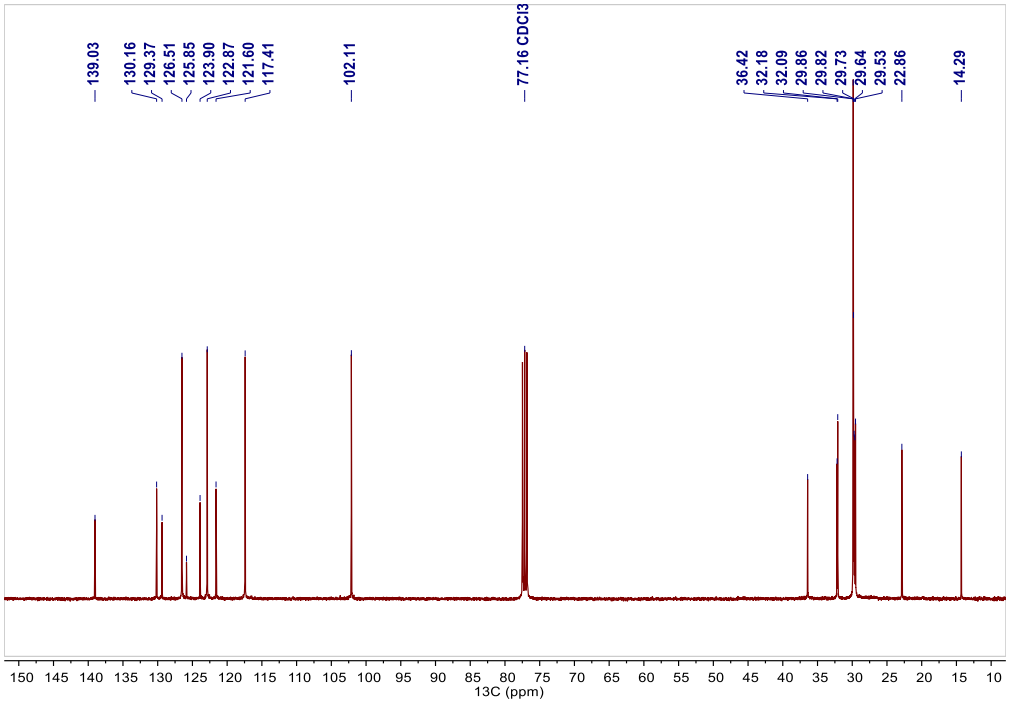

Figure 4.22. ^{13}C NMR spectrum of compound **9** in $CDCl_3$.

Compound 10

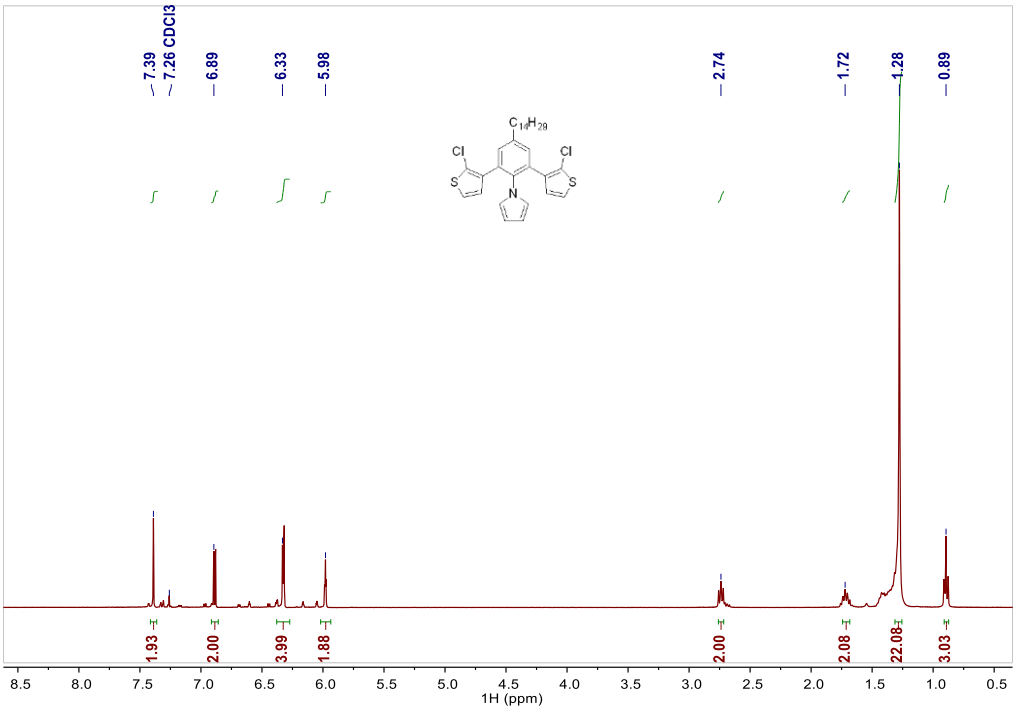

Figure 4.23. ^{1}H NMR spectrum of compound **10** in $CDCl_3$.

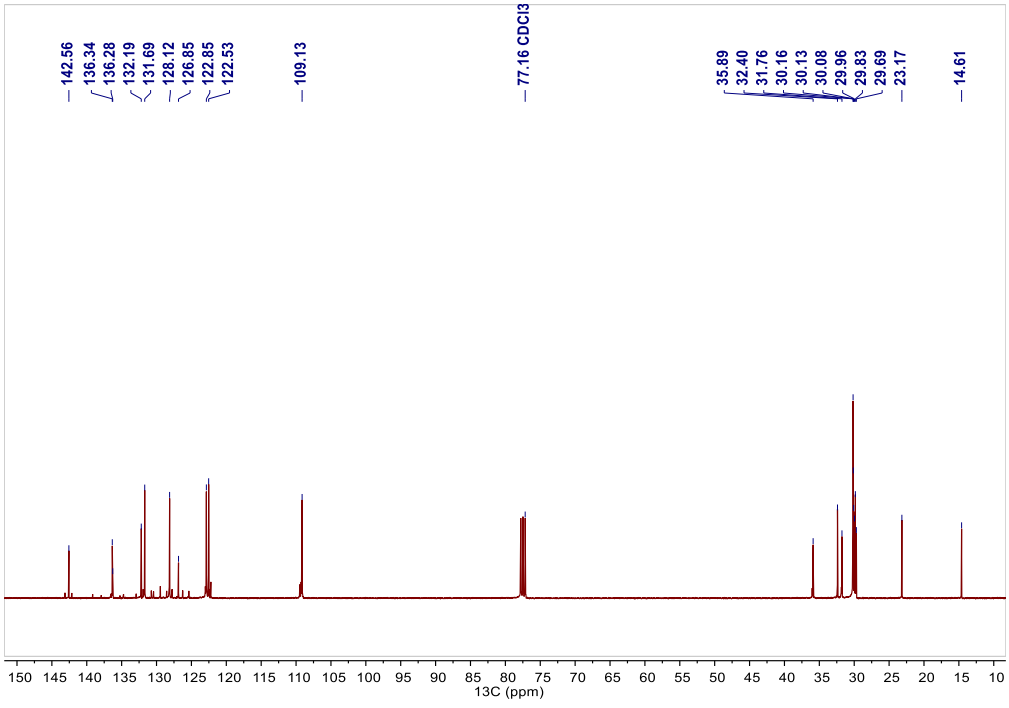

Figure 4.24. ^{13}C NMR spectrum of compound **10** in $CDCl_3$.

Compound 11

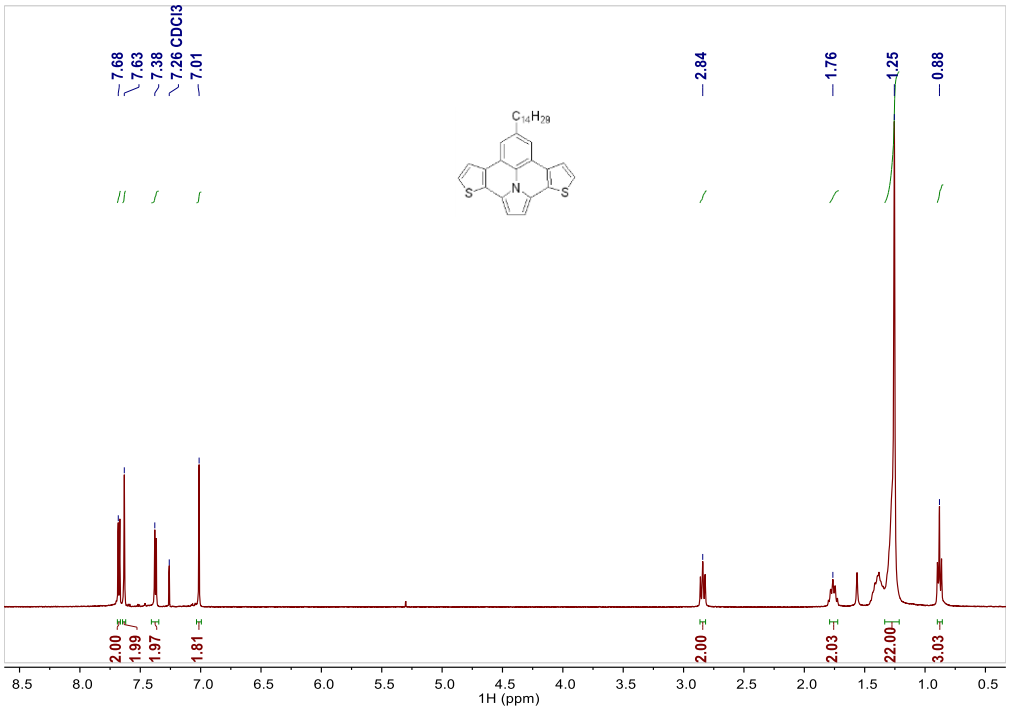

Figure 4.25. ^{1}H NMR spectrum of compound **11** in $CDCl_3$.

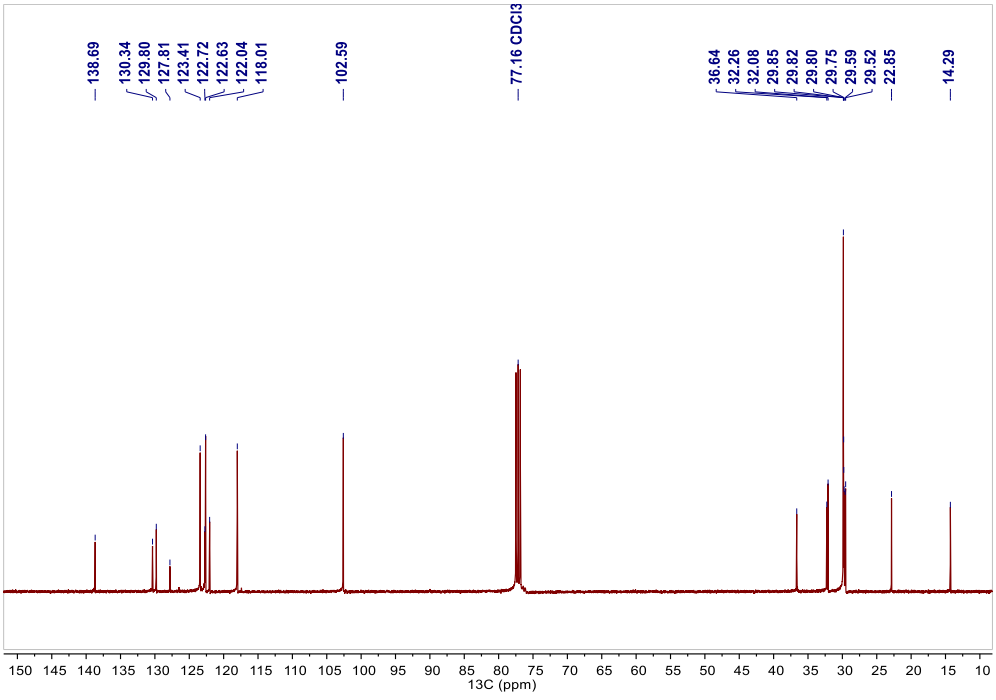

Figure 4.26. ^{13}C NMR spectrum of compound **11** in $CDCl_3$.

Compound 12

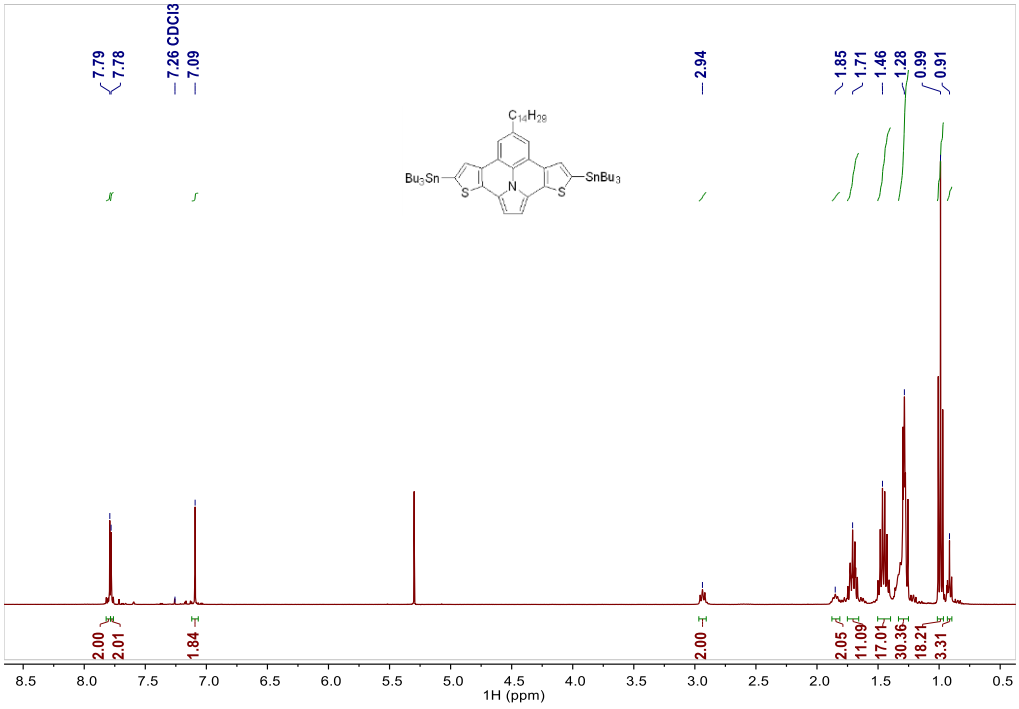

Figure 4.27. ^{1}H NMR spectrum of compound **12** in $CDCl_3$.

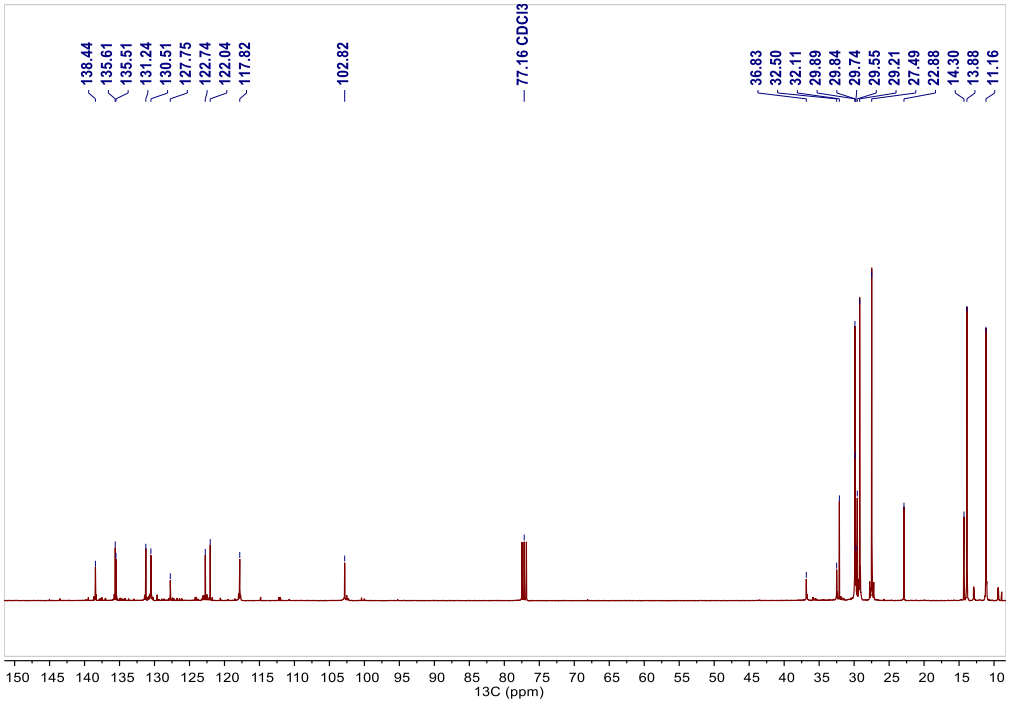

Figure 4.28. ^{13}C NMR spectrum of compound **12** in $CDCl_3$.

Polymer P1

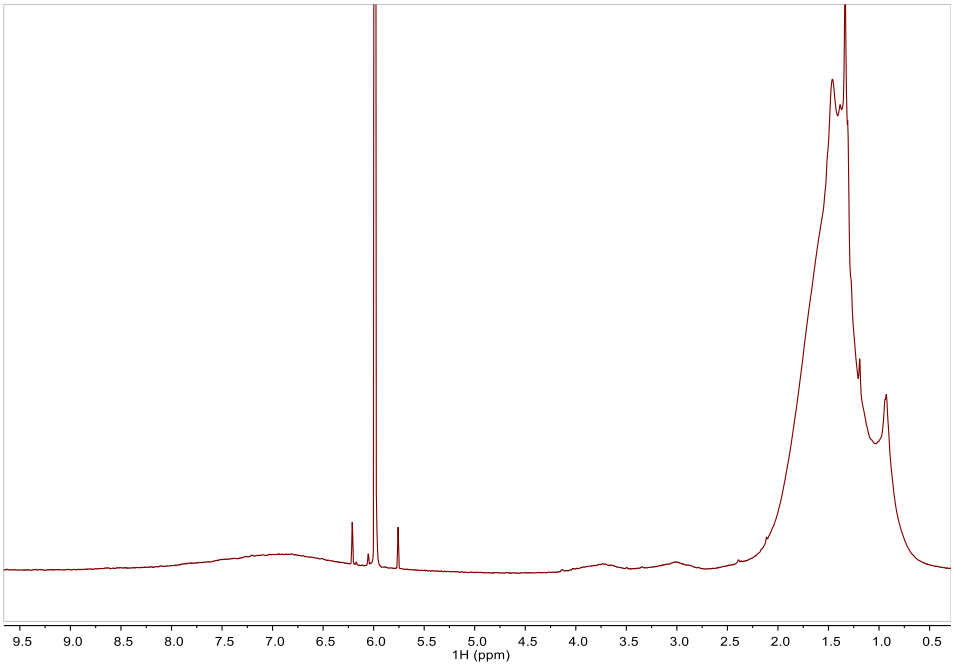

Figure 4.29. ^{1}H NMR spectrum of **P1** in TCE-d_2 at 383 K.

Polymer P2

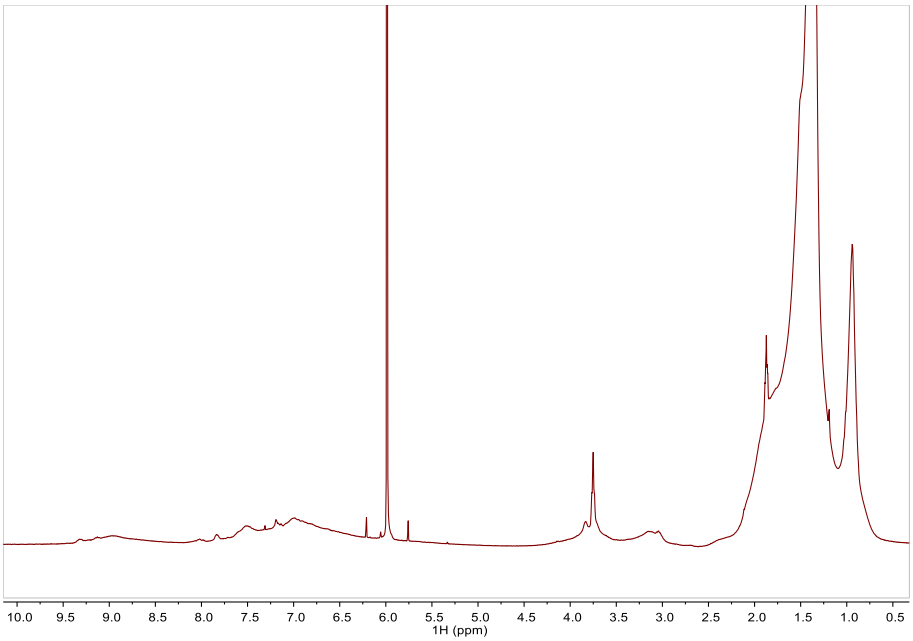

Figure 4.30. ^{1}H NMR spectrum of **P2** in TCE-d_2 at 383 K.

Polymer P3

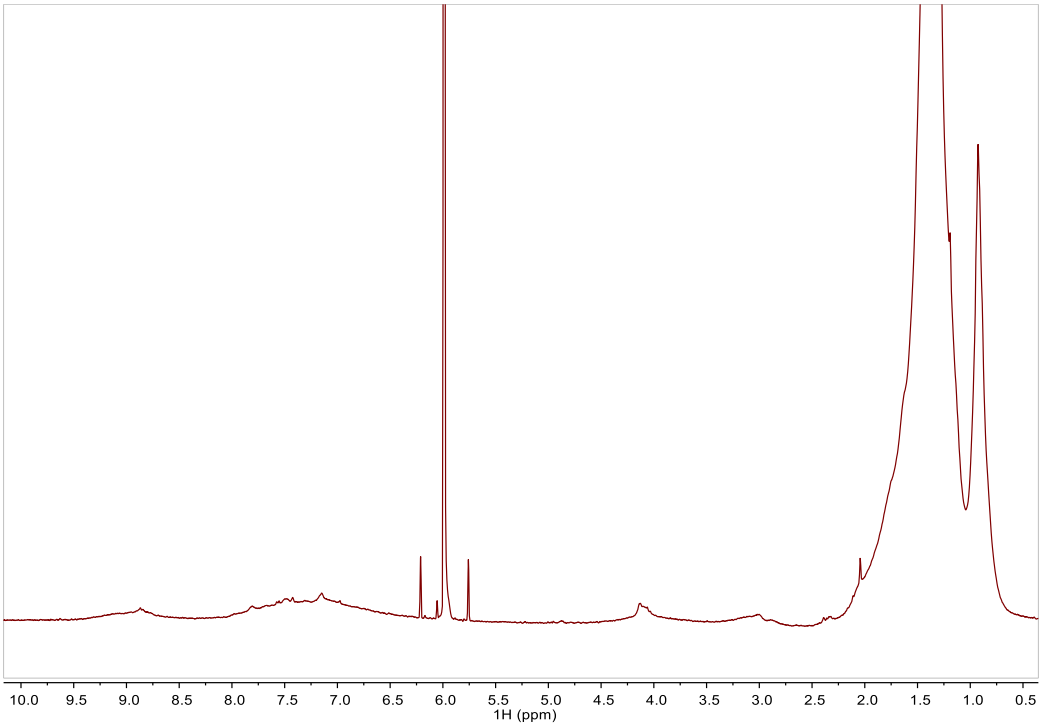

Figure 4.31. ^{1}H NMR spectrum of **P3** in TCE-d_2 at 383 K.

4.7.6. UV-visible and photoluminescence analysis

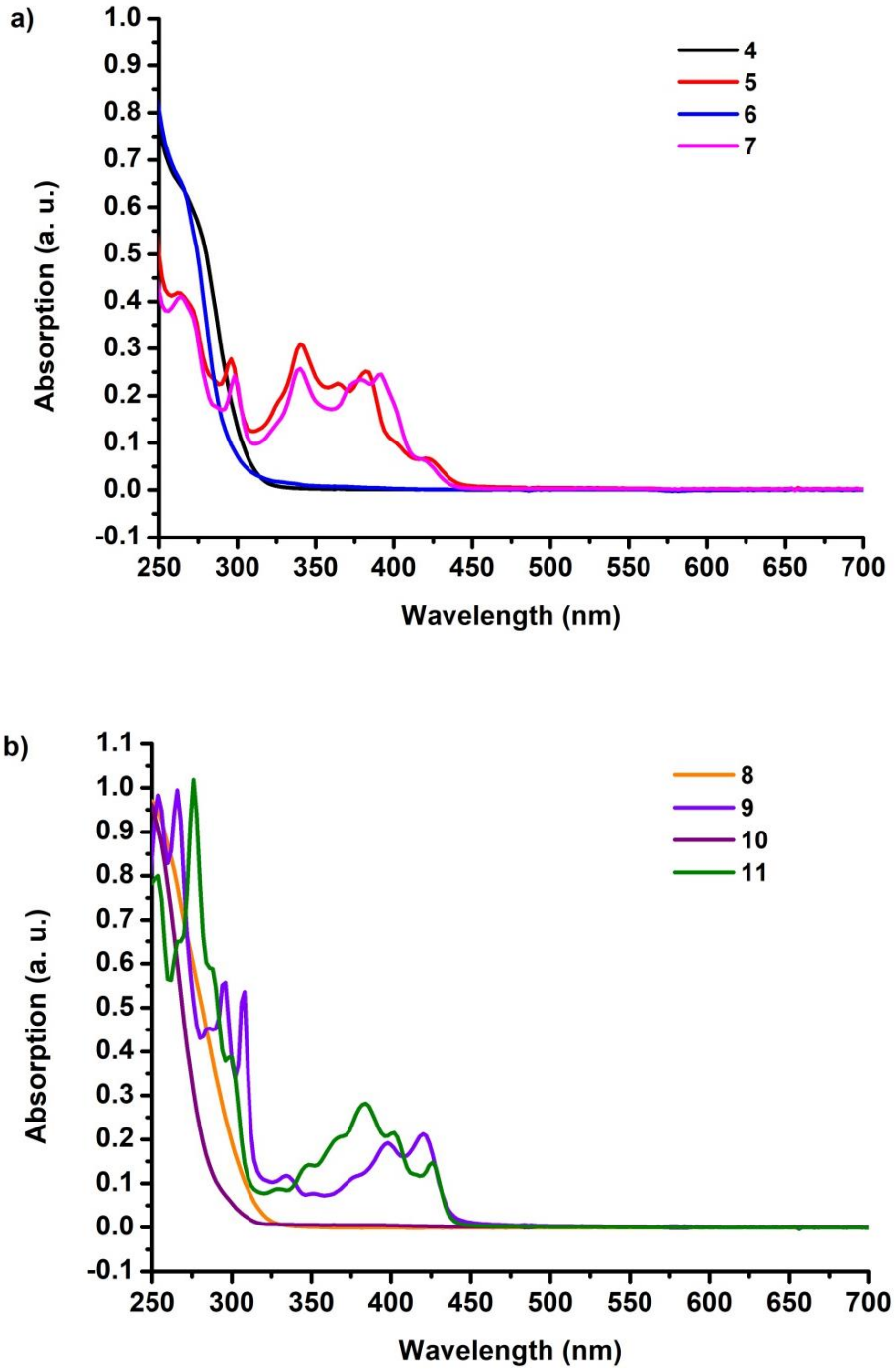

Figure 4.32. UV-vis absorption spectra of the compounds **4-7** (a) and **8-11** (b) in chloroform solution.

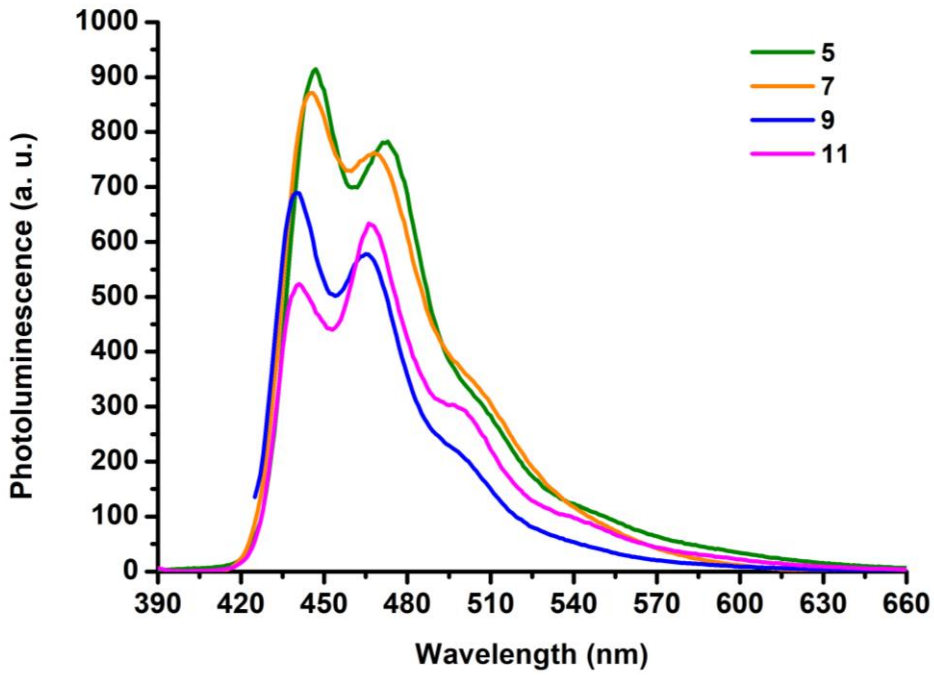

Figure 4.33. Photoluminescence spectra of the compounds **5, 7, 9** and **11** in chloroform solution (λ_{ex} = 348 nm, 400 nm, 422 nm and 388 nm, respectively).

4.7.7. Size-exclusion chromatography

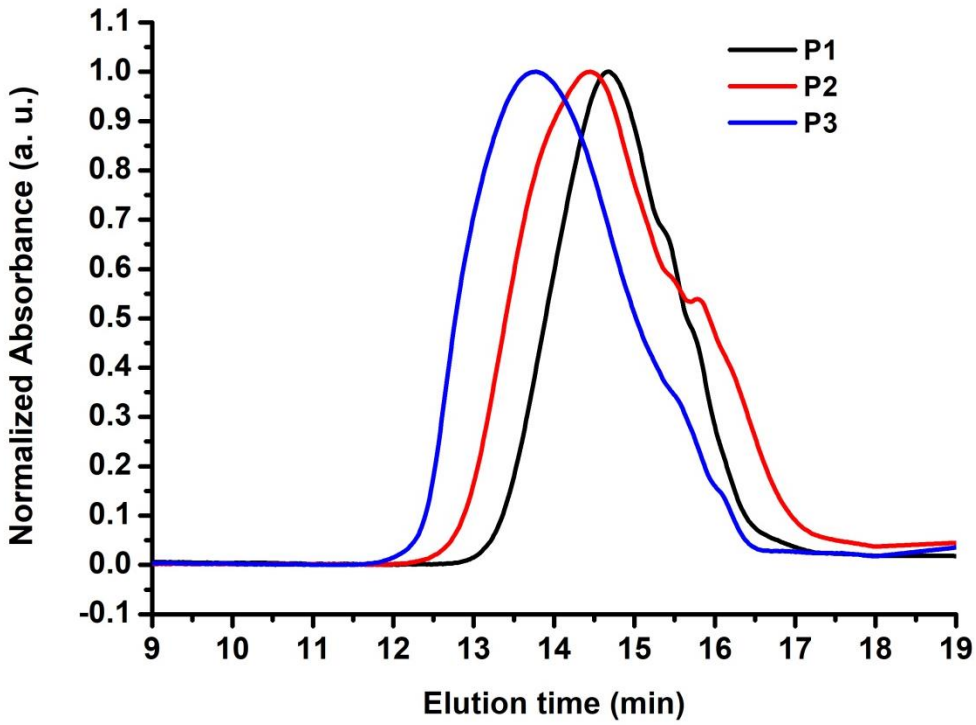

Figure 4.34. Size exclusion chromatography traces for P1 ($\overline{Mn}$: 12.5 kg mol^{-1}, $\overline{Mw}$: 22.5 kg mol^{-1}, dispersity index ($Đ$): 1.8, black trace), P2 ($\overline{Mn}$: 16.8 kg mol^{-1}, $\overline{Mw}$: 47.0 kg mol^{-1}, dispersity index ($Đ$): 2.8, red trace) and P3 ($\overline{Mn}$: 21.4 kg mol^{-1}, $\overline{Mw}$: 55.6 kg mol^{-1}, dispersity index ($Đ$) : 2.6, blue trace).

4.7.8. Thermal gravimetric analysis (TGA) and differential scanning calorimetry (DSC) thermal analysis

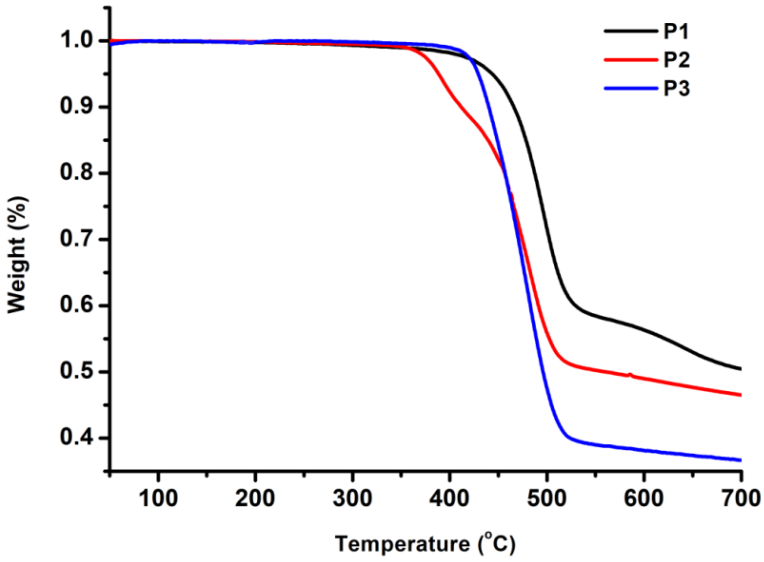

Figure 4.35. TGA plots of P1, P2 and P3 at a scan rate of 10 ℃ min^{-1} under nitrogen atmosphere.

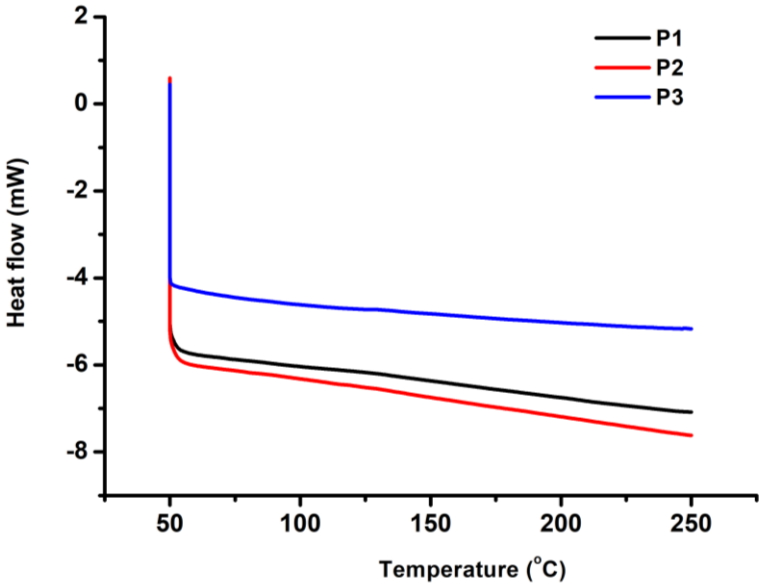

Figure 4.36. DSC plots of P1, P2 and P3 at a scan rate of 20 ℃ min^{-1} under nitrogen atmosphere.

4.7.9. Cyclic voltammetry

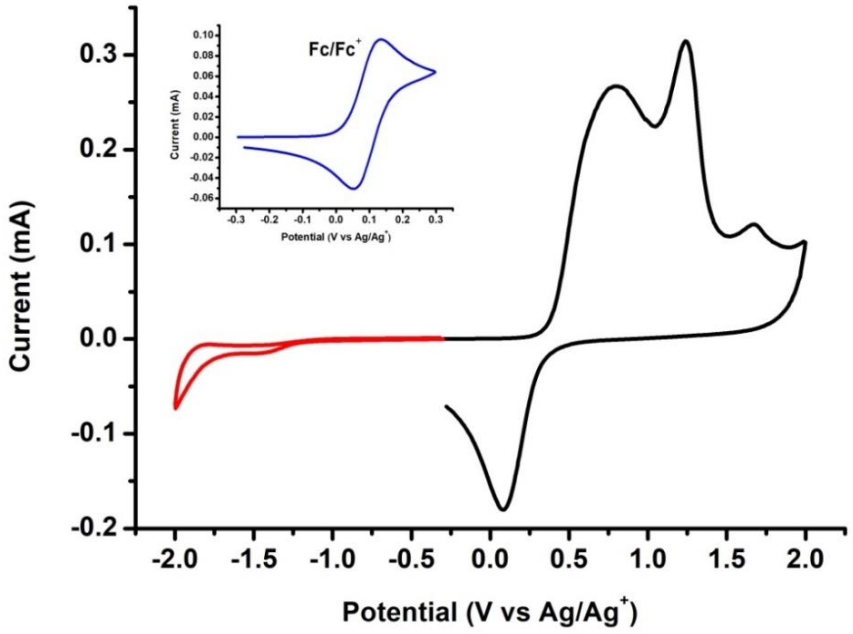

Figure 4.37. Film Cyclic Voltammetry of P1.

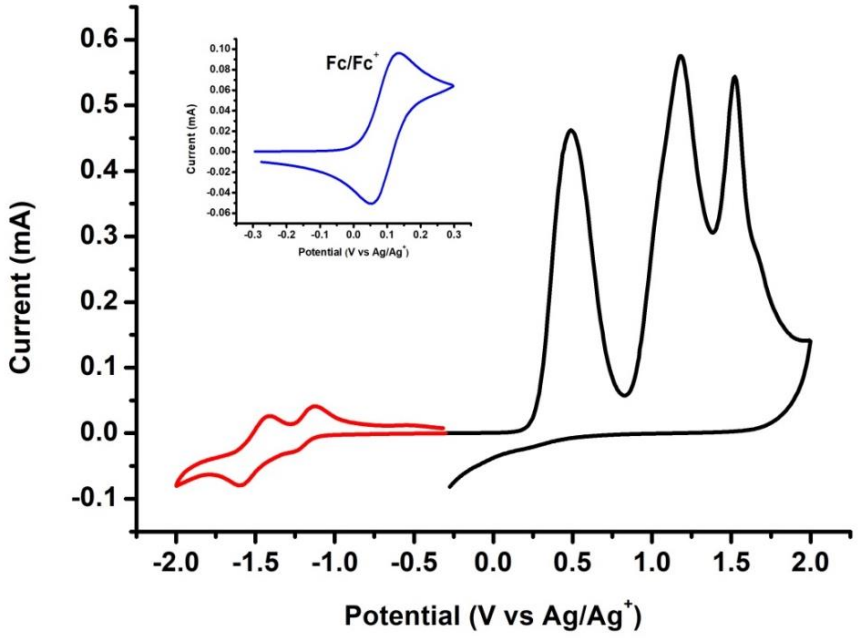

Figure 4.38. Film Cyclic Voltammetry of P2.

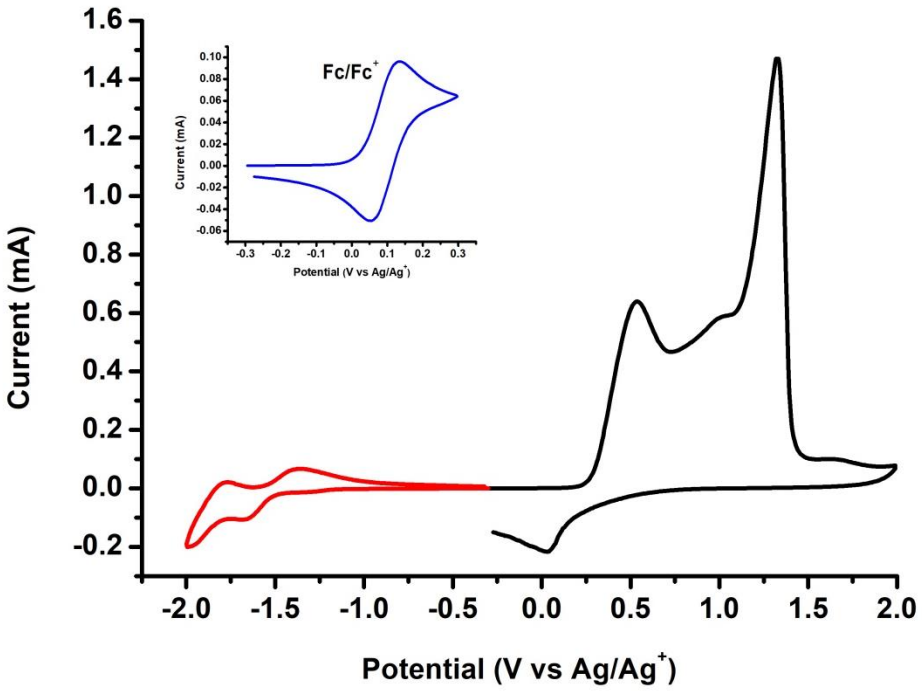

Figure 4.39. Film Cyclic Voltammetry of P3.

4.7.10. Tapping mode atomic force microscopy

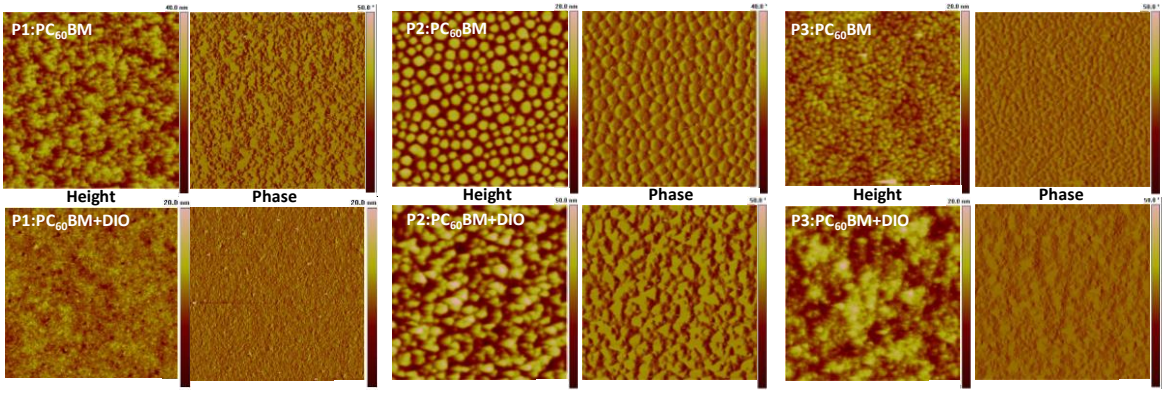

Figure 4.40. AFM images obtained in tapping mode (5 × 5 μm^2) of P1, P2 and P3 blend with $PC_{60}BM$ films without DIO (on top) and with DIO (on the bottom).

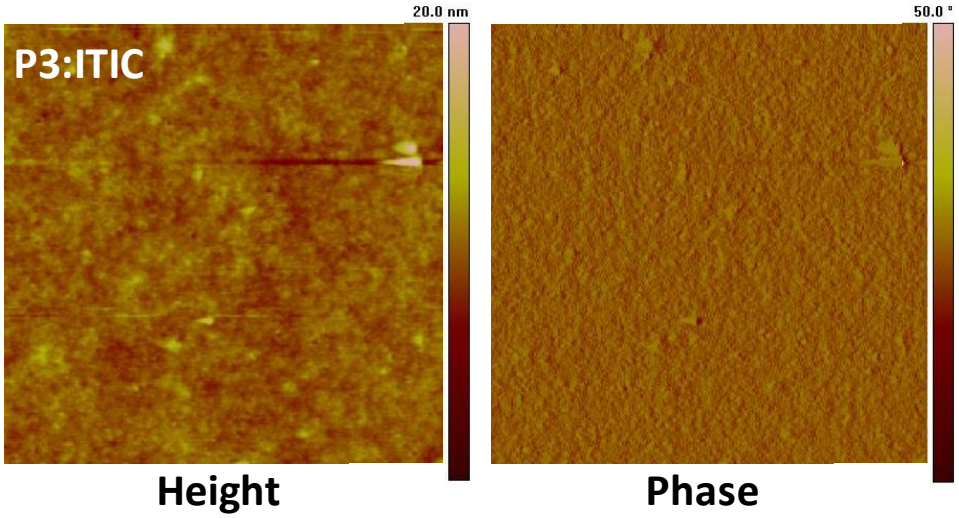

Figure 4.41. AFM images obtained in tapping mode (5 × 5 μm^2) of P3:ITIC blend film.

Conclusion and Outlook

Conclusion

In this PhD work, the bottom-up photochemical synthesis of structurally defined graphene nanoribbons with various widths and edge structures, heteroatoms doping has been achieved. Conjugated polymers, including conjugated ladder polymers (CLPs) and donor-acceptor conjugated polymers (D-A CPs) have also been prepared. The synthesis is based on the photochemical cyclodehydrochlorination (CDHC) reaction of polychlorinated polyphenylene precursors synthesized from carefully designed monomers containing chlorine atoms. The results can be concluded as follows in four parts:

1. Two narrow GNRs were prepared from polychlorinated polyphenylene precursors by the photochemical CDHC reaction (Figure C.1). The successful synthesis of both laterally symmetrical (GNR1) and unsymmetrical (GNR2) GNRs demonstrates the regioselectivity, edge configuration control, and high efficiency of the photochemical CDHC reaction. The structures were confirmed by ^{1}H NMR, FT-IR, XPS analysis and the optoelectronic properties were carefully characterized by UV-vis and photoluminescence analysis.

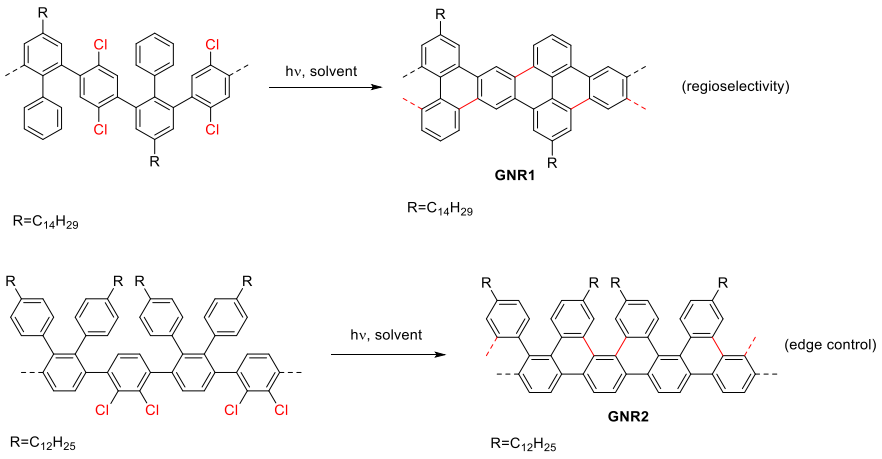

Figure C.1. Regioselective synthesis of GNR1 and GNR2 by the photochemical CDHC reaction.

2. Two narrow GNRs (*o*T-GNR and *p*T-GNR), both consist of a "ladderized" poly(*p*-phenylene) polymer backbone (in blue, Figure C.2) annulated with [2,3]thiophene units were synthesized from polychlorinated poly(*p*-phenylene) copolymers using the CDHC reaction. The synthesis *o*T-GNR and *p*T-GNR showed the versatility of the CDHC reaction, and the influence of the introduction of electron-rich functional groups on the structures and optoelectronic properties of GNRs were carefully studied.

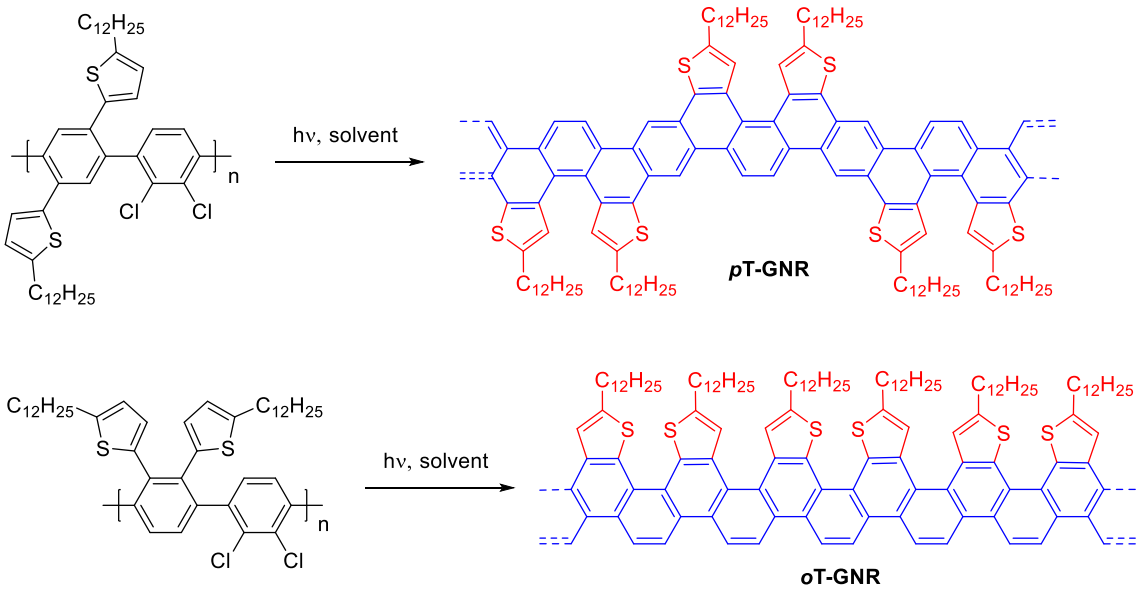

Figure C.2. Synthesis of *p*T-GNR and *o*T-GNR by the photochemical CDHC reaction.

3. Linear and helical conjugated ladder polymers (L-CLP and H-CLP) bearing electron-rich pyrrole units have been synthesized using the photochemical CDHC reaction (Figure C.3). ^{1}H NMR and XPS analysis confirmed the CLPs structures. The successful synthesis indicates the compatibility of the CDHC reaction with very electron-rich functional groups and the high efficiency of the CDHC reaction. The strong electron-donating properties of the pyrrole units in the polymer backbone make the polymer very electron-rich with moderate bandgaps and relatively high HOMO levels. Chemical titration of the CLPs was performed and the very electron-rich CLPs were easily oxidized into radical cations with a commercial oxidant.

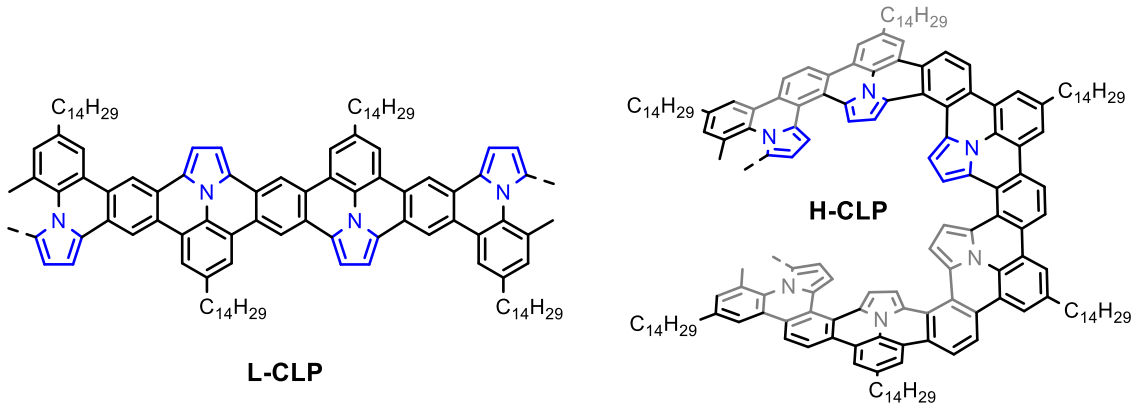

Figure C.3. Structures of the conjugated ladder polymers L-CLP and H-CLP.

4. Various π-extended ullazine derivatives annulated with either electron-poor pyridine or electron-rich thiophene units were synthesized through a metal-free, photochemical cyclodehydrochlorination (CDHC) reaction (Figure C.4). The strongest electron-donor derivative with one pyrrole and two thiophene rings was copolymerized with three electron-deficient monomers to provide a series of conjugated donor-acceptor polymers (D-A CPs). These polymers were successfully employed in the polymer solar cells and exhibited very promising performances, indicating the efficiency, versatility and practicality of the photochemical CDHC reaction.

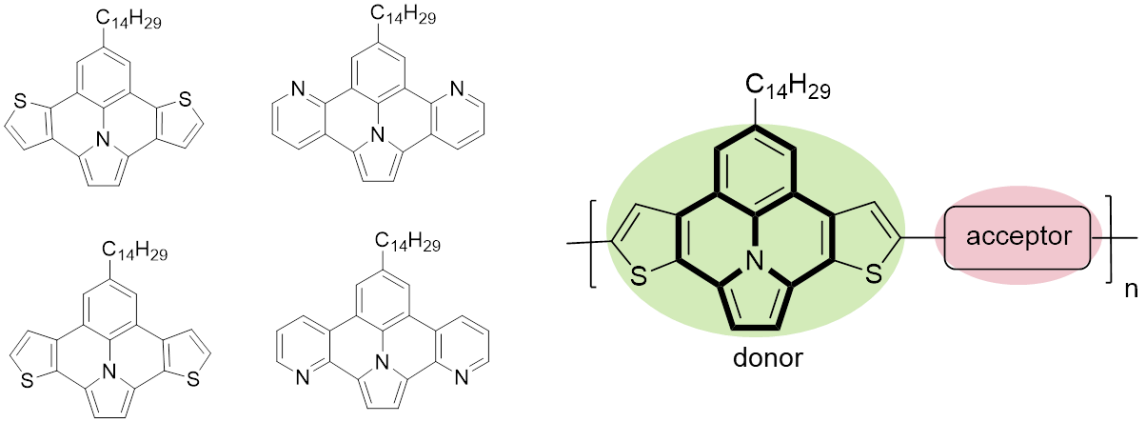

Figure C.4. Structures of the ullazine derivatives and the schematic illustration of the structures of the D-A CPs.

Outlook

With all the results we obtained above, we have proved that the photochemical CDHC reaction is useful in synthesizing various GNRs with different widths, edge structures, as well as heteroatoms doping. We have already synthesized all-phenyl GNRs, electron-rich thiophene units annulated GNRs, conjugated ladder polymes containg electron-rich pyrrole units, and a series of ullazine derivatives fused with electron-rich thiophene units or electron-poor pyridine units. The successful synthesis of these compounds demonstrated the regioselectivity, edge configuration control, compatibility with various electron-donating and electron-deficient heterocycles, high efficiency, versatility, as well as practicality of the photochemical CDHC reaction. The structures were characterized using ^{1}H NMR, FT-IR, XPS, Raman analysis and the optoelectronic properties were carefully studied by UV-vis and photoluminescence analysis.

We are trying to explore some interesting applications for the GNRs and CLPs. For example, the soluble narrow GNRs can be used for the dispersion of carbon nanotubes (CNTs), the thiophene annulated GNRs can be employed in the organic field-effect transistors (OFETs), and the CLPs containing electron-rich pyrrole units can be used in the organic light emitting diodes (OLEDs). In the future, we will put the research direction in finding useful applications for the obtained GNRs and CLPs.

In addition, all the GNRs we obtained are very narrow, in the future, we want to synthesize wider all-phenyl GNRs and wider GNRs fused with both electron-rich heterocycles or electron-poor heterocycles (Figure C.5) and find their application in the dispersion of wider CNTs. The introduction of heteroatoms is one of the best strategies to modulate the electronic energy level of π-conjugated molecules and polymers. Electron-donating atoms or groups such as sulfur and oxygen can increase the electron density, thus increasing their affinity towards n-type single-walled carbon nanotubes (SWNTs) while nitrogen and boron decrease the electron density, improving their electron transport ability (n-type materials). The preparation of wider and solution-processable GNRs doped with nitrogen and sulfur atoms by the CDHC

reaction in Figure C.5.

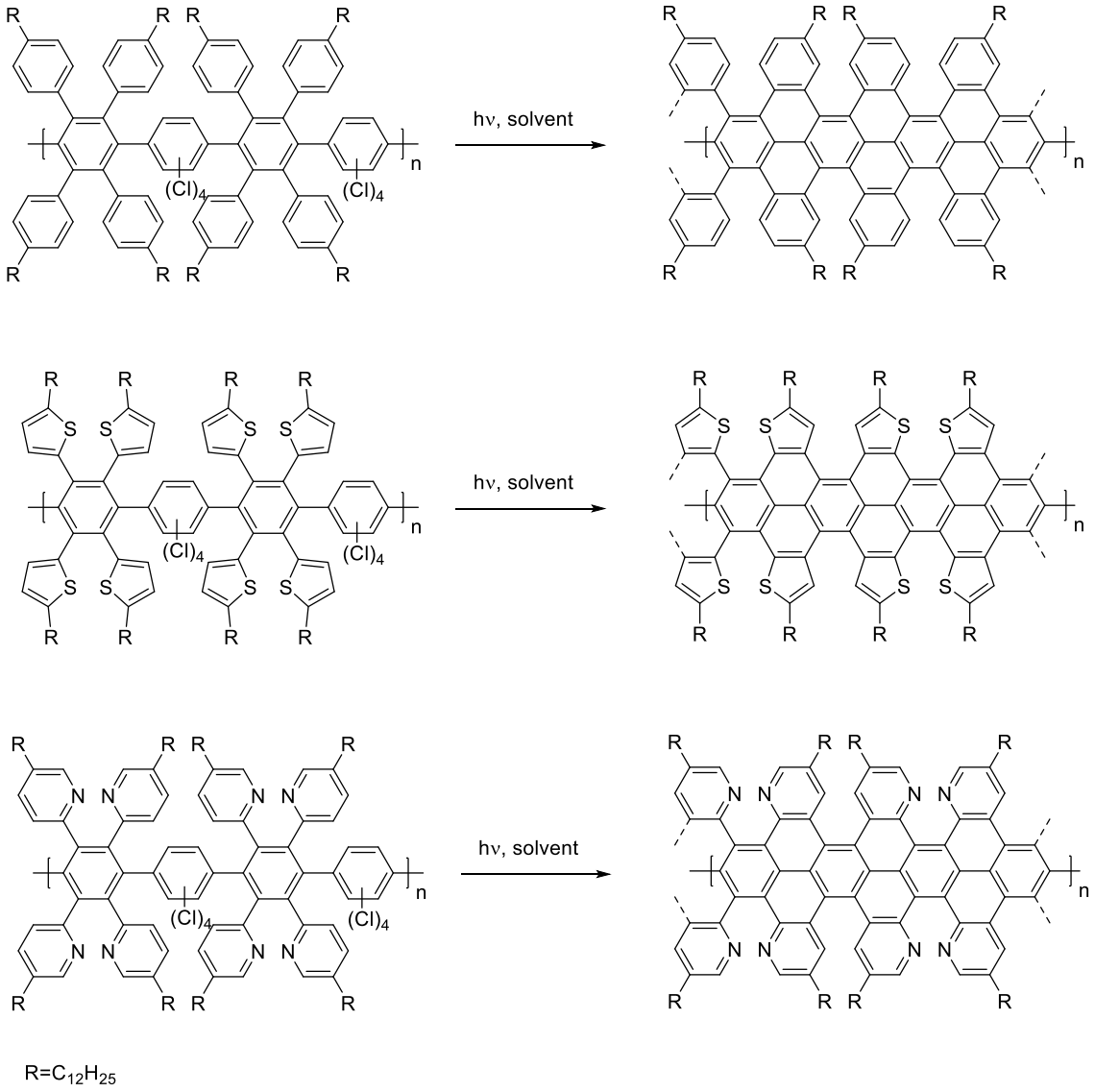

Figure C.5. Synthesis of wider all phenyl-GNR, electron-rich GNR, and electron-poor GNR by the photochemical CDHC reaction.

We propose to synthesize a GNR having a permanent dipole moment in the width axis. This feature will serve three purposes. 1) Provide the GNR with an ambipolar character, meaning that it can be both oxidized and reduced; 2) Increase the charge transport properties in the thin-film state. In fact, it has been shown that semiconducting materials with strong dipole

moment exhibit higher charge mobility in the solid state since it facilitates charge separation once a photon is absorbed; 3) Improve the morphology of the thin films since the dipole moments tend to align themselves one relative to each other, providing optimal face-to-face packing of the π-conjugated surface. The approach for the synthesis of such GNR is shown in Figure C.6. The presence of an intramolecular charge-transfer complex is expected to provide this ambipolar GNR with unique optoelectronic properties such as high absorption coefficient, low bandgap and electrochemical amphoteric character (both n-type and p-type materials).

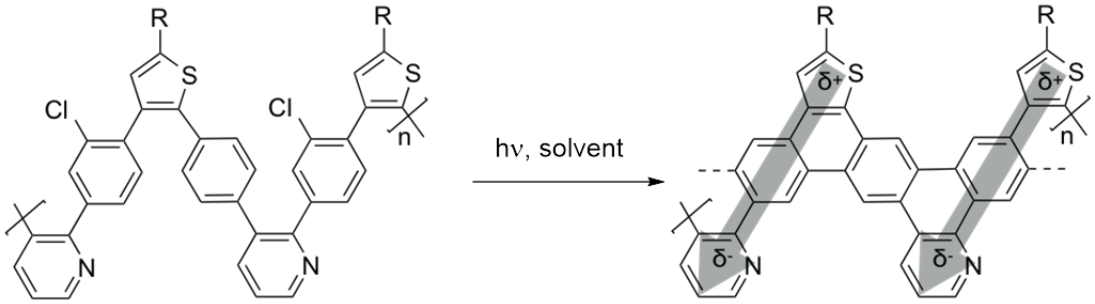

Figure C.6. Synthesis of GNR with a permanent dipole moment represented by the grey arrows.

References

(1) Novoselov, K. S.; Geim, A. K.; Morozov, S. V.; Jiang, D.; Zhang, Y.; Dubonos, S. V.; Grigorieva, I. V.; Firsov, A. A. *Science* **2004**, *306*, 666.

(2) Geim, A. K.; Novoselov, K. S. *Nat. Mater.* **2007**, *6*, 183.

(3) Orlita, M.; Faugeras, C.; Plochocka, P.; Neugebauer, P.; Martinez, G.; Maude, D. K.; Barra, A.-L.; Sprinkle, M.; Berger, C.; De Heer, W. A. *Phys. Rev. Lett.* **2008**, *101*, 267601.

(4) Stoller, M. D.; Park, S.; Zhu, Y.; An, J.; Ruoff, R. S. *Nano Lett.* **2008**, *8*, 3498.

(5) Balandin, A. A.; Ghosh, S.; Bao, W.; Calizo, I.; Teweldebrhan, D.; Miao, F.; Lau, C. N. *Nano Lett.* **2008**, *8*, 902.

(6) Lee, C.; Wei, X.; Kysar, J. W.; Hone, J. *Science* **2008**, *321*, 385.

(7) Nair, R. R.; Blake, P.; Grigorenko, A. N.; Novoselov, K. S.; Booth, T. J.; Stauber, T.; Peres, N. M.; Geim, A. K. *Science* **2008**, *320*, 1308.

(8) Westervelt, R. M. *Science* **2008**, *320*, 324.

(9) Morozov, S. V.; Novoselov, K. S.; Katsnelson, M. I.; Schedin, F.; Elias, D. C.; Jaszczak, J. A.; Geim, A. K. *Phys. Rev. Lett.* **2008**, *100*, 016602.

(10) Eda, G.; Chhowalla, M. *Nano Lett.* **2009**, *9*, 814.

(11) Müllen, K.; Rabe, J. P. *Acc. Chem. Res.* **2008**, *41*, 511.

(12) Berger, C.; Song, Z.; Li, T.; Li, X.; Ogbazghi, A. Y.; Feng, R.; Dai, Z.; Marchenkov, A. N.; Conrad, E. H.; First, P. N.; de Heer, W. A. *J. Phys. Chem. B* **2004**, *108*, 19912.

(13) Hernandez, Y.; Nicolosi, V.; Lotya, M.; Blighe, F. M.; Sun, Z.; De, S.; McGovern, I. T.; Holland, B.; Byrne, M.; Gun'Ko, Y. K.; Boland, J. J.; Niraj, P.; Duesberg, G.; Krishnamurthy, S.; Goodhue, R.; Hutchison, J.; Scardaci, V.; Ferrari, A. C.; Coleman, J. N. *Nature Nanotech.* **2008**, *3*, 563.

(14) Blake, P.; Brimicombe, P. D.; Nair, R. R.; Booth, T. J.; Jiang, D.; Schedin, F.; Ponomarenko, L. A.; Morozov, S. V.; Gleeson, H. F.; Hill, E. W.; Geim, A. K.; Novoselov, K. S. *Nano Lett.* **2008**, *8*, 1704.

(15) Alanyalıoğlu, M.; Segura, J. J.; Oró-Solè, J.; Casañ-Pastor, N. *Carbon* **2012**, *50*, 142.

(16) Su, Q.; Pang, S.; Alijani, V.; Li, C.; Feng, X.; Müllen, K. *Adv. Mater.* **2009**, *21*, 3191.

(17) Stankovich, S.; Dikin, D. A.; Piner, R. D.; Kohlhaas, K. A.; Kleinhammes, A.; Jia, Y.; Wu, Y.; Nguyen, S. T.; Ruoff, R. S. *Carbon* **2007**, *45*, 1558.

(18) Berger, C.; Song, Z.; Li, X.; Wu, X.; Brown, N.; Naud, C.; Mayou, D.; Li, T.; Hass, J.; Marchenkov, A. N.; Conrad, E. H.; First, P. N.; de Heer, W. A. *Science* **2006**, *312*, 1191.

(19) Emtsev, K. V.; Bostwick, A.; Horn, K.; Jobst, J.; Kellogg, G. L.; Ley, L.; McChesney, J. L.; Ohta, T.; Reshanov, S. A.; Röhrl, J.; Rotenberg, E.; Schmid, A. K.; Waldmann, D.; Weber, H. B.; Seyller, T. *Nat. Mater.* **2009**, *8*, 203.

(20) Ohta, T.; Bostwick, A.; Seyller, T.; Horn, K.; Rotenberg, E. *Science* **2006**, *313*, 951.

(21) Reina, A.; Jia, X.; Ho, J.; Nezich, D.; Son, H.; Bulovic, V.; Dresselhaus, M. S.; Kong, J. *Nano Lett.* **2009**, *9*, 30.

(22) Wei, D.; Liu, Y.; Wang, Y.; Zhang, H.; Huang, L.; Yu, G. *Nano Lett.* **2009**, *9*, 1752.

(23) Vitchev, R.; Malesevic, A.; Petrov, R. H.; Kemps, R.; Mertens, M.; Vanhulsel, A.; Van Haesendonck, C. *Nanotechnology* **2010**, *21*, 095602.

(24) Kim, K. S.; Zhao, Y.; Jang, H.; Lee, S. Y.; Kim, J. M.; Kim, K. S.; Ahn, J.-H.; Kim, P.; Choi, J.-Y.; Hong, B. H. *Nature* **2009**, *457*, 706.

(25) Juang, Z.-Y.; Wu, C.-Y.; Lu, A.-Y.; Su, C.-Y.; Leou, K.-C.; Chen, F.-R.; Tsai, C.-H. *Carbon* **2010**, *48*, 3169.

(26) Ismach, A.; Druzgalski, C.; Penwell, S.; Schwartzberg, A.; Zheng, M.; Javey, A.; Bokor, J.; Zhang, Y. *Nano Lett.* **2010**, *10*, 1542.

(27) Ho, K.-I.; Boutchich, M.; Su, C.-Y.; Moreddu, R.; Marianathan, E. S. R.; Montes, L.; Lai, C.-S. *Adv. Mater.* **2015**, *27*, 6519.

(28) Schwierz, F. *Nature Nanotech.* **2010**, *5*, 487.

(29) Barone, V.; Hod, O.; Scuseria, G. E. *Nano Lett.* **2006**, *6*, 2748.

(30) Han, M. Y.; Özyilmaz, B.; Zhang, Y.; Kim, P. *Phys. Rev. Lett.* **2007**, *98*, 206805.

(31) Ritter, K. A.; Lyding, J. W. *Nat. Mater.* **2009**, *8*, 235.

(32) Cai, J.; Ruffieux, P.; Jaafar, R.; Bieri, M.; Braun, T.; Blankenburg, S.; Muoth, M.; Seitsonen, A. P.; Saleh, M.; Feng, X.; Müllen, K.; Fasel, R. *Nature* **2010**, *466*, 470.

(33) Talirz, L.; Ruffieux, P.; Fasel, R. *Adv. Mater.* **2016**, *28*, 6222.

(34) Narita, A.; Feng, X.; Hernandez, Y.; Jensen, S. A.; Bonn, M.; Yang, H.; Verzhbitskiy, I. A.; Casiraghi, C.; Hansen, M. R.; Koch, A. H. R.; Fytas, G.; Ivasenko, O.; Li, B.; Mali, K. S.; Balandina, T.; Mahesh, S.; De Feyter, S.; Müllen, K. *Nat. Chem.* **2013**, *6*, 126.

(35) Wang, X.-Y.; Urgel, J. I.; Barin, G. B.; Eimre, K.; Di Giovannantonio, M.; Milani, A.; Tommasini, M.; Pignedoli, C. A.; Ruffieux, P.; Feng, X.; Fasel, R.; Müllen, K.; Narita, A. *J. Am. Chem. Soc.* **2018**, *140*, 9104.

(36) Son, Y.-W.; Cohen, M. L.; Louie, S. G. *Phys. Rev. Lett.* **2006**, *97*, 216803.

(37) Yang, L.; Park, C.-H.; Son, Y.-W.; Cohen, M. L.; Louie, S. G. *Phys. Rev. Lett.* **2007**, *99*, 186801.

(38) Li, X.; Wang, X.; Zhang, L.; Lee, S.; Dai, H. *Science* **2008**, *319*, 1229.

(39) Wu, Z.-S.; Ren, W.; Gao, L.; Liu, B.; Zhao, J.; Cheng, H.-M. *Nano Res.* **2010**, *3*, 16.

(40) Yoon, W.; Lee, Y.; Jang, H.; Jang, M.; Kim, J. S.; Lee, H. S.; Im, S.; Boo, D. W.; Park, J.; Ju, S.-Y. *Carbon* **2015**, *81*, 629.

(41) Wang, X.; Ouyang, Y.; Li, X.; Wang, H.; Guo, J.; Dai, H. *Phys. Rev. Lett.* **2008**, *100*, 206803.

(42) Kosynkin, D. V.; Higginbotham, A. L.; Sinitskii, A.; Lomeda, J. R.; Dimiev, A.; Price, B. K.; Tour, J. M. *Nature* **2009**, *458*, 872.

(43) Jiao, L.; Zhang, L.; Wang, X.; Diankov, G.; Dai, H. *Nature* **2009**, *458*, 877.

(44) Higginbotham, A.; Kosynkin, D.; Sinitskii, A.; Sun, Z.; Tour, J. *ACS Nano* **2010**, *4*, 2059.

(45) Jiao, L.; Zhang, L.; Ding, L.; Liu, J.; Dai, H. *Nano Res.* **2010**, *3*, 387.

(46) Jiao, L.; Wang, X.; Diankov, G.; Wang, H.; Dai, H. *Nature Nanotech.* **2010**, *5*, 321.

(47) Chen, Z.; Lin, Y.-M.; Rooks, M. J.; Avouris, P. *Physica E* **2007**, *40*, 228.

(48) Bai, J.; Duan, X.; Huang, Y. *Nano Lett.* **2009**, *9*, 2083.

(49) Pan, Z.; Liu, N.; Fu, L.; Liu, Z. *J. Am. Chem. Soc.* **2011**, *133*, 17578.

(50) Wang, X.; Dai, H. *Nat. Chem.* **2010**, *2*, 661.

(51) Chen, Y.-C.; de Oteyza, D. G.; Pedramrazi, Z.; Chen, C.; Fischer, F. R.; Crommie, M. F. *ACS Nano* **2013**, *7*, 6123.

(52) Bronner, C.; Stremlau, S.; Gille, M.; Brauße, F.; Haase, A.; Hecht, S.; Tegeder, P. *Angew. Chem. Int. Ed.* **2013**, *52*, 4422.

(53) Zhang, Y.; Zhang, Y.; Li, G.; Lu, J.; Lin, X.; Du, S.; Berger, R.; Feng, X.; Müllen, K.; Gao, H.-J. *Appl. Phys. Lett.* **2014**, *105*, 023101.

(54) Marangoni, T.; Haberer, D.; Rizzo, D. J.; Cloke, R. R.; Fischer, F. R. *Chem. Eur. J.* **2016**, *22*, 13037.

(55) Cai, J.; Pignedoli, C. A.; Talirz, L.; Ruffieux, P.; Söde, H.; Liang, L.; Meunier, V.; Berger, R.; Li, R.; Feng, X.; Müllen, K.; Fasel, R. *Nature Nanotech.* **2014**, *9*, 896.

(56) Cloke, R. R.; Marangoni, T.; Nguyen, G. D.; Joshi, T.; Rizzo, D. J.; Bronner, C.; Cao, T.; Louie, S. G.; Crommie, M. F.; Fischer, F. R. *J. Am. Chem. Soc.* **2015**, *137*, 8872.

(57) Kawai, S.; Saito, S.; Osumi, S.; Yamaguchi, S.; Foster, A. S.; Spijker, P.; Meyer, E. *Nat. Commun.* **2015**, *6*, 8098.

(58) Nguyen, G. D.; Toma, F. M.; Cao, T.; Pedramrazi, Z.; Chen, C.; Rizzo, D. J.; Joshi, T.; Bronner, C.; Chen, Y.-C.; Favaro, M.; Louie, S. G.; Fischer, F. R.; Crommie, M. F. *J. Phys. Chem. C* **2016**, *120*, 2684.

(59) Yang, X.; Dou, X.; Rouhanipour, A.; Zhi, L.; Räder, H. J.; Müllen, K. *J. Am. Chem.*

Soc. **2008**, *130*, 4216.

(60) Schwab, M. G.; Narita, A.; Hernandez, Y.; Balandina, T.; Mali, K. S.; De Feyter, S.; Feng, X.; Müllen, K. *J. Am. Chem. Soc.* **2012**, *134*, 18169.

(61) Osella, S.; Narita, A.; Schwab, M. G.; Hernandez, Y.; Feng, X.; Müllen, K.; Beljonne, D. *ACS Nano* **2012**, *6*, 5539.

(62) El Gemayel, M.; Narita, A.; Dössel, L. F.; Sundaram, R. S.; Kiersnowski, A.; Pisula, W.; Hansen, M. R.; Ferrari, A. C.; Orgiu, E.; Feng, X. *Nanoscale* **2014**, *6*, 6301.

(63) Narita, A.; Feng, X.; Hernandez, Y.; Jensen, S. A.; Bonn, M.; Yang, H.; Verzhbitskiy, I. A.; Casiraghi, C.; Hansen, M. R.; Koch, A. H. *Nat. Chem.* **2014**, *6*, 126.

(64) Jensen, S. A.; Ulbricht, R.; Narita, A.; Feng, X.; Müllen, K.; Hertel, T.; Turchinovich, D.; Bonn, M. *Nano Lett.* **2013**, *13*, 5925.

(65) Abbas, A. N.; Liu, G.; Narita, A.; Orosco, M.; Feng, X.; Müllen, K.; Zhou, C. *J. Am. Chem. Soc.* **2014**, *136*, 7555.

(66) Narita, A.; Verzhbitskiy, I. A.; Frederickx, W.; Mali, K. S.; Jensen, S. A.; Hansen, M. R.; Bonn, M.; De Feyter, S.; Casiraghi, C.; Feng, X. *ACS Nano* **2014**, *8*, 11622.

(67) Kim, K. T.; Lee, J. W.; Jo, W. H. *Macromol. Chem. Phys.* **2013**, *214*, 2768.

(68) Narita, A.; Wang, X.-Y.; Feng, X.; Müllen, K. *Chem. Soc. Rev.* **2015**, *44*, 6616.

(69) Qian, H.; Negri, F.; Wang, C.; Wang, Z. *J. Am. Chem. Soc.* **2008**, *130*, 17970.

(70) Huang, Y.; Mai, Y.; Beser, U.; Teyssandier, J.; Velpula, G.; van Gorp, H.; Straasø, L. A.; Hansen, M. R.; Rizzo, D.; Casiraghi, C. *J. Am. Chem. Soc.* **2016**, *138*, 10136.

(71) Morgenroth, F.; Kübel, C.; Müller, M.; Wiesler, U.; Berresheim, A.; Wagner, M.; Müllen, K. *Carbon* **1998**, *36*, 833.

(72) Feng, X.; Wu, J.; Enkelmann, V.; Müllen, K. *Org. Lett.* **2006**, *8*, 1145.

(73) Pradhan, A.; Dechambenoit, P.; Bock, H.; Durola, F. *Chem. Eur. J.* **2016**, *22*, 18227.

(74) Oded, Y. N.; Pogodin, S.; Agranat, I. *J. Org. Chem.* **2016**, *81*, 11389.

(75) Chalifoux, W. A. *Angew. Chem. Int. Ed.* **2017**, *56*, 8048.

(76) Grzybowski, M.; Skonieczny, K.; Butenschoen, H.; Gryko, D. T. *Angew. Chem. Int. Ed.* **2013**, *52*, 9900.

(77) Rempala, P.; Kroulík, J.; King, B. T. *J. Org. Chem.* **2006**, *71*, 5067.

(78) Pradhan, A.; Dechambenoit, P.; Bock, H.; Durola, F. *Angew. Chem. Int. Ed.* **2011**, *50*, 12582.

(79) Pradhan, A.; Dechambenoit, P.; Bock, H.; Durola, F. *J. Org. Chem.* **2013**, *78*, 2266.

(80) Dou, X.; Yang, X.; Bodwell, G. J.; Wagner, M.; Enkelmann, V.; Müllen, K. *Org. Lett.* **2007**, *9*, 2485.

(81) Ormsby, J. L.; Black, T. D.; Hilton, C. L.; King, B. T. *Tetrahedron* **2008**, *64*, 11370.

(82) Dötz, F.; Brand, J. D.; Ito, S.; Gherghel, L.; Müllen, K. *J. Am. Chem. Soc.* **2000**, *122*, 7707.

(83) Nobusue, S.; Fujita, K.; Tobe, Y. *Org. Lett.* **2017**, *19*, 3227.

(84) He, J.; Mathew, S.; Kinney, Z. J.; Warrell, R. M.; Molina, J. S.; Hartley, C. S. *Chem. Commun.* **2015**, *51*, 7245.

(85) Vo, T. H.; Shekhirev, M.; Kunkel, D. A.; Orange, F.; Guinel, M. J.-F.; Enders, A.; Sinitskii, A. *Chem. Commun.* **2014**, *50*, 4172.

(86) Keerthi, A.; Radha, B.; Rizzo, D.; Lu, H.; Diez Cabanes, V.; Hou, I. C.-Y.; Beljonne, D.; Cornil, J. r. m.; Casiraghi, C.; Baumgarten, M. *J. Am. Chem. Soc.* **2017**, *139*, 16454.

(87) Daigle, M.; Morin, J. F. *Macromolecules* **2017**, *50*, 9257.

(88) Miao, D.; Daigle, M.; Lucotti, A.; Boismenu-Lavoie, J.; Tommasini, M.; Morin, J. F. *Angew. Chem. Int. Ed.* **2018**, *130*, 3650.

(89) Yang, W.; Chalifoux, W. A. *Synlett* **2017**, *28*, 625.

(90) Goldfinger, M. B.; Swager, T. M. *J. Am. Chem. Soc.* **1994**, *116*, 7895.

(91) Zhu, X.; Wu, Y.; Zhou, L.; Wang, Y.; Zhao, H.; Gao, B.; Ba, X. *Chin. J. Chem.* **2015**, *33*, 431.

(92) Yang, W.; Lucotti, A.; Tommasini, M.; Chalifoux, W. A. *J. Am. Chem. Soc.* **2016**, *138*, 9137.

(93) Mohamed, R. K.; Mondal, S.; Guerrera, J. V.; Eaton, T. M.; Albrecht-Schmitt, T. E.; Shatruk, M.; Alabugin, I. V. *Angew. Chem. Int. Ed.* **2016**, *55*, 12054.

(94) Chen, T.-A.; Lee, T.-J.; Lin, M.-Y.; Sohel, S. M. A.; Diau, E. W.-G.; Lush, S.-F.; Liu, R.-S. *Chem. Eur. J.* **2010**, *16*, 1826.

(95) Li, C.-W.; Wang, C.-I.; Liao, H.-Y.; Chaudhuri, R.; Liu, R.-S. *J. Org. Chem.* **2007**, *72*, 9203.

(96) Chen, T.-A.; Liu, R.-S. *Org. Lett.* **2011**, *13*, 4644.

(97) Feng, X.; Pisula, W.; Müllen, K. *J. Am. Chem. Soc.* **2007**, *129*, 14116.

(98) Goldfinger, M. B.; Crawford, K. B.; Swager, T. M. *J. Am. Chem. Soc.* **1997**, *119*, 4578.

(99) Yang, W.; Monteiro, J. H. S. K.; de Bettencourt-Dias, A.; Catalano, V. J.; Chalifoux, W. A. *Angew. Chem. Int. Ed.* **2016**, *55*, 10427.

(100) Yang, W.; Monteiro, J. H. S. K.; de Bettencourt-Dias, A.; Chalifoux, W. A. *Can. J. Chem.* **2016**, *95*, 341.

(101) Yang, W.; Longhi, G.; Abbate, S.; Lucotti, A.; Tommasini, M.; Villani, C.; Catalano, V. J.; Lykhin, A. O.; Varganov, S. A.; Chalifoux, W. A. *J. Am. Chem. Soc.* **2017**, *139*, 13102.

(102) Takanori, M.; Taisaku, M.; Tsuyoshi, G.; Masahiro, M. *Chem. Lett.* **2011**, *40*, 40.

(103) Stężycki, R.; Grzybowski, M.; Clermont, G.; Blanchard-Desce, M.; Gryko, D. T. *Chem. Eur. J.* **2016**, *22*, 5198.

(104) Yang, W.; Kazemi, R. R.; Karunathilake, N.; Catalano, V. J.; Alpuche-Aviles, M. A.; Chalifoux, W. A. *Org. Chem. Front.* **2018**, *5*, 2288.

(105) Yang, W.; Monteiro, J. H. S. K.; de Bettencourt-Dias, A.; Catalano, V. J.; Chalifoux, W. A. *Chem. Eur. J.* **2019**, *25*, 1441.

(106) Yang, W.; Bam, R.; Catalano, V. J.; Chalifoux, W. A. *Angew. Chem. Int. Ed.* **2018**, *57*, 14773.

(107) Pati, K.; Michas, C.; Allenger, D.; Piskun, I.; Coutros, P. S.; Gomes, G. d. P.; Alabugin, I. V. *J. Org. Chem.* **2015**, *80*, 11706.

(108) Pati, K.; dos Passos Gomes, G.; Harris, T.; Hughes, A.; Phan, H.; Banerjee, T.; Hanson, K.; Alabugin, I. V. *J. Am. Chem. Soc.* **2015**, *137*, 1165.

(109) Senese, A. D.; Chalifoux, W. A. *Molecules* **2018**, *24*, 118.

(110) Jordan, R. S.; Wang, Y.; McCurdy, R. D.; Yeung, M. T.; Marsh, K. L.; Khan, S. I.; Kaner, R. B.; Rubin, Y. *Chem* **2016**, *1*, 78.

(111) Jordan, R. S.; Li, Y. L.; Lin, C.-W.; McCurdy, R. D.; Lin, J. B.; Brosmer, J. L.; Marsh, K. L.; Khan, S. I.; Houk, K. N.; Kaner, R. B.; Rubin, Y. *J. Am. Chem. Soc.* **2017**, *139*, 15878.

(112) Mallory, F. B.; Wood, C. S.; Gordon, J. T. *J. Am. Chem. Soc.* **1964**, *86*, 3094.

(113) Tang, X.-Q.; Harvey, R. G. *J. Org. Chem.* **1995**, *60*, 3568.

(114) Jørgensen, K. B. *Molecules* **2010**, *15*, 4334.

(115) Meng, D.; Fu, H.; Fan, B.; Zhang, J.; Li, Y.; Sun, Y.; Wang, Z. *Chem. Asian J.* **2017**, *12*, 1286.

(116) Schuster, N. J.; Paley, D. W.; Jockusch, S.; Ng, F.; Steigerwald, M. L.; Nuckolls, C. *Angew. Chem. Int. Ed.* **2016**, *55*, 13519.

(117) Meng, D.; Fu, H.; Xiao, C.; Meng, X.; Winands, T.; Ma, W.; Wei, W.; Fan, B.; Huo, L.; Doltsinis, N. L.; Li, Y.; Sun, Y.; Wang, Z. *J. Am. Chem. Soc.* **2016**, *138*, 10184.

(118) Endres, A. H.; Schaffroth, M.; Paulus, F.; Reiss, H.; Wadepohl, H.; Rominger, F.; Krämer, R.; Bunz, U. H. F. *J. Am. Chem. Soc.* **2016**, *138*, 1792.

(119) Sisto, T. J.; Zhong, Y.; Zhang, B.; Trinh, M. T.; Miyata, K.; Zhong, X.; Zhu, X. Y.; Steigerwald, M. L.; Ng, F.; Nuckolls, C. *J. Am. Chem. Soc.* **2017**, *139*, 5648.

(120) Zhong, Y.; Sisto, T. J.; Zhang, B.; Miyata, K.; Zhu, X. Y.; Steigerwald, M. L.;

Ng, F.; Nuckolls, C. *J. Am. Chem. Soc.* **2017**, *139*, 5644.

(121) Noller, K.; Kosteyn, F.; Meier, H. *Chem. Ber.* **1988**, *121*, 1609.

(122) Liu, L.; Yang, B.; Katz, T. J.; Poindexter, M. K. *J. Org. Chem.* **1991**, *56*, 3769.

(123) Sato, T.; Shimada, S.; Hata, K. *J. Chem. Soc. Chem. Commun.* **1970**, 766.

(124) Takeo, S.; Shigeru, S.; Kazuo, H. *Bull. Chem. Soc. Jpn.* **1971**, *44*, 2484.

(125) He, J.; Agra-Kooijman, D. M.; Singh, G.; Wang, C.; Dugger, C.; Zeng, J.; Zang, L.; Kumar, S.; Hartley, C. S. *J. Mater. Chem. C* **2013**, *1*, 5833.

(126) Lu, S.-C.; Zhang, X.-X.; Shi, Z.-J.; Ren, Y.-W.; Li, B.; Zhang, W. *Adv. Synth. Catal.* **2009**, *351*, 2839.

(127) Skonieczny, K.; Gryko, D. T. *Chem. Asian J.* **2016**, *11*, 2513.

(128) Skonieczny, K.; Yoo, J.; Larsen, J. M.; Espinoza, E. M.; Barbasiewicz, M.; Vullev, V. I.; Lee, C.-H.; Gryko, D. T. *Chem. Eur. J.* **2016**, *22*, 7485.

(129) Skonieczny, K.; Gryko, D. T. *J. Org. Chem.* **2015**, *80*, 5753.

(130) Schnapperelle, I.; Bach, T. *Chem. Eur. J.* **2014**, *20*, 9725.

(131) Daigle, M.; Picard-Lafond, A.; Soligo, E.; Morin, J. F. *Angew. Chem. Int. Ed.* **2016**, *128*, 2082.

(132) Daigle, M.; Miao, D.; Lucotti, A.; Tommasini, M.; Morin, J. F. *Angew. Chem. Int. Ed.* **2017**, *129*, 6309.

(133) Guisinger, N. P.; Arnold, M. S. *MRS bulletin* **2010**, *35*, 273.

(134) Kim, K.; Choi, J.-Y.; Kim, T.; Cho, S.-H.; Chung, H.-J. *Nature* **2011**, *479*, 338.

(135) Novoselov, K. S.; Fal, V.; Colombo, L.; Gellert, P.; Schwab, M.; Kim, K. *Nature* **2012**, *490*, 192.

(136) Lu, G.; Yu, K.; Wen, Z.; Chen, J. *Nanoscale* **2013**, *5*, 1353.

(137) Boukhvalov, D.; Katsnelson, M. *J. Phys. Condensed Matter* **2009**, *21*, 344205.

(138) Feng, H.; Cheng, R.; Zhao, X.; Duan, X.; Li, J. *Nat. Commun.* **2013**, *4*, 1539.

(139) Jeon, K.-J.; Lee, Z.; Pollak, E.; Moreschini, L.; Bostwick, A.; Park, C.-M.; Mendelsberg, R.; Radmilovic, V.; Kostecki, R.; Richardson, T. J. *Acs Nano* **2011**, *5*,

1042.

(140) Oh, J. S.; Kim, K. N.; Yeom, G. Y. *J. Nanosci. Nanotechnol.* **2014**, *14*, 1120.

(141) Obradovic, B.; Kotlyar, R.; Heinz, F.; Matagne, P.; Rakshit, T.; Giles, M.; Stettler, M.; Nikonov, D. *Appl. Phys. Lett.* **2006**, *88*, 142102.

(142) Wang, J.; Zhao, R.; Yang, M.; Liu, Z.; Liu, Z. *J. Chem. Phys.* **2013**, *138*, 084701.

(143) Dössel, L.; Gherghel, L.; Feng, X.; Müllen, K. *Angew. Chem. Int. Ed.* **2011**, *50*, 2540.

(144) Liu, J.; Li, B.-W.; Tan, Y.-Z.; Giannakopoulos, A.; Sanchez-Sanchez, C.; Beljonne, D.; Ruffieux, P.; Fasel, R.; Feng, X.; Müllen, K. *J. Am. Chem. Soc.* **2015**, *137*, 6097.

(145) Li, G.; Yoon, K. Y.; Zhong, X.; Zhu, X.; Dong, G. *Chem. Eur. J.* **2016**, *22*, 9116.

(146) Narita, A.; Feng, X.; Müllen, K. *Chem. Rec.* **2015**, *15*, 295.

(147) Schwab, M. G.; Narita, A.; Osella, S.; Hu, Y.; Maghsoumi, A.; Mavrinsky, A.; Pisula, W.; Castiglioni, C.; Tommasini, M.; Beljonne, D. *Chem. Asian J.* **2015**, *10*, 2134.

(148) Chen, L.; Hernandez, Y.; Feng, X.; Müllen, K. *Angew. Chem. Int. Ed.* **2012**, *51*, 7640.

(149) Ozaki, K.; Kawasumi, K.; Shibata, M.; Ito, H.; Itami, K. *Nat. Commun.* **2015**, *6*, 6251.

(150) King, B. T.; Kroulík, J.; Robertson, C. R.; Rempala, P.; Hilton, C. L.; Korinek, J. D.; Gortari, L. M. *J. Org. Chem.* **2007**, *72*, 2279.

(151) Bovey, F. *Polym. Eng. Sci.* **1967**, *7*, 128.

(152) Arslan, H.; Uribe-Romo, F. J.; Smith, B. J.; Dichtel, W. R. *Chem. Sci.* **2013**, *4*, 3973.

(153) Centrone, A.; Brambilla, L.; Renouard, T.; Gherghel, L.; Mathis, C.; Müllen,

K.; Zerbi, G. *Carbon* **2005**, *43*, 1593.

(154) Lee, J.; Rajeeva, B. B.; Yuan, T.; Guo, Z.-H.; Lin, Y.-H.; Al-Hashimi, M.; Zheng, Y.; Fang, L. *Chem. Sci.* **2016**, *7*, 881.

(155) Zhao, S.; Rondin, L.; Delport, G.; Voisin, C.; Beser, U.; Hu, Y.; Feng, X.; Müllen, K.; Narita, A.; Campidelli, S. *Carbon* **2017**, *119*, 235.

(156) Jordan, R. S.; Li, Y. L.; Lin, C.-W.; McCurdy, R. D.; Lin, J. B.; Brosmer, J. L.; Marsh, K. L.; Khan, S. I.; Houk, K.; Kaner, R. B. *J. Am. Chem. Soc.* **2017**, *139*, 15878.

(157) Shi, K.; Lei, T.; Wang, X.-Y.; Wang, J.-Y.; Pei, J. *Chem. Sci.* **2014**, *5*, 1041.

(158) Intemann, J. J.; Yao, K.; Ding, F.; Xu, Y.; Xin, X.; Li, X.; Jen, A. K. Y. *Adv. Funct. Mater.* **2015**, *25*, 4889.

(159) Scheuble, M.; Gross, Y.; Trefz, D.; Brinkmann, M.; López Navarrete, J.; Ruiz Delgado, M.; Ludwigs, S. *Macromolecules* **2015**, *48*, 7049.

(160) Modjewski, M.; Lindeman, S. V.; Rathore, R. *Org. Lett.* **2009**, *11*, 4656.

(161) Garden, S. J.; Torres, J.; Ferreira, A. A.; Silva, R. B.; Pinto, A. C. *Tetrahedron Lett.* **1997**, *38*, 1501.

(162) Lisowski, V.; Robba, M.; Rault, S. *J. Org. Chem.* **2000**, *65*, 4193.

(163) Nakayama, J.; Sakai, A.; Hoshino, M. *J. Org. Chem.* **1984**, *49*, 5084.

(164) Shen, H.; Vollhardt, K. P. C. *Synlett* **2012**, *2012*, 208.

(165) Hohl, B.; Bertschi, L.; Zhang, X.; Schlüter, A. D.; Sakamoto, J. *Macromolecules* **2012**, *45*, 5418.

(166) Iyer, V. S.; Yoshimura, K.; Enkelmann, V.; Epsch, R.; Rabe, J. P.; Müllen, K. *Angew. Chem. Int. Ed.* **1998**, *37*, 2696.

(167) Sakamoto, Y.; Suzuki, T. *J. Am. Chem. Soc.* **2013**, *135*, 14074.

(168) Shimo, Y.; Mikami, T.; Hamao, S.; Goto, H.; Okamoto, H.; Eguchi, R.; Gohda, S.; Hayashi, Y.; Kubozono, Y. *Sci. Rep.* **2016**, *6*, 21008.

(169) Lee, J.; Kalin, A. J.; Yuan, T.; Al-Hashimi, M.; Fang, L. *Chem. Sci.* **2017**, *8*, 2503.

(170) Wu, Y.; Zhang, J.; Fei, Z.; Bo, Z. *J. Am. Chem. Soc.* **2008**, *130*, 7192.

(171) Zeng, S.-Z.; Jin, N.-Z.; Zhang, H.-L.; Hai, B.; Chen, X.-H.; Shi, J. *RSC Adv.* **2014**, *4*, 18676.

(172) Scherf, U. *J. Mater. Chem.* **1999**, *9*, 1853.

(173) Durban, M. M.; Kazarinoff, P. D.; Segawa, Y.; Luscombe, C. K. *Macromolecules* **2011**, *44*, 4721.

(174) Grem, G.; Leising, G. *Synth. Met.* **1993**, *57*, 4105.

(175) Leising, G.; Tasch, S.; Meghdadi, F.; Athouel, L.; Froyer, G.; Scherf, U. *Synth. Met.* **1996**, *81*, 185.

(176) Piok, T.; Gamerith, S.; Gadermaier, C.; Plank, H.; Wenzl, F. P.; Patil, S.; Montenegro, R.; Kietzke, T.; Neher, D.; Scherf, U.; Landfester, K.; List, E. J. W. *Adv. Mater.* **2003**, *15*, 800.

(177) Babel, A.; Jenekhe, S. A. *Adv. Mater.* **2002**, *14*, 371.

(178) Chen, X. L.; Bao, Z.; Schön, J. H.; Lovinger, A. J.; Lin, Y.-Y.; Crone, B.; Dodabalapur, A.; Batlogg, B. *Appl. Phys. Lett.* **2001**, *78*, 228.

(179) Babel, A.; Jenekhe, S. A. *J. Am. Chem. Soc.* **2003**, *125*, 13656.

(180) Briseno, A. L.; Mannsfeld, S. C. B.; Shamberger, P. J.; Ohuchi, F. S.; Bao, Z.; Jenekhe, S. A.; Xia, Y. *Chem. Mater.* **2008**, *20*, 4712.

(181) Scherf, U.; Müllen, K. *Makromol. Chem., Rapid Commun.* **1991**, *12*, 489.

(182) Forster, M.; Annan, K. O.; Scherf, U. *Macromolecules* **1999**, *32*, 3159.

(183) Fiesel, R.; Huber, J.; Scherf, U. *Angew. Chem. Int. Ed.* **1996**, *35*, 2111.

(184) Chmil, K.; Scherf, U. *Makromol. Chem., Rapid Commun.* **1993**, *14*, 217.

(185) Yuan, Z.; Xiao, Y.; Yang, Y.; Xiong, T. *Macromolecules* **2011**, *44*, 1788.

(186) Tour, J. M.; Lamba, J. J. S. *J. Am. Chem. Soc.* **1993**, *115*, 4935.

(187) Miao, D.; Aumaitre, C.; Morin, J.-F. *J. Mater. Chem. C* **2019**, *7*, 3015.

(188) Walker, S. D.; Barder, T. E.; Martinelli, J. R.; Buchwald, S. L. *Angew. Chem. Int. Ed.* **2004**, *116*, 1907.

(189) Hecht, S.; Khan, A. *Angew. Chem. Int. Ed.* **2003**, *115*, 6203.

(190) Takase, M.; Enkelmann, V.; Sebastiani, D.; Baumgarten, M.; Müllen, K. *Angew. Chem. Int. Ed.* **2007**, *119*, 5620.

(191) Takase, M.; Narita, T.; Fujita, W.; Asano, M. S.; Nishinaga, T.; Benten, H.; Yoza, K.; Müllen, K. *J. Am. Chem. Soc.* **2013**, *135*, 8031.

(192) Gońka, E. b.; Chmielewski, P. J.; Lis, T.; Stepien, M. *J. Am. Chem. Soc.* **2014**, *136*, 16399.

(193) Dou, L.; Chen, C.-C.; Yoshimura, K.; Ohya, K.; Chang, W.-H.; Gao, J.; Liu, Y.; Richard, E.; Yang, Y. *Macromolecules* **2013**, *46*, 3384.

(194) Thompson, B. C.; Kim, Y.-G.; Reynolds, J. R. *Macromolecules* **2005**, *38*, 5359.

(195) Qiao, H.; Deng, Y.; Peng, R.; Wang, G.; Yuan, J.; Tan, S. *RSC Adv.* **2016**, *6*, 70046.

(196) Zhang, Y.; Cheema, H.; McNamara, L.; Hunt, L. A.; Hammer, N. I.; Delcamp, J. H. *Chem. Eur. J.* **2018**, *24*, 5939.

(197) Delcamp, J. H.; Yella, A.; Holcombe, T. W.; Nazeeruddin, M. K.; Grätzel, M. *Angew. Chem. Int. Ed.* **2013**, *125*, 394.

(198) Mathew, S.; Astani, N. A.; Curchod, B. F.; Delcamp, J. H.; Marszalek, M.; Frey, J.; Rothlisberger, U.; Nazeeruddin, M. K.; Grätzel, M. *J. Mater. Chem. A* **2016**, *4*, 2332.

(199) Balli, H.; Zeller, M. *Helv. Chim. Acta* **1983**, *66*, 2135.

(200) Kanno, K.-i.; Liu, Y.; Iesato, A.; Nakajima, K.; Takahashi, T. *Org. Lett.* **2005**, *7*, 5453.

(201) Wan, D.; Li, X.; Jiang, R.; Feng, B.; Lan, J.; Wang, R.; You, J. *Org. Lett.* **2016**, *18*, 2876.

(202) Boldt, S.; Parpart, S.; Villinger, A.; Ehlers, P.; Langer, P. *Angew. Chem. Int. Ed.* **2017**, *56*, 4575.

(203) Das, A.; Ghosh, I.; König, B. *Chem. Commun.* **2016**, *52*, 8695.

(204) Drigo, N. A.; Paek, S.; Huckaba, A. J.; Schouwink, P. A.; Tabet, N.; Nazeeruddin, M. K. *Chem. Eur. J.* **2017**, *23*, 17209.

(205) Parpart, S.; Boldt, S.; Ehlers, P.; Langer, P. *Org. Lett.* **2017**, *20*, 122.

(206) Zhou, J.; Yang, W.; Wang, B.; Ren, H. *Angew. Chem. Int. Ed.* **2012**, *51*, 12293.

(207) Ito, S.; Tokimaru, Y.; Nozaki, K. *Chem. Commun.* **2015**, *51*, 221.

(208) Berger, R.; Wagner, M.; Feng, X.; Müllen, K. *Chem. Sci.* **2015**, *6*, 436.

(209) Tokimaru, Y.; Ito, S.; Nozaki, K. *Angew. Chem. Int. Ed.* **2017**, *129*, 15766.

(210) Richter, M.; Schellhammer, K. S.; Machata, P.; Cuniberti, G.; Popov, A.; Ortmann, F.; Berger, R.; Müllen, K.; Feng, X. *Org. Chem. Front.* **2017**, *4*, 847.

(211) Guthrie, D. B. PhD thesis, University of Pittsburgh, 2009.

(212) Lee, D.; Lee, S.; Jung, D.; Hahn, J. *Asian J. Chem.* **2013**, *25*, 501.

(213) Zhu, W.; Ma, D. *Org. Lett.* **2006**, *8*, 261.

(214) Clar, E.; Ironside, C.; Zander, M. *J. Chem. Soc.* **1959**, 142.

(215) Istanbulluoglu, C.; Göker, S.; Hizalan, G.; Hacioglu, S. O.; Udum, Y. A.; Yildiz, E. D.; Cirpan, A.; Toppare, L. *New J. Chem.* **2015**, *39*, 6623.

(216) Ma, Z.; Wang, E.; Jarvid, M. E.; Henriksson, P.; Inganäs, O.; Zhang, F.; Andersson, M. R. *J. Mater. Chem.* **2012**, *22*, 2306.

(217) Deng, Y.; Chen, Y.; Zhang, X.; Tian, H.; Bao, C.; Yan, D.; Geng, Y.; Wang, F. *Macromolecules* **2012**, *45*, 8621.

(218) van Pruissen, G. W.; Brebels, J.; Hendriks, K. H.; Wienk, M. M.; Janssen, R. A. *Macromolecules* **2015**, *48*, 2435.

(219) Dou, L.; Liu, Y.; Hong, Z.; Li, G.; Yang, Y. *Chem. Rev.* **2015**, *115*, 12633.

(220) Huang, H.; Qiu, M.; Li, Q.; Liu, S.; Zhang, X.; Wang, Z.; Fu, N.; Zhao, B.; Yang, R.; Huang, W. *J. Mate. Chem. C* **2016**, *4*, 5448.

(221) Jenekhe, S. A.; Lu, L.; Alam, M. M. *Macromolecules* **2001**, *34*, 7315.

(222) Beaupré, S.; Shaker-Sepasgozar, S.; Najari, A.; Leclerc, M. *J. Mater. Chem. A*

2017, *5*, 6638.

(223) Li, Y.; Cao, Y.; Gao, J.; Wang, D.; Yu, G.; Heeger, A. J. *Synth. Met.* **1999**, *99*, 243.

(224) Müllen, K.; Pisula, W. *J. Am. Chem. Soc.* **2015**, *137*, 9503.

(225) Caffy, F.; Delbosc, N.; Chávez, P.; Lévêque, P.; Faure-Vincent, J.; Travers, J.-P.; Djurado, D.; Pécaut, J.; Grévin, B.; Lemaitre, N. *Polym. Chem.* **2016**, *7*, 4160.

(226) Peet, J.; Kim, J. Y.; Coates, N. E.; Ma, W. L.; Moses, D.; Heeger, A. J.; Bazan, G. C. *Nature Mater.* **2007**, *6*, 497.

(227) Sakai, J.; Kawano, K.; Yamanari, T.; Taima, T.; Yoshida, Y.; Fujii, A.; Ozaki, M. *Sol. Energy Mater. Sol. Cells* **2010**, *94*, 376.

(228) Lin, Y.; Wang, J.; Zhang, Z. G.; Bai, H.; Li, Y.; Zhu, D.; Zhan, X. *Adv. Mater.* **2015**, *27*, 1170.

(229) Piliego, C.; Holcombe, T. W.; Douglas, J. D.; Woo, C. H.; Beaujuge, P. M.; Fréchet, J. M. *J. Am. Chem. Soc.* **2010**, *132*, 7595.

(230) Zou, Y.; Najari, A.; Berrouard, P.; Beaupré, S.; Réda Aïch, B.; Tao, Y.; Leclerc, M. *J. Am. Chem. Soc.* **2010**, *132*, 5330.

(231) Wang, E.; Ma, Z.; Zhang, Z.; Vandewal, K.; Henriksson, P.; Inganäs, O.; Zhang, F.; Andersson, M. R. *J. Am. Chem. Soc.* **2011**, *133*, 14244.

(232) Wienk, M. M.; Turbiez, M.; Gilot, J.; Janssen, R. A. *Adv. Mater.* **2008**, *20*, 2556.